Sustainable Urban Air Mobility

Solving Urban Congestion in 2050
DSE Group 18

TUDelft

Sustainable Urban Air Mobility

by

Group 18

Final Report

Author:	Student number:
Anne Bart **Beijneveld**	4390458
Till M. **Blaha**	4597176
Peter A. **Bos**	4438043
Ward A. **Broeders**	4454359
Trevor A. **Gast**	4532414
Birgitte L. **Hennink**	4463064
David **Oort Alonso**	4532163
Timon L. **Rowntree**	4544927
Sidharatha S. **Thakur**	4541340
Simone F. **Veldhuizen**	4534441

Preface

This report is created by a group of 10 students as part of the Design Synthesis Exercise. This is the last phase of the Aerospace Engineering Bachelor of Science at the TU Delft, where students need to show their competence in the design process of aerospace related projects. This is the last report which includes the final design after 10 weeks of work. The team has been assigned to design a Sustainable Urban Air Mobility System.

The team would like to thank Roelof Vos for his support, knowledge and guidance during this project. Next to that, the team would like to thank Cong Li and Dmitrii Kliukin for their help, support and advice. Moreover, the team would like to thank Luciana Monteiro for the active participation during this project and the possibility to get in contact with Embraer employees. This opportunity gave us new insights, therefore we would like to thank André Stein and Carlos Ilario for their time to help us. Apart from that, the team would like to thank Yash Tambi, Marc Vizcarra and Marilena Pavel for their useful advice on various technical and design aspects of the project (on a vehicle and infrastructure level). Lastly, the team acknowledges the DSE committee and the TA's for making this project available.

Group 18
Delft, June 2019

Executive Summary

Due to the increasing urbanisation, the pressure on road transportation and public transportation networks will keep on growing in the coming years. To solve this problem and deal with the growing energy demands, a sustainable urban air mobility system (UAM) for the year 2050 is developed in this project. The system is designed for transporting passengers and not cargo, as the team wants to solve congestion. First, an extended market analysis is performed to determine what the characteristics of an "average city" are. To ensure sustainability, a sustainability development strategy is determined before the design phase starts. Hereafter, several concepts are designed and a trade-off is done to choose which vehicle would be worked-out in more detail during the rest of the project. A list of requirements for the whole system to comply with is created. Hereafter, the vehicle and the infrastructure are sized to meet the determined requirements. Finally, a preliminary investment plan is created based on estimated development, production, manufacturing and operating costs. This report is send to the tutor, the mentors and TA's.

Market Analysis   The goal of the market analysis is to determine which city corresponded most to the "average city". The focus of the analysis is on 10 prospective big cities in 2050 spread around the world which will probably have to cope with urbanisation. These cities are evaluated on several aspects, like existing transport modes, mobility demands and the geography of the city. Furthermore, also social aspects are evaluated, such as financial status of the population, political climate and the security standards. This gives a complete overview of the feasibility of a UAM in that particular city. Cities with very low average income and an unstable political climate are eliminated and average values for the different criteria are determined for the remaining cities. The cities are then ranked based on how close they are to the average of each criterion. It is found that the highest ranking city is Los Angeles (LA). This means that LA is used as a reference city throughout the rest of the design process.

LA is widely known as the city with the worst congestion problems in the United States, which brings along significant health problems to its inhabitants due to the air pollution. The UAM system could bring a solution to both problems. During the development of a UAM system, the effect of the system on the existing transport flows and air quality should be taken into account. The average user in LA requires a transport system that is most importantly time efficient, affordable and sustainable in the long run.

Data from the Census Transportation Planning Products (CTPP) is used to create a mapping of the traffic flows in LA at different times of the day. It is found that 84% of the daily commuters drives by car to their work. This clearly explains the huge congestion problem in LA. It also shows that the frequent users of the UAM system will most probably be people who commute to work by car every day. The main reason that the percentage of car-commuters is as high as it is, is because the reachability of the LA Metro system is considered to be bad and unreliable and driving a car provides users with a sense of "complete control". This gives important requirements for the UAM system, namely that it has to be easily reached and that it has to be either on demand or go on such frequent basis that the scheduling does not have to be checked.

Sustainable Development Strategy   When introducing a new transport system in a city, sustainability is one of the main priorities. In this design process not only environmental sustainability is considered, but also social and economical sustainability. During the concept trade-off multiple criteria are used that contain a form of sustainability, like the total energy usage, safety, ticket price and battery mass. In the design of the chosen concept sustainability is also implemented in various design choices. The vehicle is optimised to fly at lowest energy use with the least noise as possible to satisfy worries of environmental and social sustainability. Another social acceptance design consideration is the passenger experience and comfort, which has to meet with the expectations of users. A further optimisation on energy use and thus operational cost is done by studying the flight profile and the network. Finally the vertiport is aimed to be

self-sustainable by the use of solar panels and the social acceptance of neighbours should be investigated.

Concept Trade-off   Using the knowledge gained in the Market Analysis, criteria on the transport system are set up and ranked in importance. A numerical tool that combines vehicle and system characteristics is created to find quantitative values for the criteria. Conceptual designs for different passenger ranges (1-2 pax, 4-6 pax and 20+ pax) are created and in a two stage trade-off a winning concept is chosen. This winning concept is a four person tilt wing aircraft that scored the best in areas like energy efficiency, noise and ticket price. This concept is further developed in the final part of the DSE. The integrated tool is further developed to help designing the concept in more detail.

Vehicle Configuration and Specifications   The designed vehicle is named the Bumblebee EX, due to its likeness to a bee. It also has an appealing look which is important for social acceptance.

The vehicle is a tilt-wing rotorcraft, with 4 main wing rotors (2 m diameter each) and 2 rotors on the forward canard (1.6 m diameter). The span of the aircraft is 10 meters, and the length of the aircraft is 4.8 meters from nose to tail edge, plus 0.8 m rotor radius that extends in front of the nose. The fuselage is 1.6 meters wide, allowing 4 passengers to sit in 2 rows. The Bumblebee can carry a total payload mass of 370 kg with a maximum takeoff weight of 1,250 kg. The passengers board through a single door on the left side. Inside the aircraft, the passengers can communicate with operations/customer service via touch screens, that also provide in-flight information.

The rotors are driven by electric motors mounted directly in-line with the rotors. The tilt mechanism of the main wing is also driven by electric motors, and the wing tilt of each wing is coupled. In lieu of independent tilt, which would have meant higher structural mass, large ailerons are placed on wings to provide roll control in forward flight as well as yaw control in hover.

The vehicle uses four landing struts for vertical landing. No wheels are present, so taxiing at vertiports is completed via TaxiBot, a robot that can lift the aircraft and move it from takeoff/landing pad to the gate. The landing struts use an airbag suspension to soften landing impact. The gear are low to the ground, and can allow a belly slide in the case of an emergency horizontal landing.

A large charging port is positioned at the rear of the aircraft. Above this port is a trunk for passenger luggage which fits 2 full sized suitcases. Further storage is available in the front of the aircraft.

The vehicle flies autonomously, relying on cameras, LiDAR and inertial reference units for self-awareness. Bumblebee EX must communicate with various entities during operation, including vertiport operations, TaxiBots, fleet operations, air traffic management, nearby vehicles, remote pilots (for emergencies) and of course, the passenger. It accomplishes this through different communication systems, including backup systems to be used in an emergency.

Propulsion Characteristics   The propulsion system of the vehicle is composed of four propellers embedded in the tilt-wing and two propellers in the canard. The design of the propulsion units (wing and canard) is done independently and followed a multi-objective (noise and energy) design optimisation approach for the blade characteristics. It is found that vortex noise dominates rotational noise for an eVTOL like the Bumblebee, especially in the A-weighted sound scale. When at full payload, even with an optimised design, the vehicle is not able to meet the stringent noise requirement of 67 dBA at 250ft set out by Uber as it has a noise footprint of 73 dBA.

The propulsion system is sized to be able to withstand the failure of any of the propellers on the vehicle. The propellers are fixed-pitch, despite the performance benefits of a variable pitch, in favour of a simple and lighter option. The blades are made of carbon fibre and together with the hub weigh 10 kg for each wing propeller, and 6.5 kg for the canard propeller. The hover power required by the vehicle is 300 kW, the cruise power required is 130kW and the peak emergency power required is 425 kW.

Powertrain System Characteristics   The powertrain system includes everything from the batteries to the propulsion system. The batteries, cables, motor controllers, motors and gearboxes (where necessary) are all

sized according to the power and torque needed by the vehicle in nominal and emergency conditions. For the sizing of the electric motors and motor controllers, an interpolation of a set of EMRAX motors and compatible controllers are used as reference. Finally, the lightest combination of suitable motor, gearbox and motor controller is chosen to be used in the vehicle. The batteries are sized based on energy, system voltage, power and burst power through an optimisation of battery cell architecture and optimal cell selection from a database of existing cells. The energy requirement is based on a vehicle maximum nominal range of 60 km and a trip reserve range of 9 km.

The vehicle contains a battery pack for the main wing rotors with a mass of 310 kg, one for the canard rotors with a mass of 14 kg and one for the tilt wing mechanism with a mass of 4 kg. Based on the emergency requirements of the propulsion and tilt wing system (196 kW/prop for the main wing propellers, 32 kW/prop for the canard wing propellers and 7.3 kW/tilt mechanism), the motors, motor controllers and gearboxes for each propeller and tilt mechanism are sized, and adds to a total motor mass of 130 kg. The total mass of the lightest compatible motor controllers is 49 kg. A planetary gearbox with is used to provide a torque increase of the tilt-wing mechanism adding up to a total gearbox mass of 6 kg. The cable mass for all circuits on board adds up to a total of 23 kg.

Structural Characteristics   To size the structure of the wing, a program is adapted that is used in the sizing of the lifting surfaces in the A^3 Vahana aircraft (an aircraft that is comparable in layout). The main wings and canard consist of a composite wing skin and aluminium spars and ribs and will have a combined structural mass of 98 kg. A preliminary tilt wing mechanism has been designed and sized for yield strength and deflection criteria. This results in a mass estimation for this subsystem of 68 kg.

The fuselage structure has also been investigated and a initial sizing of the truss structure that will make up the bulk of this part has been performed as well. The sizing of this part of the vehicle is done with a Finite Element Method (FEM), from which it is found that the combined mass of all the structural elements in the truss will be 83 kg. For the carbon fibre shell around the fuselage (including windows and scatter shields), 30 kg is reserved.

Aerodynamic Characteristics and Energy Demand   An embedded lift, drag and moment tool has been realised using non-linear lifting line theory for pre-stall non-linearities from airfoil data which is validated against well know results for elliptical and tapered wings. Using inputs from stability, structures, overall packaging and this tool, a main wing planform of 8 m^2, 8 m span, resulting aspect ratio of 8 is decided that features a slight negative sweep of $-5°$, a moderate taper ratio of 0.4 and a cambered NACA2410 airfoil. The canard features a symmetric airfoil with an area 1.1 m^2. Lift over drag values of around 9 are expected during cruise.

To investigate the effect of the fuselage on the aerodynamics, a CFD analysis is performed on the body of the aircraft. RANS flow is applied on the simplified body to obtain estimates on the aerodynamic characteristics. To fly at the lowest drag, it has been found that the fuselage should be kept at an angle of attack of 6°, while moving the wing to create the necessary lift. However, this freedom still results in the fuselage causing around 50% of the vehicles drag, so further optimisation seems beneficial.

Using the aerodynamic characteristics of the wing and the body, equilibrium equations are set up to find the required thrust and angles of attack of the wing and canard during hover and cruise taking into account the lift due to the propeller and interfacing with propulsion system tools and the lifting line code mentioned before. Combining this with the flight path resulted in being able to efficiently compute the overall energy necessary for a different trips in different configurations. Thrust values in cruise are between 950 N and 1250 N while cruise continuous power is expected between 110 kW and 130 kW.

Stability & Control Characteristics   Before the stability and controllability analysis is started, the c.g. ranges at full capacity in cruise and hover configuration are analysed, as tilting of the wing causes a forward shift in c.g.. Furthermore, the most forward and aft c.g. positions for various loading configurations are analysed and resulted in the most forward c.g. at x_{cg} = -0.34 [MAC] and the most aft at x_{cg} = -0.10 [MAC].

Analysis into the c.g. ranges is followed by analysis into the moment coefficients of the aircraft-less canard, canard wing and of the complete vehicle at varying angles of attack. This led to the trim condition, which is found to be at an angle of attack of 1° around the c.g. at MTOW. The plot showing the varying moment coefficients also showed a negative C_{M_α} for the complete vehicle around the c.g. at MTOW, which corresponds to a longitudinal statically stable aircraft.

The next step is to analyse the stability and controllability of the vehicle with the defined canard wing surface area and c.g. range. The stability and controllability limits are plotted for varying c.g. positions and canard wing surface areas. The chosen canard wing surface area and c.g. range at full capacity shows to be within the stability and controllability limits, which translates into a statically stable and controllable aircraft. However, multiple other loading configurations are deemed statically unstable and the full feasible c.g. range results in -0.34[MAC] to -0.24[MAC].

The dynamic longitudinal stability of the aircraft is analysed by estimating the force derivatives based on the aerodynamics of the wings, body and propellers. This analysis can be repeated for various stages in flight from hover, to transition to cruise. Once the derivatives are estimated, a state space system is formed from the equations of motion for the states u, w (horizontal and vertical velocity), θ and q (pitch angle and pitch rate). From this analysis, four flight conditions are analysed by determining the system response and eigenmotions. The cruise condition is stable, and any disturbance quickly damps out (within a few seconds). Three conditions during transition are analysed and found to be dynamically unstable. The unstable modes are not periodic, and double in amplitude in 0.5 to 3 seconds. Artificial stability must be used to enhance the stability of the aircraft during these phases, so various methods are integratable within the system. These include thrust vectoring, applying differential thrust and tilting of the canard wing to increase the lift coefficient. The methods belonging to their respective use cases are provided in Table 1.

The fuselage of the aircraft introduces an unstable moment in the case of a sideslip angle. This moment is damped by the large main wing propellers. Sufficient response speed is available from the main rotors to provide artificial directional stability. Furthermore, the three main elements of lateral stability are the lack of dihedral and negative sweep - which are destabilising - and the high wing position, which should be stabilising. The exact aerodynamic effects and stability must be investigated further.

Table 1: Methods applied for given control use cases

Use cases	Method	
	Hover	**Cruise**
Roll	Differential thrust	Tilting of canard wing & aileron deflection
Pitch	Differential thrust	Tilting of canard wing or aileron deflection
Yaw	Thrust vectoring (aileron deflection)	Differential thrust

Autonomy   Crucial background information about the various levels of autonomous vehicles is provided, after which the applied method in order to develop a level 5 autonomous vehicle is elaborated upon. This method includes various sensors and systems providing data to the CPU. After the data has been processed, it is fed to an AI system and is distributed amongst all other vehicles within the system through a vehicle network. However, this does not come without its challenges, which include the technology readiness level of artificial intelligence amongst others.

Operations and Infrastructure   The use case of the UAM system is chosen to be a scheduled system with pre-defined routes. This use case is expected to have the most viable market by 2050, and is it offers the most efficient method to transport large amounts of people at minimum infrastructure footprint costs. The air space design implemented to operate the scheduled system in is a free flight system within allowable altitude limits. This airspace design has proven to provide low probability of collision as well as fuel efficient routing, requiring 6.2 times less energy than the other viable designs such as the flight level concept. The flight profile is defined using the applied air pace design, as well as a step up/down approach trajectory at

vertiports and a reserve mission range of 9 km.

The routes to serve are selected by computing a gain metric for all possible routes between 113 equal-population subdivision of LA (Public Use Microdata Areas PUMAs). This gain metric is used as a measure of the level of demand for commuting a certain route using the UAM system, taking into account the speed improvement achieved by travelling via the UAM system during the peak morning commute hours between 5 and 10 am compared to a car in traffic situation. These speed advantages are weighted by the number of passengers travelling that route. For the final target system size of the system, the routes offering the 600 highest gains are selected, which gives a route network between 105 vertiport locations. Using this route selection, an average time gain of 26 minutes is achieved, for trips having an average range of 18km and a net airtime of 7min. A vehicle trip model is implemented as the vehicle is either fully loaded with passenger payload or is empty, and the vehicle only goes back and forth between two hubs. In addition, the total number of passengers intended to serve is determined to 1.1% of transportation using cars. An empty-flight ("zombie") ratio of 0.45 is obtained resulting in a required fleet size of 4,470 vehicles.

The vertiport design can potentially be the bottleneck for the total passenger throughput of the system. Therefore, the area of the vertiport will be designed as efficient as possible. The vertiport design has to fulfil several criteria; the taxiway has to be 1.5 times the tip-to-span, the gates should have a diameter of the maximum dimension of the vehicle, the distance between gates should be 10 ft and the taxiway should have a clearance of 1/3 tip-to-span between gates and taxiways. An exemplary vertiport will be designed on top of the LA convention centre, because it is in the centre of LA: It has a parking garage underneath and it is just 5 minutes walk from the Pico metro station, making it easily accessible for the commuters. The total vertiport has a length of 175 meters and a width of 113 meters, making it suitable for at least 8 Touchdown and Liftoff Areas and 14 gates.

Fleet Maintenance   The maintenance plan of the system consists of three parts. The first part is the daily maintenance, this is a visual check for damage performed after every flight. The second part, is the software and hardware check performed by the autonomy kit prior to every flight. It verifies that the system responds adequately to certain inputs. The final part is the so called ABC check system. The A and B checks are more focused on visual checks, while the C and D checks are much more thorough as also satisfactory functioning of sub-components is tested. The A check is done every 300 cycles, the B check every 1,500 cycles, the C check every 5,000 and finally the D check every 25,000 cycles. For every check a detailed checklist will be created that should be run through point per point without skipping any of the steps mentioned in the procedures. Once the vertiport design is set, a preventive maintenance plan for the vertiports will be created in a similar manner to how these plans are created for airports.

Ticket Price   The ticket price is based on the production and operational costs. These costs are calculated for the vertiports and the vehicles. The production costs for the vehicles are dependent on battery costs (20,000 USD), structural costs (6,000 USD), autonomy kit (120,000 USD), propulsion units (140,000 USD) and manufacturing costs (910,000 USD). This otals to a production costs of 1,200,000 USD for one vehicle. However, the expectation is that costs of most subsystems will decrease by 2050. Next to that, once the vehicle production is doubled, the production costs will decrease by 15%, which is a typical learning curve for aerospace and automotive products[1]. The production costs of one vertiport is estimated to be 3.6 million dollars, including the required modifications to buildings and 12 high voltage chargers for each vertiport. These costs are expected to be amortised within a time period of 30 years. The total production costs are the sum of these costs.

The operational costs are also calculated for the vehicle and for the vertiport. The operational costs for the vehicle are based on the energy usage of the vehicle per trip, which is set at 0.12 USD per kWh. The operating costs of the vertiports consist of lease, maintenance, personnel, security etc. and is 300 USD per day per vehicle. The break even point is set at 15 years, meaning that the ticket price will be 1.70 USD per km per passenger. The vehicle and system need to be incurred from initiation to implementation, therefore

---

[1] https://www.uber.com/elevate.pdf [accessed 20.06.19]

development costs are added. There will be 1-4 million USD allocated for concept exploration, 10-90 million USD for concept validation, 200-600 million USD for the development and 200-300 million USD for the industrialisation for the system [2].

RAMS   To find the reliability of the transport system, different failure modes are studied and the components prone to failure are identified. The autonomous system has to be extensively tested, to ensure the vehicle to be reliable enough for use within a city. Also, the batteries, electric motors and the tilt-wing mechanism are crucial elements that need to be very reliable before the system can safely operate. For efficient maintenance, the preventive maintenance should be scheduled so that the downtime is minimised. Also, critical components of the vehicle should be accessible for inspection and repair. In order determine the availability of the system, a more detailed design and study into the numerical values for reliability and maintenance has to be performed. Finally, safety is one of the top priorities when flying in a populated area, therefore emergency plans have to be worked out for different scenarios. When the vehicle is on the ground, no electrical hazards may occur and the time users spend at the gate should be minimised to mitigate the risk of accidents.

Production Plan

The fuselage, wing and canard are built in the factory. All components such as the rotors, motors and batteries are bough from the market. The fuselage is built up of aluminium members, which are bought from a supplier. They will be cut by a shearing operation on the members, which are welded together in a welding jig. The aluminium ribs in the wing and canard are made by rubber forming of aluminium sheets. The composite spar is made by laying carbon Fibre pre-preg by means of an Automatic Fibre Placement machine on a rotating mandrel. This machine is be used to lay pre-preg for the skin. These composite parts are cured afterwards. The battery cells are bought from a supplier and assembled into a battery pack. A more detailed business plan are necessary to compute the delivery interval of the production process.

Recommendations   For optimal operation and integration in LA, a more detailed demand analysis using agent based modelling should be performed, for instance using MATSim. With improved sources on demand and a better decision on hub locations, a minimum cost flow problem can be setup and solved to minimise fleet size, operational energy efficiency and maximised availability. The power grid is expected to constrain the power demand ($\approx 300kW$ per vehicle) at charging locations, even in the mid-future, and expanding suitable power lines is expected to cost around 1 million USD per kilometre. This effect could outweigh the higher vehicle cost and lower efficiency of increasing range such that outfitting only some convenient hubs with charging stations may decrease investment costs sufficiently. Once the design has reached a more detailed maturity, reliability of all components must be evaluated and confirmed to satisfy regulations. Furthermore, maintenance schedules and reduced equipment lists should be developed to minimise downtime and ensure that significant maintenance only has to occur at convenient hub locations.

Noise can be further reduced by analysing more elaborate rotor features like tip sweep or porosity, which requires more powerful tools like PowerFLOW that can also evaluate interaction effects with the wing, canard and fuselage. Also, the current noise metrics need to be replaced by more indicative metrics that take into account fleet noise and the profile of noise due to the flight path. It should be investigated whether more continuous interpolation or fitting of motor or battery data bases can achieve a more optimal design with faster and more predictable convergence than the current discrete approach. Also, values should be extrapolated to yield probable specs by 2050.

Bending and buckling load cases of the chassis members should be included in the structural analysis to compute a more complete structural mass. Any form of vibrational analyses have been excluded in the sizing so far, but it seems necessary to evaluate fatigue loading on the wing connection. Future improvements in new process technologies like additive manufacturing should be exploited in detailed design to minimise mass of, for example, structural connections in tight spaces. A better trade-off between the aerodynamics, stability, structures and operations departments would have yielded a lighter wing design using

---

[2] https://fedotov.co/wp-content/uploads/2018/03/Future-of-Vertical-Mobility.pdf [accessed 20.06.19]

a thicker airfoil at the cost of slightly higher cruise drag. Furthermore, the aerodynamics of the fuselage should be improved to achieve lower drag and more favourable stability and trim condition as compared to the current highly destabilising design. Finally, an alternative method for yaw control during hover exploiting the spinning directions of the main wing rotors is proposed to eliminate the need of the ailerons if enough cruise roll authority can be provided by the canard wing. This requires further analysis and a more integrated interface with aerodynamic analyses to evaluate this configuration. Lateral and directional stability during cruise must be guaranteed, preferably without a large vertical tailplane, but by controlling differential thrust of the wing. Also, a fully integrated simulation should be developed to test these control strategies and autonomous flight software.

Contents

Nomenclature

Latin Symbols

$\bar{c}$	Mean aerodynamic chord	m
$\bar{c}_c$	Mean aerodynamic chord canard wing	m
$\bar{x}_{ac}$	x-coordinate aerodynamic centre	[MAC]
$\bar{x}_{cg_A}$	x-coordinate centre of gravity component A	[MAC]
$\bar{x}_{cg}$	x-coordinate centre of gravity	[MAC]
$\bar{x}_{np}$	x-coordinate neutral point	[MAC]
Δcg_x	Offset from cg (forward positive)	m
Δx_{tilt}	x-offset from wing tilt axis to leading edge of root chord	m
$\dot{m}$	Mass flow rate	kg/s
$\dot{q}$	Pitch acceleration	rad/s^2
$\dot{u}$	Accaleration in x-direction	m/s^2
$\dot{w}$	Accaleration in z-direction	m/s^2
$\underline{\underline{K}}$	Global stiffness matrix	N/m
$\underline{\underline{k}}$	Local stiffness matrix	N/m
$\underline{\underline{T}}$	Local to global transformation matrix	-
γ_{climb}	Climb angle	-
d	Differential of variable	-
$\underline{\delta}$	Local deformation matrix	m
$\mathbf{F}$	Externally applied forces	N
$\underline{\mathbf{y_p}}$	Spanwise propeller locations	m
$\underline{\mathbf{y}^{ii}}$	Circulation control points grid	m
$\underline{\mathbf{y}^{i}}$	Horseshoe vortex grid	m
A	Cross sectional area	mm^2
a	Acceleration	m/s^2
A_a	Achieved Availability	-
a_c	Speed of sound	m/s
A_i	Inherent Availability	-
A_o	Operational Availability	-
A_{cable}	Area of a cable	m^2
A_{new}	Cross sectional area, next iteration	mm^2
A_{old}	Cross sectional area, current iteration	mm^2
A_{rotor}	Rotor area	m^2
AR	Wing aspect ratio	-
AT	Air time	s
b	Wing span minus fuselage width	m
c	Local blade/wing/canard chord	m

$C(t_{day})$	Congestion Ratio	-
C_1, C_2	Constants of integration	m
C_D	Finite wing drag coefficient	-
c_d	Local airfoil drag coefficient	-
C_L	Finite wing lift coefficient	-
c_l	Local airfoil lift coefficient	-
$C_{M_{A\text{-}c}}$	Moment coefficient induced by the aircraft-less canard	-
C_P	Power coefficient	-
C_r	Root chord	m
C_T	Thrust coefficient	-
C_t	Tip chord	m
$C_{burst,cell}$	Cell burst C-rate	1/h
C_{d_0}	Zero-angle-of-attack profile drag coefficient	-
C_{D_b}	Drag coefficient of the body	-
C_d	Blade sectional profile drag coefficient	-
$C_{L_{A\text{-}c}}$	Lift coefficient of aircraft-less canard	-
C_{L_c}	Lift coefficient canard wing	[-]
C_{L_w}	Lift coefficient main wing	-
C_{L_b}	Lift coefficient of the body	-
$C_{L_{\alpha_{A\text{-}c}}}$	Lift slope aircraft-less canard	-
$C_{L_{\alpha_c}}$	Lift slope canard wing	-
C_{l_α}	Lift slope of airfoil blade	1/rad
C_{L_c}	Lift coefficient of canard wing	-
$C_{m_{ac}}$	Moment coefficient around aerodynamic centre	-
C_{m_b}	Moment coefficient body	[-]
C_{M_c}	Moment coefficient induced by the canard wing	-
C_{m_c}	Aerodynamic moment coefficient canard wing	-
C_{m_w}	Aerodynamic moment coefficient main wing	-
$c_{m_{ac}}$	Local airfoil moment coefficient	-
$C_{m_{y_b}}$	Moment coefficient of the body	-
C_M	Moment coefficient of the complete aircraft	[-]
$C_{nom,cell}$	Nominal cell C-rate	1/h
c_{zombie}	Ratio empty to full flights	-

Contents

D	Aerodynamic drag	N
D	Direct distance from origin to destination	m
d	Diameter of tilt bar	m
$D1$	Linear term coefficient in quadratic drag polar	1/rad
$D2$	Quadratic term coefficient in quadratic drag polar	$1/\text{rad}^2$
D_b	Aerodynamic drag of the body	N
D_c	Aerodynamic drag of the canard	N
D_i	Lift induced drag	N
D_p	Profile drag	N
D_w	Aerodynamic drag of the main wing	N
D_N	Total distance travelled at flight phase N	m
D_b	Drag on the aircraft fuselage	N
D_{cp}	Drag of the canard propellers	N
D_{total}	Total (incompressible and inviscid) drag	N
D_{wp}	Drag of the main wing propellers	N
E	Young's modulus	MPa
e	Oswald span efficiency factor	-
E_{cell}	Cell capacity	Ah
E_{day}	Energy per day	J
$E_{max,pack}$	Maximum required energy from a battery pack	Wh
$E_{revenue}$	Energy full flight	J
E_{zombie}	Energy zombie flight	J
F	Prandtl Tip Loss function	-
f	Exponent in Prandtl Tip Loss function	-
F_1, F_2	Forces	N
f_{peak}	Vortex noise peak frequency	1/s
g	Gravitational acceleration	9.81 m/s^2
$G(\text{trip}, t_{day})$	Demand gain metric for a trip	pax s/m
h	Projected blade thickness	m
h_c	Vertical distance from c.g. to a.c. canard wing	m
h_{ac}	Vertical distance from c.g. to a.c. of the main wing	m
h_{cruise}	Cruise altitude	m
$h_{emergency}$	Emergency flight level altitude for cruise	m
I	Current	A
i_w	Tilt angle of the main wing	rad
I_{xx}	Area moment of inertia of tilt bar	m^4
I_{yy}	Aircraft inertia about the Y-axis	kg m^2
$J_{mN_b}(x)$	Bessel function of the first kind of order mN_b and argument x	-
k	Number of discrete spanwise control points	-
K_2	Semi-empirical constant for vortex noise	(s/m)^3
k_e	Equivalence factor between noise and energy	-
L	Lift	N
l	Length of structural member	m
L'	Spanwise sectional lift	N/m
L/D	Lift to drag ratio	-
L_c	Canard Lift	N
L_w	Wing Lift	N
l_{ac}	Distance from c.g. to a.c. of the main wing	m
L_{cable}	Length of a cable	m
l_c	Canard length	m
m	Mass	kg
m_h	Harmonic number	-
M_u, M_w, M_θ, M_q	Moment derivatives about the Y-axis	
m_A	Mass component A	kg
M_x	Bending moment in tilt bar	Nm
M_x, M_y	Moments around x and y axes respectively	Nm
$M_{0.25\text{MAC}}$	Aerodynamic moment around quarter chord of MAC	Nm
M_{ac}	Aerodynamic moment around ac of the main wing	Nm
$m_{battery}$	Battery mass	kg
M_{body}	Aerodynamic moment of the body	Nm
M_{cp}	Pitching moment of the canard propellers	Nm
M_c	Aerodynamic moment of the canard wing	Nm
M_c	Aerodynamic moment of the canard wing	N
m_{prop}	Propeller mass	kg
M_t	Total aerodynamic moment applying at tilt mechanism	Nm
M_{wp}	Pitching moment of the main wing propellers	Nm
M_w	Aerodynamic moment of the main wing	Nm
$MTOW$	Maximum take-off weight	kg
N	flight phase index	-
n, j, i, s	Arbitrary indexing variables	-
N_b	Rotor number of blades	-

N_r	Number of rotors	-
$n_{parallel}$	Number of cells in parallel	-
n_{pax}	number of passengers	-
n_{series}	Number of cells in series	-
P_N	Total thrust power required at flight phase N	N
P_{loss}	Power loss	W
p_{m_L}	Root Mean Square (RMS) loading sound pressure	Pa
p_{m_T}	Root Mean Square (RMS) thickness sound pressure	Pa
$P_{nom,pack}$	Nominal cell C-rate	W
$P_{prop,max}$	Maximum propeller power	kW
P_{prop}	Propeller power	N
p_{ref}	Reference sound pressure (2×10^{-5})	Pa
$pax(\bar{R})$	Maximum passengers on the inverse route	-
$pax(R_i)$	Maximum passengers on the route	-
pax_{km}	Passenger kilometres	km
Q	Rotor Torque	Nm
q	Pitching rate	rad/s
R	Rotor radius	m
r	Normalized radial location on rotor blade	-
R_e	Effective rotor radius	m
R_i	Radius of rotor i	m
R_{cable}	Electrical Resistance of a Cable	Ω
r_{max}	Maximum vehicle range	m
Re	Reynolds number	-
ROC	Rate of climb	m/s
S	Surface area main wing	m^2
$s.m.$	Stability margin	0.05 [MAC]
S_c	Surface area canard wing	m^2
SM	Safety margin	0.02 [MAC]
T	Rotor thrust	N
t	Blade maximum thickness	m
T/A_{rotor}	Disk loading	-
T/W	Trust to Weight ratio in hover	-
$t_{\frac{1}{2}}$	Time to half amplitude	s
T_c	Normalised thrust in cruise	-
t_r	Tilt bar wall thickness	m
T_u	Annulus thrust	N
T_N	Total airtime to required to fly flight phase N	s
t_{away}	Time away from vertiport	min
$t_{boarding}$	Boarding time	min

$t_{charging}$	Charging time	min
t_{climb}	Climb time	s
T_{cp}	Thrust of the canard propellers	N
t_{cruise}	Cruise time	s
t_{day}	Time of day at which trip is evaluated	hour
t_{hover}	Hover time	s
t_{peak}	Peak day time	h
T_{req}	Thrust required	N
t_{taxi}	Taxiing time	min
$t_{turnaround}$	Turnaround time	min
T_{wp}	Thrust of the main wing propellers	N
$T_{t_{car,avg}}$	Time a car needs in normal traffic for a trip	s
$T_{t_{car}}$	Time a car needs in traffic for a trip	s
$T_{t_{UAM}}$	Time the UAM is estimated to take for a trip	s
TT	Turnaround time	s
u	Velocity in the X-direction	m/s
u_1	Velocity after disk	m/s
u_2	Velocity sufficiently far away from rotor	m/s
V	Free stream velocity	m/s
V	Resultant velocity of blade element	m/s
v	Velocity in the Y-direction	m/s
V_0	Undisturbed air velocity	m/s
v_i	Induced velocity	m/s
V_p	Axial rotor velocity	m/s
V_T	Tangential velocity of rotor	m/s
$V_{u,v,w}$	Airspeed in the X, Y, Z-direction	m/s
V_N	Vehicle velocity at flight phase N	m/s
V_{cell}	Cell voltage	V
$V_{circuit}$	Circuit voltage	V
V_{climb}	Climb speed	m/s
V_{cruise}	Cruise speed	m/s
V_c	Velocity canard wing	m/s
V_{desc}	Rate of descent	m/s
V_{eff}	Effective velocity	m/s
$v_{x'_p}$	Propeller induced velocity ‖ propeller axis	m/s
v_{x_p}	Propeller induced velocity ‖ freestream	m/s
V_x	Velocity in x- direction, expressed in the aerodynamic reference frame	m/s
V_y	Velocity in y- direction, expressed in the aerodynamic reference frame	m/s

$v_{z'_p}$	Propeller induced velocity $\perp$ propeller axis	m/s
v_{z_p}	Propeller induced velocity $\perp$ freestream	m/s
V_z	Velocity in z- direction, expressed in the aerodynamic reference frame	m/s
veh_{pax}	Passengers per vehicle	-
W	Weight	N
w	Velocity in the Z-direction (normal to Earth surface)	m/s
w_0	Local chordwise velocity component	m/s
w_i	Wing induced velocity (upwards positive)	m/s
X_u, X_w, X_θ, X_q	Force derivatives in the X-direction	
x_{ac_w}	x-coordinate aerodynamic centre main wing	m
x_A	x-coordinate A	m
y	Spanwise location	m
z	Coordinate along tilt rod	m
z	Separation between rotors	m
Z_u, Z_w, Z_θ, Z_q	Force derivatives in the Z-direction	
z_A	z-coordinate A	m
z_{ac_w}	z-coordinate aerodynamic centre main wing	m
z_{cg}	z-coordinate c.g.	m

Greek Symbols

α	Angle of attack of a blade element	rad
α_0	Zero-lift angle of attack of the rotor blade airfoil	rad
α_b	Angle of attack of body	deg
α_c	Angle of attack of the canard	deg
α_{off_b}	Body offset angle w.r.t. the ground	°
α_{off_c}	Canard wing offset angle w.r.t. the ground	°
α_{off_w}	Main wing offset angle w.r.t. the ground	°
α_{eff}	Effective angle of attack	deg
α_w	Geometric Angle of attack of the main wing	deg
ΔS	Distance between the rotor and the observer	m
δ	Axial deformation	m
δ_c	Canard angle input	rad
δ_i	Induced drag factor	-
$\dot{\theta}$	Pitch rate	rad/s
ϵ	Observer elevation angle	rad
η_p	Propulsive efficiency	-
$\eta_{operational}$	Usable fraction of the battery pack capacity	-

Γ	Spanwise circulation distribution	m^2/s
γ	Flight path angle	rad
Γ_0	Spanwise maximum circulation	m^2/s
γ_{num}	Numerical damping factor	-
κ	Rotor-induced power factor	-
λ	Eigenvalue	s^{-1}
λ_c	Taper ratio of the canard	-
λ_i	Induced inflow ratio	-
λ_P	Axial inflow ratio	-
λ_r	Inflow ratio	-
λ_T	Tangential inflow ratio	-
λ_w	Taper ratio of the main wing	-
$\Lambda_{0.25}$	Quarter chord sweep (backwards positive)	rad
ν	Transverse deflection of tilt bar	m
Ω	Rotational velocity of rotor	rad/s
ω_s	Rotor wake swirl velocity	rad/s
Φ	PUMA vehicle flux	- / hr
ϕ	Inflow angle	rad
Ψ	Route vehicle flux	- / hr
ψ	Azimuthal angle on the rotor	rad
ρ	Air density	kg/m^3
ρ_t	Radial location on tilt bar	m
ρ_{copper}	Electrical Resistivity of copper	Ωm
σ	Rotor solidity	-
σ_z	Normal stress in tilt bar	MPa
σ_{ult}	Ultimate stress of the isotropic material	MPa
σ_{yield}	Yield stress of the isotropic material	MPa
τ_t	Normalised spanwise decaying factor of propeller interference $\perp$ freestream	-
τ_x	Normalised spanwise decaying factor of propeller interference $\parallel$ freestream	-
θ	Aircraft pitch angle	rad
θ_b	Blade element pitch angle with respect to the rotor plane	rad
ε	Canard downwash angle	°
$\underline{\delta}$	Nodal deflections	m
ζ	Share of commuters served on selected routes	-
η_{charge}	Charge/discharge efficiency	%
η_c	Cruise/climb efficiency	%
η_h	Hover efficiency	%
η_{zombie}	Zombie flight efficiency	%
σ_1, σ_2	Stresses for each member of respective load case	MPa

Glossary

(e)VTOL (electrical) Vertical Take-off and Landing

a/c Aircraft

ADC Air Data Computer

ADS-B Auto. Dependent Surveillance Broadcast

AGL Above Ground Level

AI Artificial Intelligence

AMP Approved Maintenance Plan

ANSP Air Navigation Service Provider

ASL Above Sea Level

ATCo Air Traffic Controller

ATL Automated Tape Layer

ATM Air Traffic Management

BEMT Blade Element and Momentum Theory

BMS Battery Management System

c.g. Centre of gravity

CD&R Conflict Detection and Resolution

CO$_2$ Carbon Dioxide

CPU Central Processing Unit

CTPP Census Transportation Planning Products

DOD Depth of Discharge

DSE Design Synthesis Exercise

EBD Electrical Block Diagram

FAA Federal Aviation Administration

FBS Functional Breakdown Structure

FC Flight Control

FDAL Function Development Assurance Levels

FEM Finite Element Method

FFD Functional Flow Diagram

GA Genetic Algorithm

GNSS Global Navigation Satellite System

IMU Inertial Measurement Unit

LA Los Angeles

LiDAR Laser Imaging Detection and Ranging

MAC Mean Aerodynamic Chord

MCFP Minimum Cost Flow Problem

MDT Mean Downtime

MTBF Mean Time Before Failure

MTBM Mean Time Between Maintenance

MTOW Maximum Take-off Weight

MTTR Mean Time To Repair

NAA National Aviation Authority

OEW Operational Empty Weight (w/o batteries)

pax Passenger(s)

PREE Payload·Range per Unit Energy [-]

PUMAs Public Use Microdata Areas

PVB Polyvinyl butyral

RAMS Reliability, Availability, Maintainability, Safety

RMS Root Mean Square

rpm revolutions per minute

SMT Simple Momentum Theory

SPL Sound Pressure Level

T/L Thrust/Lift

TAWS Terrain Awareness Warning System

TCAS Traffic Collision Avoidance System

TCAS III Traffic Collision Avoidance System III

TLOF Touchdown and Liftoff Area

TO Take-off

UAM Urban Air Mobility

USD United States dollar

VHF Very High Frequency

VRS Vortex Ring State

Introduction

The world is becoming increasingly urbanised. The United Nations predicts that by 2050, 68% of the world population will live in urban areas[1]. Currently, cities have to cope with pollution, traffic congestion and a continuously decreasing amount of space. The increasing urbanisation and population growth will amplify these problems in the future. As of now, the only way to transport people within a city is either over or underneath the ground using existing roads or railways. This limits the amount of people that can be transported over a certain distance at once. Together with the increasing urbanisation, these are the main causes of the congestion problems within large cities. An aerial transport system could play an important role in resolving the congestion problem in big cities as it is a three-dimensional transport system and there is a lot of unused space above cities.

Major air pollution is another problem associated with traffic congestion, which leads to another reason for the need of implementing a new transport system. Furthermore, sustainability and environmental impact are becoming more and more important in today's society. Therefore, it is crucial that a new transport system is sustainable as well. So, everything from the operation of the system to the sourcing of raw materials, manufacturing and recycling of any component of the whole system is something that will have to be carefully thought through.

The purpose of this report is to design an urban air mobility system. In order to determine the demands for the system, an extensive market analysis into Los Angeles (LA) is done. This analysis is used to determine the locations within LA where the system is to be implemented leading to a network of various routes. After a two step trade-off a preliminary vehicle design is chosen. The vehicle is further designed to make it stable, controllable, sustainable and above all, socially accepted. Moreover, the operations and infrastructure are designed to make sure the system is competitive with existing transport modes.

This design process is fulfilled by the team and the specific tasks can be found in Chapter 2. In Chapter 3, the Market Analysis is discussed, followed by the Sustainable Development Strategy for this project in Chapter 4. Then, a recap of the trade-off between the concepts is explained in Chapter 5. In this chapter also the weight factors of the criteria and the updated tool are explained. Hereafter, the requirements for the system will be discussed in Chapter 6, also the requirements for the infrastructure and operations as well as the vehicle requirements are described. Afterwards, the vehicle specifications are discussed in Chapter 7. Then the vehicle is shown in Chapter 8, as well as the software block diagram and communications flow diagram. Hereafter, the design for the different subsystems is discussed in Chapter 9. The operations and infrastructure is presented in Chapter 10. Once the design is known a budget breakdown is made in Chapter 11. Hereafter, the sensitivity analysis is discussed in Chapter 12. The reliability, availability, maintainability and safety (RAMS) about this system are discussed in Chapter 13. The technical risk assessment is discussed in Chapter 14. As a final phase for the design the production plan is presented in Chapter 15. Afterwards, the compliance matrix is shown in Chapter 16. Then, the post DSE plan is shown in Chapter 17. This is followed by the conclusions of the final design in Chapter 18. Finally, the recommendations for further development of this design are discussed in Chapter 19.

---

[1] `https://www.un.org/development/desa/en/news/population/2018-revision-of-world-urbanisation-prospects.html`[accessed 02.05.19]

2

Project Organisation and Objectives

In a large project such as the Design Synthesis Exercise, a planning and task division have to be made and followed in order to keep the design process organised. In Figure 2.1, the organigram of the team can be found. It shows which team member is responsible for which aspects of the design process.
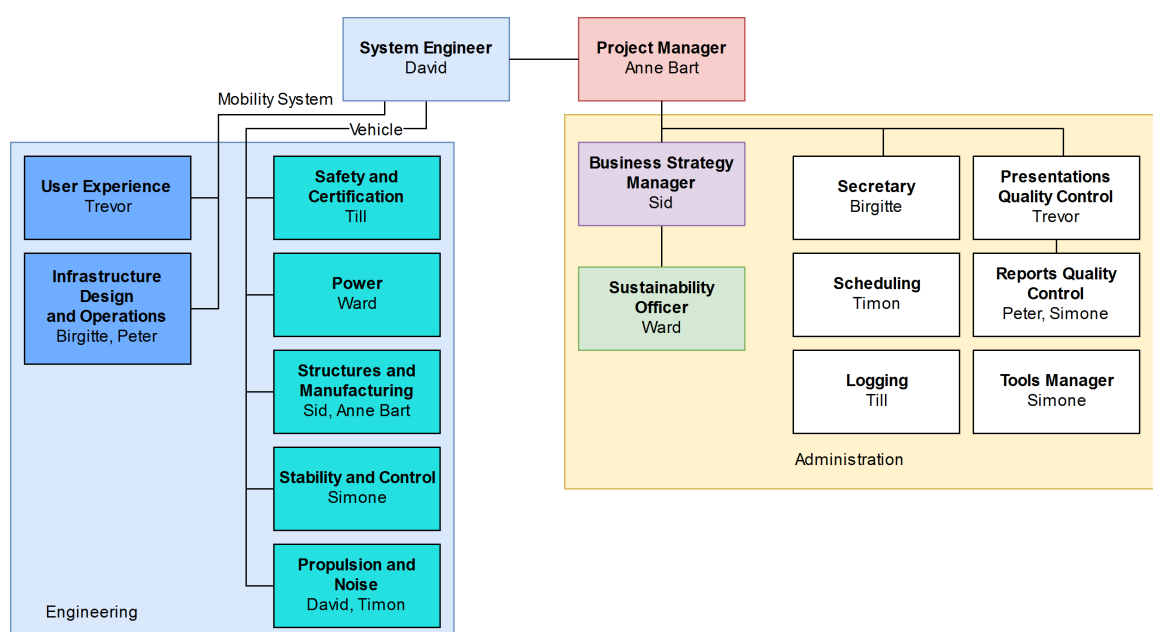
Figure 2.1: Team organigram

The Mission Need Statement states the overall goal and lays out the core purpose that needs to be fulfilled by the project. The mission statement is formulated as follows:

"To provide an environmentally sustainable, socially acceptable and economically competitive solution to meet urban transport demands of 2050 due to increasing urbanisation, congestion and energy demands."

The Project Objective Statement is focused on the project group itself and what the team wants to achieve during the project.

"To design a sustainable Urban Air Mobility System with a high probability of social acceptance which will be further developed by EmbraerX, with 10 students in 10 weeks."

<div align="right"># 3</div>

Market Analysis

The market analysis is of great importance as it determines some requirements and a reduction in the design space. Firstly, the city where a UAM should be designed for is determined in Section 3.1. After the city is chosen the characteristics of commuters are determined in Section 3.2. The stakeholders are shown in Section 3.3. After this the legislation for a UAM system is researched in Section 3.4. Finally, other transport modes are researched as these modes of transport can aid in accomplishing a reduction in congestion. This will be discussed in Section 3.5.

3.1. City Trade-off

For a UAM system to be feasible, first the right place to implement the system should be found. However, this market should also not be so specific that the system can only be implemented in one particular city. Large cities and metropolitan areas on different continents are selected and investigated to find similarities and differences. The cities chosen are: Sao Paulo, Mexico City, LA, San Fransisco, Tokyo, the Randstad, Dubai, New York, Bangkok and Kinshasa. All these cities are subject to urbanisation and are prospective metropolitan areas in the year 2050.

3.1.1. City Trade-off Criteria

Multiple factors have an influence on the feasibility of a UAM system, which can differ significantly in different cities and continents. To clarify these influences, a list of criteria is made to compare the different cities and urban areas.

Existing Transport Modes and Mobility Demands   This criterion establishes (in broad terms) the need for a new mobility system. Moreover, the competition with other transport systems can be faced. Mobility demands are good indicators of demand for a UAM system and the type of competition present with other transportation modes. The success of a UAM system will also depend on the connection and compatibility to existing modes of transport, since the future of urban transportation will most likely be multi-modal to facilitate the diverse trip profile demands. Existing modes of transport should lend themselves to a future where they can interact with an air travel segment.

City Planning   A city showing a high level of urban sprawl would be favourable to a UAM system since the likely advantages are higher speed, at the cost of longer boarding times and possible waiting times. Also, any low speed section of the flight legs are significantly less efficient which would result in higher fuel/power consumption and higher prices per flown distance. Moreover, an extremely high population density could point to a poor city with low economic development. Therefore, vertical density is also considered. A high vertical density often goes hand in hand with a higher economic development, which would lead to a larger market for the UAM system.

Geographical/Natural Environment   Bad weather conditions pose risks on the safety of the vehicle and payload. The climate factor encompasses various weather conditions ranging from average wind conditions to thunderstorms and natural disasters like hurricanes and tsunamis. Apart from the local climate, the topography of the city is also considered. In a very hilly city, the use of public transports like metros

or trains can be difficult, resulting in people using cars. Also, rivers or other waterways can obstruct the existing transport systems, because of the lack of bridges or tunnels. These problems can be solved by the air mobility system as this will not be an issue for this system.

Political Climate The political climate encompasses aspects such as the openness of a city government to new projects, the budget allocated to transportation, the regulations for infrastructure construction and airspace use, certification regulations in the area, etc.

Financial As the UAM system probably will be at least as expensive as traditional public transport methods, a sufficient part of the city population has to be able to afford the system to make it profitable. The financial distribution of the population of the city is therefore analysed. Not only the financial state of the people living in a city is important, but also the finances of the city as a whole. Investment from the city is necessary to build the first 'stations' and to integrate the UAM system in the existing transport system. A prosperous economy is therefore favoured to start up the system.

Security and Social Stability Transporting people above urbanised areas requires unprecedented levels of security for public acceptance (comparable to or higher than civil aviation) [1]. For the system to be feasible, it should be incorporated in environments where civil safety and security standards are high. A politically and economically stable environment is also beneficial for the viability of the system.

Social Acceptance One of the most important factors that determines the success of the system is the social acceptance. A study by Airbus[1] shows that the main concerns of the public are safety, noise, time of the day the system operates and the altitude at which the vehicles fly. However, it is very difficult to predict the social acceptance in different cities in 2050

3.1.2. Result

Using these criteria, quickly Kinshasa and Bangkok can be written off as possible cities for a UAM system. The low average income and political instability create large threats for the feasibility of such a system. By analysing the similarities of the remaining options, the city that corresponds most to the average city is chosen as the reference city for which the mobility system shall be designed for. In order to find the city that correlates most with the average values for the various criteria, the difference between the global average and city averages for each of the criteria is determined. The next step is to implement a ranking system which ranks the numerical values for the criterion and accordingly assigns scores. The city with the highest score corresponded most to the "average city". After having applied this ranking method to the cities, **LA** is the winner, and is therefore used as a reference throughout the rest of the design process.

3.2. Los Angeles

LA is widely seen as the city with the worst congestion problem in the United States. Knowing the effects of the congestion is of great importance in understanding how to solve this problem. Furthermore, understanding why commuters keep on using cars instead of existing public transport systems can provide an insight in how the UAM system should be designed, so that it answers the wishes and needs of possible users.

3.2.1. Effects of Congestion

Traffic in LA is of vast majority composed of petrol engine cars, of which emissions include gasses such nitrogen oxides and carbon monoxide which pose extremely hazardous risks on the personal health of the urban population. They are known to have adverse consequences on global warming[2]. In urban car con-

---

[1] https://www.airbus.com/newsroom/news/en/2019/02/urban-air-mobility-on-the-path-to-public-acceptance.html [accessed 30.04.19]

gestion, the car is often busy with either accelerating, decelerating or with the engine left idling, which is when the car is least efficient and most polluting.

The Environmental Protection Agency (EPA) has set the so called National Ambient Air Quality Standards (NAAQS) to provide public health protection. According to these standards the maximum concentration of PM2.5 annual mean, averaged over 3 years, is 12 $\mu g/m^3$ [1]. It is however measured that concentrations of of PM2.5 go far above 20 $\mu g/m^3$, especially in proximity to the ring road highways around central LA [3]. These concentrations are extremely bad for the health of the community living close to these highways.

3.2.2. Ways to Decrease Congestion

In LA, there have been multiple studies and proposals about decreasing the congestion problems. The most recent method that is now taken into serious consideration, is a 4 USD tax for cars travelling in so called 'Mobility Go Zones' [4]. These zones would be implemented in the most congested parts of LA to reduce the amount of cars and stimulating the use of public transport. In a feasibility study it is found that in 2035 this measure would decrease the amount of cars used during peak hours by 19%, while increasing the use of other transit systems by 9%. This decrease of car usage would decrease the vehicle hours travelled by almost 24%. This gives an indication of the amount of passengers the UAM system should have to transport to significantly reduce the congestion and time that people spend in traffic jams.

Furthermore, lots of research is done about public transport systems. In 2015, a study [5] investigated the effect of implementing a light rail connection in downtown LA on road congestion. The results indicate that reduction in road congestion would be small and local, although the overall transit use would increase. A small percentage of total car users would shift to the public transport system. Additionally, possible new local congestion could occur at park-and-ride-facilities of the station. This should be taken into account during the development of the UAM system, as vertiports will likely attract extra traffic in their near surroundings. In addition to this, to really make a serious impact on the total road congestion of LA, the system shall cover a large area.

3.2.3. User Needs

Based on an extended analysis, the primary transport related problem in LA is congestion. Congestion in LA is caused by the combination of 84% of the daily commuters using a car and driving alone, and the fact that almost 46% of the population lives in urban areas surrounding LA. This shows that the frequent users will be the people who mainly use a form of private motorised transport to commute to work every day. This leads to the question of why the percentage of daily commuters using private transport is as high as it is.

The known problems with the LA Metro system influence users to rely on private transport rather than public. One of the problems is the low amount of rail stations due to the very spread-out layout of Greater LA. The amount of rail stations in LA is a little over 110 [2], whereas the area of Greater LA is 88,000 km^3 [3]. This indicates that the reach-ability of the rail stations is bad, resulting in the need for a prior form of transport for last-mile travel. Furthermore, the general image of the LA Metro system is bad due to the limited carrying capacity, which was clearly seen after the extension of the expo line (Santa Monica) and overcrowding of the trains. This caused the smell to become unpleasant and the trains becoming dirty; the general image became "cheap". This consequently resulted in 30% of the users feeling unsafe and staying away even after considering the fact that the LA Metro system is very safe compared to the neighbourhoods surrounding the various stations. Another reason why the LA Metro ridership is so relatively low compared to the expected ridership is due to the sense of control aspect experienced by the commuters. The fact that owning and driving a car provides users with a sense of "complete control" is acknowledged, as the user has the freedom

---

[1] https://www.epa.gov/criteria-air-pollutants/naaqs-table [accessed 10.05.19]
[2] https://media.metro.net/documents/8f0fe43e-da3b-4a10-bd8e-4cfd54e30eb3.pdf [accessed 17.05.19]
[3] https://simple.wikipedia.org/wiki/Greater_Los_Angeles_Area [accessed 17.05.19]

to choose when and where to go without the need of checking any schedules[4].

Moreover, the bus system is analysed. It is found that there are more than 20,000 bus stations in Greater LA. This corresponds to a better reach-ability than the metro system. However, around 23% of the busses in 2016 were late. This reliability problem paired with the low frequency of busses makes a 10 minute ride by car turn into a trip which can easily take 50 minutes by bus (due to waiting time, the lower average speed at which a bus generally drives compared to a car, and the amount of stops the bus makes along the way).

After the analysis of the main aspects which resulted in a low ridership rate of the LA Metro and bus systems, the main aspects of user needs are considered by the design team:

1. Sense of safety
2. Sense of Luxury : clean environment, aesthetics, level of technology, comfort
3. Reliability and availability : waiting time, carrying capacity, amount of vehicles
4. Reachability
   - Hub-to-hub system : Commute distance to a hub
   - On demand system : Accuracy take-off and land locations
5. Commute time : Always lower than any other form of transport
6. Sense of control
7. Cost : ticket fare or cost per kilometre
8. Integration within the city : with other modes of transport (public transport)

3.2.4. Quantitative Market Analysis

The worker population of LA metropolitan area is considered to be the target group of this mobility system. They would be the likely users of the system. This metropolitan area consists of LA city and other areas. Data from the "Census Transportation Planning Products" (CTPP) is used to identify travel patterns of the worker population. This data-set has information about the number of workers, their residence locations, their workplace location and the start time of the their commute[5].

The residence locations of the workers are given in terms of "Public Use Microdata Areas" (PUMAs). A PUMA is geographical area that consists of about 100,000 to 200,000 residents. The use of a PUMA gives a relatively accurate indication of the starting point of a commute. It is found that a PUMA could not be used to classify workplace locations; the CTPP data did not have sufficient data concerning the workplace locations within a PUMA. Therefore, the workplace location of the workers are given in terms of "Principal Cities of the Metropolitan Statistical Area of LA". The Principal City is the most important city of the Metropolitan Area with a high percentage of working people in comparison to the residents. The locations of these principal cities are found on a map and this was translated to a location within a PUMA. An inconvenience is that, in the data-set, LA city as a whole is considered as a principal city. It would have been better if it is sub-divided into regions within the city. However, it is found that LA city has four main workplace areas; Downtown, Westwood, Koreatown and Hollywood. The number of working people in LA city is divided into these four areas. The ratio used to divide the people is found using another source[6].

The start time of the commute is between 5:00 am and 9:00 am in steps of one hour (e.g. 5:00, 6:00 ...). No accurate CTPP data for the evening rush hour is unfortunately available. Therefore, only the morning is observed and it is assumed that this also represents the evening rush hour. The original data-set is processed using Python, where a list of 10,000 routes is compiled for each time frame. Each route has information about the source, destination and the number of workers on that route for that time frame. A Google MAPS API (Application Programming Interface) is then used to further find characteristics of the route. These characteristics include the distance, time taken in traffic and time taken without traffic. These

---

[4] `https://www.citymetric.com/transport/los-angeles-metro-great-so-why-aren-t-people-using-it-2742` [accessed 17.05.19]

[5] `https://ctpp.transportation.org/2012-2016-5-year-ctpp/` [accessed 08.05.19]

[6] `http://ccdphila.maps.arcgis.com/apps/OnePane/basicviewer/index.html` [accessed 08.05.19]

metrics enable the team to identify which routes are the most congested. The visualisation of the PUMAs and the routes helps the team identify infrastructure patterns of the various systems. A MAP tool is used which outputs a map for each time-frame. The top N routes based on the gain metric is drawn on this map. The method to find the gain metric is elaborated in subsection 10.4.1.

3.3. Stakeholders

As shown in figure 3.1, six groups of stakeholders are identified, where each group has likely subsidiaries or distinguishable groups. As the product life-cycle continues, more and more stakeholders may be discovered and may possess individual and differing company philosophies and requirements.
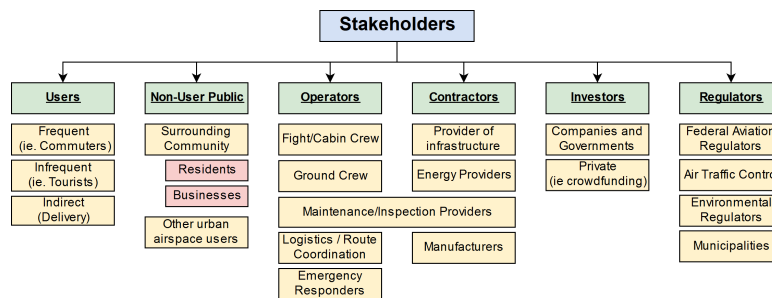

Figure 3.1: Overview of all stakeholders in the project

3.4. Legislation

There is a huge market for Unmanned Aircraft Systems (UAS), often referred to as drones. The market ranges from industrial inspection or aerial photography, but also to transport people. Officially, drones can only be used below navigable airspace. The Federal Aviation Administration (FAA) owns the airspace and has the exclusive authority to regulate all aircraft vehicles, manned or unmanned, within navigable airspace. The FAA defines navigable airspace as the airspace that is required for safe takeoff and landing of airplanes, combined with the airspace above the minimum flight altitudes[7]. New rules are required to regulate the use of UAS in low-altitude airspace. Two years ago, a new program is started: The UAS Integration Pilot Program (IPP). By bringing together the different governments with private parties, national and local interests are being identified, while at the same time taking into account security and privacy issues that might arise. The goal of the program is to increase the speed at which new rules are created and authorised[8].

In addition to the IPP, the FAA started in 2007 on modernising the overall aviation system. This project, which is referred to as 'NextGen', should lead to an aviation system which is safer, more efficient, has a higher capacity and predictability. The target of NextGen is to have all major components implemented by 2050[9]. The major changes will be in navigation and communication. By switching towards satellite-enabled navigation, optimum routes can be determined more easily, as it is much more accurate than ground-based navigation. Moreover, the new data communication system will allow for quicker and easier communication in air traffic. In addition, it will reduce the risk of miscommunication that occurs due to radio messages over busy frequencies[10]. It is clear from all the ongoing projects and their desired results, that by 2050 major changes will have occurred in the overall legislation. The system will adapt its ATM method such that it will comply with these new regulations. It is expected that local airports and the location of hospitals with emergency helipads will have the largest influence on the allowable flight routes of the system. Furthermore, it is assumed that satellite-based navigation, will make it possible to travel safely through low-altitude airspace.

---

[7] https://www.faa.gov/airports/engineering/airspace_analysis/ [accessed 08.05.19]

[8] https://www.faa.gov/uas/programs_partnerships/integration_pilot_program/ [accessed 08.05.19]

[9] https://www.faa.gov/nextgen/what_is_nextgen/ [accessed 08.05.19]

[10] https://www.faa.gov/nextgen/how_nextgen_works/ [accessed 08.05.19]

They do so, by providing very accurate data of current locations and estimated flight routes of all other vehicles that are in operation in the near surroundings.

3.5. Non-airborne Solutions

A UAM system is not the only mode of transport which can help reduce congestion issues. Other modes of transport that can aid in accomplishing this mission should be investigated. These could act both as competition and complement to the system. The modes of transportation considered are cars, busses and trains.

3.5.1. Electric Cars

It is expected that cars will remain a main mode of transportation in 2050. These cars will likely be electric. This assumption is based on the the current development in the market of electric vehicles and the growing number of manufacturers introducing electric cars[11]. The use of electric cars will decrease air pollution and help tackle climate change, provided that the energy comes from a renewable source. To accommodate the city's traffic, a 3D network of roads will have to be created to make a solution with only cars viable[12]. This could be done by having multiple levels of roads above the ground or having a network of tunnels below the city. There will have to be investments for the construction of such 3D road networks. Furthermore, the group envisions that in 2050 cars are controlled autonomously. This is expected to enhance safety, as technology is rapidly moving towards a point where computers will make less mistakes than humans.

3.5.2. Rail and Bus Networks

Another option to alleviate congestion in LA is the use of rail networks. Again, it is assumed that all the energy used to power this system is of renewable origin. Currently, LA does not have a widespread rail network. Just as in the case of road networks, there will have to be large infrastructure development and construction costs to realise such a system. Bus networks can potentially allow for energy efficient transportation by having a large amount of people being carried in a single vehicle. It is questionable how much this would improve traffic situations, as numerous vehicles are nevertheless needed to effectively accommodate large demands.

3.5.3. Energy Efficiency of Other Transport Modes

The PREE (Payload·Range per Unit Energy) is a metric that finds the efficiency at which a vehicle can move payload. It is dimensionless parameter and a high value indicates a better efficiency at moving payload over a distance. Including these numbers at this stage allows for a comparison of the relative energy efficiency of a UAM system to other modes of transport. For cars in the US a PREE was found of 0.76, which is based on an average occupancy of 1.5 pax per vehicle. For busses it lies at 3.32 with an occupancy of 9.1 pax per vehicle at any one time. For rail networks the PREE is 27.9 with an average occupancy of 31.7 pax. The transportation PREE was computed from the data of Oak Ridge National Laboratory[13].

---

[11] https://www.eesi.org/articles/view/transportation-2050-more-evs-but-conventional-vehicles\ -will-still-dominate [accessed 17.05.19]

[12] https://www.ericsson.com/en/blog/2018/6/we-need-three-dimensional-traffic-congestion-solutions [accessed 17.05.19]

[13] https://tedb.ornl.gov/data/, [accessed 01.07.19]

4

Sustainable Development Strategy

To make sure sustainability is considered throughout the complete design process, a description of the approach to sustainable design is provided in every report. For each major step taken in the process leading up to the Midterm Report, an explanation of sustainability is taken into account. A division is made between the three forms of sustainability, namely environmental, social and economic sustainability. In Section 4.1 these definitions are explained, followed by the phases of the project where sustainability is most taken into account. A short recap on the trade-off in the Midterm Report is made in Section 4.2, followed by the sustainability strategies for the design of the vehicle, operations and infrastructure (Section 4.3, Section 4.4 and Section 4.5 respectively). Some recommendations for the next development phase of the UAM system is discussed in Section 4.6.

4.1. Definition

Environmental sustainability is the best known form of sustainability. It describes all aspects of the system which have an impact on the environment, like pollution, usage of scarce materials and energy use during manufacturing and operations. To enable the development of the system, it has to be economically feasible, but better yet economically sustainable. Various considerations are to be taken into account in order to minimise the development, manufacturing and operation costs, but also the ticket prices have to be affordable. Social sustainability describes whether a product or system adds something to the quality of life. This could be interpreted in several ways; a product or system could provide a way to improve the health of the society, or it could improve access to other places by providing a transport service. Although the three different forms of sustainability are described separately, often the definitions overlap and interact with each other.

4.2. Sustainability Trade-off Criteria

During the concept generation and the trade-off performed in the Midterm Phase of the DSE, sustainability was an important factor that was taken into account. By implementing the different forms in sustainability in the criteria used to score the concepts, the trade-off provided a sustainable concept that is designed in more detail in the Final Phase of the DSE. Some criteria with the highest weights are described below. A brief recap on the trade-off is discussed in Chapter 5.

The criterion with the highest score is the **PREE**, that finds the efficiency at which the vehicles can move passengers. By increasing this value, less energy is necessary to move each passenger and the system is more environmentally friendly. Also the ticket price can be decreased if less energy is necessary during operations, which increases the economical sustainability. When developing a flying transport network within a city, **Safety** is a major factor to get accepted by the residents of the city and municipalities. Low safety standards or large consequences in case of an accident will decrease the willingness of people to use the system. As a result the congestion and pollution will not be solved and the social sustainability will not improve. Another criteria that influences the social part of sustainability is **Ticket price**. Overpriced tickets will decrease the amount of people who can afford the system, making the system only available for the

higher class. Furthermore, enough people have to make use of the system to make it economically feasible for the operator. Finally, the **Battery mass** is a factor that should be minimised in the system, due to the scarce materials used in batteries and the hazardous disposal after its lifetime. To be as environmentally sustainable as possible, a low battery mass is ideal.

4.3. Vehicle

With the concept selected (further elaborated in Chapter 5), a detailed design is created in this report. In this design, the vehicle is optimised for different design factors, which are closely related to different forms of sustainability.

Energy   As also explained in the section of the trade-off (Section 4.2), the energy use of the system is very important. To optimise the vehicle for energy use, not only the cruise phase is looked at, but also the hover and transition period. This has a large influence on the design of the rotors, fuselage and wings. The behaviour of these components is investigated for vertical take-off and landing (VTOL) and cruise. In this design, also a trade-off between efficiency and noise of the rotor is made. High blade number and high solidity rotors generally are more efficient, but generate more noise than rotors with fewer blades and a lower solidity. The chosen rotor is a compromise between the two, to keep the efficiency relatively high but the noise down to a socially acceptable level (72 dBA at 250 ft). The most efficient cruise position of the fuselage is (6° α_b), however no optimisation of the aerodynamics on the body is performed. Also the tilting wing has to be studied in more detail, mostly considering the transition phase. To keep the vehicle environmentally sustainable, the energy over the complete trip is minimised.

Noise   Next to the energy constraints on the vehicle, noise is a crucial factor in the design, relating to social sustainability. As one of the largest concerns of the public is the amount of noise the system will create during operations, a low noise is essential for the social acceptance. For this, the noise levels during multiple phases of the flight are studied and minimised. As already explained this is taken into account during the rotor design, which produces the most noise of the vehicle. This noise is computed for different phases of flight and at different altitudes. If the noise observed from the ground is still too high, changes in flight paths are considered (Section 4.4). Furthermore, not much is known about the effect of a fleet of vehicles simultaneously flying through a city. This will be investigated in later stages of the design.

Passenger Experience   Social sustainability is not only applied on non-users, but is also considered for the passengers of the system. One of the goals of the UAM system is to improve quality and speed of transport, so the vehicle has to be as comfortable as cars in terms of cabin noise and legroom. People have to feel safe inside the vehicle and should not get nauseous during the flight. If the travelling experience lives up to the price people pay, they will be more willing to use the service again. The seat pitch in the Bumblebee is 1 meter, which gives around 20 cm more leg room than average economy class seats[1]. Phone caddies are installed for safe and comfortable in-flight phone use and screens will clearly communicate the destination and other information to the passengers. Finally, due to the fixed angle of attack of the body, the passengers are comfortably reclined 6 degrees backwards.

Materials and Manufacturing   The production of the vehicles is one of the main factors where sustainability is taken into account. The majority of the structure of the vehicle consists of aluminium, which is easily recyclable and relatively cheap to buy and process, to gain both environmental and economical sustainability. However, for the skin, carbon fibre is used due to its low mass. Although carbon fibre itself is less sustainable, the lower weight results in less battery mass necessary, which is minimised to remain environmentally sustainable as well. This trade-off between sustainable materials and battery mass is performed with care to end up with the most sustainable solution as possible. During manufacturing, the necessary energy to produce parts is minimised and the amount of waste is reduced as much as possible. More specifics on the production are explained in Chapter 15, but more details will be found later in the design process.

---

[1]`https://www.airlinequality.com/info/seat-pitch-guide/`[accessed 01.07.19]

4.4. Operations

The design of the operations has a large influence on energy usage, social acceptance and the operational costs. This is shortly described below and related to their corresponding form of sustainability.

Flight Profile and Flight Path   The flight profile describes the vertical path that the vehicle takes during a route. The optimal flight path considering energy usage is as low as possible, to lose the least energy during the climb phase. However, for the social acceptance of the non-users, the vehicle has to fly as high as possible. A compromise between this is set by a mandatory vertical step up manoeuvre of 200 m before starting transition into forward flight. This reduces the noise disturbance to neighbouring areas and keeps the flight relatively energy efficient.

Route Network and Scheduling   When the system is implemented in a city, the network and locations of vertiports and landing pads are very important for the success of the system. In order to increase the quality of travel and the social sustainability, commuters have to be able to board close to home and land near their final destination. If people first have to travel a long way or the connection to the various public transport modes is bad, they will probably switch back to travelling by car and accept the congestion. The scheduling is important for the energy use; it should be optimised for as few empty flights as possible.

4.5. Infrastructure

Finally, during the design of the vertiports and landing pads, sustainability is also taken into account, not only for the design, but also the placement within the city and the operations taking place on the vertiport.

Vertiport Design and Location   In the design of the vertiport, the focus is laid on using sustainable materials, implementing good insulation and minimising energy costs. When rooftops of existing buildings are used, some rooms could be redesigned and turned into waiting rooms to lower the construction costs. Furthermore, rooftops are partially covered with solar panels, to make the vertiport itself a CO_2 neutral building. The location of a vertiport has a large influence on its surroundings and the social sustainability of the residents. The people living close to the landing pads will probably hear the vehicles landing and taking off and congestion around the vertiport may arise. As a lot of people will travel to the vertiport, parking facilities should be created and connections to public transport modes should be extended. By doing this, the social acceptance of the citizens will be higher, thus giving the system a higher chance of success. Finally, as vertiports are implemented on top of existing buildings (where possible), the costs are reduced compared to the construction of a completely new building.

4.6. Future Design Plan

After this first preliminary design, the vehicle and system can be further developed. A more detailed sizing of the vehicle can be performed and the production can be analysed in more detail. Sustainable and recyclable materials should be used to improve the environmental sustainability and for the economic sustainability, these materials should also be affordable to minimise the costs. Additionally, mass production could drive the production costs of the vehicle down, so the scalability and expansion of the system to different cities should also be investigated. The routes and schedule should be optimised in order to minimise the energy usage. For this, a more thorough analysis into the moving patterns and demand should be performed. If this schedule is optimised, this will add to the environmental sustainability in terms of energy usage and social sustainability in terms of reducing commute times.

Concept Trade-off

Multiple design choices have to be made during a design process and in order to do so, often trade-offs are performed. The main trade-off during the Midterm Phase of the DSE was to determine the optimal vehicle capacity and with it, the concept that would be further developed. This is described in Section 5.1, followed by the trade-offs performed in the detailed design during the final phase (Section 5.2).

5.1. Concept Trade-off Process

From a design option tree, the team designed multiple preliminary concepts for different passenger ranges. In order to come up with a single concept to be designed in further detail, two trade-offs are performed. The intermediate trade-off narrows down all the concepts to one concept for each passenger capacity. The result of the final trade-off is the 'winner' and is designed in further detail in the final phase.

5.1.1. Selection Criteria

To perform these trade-offs, a list of criteria is created and can be found in Table 5.1. Four main criteria are divided into sub-criteria. For the intermediate trade-off, only the quantitative criteria are used and during the final trade-off, the qualitative criteria are also taken into account.

The weights of the criteria and sub-criteria are determined through a pairwise comparison between the criteria, following the Analytical Hierarchy Method [6]. This comparison is performed by all team members, the tutor and coaches to get a well substantiated weighting. The most important criteria are the PREE, safety and the ticket price. All weights can be found in Table 5.1 and a more extensive description of the criteria can be found in the Midterm Report [7].

5.1.2. Method Description

To compare the different designs in a quantitative way, a program (later referred to as tool) is written and takes vehicle parameters as input and outputs the values for the quantitative criteria. Figure 5.1 shows a simplified version of the flowchart of the tool. The tool can be divided into four parts: People, Vehicle, Infrastructure and Cost.

People: In the people section, the transport flows of commuters are combined with some parameters of the vehicle, like cruise velocity and range, to find the optimal routes for the vehicle.

Vehicle: The characteristics of the vehicle such as amount of passengers, and the number and size of the propellers are used to determine a MTOW and a battery size. From this, the noise and downwash are determined as well, which are criteria.

Infrastructure: This part of the program is used to find the total fleetsize and details on the vertiports. Criteria like PREE and total battery mass can be found subsequently.

Cost: The final section is used to find the ticket price. This is done by setting a break even point and finding all the costs for developing such a system.

This tool is further modified in the final phase of the project and is described in more detail in Section 5.2.
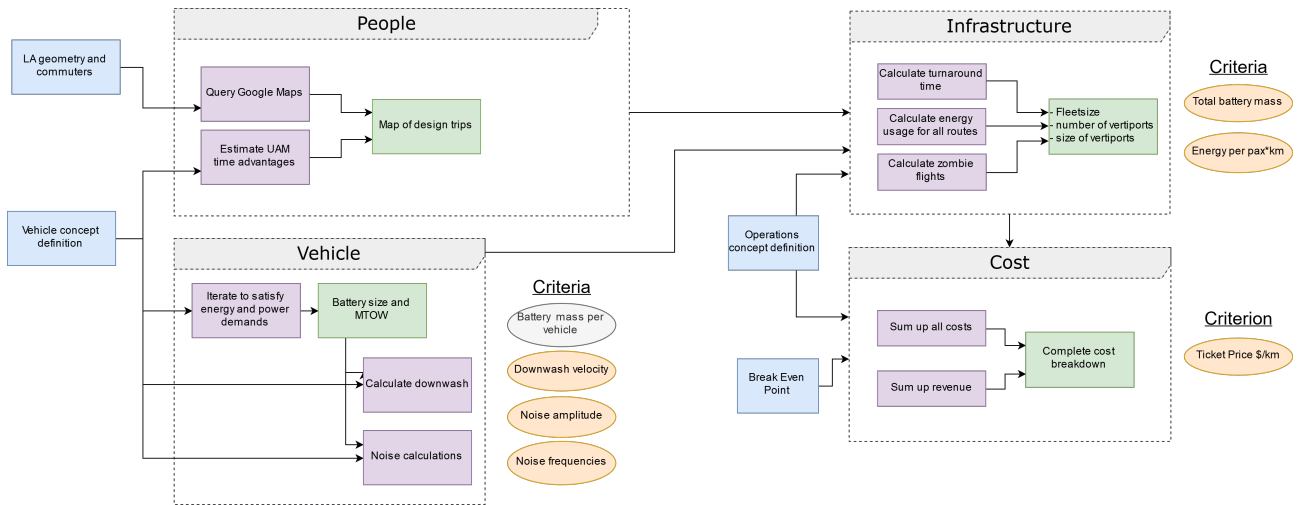
Figure 5.1: Simplified flowchart of the method

5.1.3. Concepts

For each of the three passenger capacities (1-2, 4-6 and 20+), three conceptual designs were made and scaled using the tool. The intermediate trade-off with only the quantitative criteria resulted in the three concepts shown in Figure 5.2.

(a) 2 passenger concept

(b) 4 passenger concept

(c) 20 passenger concept
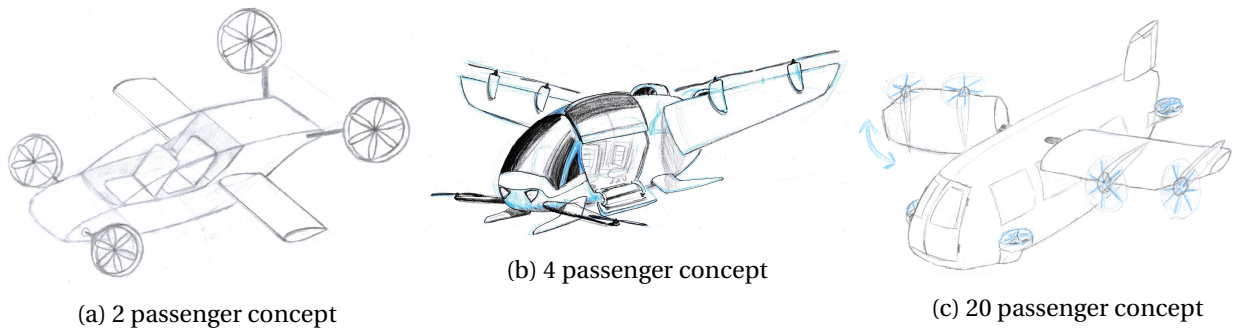
Figure 5.2: Winning concepts of each passenger capacity

After determining the scores for the qualitative criteria through individual scoring by all team members, the tutor and the coaches, the final trade-off could be performed. The trade-off summary table is shown in Table 5.1 and the trade-off clearly results in the 4 passenger vehicle being the winner. In the following few chapters, this concept is worked out in more detail, together with the accompanying infrastructure and operations. The updated tool for this phase and the approach for optimisation are described in Section 5.2.

Table 5.1: Trade-off summary table

Criteria	Sub-Criteria	Total Weights	2 pax	4 pax	20 pax
Ecologic Sustainability	PREE	0.28	5	5	3
	Battery mass	0.078	4	5	3
	Safety	0.19	2.9	3.3	2.5
Social Acceptance	Passenger experience	0.056	4.1	3.7	2.7
	Noise	0.055	5	5	2
	Downwash	0.017	5	5	4
Cost/Profit	Development cost	0.036	4	3	1.8
	Ticket price	0.15	2	5	2
	ATM/UTM efforts	0.081	1.4	2.7	2.9
Technical Risk	Weather conditions	0.043	2.1	2.7	3.7
	Modification of regulations	0.018	3.7	3	1.5
Sum of Weighted Scores			**3.6**	**4.2**	**2.7**

5.2. Trade-off Method for Detailed Design

The trade-off method in the detailed design phase is governed by the same criteria as in the Midterm phase, except that for the detailed design, the trade-offs are mostly done on a subsystem level and do not require a scoring by all team members but only by the engineers involved in the respective departments. When possible, a trade-off is done quantitatively, which requires some form of an analysis tool, similar to the one developed in the Midterm phase but with an emphasis on detailed vehicle sizing (on a subsystem level). What in the Midterm was the batConverge function which converges the battery mass for a fixed value of the OEW/MTOW fraction, is now a much bigger MTOWconverge function which sizes each of the vehicle components as a function of the MTOW until it converges. The layout of the tool is presented on page 15.

The input of the tool consists of variable and fixed parameters, which are grouped in *Atmospheric, Vehicle* or *Operational* parameters. The variable parameters are indicated by magenta diamond shapes in the flowchart and are those that change with the MTOW. This includes parameters like battery mass, thrust required, rotor geometry, fleet size (which is influenced by trip energy due to changing charging time and therefore turnaround time), etc. Fixed parameters are the selected trips to serve (which depends on a specified cruise velocity, target time gain, minimum trip range and maximum vehicle range), the market share, the flux of passengers in and out of PUMAs, etc..

With an initial instance of the Vehicle and Operations objects, the top N trips where the system provides the largest time gain is found using data about commuting patterns in LA from the `People` subtool. This trip selection procedure takes into account a more sophisticated way of assigning trip flight profiles (and thus air times) based on range, done in `flightphases.m`. Concurrently, the initial Vehicle object is passed to the `MTOWconverge.m` function which performs an iteration in which the vehicle subsystems are sized and automatically optimised as a function of the MTOW and the average trip profile. Once the vehicle converges, downwash and noise are computed, which define its main footprints.

With the converged vehicle, it is also possible to compute the turnaround time at the vertiport (based on charging time) and find the fleet size required to serve the demand, based on a simple operational model of the vehicles. The fleet size allows to calculate the total battery mass of the system. Using the number of take-offs and landings per hour at each hub, the number of landing pads required is calculated. The ratio between taxi time and charging time drives the ratio of landing pads and gates, which is used to determine the number of gates needed at the hub and a total ground footprint. Finally, the number of vehicles, the vehicle specifications, and the operational and infrastructure requirements of the system are used in a cost tool, which together with a specified break even point calculates the ticket price/pax/km.

Integrated Tool Flow Chart and Functional Descriptions

MTOWconverge.m

While not converged

auxSizing.m	Add outside shell, interior, seats and avionics
rotorSizing.m	Optimize blade characteristics for noise and energy
	Size rotors for required thrust and dimensions
powertrainSizing.m	Select motors/ controllers and size gearbox
	Compute cable losses and masses
batSizing.m	
	Optimize battery pack architectures and select optimal cell
structureSizing.m	Truss finite element analysis and weight optimization
	Size wingbox and tilt mechanism

MTOW_(t+1) = MTOW_t + 1.4*(Sum_of_components- MTOW_t)

BEMT.m

NewRPM = OldRPM -k*(BEMT_Thrust-Thrust_req)

k = 0.001

Tripenergy.m

For every flightphase

Powered lift? yes/no

solveHover.m solveCruise.m

Iterate mainly thust Iterate mainly incidence angles

BEMT.m LiftingLine.m / BEMT.m

Converged?

Integrate power over flightphases

Trip Energy

Noise.m

Calculate Tonal Noise
Calculate Thickness Noise
Calculate Loading Noise
Apply A-weighting
Apply atmospheric attenuation

Calculate Broadband Noise
Apply A-weighting
Apply atmospheric attenuation

Sum SPL across frequencies & propulsion units

Total Noise signature in dB, dBA

Legend:

Fixed parameters	(green)	Logical block	(pink)
MTOW dependent parameters	(brown)	Functional block	(grey)
MATLAB function	(blue)	User input	(yellow)
MATLAB script	(purple)	Tool output	(orange)

15

<div style="text-align: right; font-size: 3em;">6</div>

Mobility System Requirements

This section shows all requirements set for the transport system, operations and vehicle. Section 6.1 shows the system requirements of the complete transport system and the top-level requirements of the Operations and Infrastructure. The system and subsystem requirements for the vehicle are shown in Section 6.2.

6.1. Infrastructure and Operation Requirements

The system requirements of the complete transport system are stated in Table 6.1. In Section 6.1, the top-level requirements for the vertiports, infrastructure and operations are described.

Table 6.1: Transport system requirements

Code	Requirement
SYS-01	The average ticket price shall not exceed 2.90 USD/(passenger· km)
SYS-02	The system shall provide a gain in total travel time with respect to other viable modes of transport
SYS-03	The peak power demand of the system shall not exceed 800 MW
SYS-04	The break-even time for the system shall be within 15 years
SYS-05	The system shall provide a passenger energy efficiency of maximum 5,200 J/(m· passenger)
SYS-06	The system shall provide an ATM system that allows for safe operation in high density urban areas

Table 6.2: Top level system requirements of operations & infrastructure

Code	Requirement
TL-VERTP-01	The landing pad shall cost maximum 4 million USD to construct
TL-VERTP-02	The landing pad shall provide a surface area of at least 330 m^2 per vehicle
TL-VERTP-03	The number of landing pads at vertiport shall allow for the vehicle throughput demand at site to be satisfied
TL-VERTP-04	The landing pad configuration shall allow for safe landing and take off operation of multiple vehicles at vertiport
TL-VERTP-05	The size of the landing site shall scale with the maximum passenger throughput of that site
TL-VERTP-06	Parking infrastructure shall be provided in proximity of all vertiports located in peripheral pumas
TL-VERTP-07	The vertiport shall provide waiting area for all waiting passengers
TL-VERTP-08	There shall be a safety landing spot available at every vertiport at all times
TL-VERTP-09	Every vertiport shall provide charging facility
TL-VERTP-10	The total vertiport charging facilities shall be able to provide a peak power supply of 800 MW
TL-VERTP-11	The total deboarding and boarding procedures shall be completed within 5 minutes
TL-VERTP-12	The taxi speed shall be 15 km/h
TL-VERTP-13	Boarding facility shall provide safe and comfortable passenger boarding
TL-INFR-01	The maximum route distance shall not exceed 55 km
TL-INFR-02	The target size of the system shall incorporate minimum 105 vertiport locations throughout LA
TL-INFR-03	The safety and (de)boarding procedures shall be clearly communicated to the users

Code	Requirement
TL-INFR-04	The system shall possess means of informing passengers about schedules and/or on-demand procedures
TL-INFR-05	The system shall be manufactured with at least 25 % of recycled materials
TL-INFR-06	The vertiports shall be positioned such that the average last minute travel is less than 10 minutes
TL-OPER-01	The operations shall produce no more than 0 kg of greenhouse gasses per km travelled
TL-OPER-02	The operations shall produce no more than 0 kg of Nitrogen Oxides gasses per km travelled
TL-OPER-03	The system shall not accommodate single use plastic during the operation
TL-OPER-04	The system shall not accommodate the use of paper during the operation
TL-OPER-05	The maximum waiting time at any vertiport shall be less than 10 minutes
TL-OPER-07	The system shall have an operating time from 5 AM to 10 PM
TL-OPER-08	The ATM system shall enable real time changes to the scheduling due to delays
TL-OPER-09	The passengers and cargo shall be (un)loaded in a safe manner
TL-OPER-10	There shall be sufficient battery reserve at all times to allow for 9 km reserve range at emergency cruise altitude
TL-OPER-11	The vehicles shall have up to date knowledge of position, velocity, trajectory and identity of all surrounding vehicles during operation
TL-OPER-12	The system shall have direct communication with the ANSP at all times for remote piloting in case of unpredictable traffic situations
TL-OPER-13	Buildings and urban infrastructure must have a clearance of at least 100 meters from vehicle flight trajectory
TL-OPER-14	An emergency cruise flight layer shall be specially designated for vehicles in turnaround or emergency flight.
TL-OPER-15	Cruise altitude shall not exceed altitude of 1,370 m ASL
TL-OPER-16	The vertical separation between aircraft must be at least 30 meters
TL-OPER-17	The horizontal separation between aircraft shall be at least 500 meters
TL-OPER-19	The approach fix of vertiport shall be placed at a maximum horizontal distance of 135 meters from the landing pad and at an altitude of 200 meters

6.2. Vehicle Requirements

The top-level requirements for the vehicle are shown in Table 6.3. Also, requirements from the proposed special condition for VTOL aircraft are added [8], followed by the requirements for manufacturing. The requirements for the subsystems can be found in tables on the following pages. Table 6.4 contains requirements for the Propulsion and Power subsystems, Table 6.5 contains the Structures and Stability & Control subsystem and in Table 6.6 the requirements for Aerodynamics, the Electrical subsystem and the interior and auxiliary systems are stated. For each subsystem, the associated regulations for VTOL aircraft are added. A few of these regulations apply for more than one subsystem but for the sake of completeness they are added to all of them.

Table 6.3: Top level system requirements of vehicle and manufacturing requirements

Code	Requirement
TL-VEHI-01	The vehicle shall be able to transport at least 4 passengers in one trip
TL-VEHI-02	The vehicle shall not transport non passenger cargo
TL-VEHI-03	The vehicle shall be able to carry a payload of at least 400 kg in one trip
TL-VEHI-04	The vehicle shall comply to the proposed VTOL regulations
TL-VEHI-05	The vehicle shall be able to perform vertical take-off and landing
TL-VEHI-06	The vehicle shall be able to transport payload over a distance of at least 60 km without recharging or refuelling
TL-VEHI-07	The vehicle shall be able to transport payload at a minimum cruise velocity of 60 m/s
TL-VEHI-08	The vehicle shall be able to perform an emergency landing at any time during operations
TL-VEHI-09	The vehicle shall be stable and controllable across the complete flight envelope
TL-VEHI-10	The vehicle shall be able to navigate to a set destination

Code	Requirement
TL-VEHI-11	The vehicle shall avoid collisions with any objects in its environment
TL-VEHI-12	The vehicle shall operate normally in a temperature range of -10°C to 50°C
TL-VEHI-13	All flight critical systems on board the vehicle shall be protected against all cyber attacks
TL-VEHI-14	All physical component of the pax cabin must be strong enough to resist accidental damage by pax
TL-VEHI-15	All critical mechanical components reachable by passengers or outsiders need to be able to resist vandalism
TL-VEHI-16	All critical components ensuring safe operation of ground based structure need to be able to resist vandalism
TL-VEHI-17	Chance of passenger survival must be larger than 95% following an impact at 24 m/s vertical acceleration
TL-VEHI-18	Each item of mass that can injure an occupant shall not detach in the event of a crash with 20 g vertical acceleration
TL-VEHI-19	The vehicle shall have sufficient manoeuvrability in one-engine-out operation
TL-VEHI-20	The vehicle shall have a residual range of half the nominal range to perform an emergency landing in one-engine-out operation
TL-VEHI-21	The vehicle shall have capability to warn pedestrians in case of an emergency landing that cannot be carried out on a landing pad
TL-VEHI-22	The vehicle shall have capability avoid obstacles in case of an emergency landing that cannot be carried out on a landing pad
TL-VEHI-23	The vehicle shall have structure strong enough to resit impacts of birds at maximum operating speed without danger to passengers or pilots
TL-VEHI-24	The vehicle shall have structure strong enough to resit impacts of hailstones at maximum operating speed without danger to pax or pilots
TL-VEHI-25	The vehicle shall have control and manoeuvrability capability to avoid impacts with obstacles
TL-VEHI-28	The vehicle shall emit a noise level of less than 67 dBA at ground level at 250 ft (76 m) altitude
TL-VEHI-29	The system shall not operate between 10pm and 5am
TL-VEHI-30	The noise of the vehicle as perceived by any non-user bystanders during take off / landing on a landing pad shall be limited to 80 dBA
TL-VEHI-31	The noise of the vehicle as perceived by any non-user bystanders during cruise shall be limited to below 70 dBA
TL-VEHI-32	The noise of the vehicle as perceived by ground personnel and other persons on or close to a landing pad shall be limited to 84 dB
TL-VEHI-33	The noise of the vehicle as perceived by the occupants during take off / landing on a landing pad shall be lower than 80 dB
TL-VEHI-34	The noise of the vehicle as perceived by the occupants during cruise shall be lower than 80 dBA
TL-VEHI-36	The interior layout of the vehicle shall not compromise the comfort of the passengers during operation
TL-VEHI-37	The interior temperature shall be regulated between 15 to 25 degrees Celsius
TL-CERT-01	VTOL.2005b(1): Must be able to land at an operating site after critical malfunction of thrust/lift if flight over congested area is required
TL-CERT-02	VTOL.2105a(2)(ii): Must meet all performance requirements in chosen operations envelope concerning ambient atmospheric conditions and temperatures
TL-CERT-03	VTOL.2105(d): Performance data must account for cooling needs, downwash considerations and other demands on power sources
TL-CERT-04	VTOL.2110: Flight envelopes (normal, operational and limit) must be determined for most adverse conditions in each flight condition
TL-CERT-05	VTOL.2115(c): TO performance must be determined taking into account critical malfunction of thrust/lift
TL-CERT-06	VTOL.2120(b)(2): Minimum climb performance out of ground effects must be compliant with critical malfunction of thrust/lift
TL-CERT-07	VTOL.2130: Calculate ground area necessary for safe landing or go around of average crew skill using critical flight conditions. Also list procedures and configurations

Code	Requirement
TL-CERT-20	VTOL.2250(c): Failure of a part with critical characteristics must not have catastrophic effect
TL-CERT-37	VTOL.2500(c): Failure conditions that would prevent continued safe flight and landing of the aircraft are considered catastrophic
TL-CERT-38	VTOL.2510(a)(1): Catastrophic failure must not result from a single failure
TL-CERT-39	VTOL.2510(c): Adequate in-service monitoring of systems which failure may have hazardous or catastrophic consequences must be established
TL-CERT-43	VTOL.2625(d): Document and implement procedures to prevent structural failures due to foreseeable causes of strength degradation
TL-CERT-44	AMC VTOL.2510 Quantitative safety objectives (FDAL): minor <=1e-3, incidents/hr, major <=1e-5/hr, hazardous <=1e-7, catastrophic <=1e-9
TL-MANU-01	The manufacturing process of the vehicle shall limit the emission of greenhouse gasses
TL-MANU-02	The manufacturing process of the complete system shall limit the emission of greenhouse gasses
TL-MANU-03	The manufacturing process of the system shall limit the generation of waste
TL-MANU-04	No waste of the manufacturing process shall end up in the environment
TL-MANU-05	The manufacturing process shall limit the use of scarce materials

Table 6.4: Subsystem requirements for propulsion and power

Code	Requirement
VEH-PROP-01	The T/W shall be at least 1.1 in all take-off & landing conditions
VEH-PROP-02	The propulsion system shall produce less than 67 dB(A) of noise at 250 ft
VEH-PROP-03	The rotors shall despin in less than 5 seconds for safe boarding
VEH-PROP-04	The propulsion system shall have sufficient redundancy to land safely in case of a motor failure
VEH-PROP-05	Rotor tip mach shall be less drag than divergence Mach number
TL-CERT-16	VTOL.2215(a) critical flight loads must be calculated with any (a)symmetrical loading conditions from min to max mass and with likely failure of systems
TL-CERT-19	VTOL.2225(c) Determine design loads on rotor assemblies as result of flight and ground conditions, as well as limit input torques
TL-CERT-27	VTOL.2400(c) T/L system must account for all likely operating conditions, including foreign object threats and hazards in operation or to ground personnel
TL-CERT-28	VTOL.2405(b) single failure or likely combination failures of T/L controls systems must not prevent controlled emergency landings
TL-CERT-29	VTOL.2405(c) Inadvertent operation of T/L systems must be impossible or not unsafe
TL-CERT-30	VTOL.2405(d) provide means of verifying operation of automatic control systems of T/L system; enable override function; prevent inadvertent deactivation
TL-CERT-36	VTOL.2435(h) Any likely single failures of T/L configuration and able to react accordingly
VEH-POW-01	The cabling in the vehicle shall have a mass of less than 25 kg
VEH-POW-02	The battery shall have a capacity of 50 kWh
VEH-POW-03	The battery shall be able to charge 100 % within 10 minutes
VEH-POW-04	Battery mass shall be less than 330 kg
VEH-POW-05	The powertrain efficiency shall be at least 95 percent
VEH-POW-06	The battery shall be able to withstand 5,000 charge/discharge cycles in its lifetime
VEH-POW-07	The battery shall not exceed temperatures of 60 °C
VEH-POW-08	The powertrain subsystem shall not occupy a volume more than 0.007 m^3 per rotor
VEH-POW-09	In the event of crash landing the battery shall not endanger the passengers or emergency responders
TL-CERT-26	VTOL.2335 Mitigate probability or adverse effects of lightning
TL-CERT-31	VTOL.2430(a)(1) Each T/L system must provide independence between multiple energy storage and supply systems
TL-CERT-32	VTOL.2430(a)(3-4) Each T/L system must provide adequate margins to ensure safe functioning accounting for likely component failures and energy fluctuations
TL-CERT-33	VTOL.2430(a)(5-6) Each T/L system must provide a means to safely remove or isolate the energy stored within the system and minimise hazards to people to occupants or people on the ground taking into account failure of the landing system

Code	Requirement
TL-CERT-28	VTOL.2405(b) single failure or likely combination failures of T/L controls systems must not prevent controlled emergency landings
TL-CERT-29	VTOL.2405(c) Inadvertent operation of T/L systems must be impossible or not unsafe
TL-CERT-30	VTOL.2405(d) provide means of verifying operation of automatic control systems of T/L system; enable override function; prevent inadvertent deactivation
TL-CERT-36	VTOL.2435(h) Any likely single failures of T/L configuration and able to react accordingly
TL-CERT-35	VTOL.2430(b)(3-4) T/L systems must prevent significant loss of stored energy and provide energy for a sufficient reserve based on a standard flight

Table 6.5: Subsystem requirements for structures and stability & control

Code	Requirement
VEH-STRUC-01	The structure of the vehicle shall be able to withstand 1.5 times the limit load
VEH-STRUC-02	The OEW shall be less than 50% of the MTOW
VEH-STRUC-03	The landing struts shall be able to withstand the landing loads
VEH-STRUC-04	The manufacturing process of the vehicle shall limit the emission of greenhouse gasses
VEH-STRUC-05	The aircraft shall perform 90,000 trips in its lifetime
VEH-STRUC-06	The structure shall be able to accommodate the usage of windows
VEH-STRUC-07	The structural components shall be corrosion resistant
VEH-STRUC-08	The fuselage shall be able to protect the passengers in case of a bird strike
VEH-STRUC-09	The landing gear shall be able to withstand free-fall landing from 0.33 m
VEH-STRUC-10	TaxiBots shall be capable of lifting the aircraft from the base for ground transport
VEH-STRUC-11	The tilting wing mechanism shall be able to operate in at least 100,000 cycles in its lifetime
TL-CERT-14	VTOL.2160(a) No excessive vibration throughout limit flight envelope
TL-CERT-17	VTOL.2240(a-b) Develop procedure to detect structural damage before it results in structural failure
TL-CERT-22	VTOL.2270(a) items of mass or impacts during emergency landings themselves may not injure occupants precluding egress
TL-CERT-24	VTOL.2320(b) protect occupants from serious injuries due to bird strikes and keep flight crew operational
TL-CERT-25	VTOL.2325 Minimise risk of fire initiation and propagation in survivable emergency landing and through equipment overheating
TL-CERT-26	VTOL.2335 Mitigate probability or adverse effects of lightning
VEH-STAB-01	The vehicle shall be statically stable (in hover, powered and unpowered flight)
VEH-STAB-02	Cm-alpha shall be <0
VEH-STAB-03	The vehicle shall be stable during the transition period
VEH-STAB-04	The vehicle shall be able to withstand gusts of 6 m/s
VEH-STAB-05	The rotors on the canard will not destabilise the vehicle
VEH-STAB-06	The vehicle shall be able to manoeuvre within the city
VEH-STAB-07	The vehicle shall maintain stable hover without forward props at less than -10 degrees from level
VEH-STAB-08	The vehicle shall not descend at a rate larger than one-fourth of the induced velocity of its rotors in hover
VEH-STAB-09	The vehicle shall not tip over on the ground during loading
TL-CERT-08	VTOL.2135(a)(3-5) maintain control in all flight phases with avg pilot skills, alertness and effort with degraded electronics and FC modes; with likely T/L malfunctions
TL-CERT-09	VTOL.2135(a)(6) demonstrate controllability with wind limit from all azimuths
TL-CERT-11	VTOL.2140(c) Trim control max not introduce undesirable control force gradient discontinuities. during critical malfunction control forces may not be distracting
TL-CERT-12	VTOL.2145(b) no divergent stability characteristics within flight envelope that unacceptably increase workload of flight crew
TL-CERT-13	VTOL.2150(a) Controllable stall characteristics with warnings sufficiently to provide margin
TL-CERT-21	VTOL.2250(d) FC system free from jamming when a/c subjected to limit air loads

Table 6.6: Subsystem requirements for aerodynamics, electrics and the interior

Code	Requirement
VEH-AERO-01	The L/D of the vehicle shall be at least 9
VEH-AERO-02	Drag of the canard rotors shall be minimised during cruise
TL-CERT-16	VTOL.2215(a) critical flight loads must be calculated with any (a)symmetrical loading conditions from min to max mass and with likely failure of systems
VEH-ELEC-01	The vehicle shall have sufficient primary sensors
VEH-ELEC-02	The power system shall communicate battery capacity and charge at all times
VEH-ELEC-03	The power system shall communicate battery (dis)charge rate
VEH-ELEC-04	The power system shall complete self diagnostics report health
VEH-ELEC-05	The vehicle shall have 3 redundant sets of sensors
VEH-ELEC-06	The vehicle shall communicate complete telemetry to ground station between 118 and 136.975 Hz
VEH-ELEC-07	The vehicle shall maintain constant ground communication
VEH-ELEC-08	The vehicle shall be remotely controllable via secure channel
VEH-ELEC-09	The vehicle shall communicate via VHF from 118-137 MHz
VEH-ELEC-10	The communications shall be 99.9% reliable over 100,000 km
VEH-ELEC-11	The system shall only operate when all seat belts are fastened
VEH-ELEC-12	The system shall determine its c.g. before flight
VEH-ELEC-13	The vehicle shall indicate when it is safe to approach/board
VEH-ELEC-14	The vehicle shall have redundant power systems for control, communications and safety systems
TL-CERT-40	VTOL.2515(a) Electric systems not adversely affected by lightning, unless lightning strike shown to be improbable
TL-CERT-41	VTOL.2520(a) protection against High Intensity Radiated Fields (HIRF) and fast recovery after an event
TL-CERT-42	VTOL.2555(f) flight data recorders must be installed but may transmit data to be remotely recorded
VEH-INTER-01	Passengers shall be secured in seats by a seat belt
VEH-INTER-02	Passengers shall have neck and head support
VEH-INTER-03	All passenger items shall have a secured position
VEH-INTER-04	The passengers shall be able to request ground contact with a human via audio/video
VEH-INTER-05	The vehicle shall provide location, altitude, temperature etc to passengers during flight
VEH-INTER-06	The vehicle shall confirm passenger destination before flight
VEH-INTER-07	Passengers shall be able to board and deboard the vehicle safely
VEH-INTER-08	The vehicle shall maintain interior temperature between 15-25 °C, ambient humidity
VEH-INTER-09	The vehicle shall provide in-flight entertainment via Wi-Fi
TL-CERT-15	VTOL.2165(a) icing
TL-CERT-22	VTOL.2270(a) items of mass or impacts during emergency landings themselves may not injure occupants precluding egress
TL-CERT-34	VTOL.2430(b)(2) T/L must be be isolated from personnel compartments and protected from hazards

Vehicle Specifications

The Bumblebee EX is designed to meet its mission requirements. To further define the specifications, Table 7.2 is given to show the mass and placement of the major systems. All mass is accounted for in this sheet. Any components not explicitly listed are included in another items.

7.1. Mass Budget and C.G.

The mass of each subsystem component group is listed in Table 7.2. Contingencies for the current design have to be determined. However, since the goal of this section is to show the current design of the vehicle, the contingency management is discussed later, in Section 19.3. The datum point for the centre of gravity is at the nose of the aircraft, located at the base of the landing gear. Note that the canard is swept forward and is actually in front of the nose. Figure 7.1 gives a visual breakdown of the major component groups. Furthermore, the moment of inertia is estimated to be able to perform the stability analysis. The moment about the y-axis I_{yy} is estimated to be 1,340 kg m^2. This is slightly less than for a Piper Cherokee PA-28[1], a conventional aircraft of similar weight, that is longer than the Bumblebee EX.
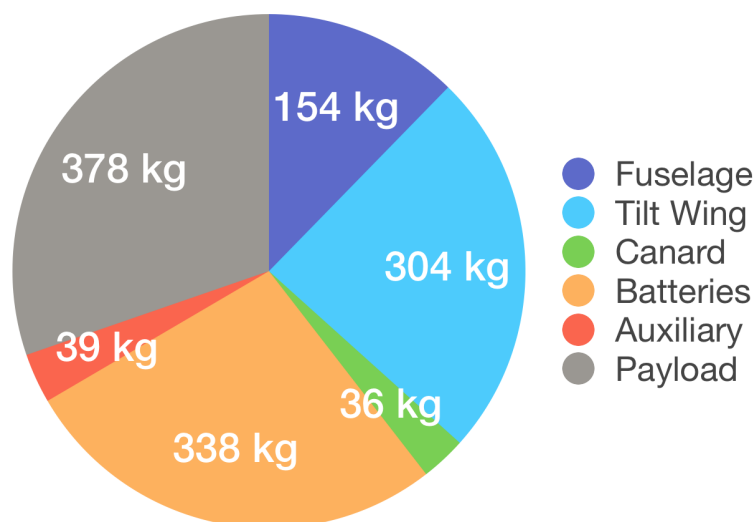

Figure 7.1: The mass of all components are grouped to show the relative percentages allowed for each group. This chart includes all mass up to MTOW of 1,250 kg.

[1] `http://jsbsim.sourceforge.net/MassProps.html` [accessed 18.06.19]

7.2. System Power

Table 7.1: Power budget of the Bumblebee EX

| Category	Component (Qty)	Voltage [V]	Peak power [W]
Main Propulsion and Control	Wing propellers (4)	750	200k
	Canard propellers (2)	100	70k
	Wing Tilt actuators (2)	100	7,500
	Canard actuators (2)	100	500
	Aileron actuators (2)	100	500
Auxiliary systems	TCAS	28	100
	IMU (2)	10-28	2.5
	LiDAR	12-28	90
	ADC/CPU	28	<5
	Cameras (4)	3.6-5.5	1.4
	Radio	12-28	9
	Air Conditioning	60-240	2,000
	Internal/external lights	28	100
	Screens and audio	28	100
Total			**550,000** [2]
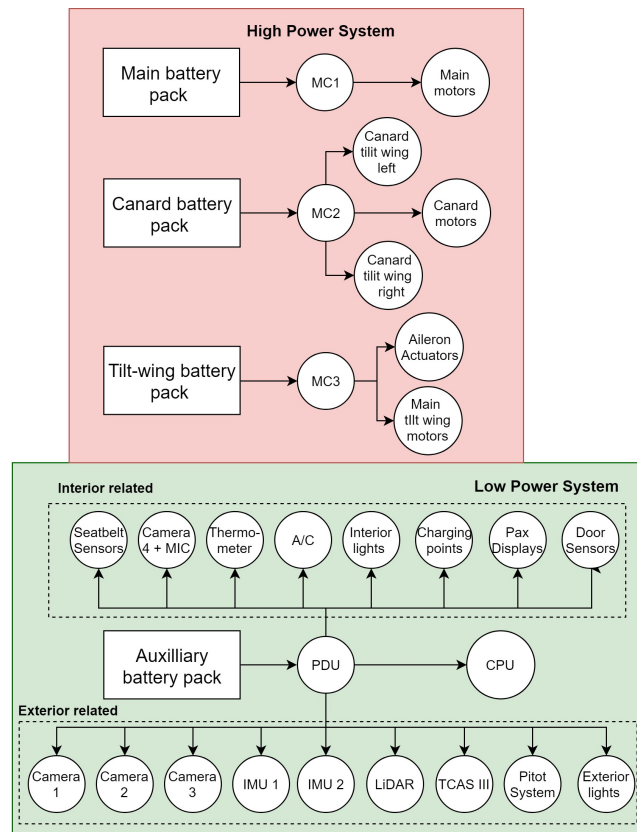
Figure 7.2: The Electrical Block Diagram EBD of the Bumblebee

---

[2]The peak total power output required, only includes running 2 of the 4 main wing propellers and only one tilt actuator. This is because the main wing motors are sized to maintain hover with 2 rotors off. Likewise the wing tilt actuator uses peak power when only one actuator is out.

7.3. Specifications

Some general specifications of the Bumblebee EX are given for reference. Some additional subsystems are detailed in this chapter, while other systems are treated elsewhere.

MTOW	1,250 kg	- Material	Aluminium 2014-T6
- OEW/MTOW	0.44	- Yield stress	414 MPa
Passengers	4 (400 kg)	- Density	2.8 kg/m^3
Doors	1		
Structure mass	150 kg		

Wing span	10 m (8.4 m net)	**Canard** span	2.7 m (net)
- Aspect ratio	8	- Aspect ratio	6.8
- Tilt range	-4° to 120°	- MAC	0.4
- MAC	1 m	- Sweep	-10°
- Sweep	-5°	- Taper ratio	0.6
- Taper ratio	0.4	- Airfoil	NACA0010
- Airfoil	NACA2410		

Main wing rotors	4	**Canard Rotors**	2
- Solidity	0.17	- Solidity	0.18
- Blade & Hub mass	10 kg	- Blade & Hub mass	6.5 kg
- Motor diameter	29 cm	- Motor diameter	19 cm
- Motor width	9 cm	- Motor width	8 cm
- Motor mass	26 kg	- Motor mass	7.3 kg
- Motor cont. power	90 kW	- Motor cont. power	26 kW
- Hover Power req.	70kW/rotor	- Hover Power req.	11 kW/rotor
- Peak power req.	200 kW/rotor	- Peak power req.	32 kW/rotor
- Max Tip Mach	0.43	- Max Tip Mach	0.2

Main Battery mass	310 kg	**Canard Battery** mass	14 kg	**Wing Tilt Battery** mass	4 kg
- Volume	0.1 m^3	- Volume	0.02 m^3	- Volume	0.005 m^3
- Usable Capacity	48 kWh	- Usable Capacity	1.3 kWh	- Usable Capacity	400 Wh
- Peak power output	2.4 MW	- Peak power output	78 kW	- Peak power output	22 kW
- Energy density	155 Wh/kg	- Energy density	93 Wh/kg	- Energy density	100 Wh/kg
- Power density	2,100 W/kg	- Power density	2,800 W/kg	- Power density	2,800 W/kg
- Full Charge time	8 minutes	- Full Charge time	7.5 minutes	- Full Charge time	7.5 minutes
- Architecture	68S16P	- Architecture	2S7P	- Architecture	4S1P
- Cell [3]	SLPB065070180	- Cell [4]	c1	- Cell [4]	c1

Backup Radio System		- Band	VHF 118-137 MHz

Performance Specs		Vertical climb rate	10 m/s
Cruise speed	65 m/s	Vertical descent rate	-4 m/s
Range	60 km	Noise	73 dBA (250 ft)
Operating altitude	300-1300 m	Hover Downwash	37 m/s
Climb/descent rate	5-7 m/s	Wing tilt speed	20 deg/s

---

[3] http://kokam.com/data/Kokam_Cell_Brochure_V.1.pdf?PHPSESSID=127ce197928d82d81619847c0b83f2f5 [accessed 02.05.19]

[4] https://hobbyking.com/en_us/turnigy-nano-tech-8400mah-3s-30c-lipoly-battery-w-traxxas-connector.html [accessed 02.05.19]

Canard tilt speed	30 deg/s	Max passenger g-force	1.3
L/D	9.5	Nominal energy during 30km trip	22kWh
Cruise (wing) angle of attack	2°	PREE	0.11 [-]
Cruise cabin pitch	6°		

Environmental System   Since it is hot in LA, the Bumblebee EX is equipped with a small car-style air conditioning system. This small system consumes 2 kW when running, so a 1 kWh battery is installed to provide cooling for single flight on a full charge. Furthermore, the system weighs 5 kg, plus a 4 kg battery unit. Forced air is used as an intake in flight. The cooler air at altitude helps the system keep cool without using too much power. This unit can be removed for operation in different climates.

Backup Systems   The auxiliary power system includes charge for 8 hours or more (with backup) not including the environmental system. This includes power for an analogue radio system that can reach aircraft emergency channels, assuming they are still in use in 2050.

Table 7.2: Mass budget of the Bumblebee EX

Category	Component	Mass [kg]	x_location [m]	z_location [m]
Wing	Wing structure and skin	90	3.25	1.1
	Wing Tilt mechanism	68	3.3	1.5
	Outboard motor(s)	27x2	2.6	1.7
	Inboard motor(s)	27x2	2.7	1.7
	Outboard rotor(1)	10x2	2.6	1.7
	Inboard motor(s)	10x2	2.7	1.7
Canard	Canard wings	8	-0.1	0.65
	Canard motor(s)	7.3x2	-0.1	0.65
	Canard rotor(s)	6.5x2	-0.1	0.65
Fuselage	Airframe and skin (including landing gear)	83	2.1	0.8
	Cabling	23	2.1	0.8
	Main wing motor controllers	27	3.55	0.95
	Wing tilt motor controller	10	3.55	0.95
	Canard motor controllers	10	0.45	0.7
Battery	Auxiliary system batteries	12	0.5	0.45
	Battery group 1	160	3.3	0.3
	Battery group 2	160	3.6	0.65
Auxiliary System	Front Passenger seats	8	1.9	0.8
	Rear Passenger seats	8	2.9	0.8
	Radio	2	0.4	0.95
	CPU	1	0.4	0.8
	LiDAR	5.3	0.35	0.6
	IMU(s)	0.4	3.2	0.85
	User interaction screens	2	1.5	1.0
	Air conditioning unit	5	2.1	0.8
	TCAS	7.5	0.35	0.8
Payload	Passenger 1	77	1.7	0.9
	Passenger 2	77	1.7	0.9
	Passenger 3	77	1.7	0.9
	Passenger 4	77	1.7	0.9
	Cargo in trunk	60	3.65	1.15
	Small luggage	10	0.5	0.75
Total		**1,250**	**2.68**	**0.92**

Vehicle Configuration and User Experience

In this chapter, a broad overview of the vehicle configuration is given. First, drawings and renders are provided to show the major components of the vehicle, their position and orientation. Most of the internal components are demonstrated as blocks. In many cases the block dimensions are the largest dimensions of the item. Some items may actually be quite a bit smaller. Also, by 2050, some of the components may be replaced by smaller, lighter models. Finally, the structural connections are not detailed in the drawings, but sufficient space has been left for their implementation.

8.1. Vehicle Configuration

The A3 drawings on page 28 and 29 show the major dimensions of the vehicle in meters. The diameter of the motors and rotors are given and the major internal components are also identified with bubbles. Their exact c.g. location and mass are given in Chapter 7. In addition to the components shown on the drawings, some additional components are placed in renders.

Figure 8.1: The Bumblebee EX has a rear loading trunk that fits two full-size suitcases. Below the trunk is the charging port.

Charging   A charging port is located on the back underneath the trunk access handle (pictured in Figure 8.1). The size of this port may depend on standards that do not yet exist. It is likely to be large in order to accommodate fast charging.

Cameras and Screens   Three cameras are placed on the lower portion of the vehicle for use by the autonomous pilot and remote pilot. One is placed in the front, one in the middle (on the belly) and one in the back, all pointing downward. These cameras are used for landing, and as proximity detectors on the ground.

There is also a camera and microphone placed inside the vehicle for 2-way communication with the passengers. The customers also have access to 2 sets of video screens (one set for the forward seated passengers, one set for the back seats), which have three purposes. First, the screens show the interface for the Virtual

Boarding Assistant, that provides important information and instructions to the customer during boarding and de-boarding. Second, it displays flight status information and act as the interface for the customer to set the environmental controls and other comfort settings. Finally, it is the interface for communication with customer service and remote pilots in the event of issues or emergencies.

Landing Gear Suspension   The landing gear of the vehicle are semi-rigid carbon-fibre struts. Inside the chassis, the struts are connected to the airframe via airbags, which soften the landing. The four landing struts of the vehicle are intended for vertical landing but in extreme cases, the vehicle can land horizontally without wheels. The airbag suspension will soften the initial impact. The ground clearance of the vehicle is 20 cm. This keeps the vehicle low for easy accessibility.

In the case of an emergency horizontal landing, the struts take the force of initial impact but can be lowered to allow for belly sliding. They are swept back to allow sliding. Two large beams of the airframe run directly along the belly, allowing the vehicle to easily slide (like sled runners). While a belly landing is not ideal, it allows the vehicle to land horizontally at an airfield in an emergency situation.

Wing Features   Ailerons are placed on the wings for roll control in forward flight as well as yaw control in hover. The control mechanism for the ailerons is placed inside the wing.

Static wicks are also placed along the back of the main wing and ailerons. These allow the vehicle to discharge static buildup that occurs when flying through precipitation, without interfering with the electrical and radio equipment.

The outboard rotors leave a clearance of 2.15 m when tilted up.
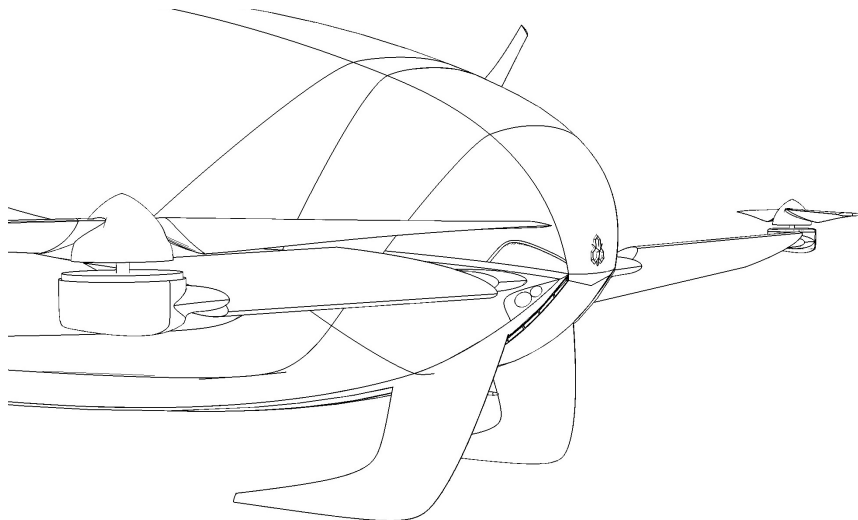

Figure 8.2: The canard wings are fully tiltable and independent, providing complete control.

Canard Features   The canard wing at the front of the vehicle is fully tiltable along the quarter-chord line as shown in Figure 8.2. However, the forward rotors are fixed and do not tilt, always pointing upwards.

TU Delft DSE 18

DRAWING TITLE
Bumblebee EX - Outboard

SIZE	DRAWN BY	DATE	REV
A3	Trevor Gast	21-6-2019	

SCALE 1:50	WEIGHT(kg) 870 kg	SHEET 1/2

This drawing is our property.
It can't be reproduced or communicated
without our written agreement.

Top view
Scale: 1:50

Static wicks

10.01
1.27
0.61
4.82
0.06
4.01
0.48
∅190
1.57
3.77
∅1.62

Measurements in meters

Isometric view
Scale: 1:50

∅292
0.95
1.62
∅2.04

Front view
Scale: 1:50

1.29
1.71
4.4

Right view
Scale: 1:50

28

TU Delft DSE 18

DRAWING TITLE
Bumblebee EX - Inboard

SIZE A3	DRAWN BY Trevor Gast	DATE 21-6-2019	REV
SCALE 1:50	WEIGHT(kg) 870 kg		SHEET 2/2

This drawing is our property.
It can't be reproduced or communicated
without our written agreement.

Top view
Scale: 1:50

2.56

1.6

Section view B-B
Scale: 1:50

Isometric view
Scale: 1:60

Right view
Scale: 1:50

2.15
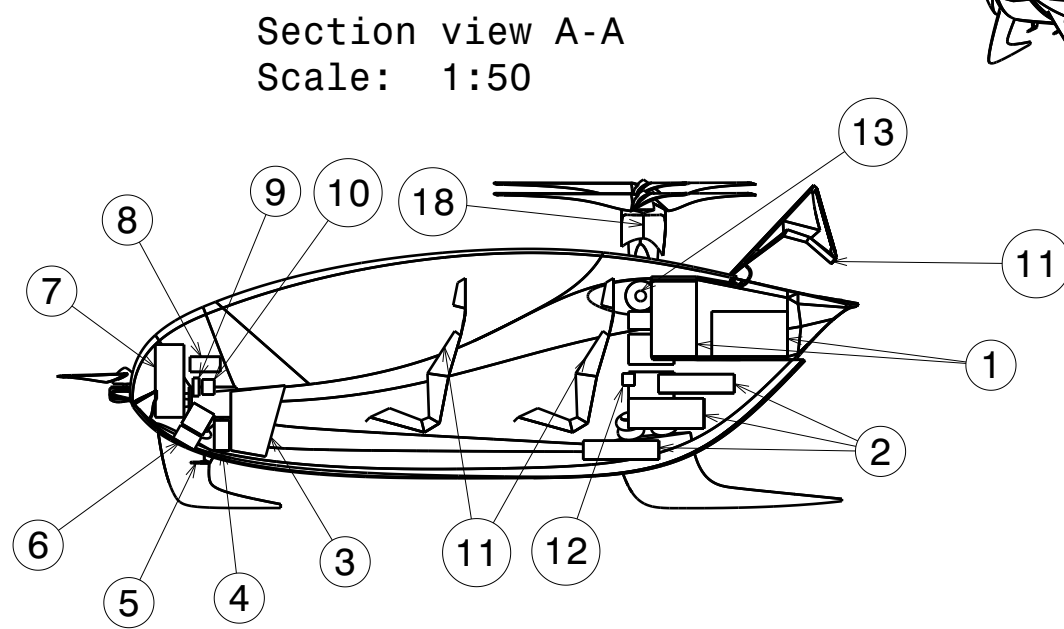
Section view A-A
Scale: 1:50

1 – Passenger Cargo
2 – Propulsion Batteries
3 – Hand luggage space
4 – Aux System Batteries
5 – Pitot tube(s)
6 – LiDAR
7 – Air Conditioning
8 – Radio Transceiver

 9 – TCAS
10 – CPU
11 – Passenger Seats
12 – IMU(s)
13 – Wing tilt actuator
14 – Canard Motor Controllers
15 – Main Motor Controllers
16 – Canard actuators
17 – Landing gear
        airbag suspension
18 – Wing motors
19 – Canard motors

29
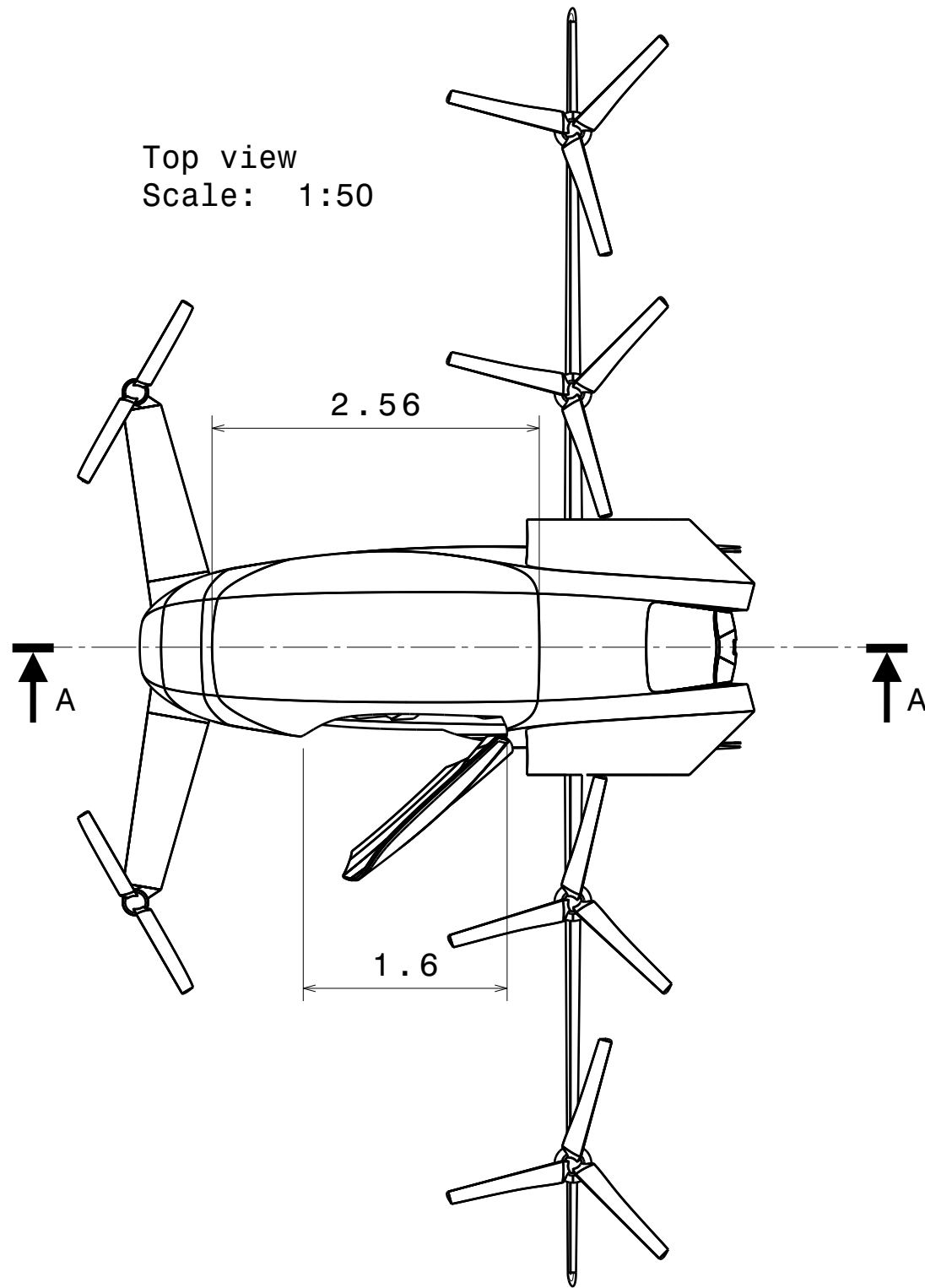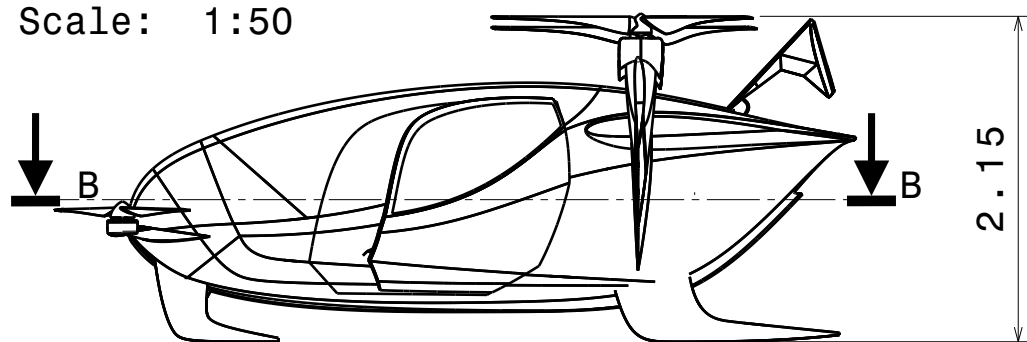
8.2. Vehicle Communication Flow

Throughout operations, the vehicle must communicate with various entities. Since the vehicle is piloted autonomously, additional information must be conveyed to those entities during flight. The communication flow from the perspective of the autonomous pilot is shown in Figure 8.5. Some lines of communication are continuous throughout flight and operation, while other lines may be limited to a specific flight phase.

The "communication" between the pilot and the landing site takes the form of visualisation between the cameras and the LiDAR. Those systems will be able to detect obstacles, uneven ground, clearance, and judge ground solidity (e.g. to avoid landing on bodies of water). Such systems are already in development and should reach maturity well before 2050[1].
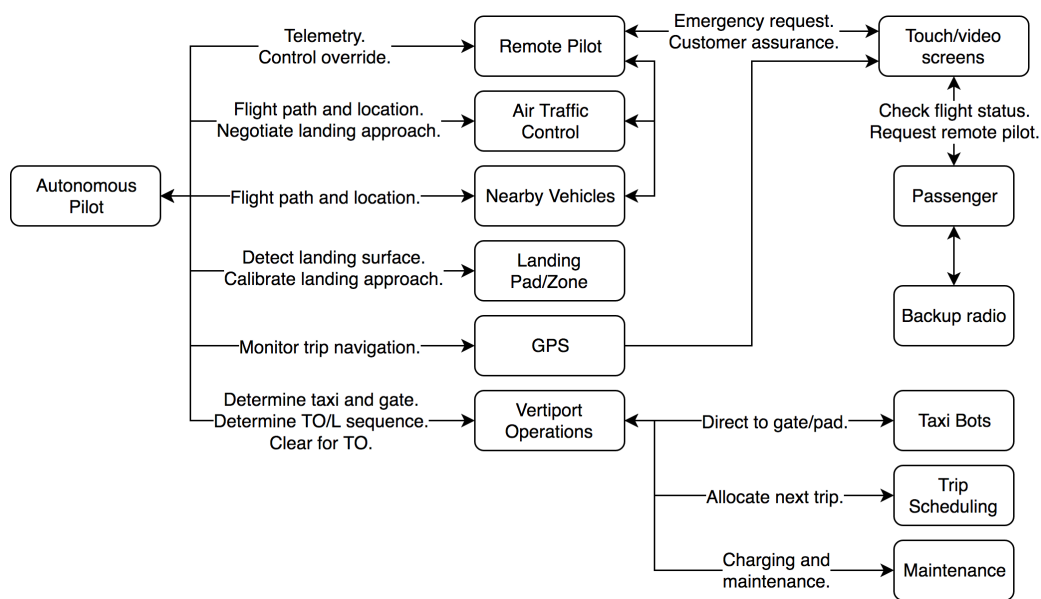
Figure 8.5: The communication flow from the vehicle perspective.

8.3. Software Configuration

Since the vehicle is autonomous, its core software is responsible for the various roles the vehicle must perform; from pilot, to cabin crew, to communications. The core software flow is shown in Figure 8.6, indicating input with a blue arrow and output with a green arrow. The primary output of the control system is the propeller, tilt-wing and canard control, given in the green box. The control input comes from the set of sensors which provide information about location, altitude, and attitude, as well as information about nearby vehicle, obstacles, and ground geometry. The CPU is responsible for the autonomous piloting. This is further discussed in subsection 9.5.5.

In addition to the flight control system, customer communication and safety systems are also present. Furthermore, sensors are required on the seat belts and doors, as well as the hand luggage compartment. This is to prevent the vehicle from putting the passengers at unnecessary risk.

---

[1] https://www.nearearth.aero [accessed 21.06.19]

Figure 8.6: Block diagram of the software/data connections of the vehicle.

8.4. User Experience

The passenger experience is especially important, as this service accommodates a large number of passengers, very quickly. The phases of this journe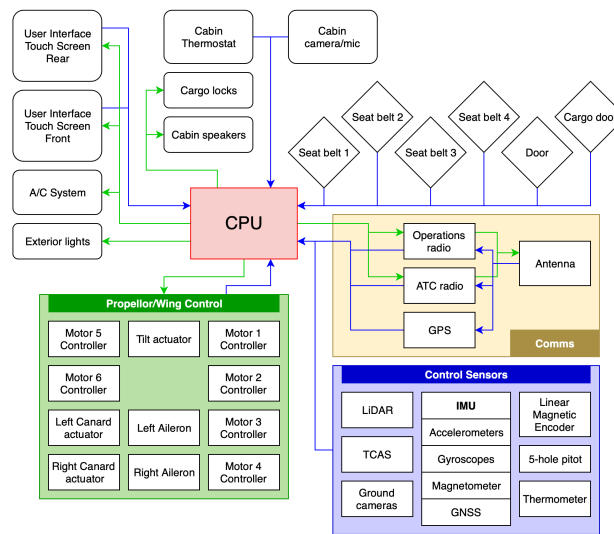y are described here in 3 segments: boarding, flight and arrival. Moreover, the ticketing procedure can take many forms, from purchase via phone, or website. Most likely customers can request flights directly via an app.

Boarding The passengers board the vehicle from one side, which means the passenger traffic is managed to follow a single path. The likelihood of customers bumping into rotors is therefore minimised, since they will not need to walk around the vehicle. Before boarding, the on-board Virtual Boarding Assistant directs the passengers to secure their hand luggage either in the trunk in the back, or if full, in the cargo space in the front of the nose. The luggage in the front should be secured with a strap, and the compartment automatically locks once taxiing begins.

Passengers will always board the front seats first. The seat pitch is 1 m, and has sufficient leg/head room for a passenger over 2 m tall. Once the passengers are seated, the door is closed, and each passenger is directed to secure their personal digital devices in the provided caddies, such that they cannot be "dropped" and that the devices do not fly about the cabin in case of an emergency manoeuvre. This complies with the CS regulations regarding loose items in the cockpit. In addition it prevents passengers from dropping their device while in flight, so they do not need to unlock their seat belt during flight.

Once the device is secured, the passenger is directed to connect the lower portion of their five-point seat belt first, then the over-shoulder straps. Once complete, the boarding assistant indicates on the screen that the passengers are secured, and ready for flight. An optional pre-flight safety instruction is offered. The passengers are then asked to confirm their destination on the screen. If it is incorrect, it is updated. Also available on the boarding assistant is flight information, including information on time, location, speed, altitude, etc.. The customer may also request direct video-phone communication with a human ground agent. In emergency situations, a remote pilot is connected to monitor the flight and intervene if necessary.

Once the door is closed and the passengers are prepared for flight, exterior lights are used to indicate the vehicle is not safe to approach (as can be seen in Figure 8.7). The vehicle will run self diagnostics to confirm proper operation of tilting mechanisms, ailerons, canard, and motor controllers. TaxiBots then approach and lift the vehicle to take it to the Touchdown and Liftoff Area (TLOF) pad. Once the TaxiBots have left the vehicle at the pad, the vehicle begins to spin up the rotors and takes off.

During transition and cruise, the vehicle is trimmed to tilt back at a slight angle of attack. This, in addition to the acceleration rate means the vehicle slightly reclines the customers to a comfortable angle. This is especially nice, since the seats are not adjustable. During transition from cruise to hover, the deceleration removes some of the reclining effect, but the pitch angle of the vehicle increases as it slows to counter this.

Figure 8.7: Red lights on the fuselage indicate the vehicle is not safe to approach. The lights turn green when it is safe to approach.

In-Flight   While in flight, the screen also provides options for environmental (temperature) control. The cabin is not pressurised, but does have intake to bring in airflow from outside. LA can be hot, so a small air conditioning unit is present. Furthermore, Wi-Fi is available on board during cruise phase, so the passengers can quickly connect and use their personal digital devices in the caddies.

An emergency call button is available that connects the vehicle directly to a remote pilot.This also engages the secondary emergency radio system (audio only). While remote pilots should not be necessary for the majority of operations, having remote pilots available is an important feature to improve the likelihood of social acceptance.

At the end of cruise, the autonomous pilot indicates that transition back to hover will occur. This phase tends to apply a wider range of forces on the passengers. Initially there is reduced g-force, followed by tilting back (to decelerate) at a g-force higher than 1.

Arrival   Once the vehicle has landed, the rotors spin down and TaxiBots approach the vehicle to take it to the gate. Once at the gate, a quick visual safety inspection is completed by the vertiport staff before the doors open. Next to that, the software and hardware checks are performed by the autonomy kit. The rotors must all be locked, then the lights indicate the vehicle is safe to approach. Hereafter the door unlocks and can be opened. The customers collect their luggage and leave. In the meantime, maintenance crews check over the vehicle and connect the charging cable in preparation for the next flight. Throughout the journey, the passenger has multiple contacts with operations. Figure 8.8 shows the lines of communication during the journey and the relevant information transferred between entities.
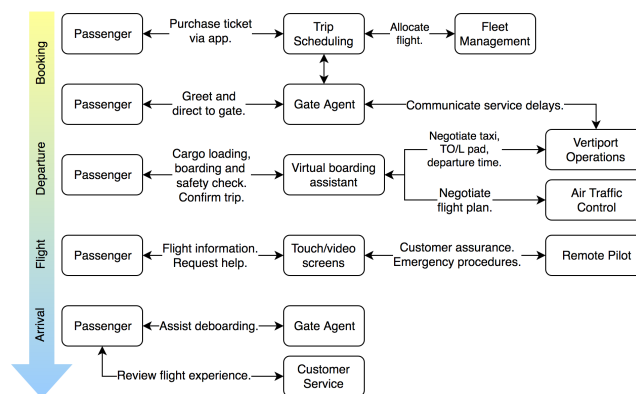

Figure 8.8: Block diagram of the communications throughout a single passenger journey (from the customer perspective).

Vehicle Analysis & Sizing

To find the specifications for the vehicle given in Chapter 7, different tools and methods were used. This chapter discusses the approach used for the different subsystems. In Section 9.1 the sizing of the propulsion subsystem and the calculations for the noise are discussed. The computations for the powertrain and battery are described in Section 9.2 followed by the aerodynamics subsystem in Section 9.3. This section also contains the calculation for the thrust and power of the vehicle. An analysis of the loads on the vehicle and the structure is performed in Section 9.4. Finally, the characteristics of the stability and control are calculated in Section 9.5.

9.1. Propulsion Subsystem

The propulsion subsystem of the vehicle is responsible for producing a propulsive force capable of lifting the vehicle off the ground vertically during take-off and for propelling the vehicle at the required cruise velocity, whilst being as quiet and efficient as possible.

In the Midterm Report [7] several propeller performance tools such as the Blade Element and Momentum Theory (BEMT), Noise and Downwash tools were developed to aid in the quantitative concept trade-off process. During the detailed design phase, these tools are developed and verified further and are used for propeller design optimisation and vehicle stability assessment.

9.1.1. Blade Element & Momentum Theory (BEMT) Method

A BEMT tool is developed for rotor performance calculations. In the current tool, the BEMT code is used to calculate the rotational speed of a rotor (with a designed solidity, number of blades, twist, airfoil and radius) and the torque it generates for a given value of thrust required. The MATLAB tool developed in the Midterm Phase was able to predict the performance of a single and a coaxial rotor in hover, but the model is extended in the Detailed Design phase to predict the performance of a single rotor in axial flow (for climb and cruise) and tangential flow (during transition). For the sake of completeness, the theory behind the tool is presented again in this report along with the extensions that are made. The implementation is based on [9], which describes a modelling approach for coaxial rotors in axial flight and hover. The approach is also applicable to single rotors. The advantage of BEMT is that it is based on solid physical principles (mass, momentum and energy conservation laws) and is relatively free of empirical parameters.

Leishman Method   The theory developed by Leishman discretises the rotor disk into rotor annuli and applies momentum theory to each.

The main assumption of BEMT is that successive blade elements have no mutual effects on each other (a two-dimensional assumption). Classic Prandtl "tip loss" effects have been included into the BEMT, giving a first approximation of the three-dimensional effects that occur due to tip and root vortices.

Momentum theory principles relate the thrust produced by an annulus to the product of the mass flow rate through it and the induced velocity there. The incremental thrust on the annulus is:
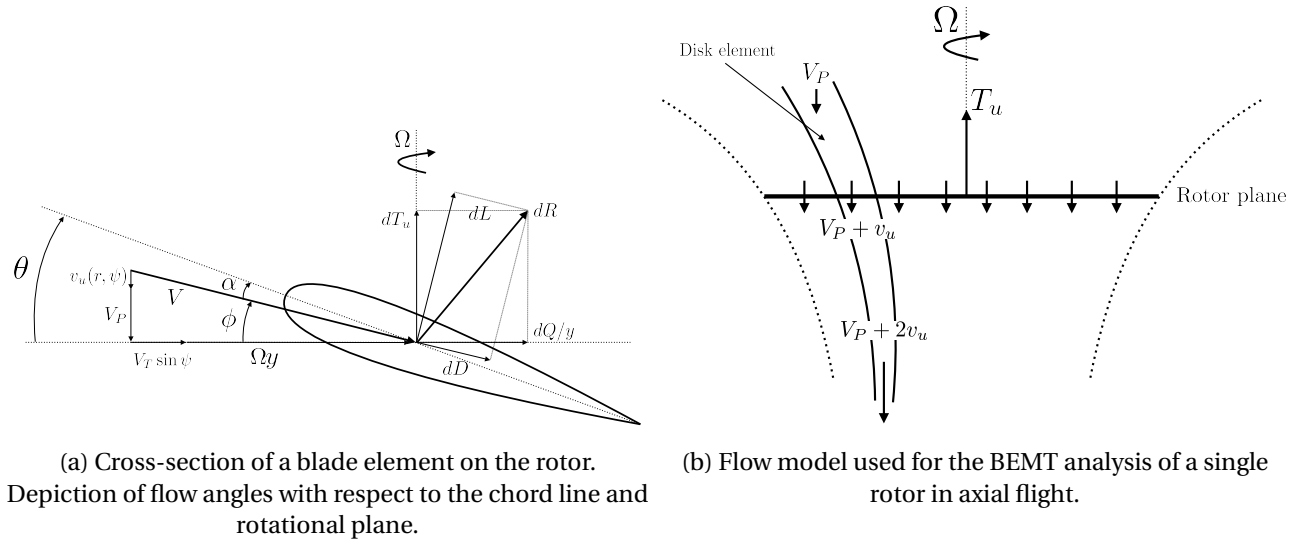
(a) Cross-section of a blade element on the rotor. Depiction of flow angles with respect to the chord line and rotational plane.

(b) Flow model used for the BEMT analysis of a single rotor in axial flight.

Figure 9.1: Modelling approach for rotor blade elements in (a) and for the flow model in (b).

$$\mathrm{d}T = 2\mathrm{d}(\dot{m}\, v_\mathrm{i}) \tag{9.1}$$

$$\mathrm{d}\dot{m} = \rho(V_\mathrm{P} + v_\mathrm{i})\,\mathrm{d}A = 2\pi\rho(V_\mathrm{P} + v_\mathrm{i})\, y\,\mathrm{d}y, \tag{9.2}$$

where $\mathrm{d}\dot{m}$ is the mass flow rate over the annulus, V_P is the axial velocity of the rotor, v_i is the induced velocity at a specific rotor annulus, and $\mathrm{d}A = 2\pi y\,\mathrm{d}y$ is the area of a rotor annulus which is at a radial distance y from the rotation axis of the rotor.

After non-dimensionalising Equation 9.1 by $\rho\pi R^2(\Omega R)^2$, where R is the rotor radius and Ω the rotational speed of the rotor, the expression for the thrust coefficient of the annulus is obtained:

$$\mathrm{d}C_\mathrm{T} = 4F\lambda_\mathrm{r}\lambda_\mathrm{i}r\,\mathrm{d}r \tag{9.3}$$

where $r = y/R$, $\lambda_\mathrm{r} = \lambda_\mathrm{P} + \lambda_\mathrm{i} = \frac{V_\mathrm{P}+v_\mathrm{i}}{\Omega R}$ and F is the Prandtl tip loss function:

$$F = \frac{2}{\pi}\cos^{-1}(\exp(-f)). \tag{9.4}$$

f is a function of the number of blades N_b, the radial position of the blade element r, and the inflow angle ϕ (equal to $\lambda_\mathrm{r}(r)/r$ with a small angle assumption):

$$f = \frac{N_\mathrm{b}}{2}\left(\frac{1-r}{r\phi}\right) \tag{9.5}$$

Using the circulation theory of lift, with small angle assumptions, Equation 9.3 is equated to:

$$\mathrm{d}C_\mathrm{T} = \frac{1}{2}\sigma r^2\mathrm{d}r = \frac{1}{2}\sigma C_{\mathrm{l}_\alpha}(\theta_\mathrm{b} - \phi - \alpha_0)r^2\mathrm{d}r$$

$$= \frac{\sigma C_{\mathrm{l}_\alpha}}{2}(\theta_\mathrm{b}r^2 - \lambda r)\mathrm{d}r \tag{9.6}$$

where θ_b is the blade pitch distribution on the rotor, as shown in Figure 9.1a. α_0 and C_{l_α} are the zero-lift angle of attack and the lift curve slope of the airfoil at that blade section, respectively. σ is the solidity of the rotor.

Combining the expressions from Equation 9.3 and Equation 9.6 allows to solve for the non-dimensionalised inflow ratio at the rotor annulus:

$$\lambda_r(r, \lambda_P) = \sqrt{\left(\frac{\sigma C_{l_\alpha}}{16F} - \frac{\lambda_P}{2}\right)^2 + \frac{\sigma C_{l_\alpha}}{8F}\theta_b r} - \left(\frac{\sigma C_{l_\alpha}}{16F} - \frac{\lambda_P}{2}\right). \tag{9.7}$$

Since λ_r is a function of F and viceversa, a fixed-point iteration (which typically takes 5-10 iterations to converge) is performed to solve for λ_r and consequently for dC_T, based on an initial guess of $F = 1$. The incremental power coefficient is found as the sum of induced and profile sources:

$$dC_P = \lambda_r dC_T + \frac{1}{2}\sigma C_d r^3 dr \tag{9.8}$$

where C_d is the sectional profile drag coefficient. In this first analysis, $C_d = C_{d_0} + D_1\alpha + D_2\alpha^2 + D3\alpha^3 + D4\alpha^4$, according to the fit shown in Figure 9.2b for a NACA 0012 airfoil at $Re = 1 \times 10^6$.
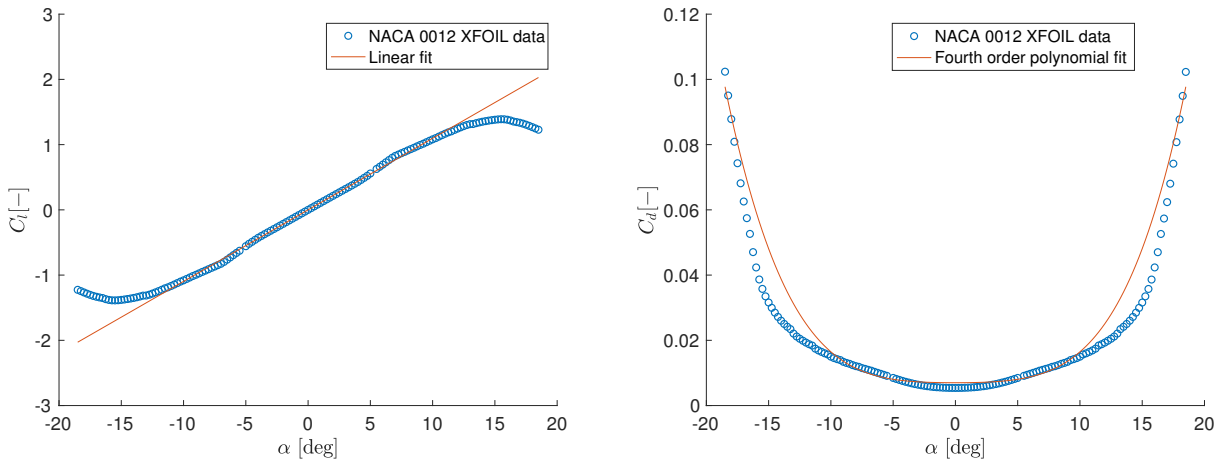
(a) Lift coefficient is modelled as a linear function of angle of attack with a lift curve slope of $C_{l_\alpha} = 2\pi$ [1/rad]

(b) Profile drag coefficient is modelled as a quadratic function of angle of attack with $D1 = D3 = 0$, $C_{d_0} = 0.007$ [-], $D2 = 0.08$ [1/rad^2] and $D4 = 7$ [1/rad^4]

Figure 9.2: Linear lift (a) and quadratic drag (b) polar fits with reference to XFOIL [10] data computed for a NACA 0012 airfoil at $Re = 1 \times 10^6$

Non-axial Flow Extension   The extension made to the model discretises the disk into disk elements (radius and azimuth) to be able to capture the loading asymmetry as the blade performs a full revolution. Figure 9.1a shows the inflow velocities of a blade element as a function of both radius and azimuth.

Each disk element has an area of $dA = r\,dr\,d\psi$. To each of these disk elements, the relation found in Equation 9.1 from momentum theory can be applied, which relates the incremental thrust of each disk element and the inflow ratio there:

$$dT = 2\rho(V_P + v_i)v_i dA = 2\rho(V_P + v_i)v_i y\,dy\,d\psi \tag{9.9}$$

$$dC_T = \frac{dT}{\rho(\pi R^2)(\Omega R)^2} = \frac{2\rho(V_P + v_i)v_i y\,dy\,d\psi}{\rho(\pi R^2)(\Omega R)^2} \tag{9.10}$$

which simplifies to:

$$\mathrm{d}C_{\mathrm{T}} = \frac{2}{\pi} F \lambda_{\mathrm{r}} \lambda_{\mathrm{i}} r \mathrm{d}r \mathrm{d}\psi \tag{9.11}$$

where F is the Prandtl Tip loss function given by Equation 9.4 and is a function of the inflow angle ϕ, which in this case is equal to (based on Figure 9.1a):

$$\phi = \tan^{-1}\left(\frac{V_{\mathrm{P}} + v_{\mathrm{i}}}{\Omega y + V_{\mathrm{T}} \sin \psi}\right) = \tan^{-1}\left(\frac{\lambda_{\mathrm{r}}}{r + \lambda_{\mathrm{T}} \sin \psi}\right) \tag{9.12}$$

$$\approx \frac{\lambda_{\mathrm{r}}}{r + \lambda_{\mathrm{T}} \sin \psi} \tag{9.13}$$

where the last step uses a small angle assumption ($\phi << 1$). $\lambda_{\mathrm{T}} = \frac{V_{\mathrm{T}}}{\Omega R}$ is the non-dimensionalised tangential flow ratio. It is assumed that $\phi << 1$ (small angle assumption), using conventional blade-element theory, the following is written:

$$\mathrm{d}T = N_{\mathrm{b}} \mathrm{d}L \frac{\mathrm{d}\psi}{2\pi} = N_{\mathrm{b}} \frac{\rho}{2} C_{\mathrm{l}} V^2 c \mathrm{d}y \frac{\mathrm{d}\psi}{2\pi} \tag{9.14}$$

where C_{l} and V are expanded, respectively, as:

$$C_{\mathrm{l}} = C_{\mathrm{l}_\alpha}(\alpha - \alpha_0) = C_{\mathrm{l}_\alpha}(\theta_{\mathrm{b}} - \phi - \alpha_0) \tag{9.15}$$

$$V = V_{\mathrm{T}} \sin \psi + \Omega y \tag{9.16}$$

which is inferred from Figure 9.1a using small angle assumptions (ϕ is given by Equation 9.13). Writing Equation 9.14 in non-dimensional form, the following equation applies:

$$\begin{aligned}
\mathrm{d}C_{\mathrm{T}} &= \frac{N_{\mathrm{b}} c}{\pi R} \frac{C_{\mathrm{l}_\alpha}}{2}(\theta_{\mathrm{b}} - \phi - \alpha_0)\left(\frac{V_{\mathrm{T}}^2 \sin^2 \psi}{(\Omega R)^2} + \frac{2 V_{\mathrm{T}} \sin \psi \Omega y}{(\Omega R)^2} + \frac{(\Omega y)^2}{(\Omega R)^2}\right)\mathrm{d}r \frac{\mathrm{d}\psi}{2\pi} \\
&= \sigma \frac{C_{\mathrm{l}_\alpha}}{2}(\theta_{\mathrm{b}} - \phi - \alpha_0)(\lambda_{\mathrm{T}}^2 \sin^2 \psi + 2\lambda_{\mathrm{T}} r \sin \psi + r^2)\mathrm{d}r \frac{\mathrm{d}\psi}{2\pi}
\end{aligned} \tag{9.17}$$

where σ is the rotor solidity, by definition. Equating the above expression to the one previously found in Equation 9.11, and defining $\mu(r, \psi) = \lambda_{\mathrm{T}}^2 \sin^2 \psi + 2\lambda_{\mathrm{T}} r \sin \psi$ for brevity, it is obtained:

$$\sigma \frac{C_{\mathrm{l}_\alpha}}{2}\left(\theta_{\mathrm{b}} - \frac{\lambda_{\mathrm{r}}}{r + \lambda_{\mathrm{T}} \sin \psi} - \alpha_0\right)(\mu + r^2)\,\mathrm{d}\cancel{r}\,\frac{\mathrm{d}\cancel{\psi}}{2\cancel{\pi}} = \frac{2}{\cancel{\pi}}F\lambda_{\mathrm{r}}(\lambda_{\mathrm{r}} - \lambda_{\mathrm{P}})r\,\mathrm{d}\cancel{r}\,\mathrm{d}\cancel{\psi} \tag{9.18}$$

$$\frac{\sigma C_{\mathrm{l}_\alpha}}{8Fr}(\theta_{\mathrm{b}} - \alpha_0)(\mu + r^2) - \frac{\sigma C_{\mathrm{l}_\alpha}}{8Fr} \frac{\lambda_{\mathrm{r}}}{r + \lambda_{\mathrm{T}} \sin \psi}(\mu + r^2) = \lambda_{\mathrm{r}}(\lambda_{\mathrm{r}} - \lambda_{\mathrm{P}}) \tag{9.19}$$

$$\lambda_{\mathrm{r}}^2 + \left(\frac{\sigma C_{\mathrm{l}_\alpha}}{8Fr} \frac{\mu + r^2}{r + \lambda_{\mathrm{T}} \sin \psi} - \lambda_{\mathrm{P}}\right)\lambda_{\mathrm{r}} - \frac{\sigma C_{\mathrm{l}_\alpha}}{8Fr}(\theta_{\mathrm{b}} - \alpha_0)(\mu + r^2) = 0 \tag{9.20}$$

$$\lambda_{\mathrm{r}}(r, \psi) = \sqrt{\left(\frac{\sigma C_{\mathrm{l}_\alpha}}{16Fr} \frac{\mu + r^2}{r + \lambda_{\mathrm{T}} \sin \psi} - \frac{\lambda_{\mathrm{P}}}{2}\right)^2 + \frac{\sigma C_{\mathrm{l}_\alpha}}{8Fr}(\theta_{\mathrm{b}} - \alpha_0)(\mu + r^2)} - \left(\frac{\sigma C_{\mathrm{l}_\alpha}}{16Fr} \frac{\mu + r^2}{r + \lambda_{\mathrm{T}} \sin \psi} - \frac{\lambda_{\mathrm{P}}}{2}\right). \tag{9.21}$$

Note that Equation 9.21 reduces to the expression derived in [9] (Equation 9.7) in axial flight ($\lambda_T = 0$). The same iteration is required between λ and F.

Obtaining the incremental torque coefficient is straightforward having found λ_r and dC_T. By using a small angle assumption, the profile and induced torque coefficients are found:

$$dC_{Q_p} = \frac{N_b y \frac{d\psi}{2\pi} dD}{\rho(\pi R^3)(\Omega R)^2} = \frac{N_b y \frac{d\psi}{2\pi} \frac{1}{2}\rho V^2 C_d c dy}{\rho(\pi R^3)(\Omega R)^2} = \frac{N_b c}{\pi R}\frac{y}{R}\frac{dy}{R}\left(\frac{V}{\Omega R}\right)^2 \frac{C_d d\psi}{4\pi} = \sigma r dr d\psi \frac{C_d}{4\pi}(\mu + r^2). \tag{9.22}$$

$$dC_{Q_i} = \lambda_r dC_T = \frac{2}{\pi}\lambda_r^2 \lambda_i r dr d\psi = \frac{2}{\pi}\lambda_r^2(\lambda_r - \lambda_P) r dr d\psi \tag{9.23}$$

Integrating the incremental thrust and torque coefficients over the disk yields:

$$C_T = \int_0^{2\pi}\int_0^1 dC_T = \int_0^{2\pi}\int_0^1 \frac{2}{\pi}F\lambda_r\lambda_i r dr d\psi \tag{9.24}$$

$$C_P = \int_0^{2\pi}\int_0^1 dC_{Q_i} + dC_{Q_p} = \int_0^{2\pi}\int_0^1 \left(\frac{2}{\pi}\lambda_r^2(\lambda_r - \lambda_P) + \sigma\frac{C_d}{4\pi}(\mu + r^2)\right) r dr d\psi. \tag{9.25}$$

A sample output of the model for specific operating conditions of the wing rotor is shown in Figure 9.3.
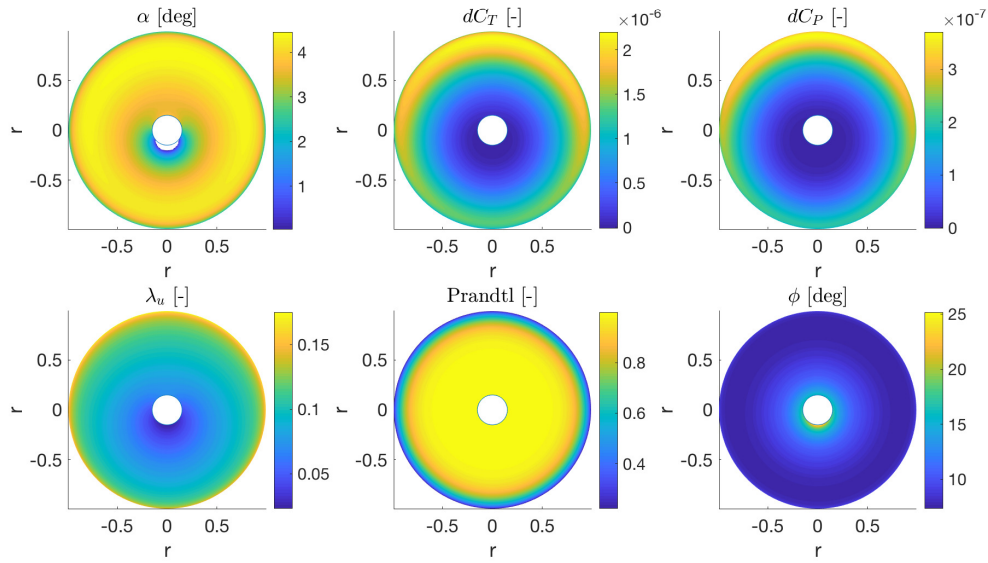

Figure 9.3: Sample output from the BEMT tool for an axial velocity of 10 m/s and tangential velocity of 30 m/s (coming from the left). The rotor is spinning in counter-clockwise direction. The advancing and retreating sides of the disk are clearly visible.

Downwash and Swirl Calculation   The downwash that is created by the propulsion system will be a factor in the social acceptance of a UAM system. It is most critical in the take off phase of the flight. A large downwash disturbs day to day business of an urban environment to a greater extent than a system with a small downwash. Also, it increases the amount of clearance needed around the landing site. Moreover, the downwash from the wing propellers has an impact on the performance of the wing by increasing the local free-stream velocity. Downwash in the vicinity of the rotor (assuming no contraction in the wake) is simply v_i, which is calculated through a mass-flow-weighted average over the rotor disk elements. Lastly, the induced velocity of the rotor is important for a controlled vertical descent of the vehicle. According to Marilena Pavel [11], the following rule of thumb can be used to calculate the maximum rate of descent of the vehicle: for a rate of descent $v_i/4 < V_{desc} < 2v_i$ the rotor enters a Vortex Ring State (VRS) where it ingests its own wake and becomes highly uncontrollable. Beyond $2v_i$ the rotor enters a state of autorotation. Therefore, the maximum rate of descent cannot be larger than one-fourth of the smallest induced velocity between the canard and wing propellers in hover.

Knowing the torque and rotational speed of the rotor, it is possible to calculate the swirl that the rotor creates in its wake. Assuming there is no swirl in the flow ingested by the rotor, the relation between incremental torque on a disk element and the rotational speed it creates in the flow is:

$$dQ = d\dot{m}\omega_s y^2 = \rho(V_\text{P} + v_\text{i})\, y\, dy\, d\psi\, \omega_s\, y^2 \tag{9.26}$$

$$dC_\text{P} = \frac{dQ}{\rho \pi R^3 (\Omega R)^2} = \frac{r^3 \lambda_\text{r}\, dr\, d\psi\, \omega_s}{\pi\Omega} \tag{9.27}$$

$$\omega_s = \frac{dC_\text{P}\pi}{\lambda_\text{r}\, dr\, d\psi\, r^3} \tag{9.28}$$

The resulting rotational speed in the wake is calculated in a similar way as the downwash; by doing a mass-flow-weighted average of ω_s across the disk.

Rotor Drag and Pitching Moment Calculation   Having computed the thrust and torque distribution across the disk as shown in Figure 9.3, it is possible to extract additional forces and moments acting on the rotor hub which play a role in the stability of the aircraft as discussed in Section 9.5. The drag on the rotor is computed by integrating $\frac{dC_\text{P}}{r}\sin\psi$ over the disk. Note that this would result in 0 drag in hover, which is logical.

To compute the rolling moment on the rotor disk one has to integrate $dC_\text{T} r \sin\psi$ over the rotor disk. For the pitching moment the integration is done for $dC_\text{T} r \cos\psi$.

Verification and Validation   The Midterm report presented a verification of the BEMT tool against results from a Free-Vortex Method [9]. To validate the tool, the Harrington 1 and Harrington 2 single rotor parameters [12] form an input for the tool, and the results are compared against experimental data. For the comparison with experimental data, the propeller is simulated at different collective angles and the thrust and power coefficients are calculated. They aer plotted in Figure 9.4 for both the Harrington 1 and Harrington 2 rotors. As can be seen, the agreement is much better than that of Simple Momentum Theory (SMT), which is governed by a semi-empirical equation:

$$C_\text{P} = \frac{\kappa C_\text{T}^{3/2}}{\sqrt{2}} + \left(\frac{\sigma C_{\text{d}_0}}{8}\right) \tag{9.29}$$

where $\kappa = 1.15$ is the rotor-induced power factor and is derived empirically.

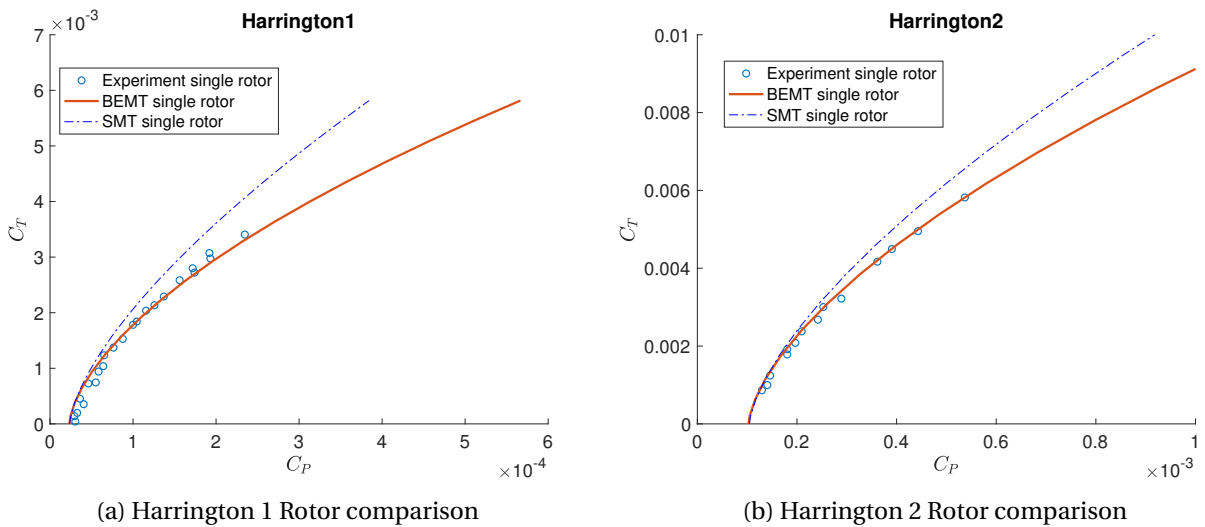(a) Harrington 1 Rotor comparison   (b) Harrington 2 Rotor comparison

Figure 9.4: Validation of the BEMT for a single hovering rotor against measurements of thrust and power. The BEMT significantly outperforms SMT in terms of its empirical-free predictive capabilities

The correct prediction of induced velocities by the BEMT tool is verified by developing a simple downwash tool based on Momentum theory for an isolated rotor. This theory is governed by the equation relating thrust of a rotor and the average induced velocity at the disk:

$$T = 2\rho \cdot A_{\text{rotor}} \cdot (V_{\text{P}} + v_{\text{i}}) \cdot v_{\text{i}}. \tag{9.30}$$

The equation above is insensitive to rotor solidity, blade planform, etc. Nevertheless, there is very good agreement between Momentum Theory and the BEMT as shown in Figure 9.5a.
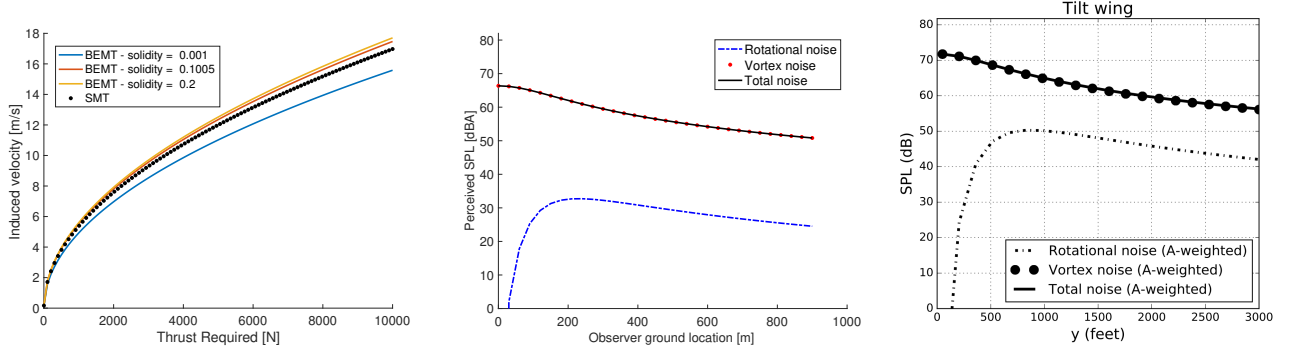
(a) Downwash velocity for different values of thrust required. The output of the BEMT is sensitive to rotor solidity, collective angle and blade design, whilst SMT is only sensitive to rotor area.

(b) Noise footprint of the Bumblebee as a function of observer ground location

(c) Predicted noise footprint of the Airbus Vahana concept in [13] as a function of observer ground location

Figure 9.5: Verification plots for BEMT (downwash) in (a) and Noise tool in (b) and (c), for a constant vehicle hovering height of 152 m

9.1.2. Vehicle Noise

The noise tool implemented for this stage of the project is based on [13], which presents a procedure for estimating harmonic and vortex noise for a rotorcraft in hover.

Harmonic Noise Also referred to as rotational or tonal noise and can be divided into loading noise, which is a direct consequence of thrust generation, and thickness noise, caused by finite rotor blade thickness. What makes this type of noise characteristic is that it is emitted at discrete frequency harmonics of the fundamental frequency (which is ΩN_{b} for a single rotor). Appendix C in [13] derives the Gutin and Deming formulae in equivalent-radius form. They are presented here in final form for brevity:

$$p_{\text{m}_{\text{L}}} = \frac{m_{\text{h}} N_{\text{b}} \Omega}{2\sqrt{2}\pi a(\Delta S)} \left(T\cos\epsilon - Q\frac{a_c}{\Omega R_e^2} \right) J_{mN_{\text{b}}}\left(\frac{mN_{\text{b}}\Omega}{a} R_e \sin\epsilon \right) \tag{9.31}$$

$$p_{\text{m}_{\text{T}}} = \frac{-\rho (m_{\text{h}} N_{\text{b}} \Omega)^2 N_{\text{b}}}{3\sqrt{2}\pi(\Delta S)} c t R_e J_{mN_{\text{b}}}\left(\frac{m_{\text{h}} N_{\text{b}} \Omega}{a} R_e \sin\epsilon \right) \tag{9.32}$$

$$SPL = 10\log_{10}\left[N_r\left(\frac{p_{\text{m}_{\text{L}}}^2 + p_{\text{m}_{\text{T}}}^2}{p_{\text{ref}}^2} \right) \right] \tag{9.33}$$

$p_{\text{m}_{\text{L}}}$ and $p_{\text{m}_{\text{T}}}$ are the root mean square (RMS) sound pressures for loading and thickness noise, respectively. SPL is the sound pressure level (in dB), p_{ref} is a reference sound pressure of 2×10^{-5} Pa, m_{h} is the harmonic number (a positive integer), N_r is the number of rotors, N_{b} is the blade number per rotor, Ω is the rotor angular velocity (which is found in the BEMT tool in an iteration), a_c is the speed of sound, and ΔS is the

distance between the rotor and the observer. T is the rotor thrust, Q is the rotor torque (also coming from the BEMT), and ϵ is the elevation angle (in rad) plus $\frac{\pi}{2}$ between the observer and the rotor hub. ρ is the air density, c is the blade chord and t is the blade maximum thickness. J_{mN_b} is a Bessel function of the first kind of order $m_h N_b$. An effective rotor radius of $R_e = 0.8R$ is recommended in [13] and is an assumption that approximates the integral that should be used for more accurate predictions.

Vortex Noise   Also referred to as broadband noise has a continuous frequency spectrum. A model for vortex noise is derived in Appendix D.A of reference [13], but is only presented in final form here:

$$SPL = 20\log_{10}\left[K_2 \frac{\Omega R}{\rho(\Delta S)}\sqrt{\frac{N_r T}{\sigma}\left(\frac{T}{\pi R^2}\right)}\right] \tag{9.34}$$

$$f_{\text{peak}} = \frac{0.7\Omega R \text{St}}{h} \tag{9.35}$$

where T/A_{rotor} is the rotor disk loading, K_2 is a semi-empirical constant. Although vortex noise is broadband it has a peak frequency f_{peak}, which is a function of 0.7 times the tip speed, the projected blade thickness h and the Strouhal number St. With the peak frequency known, the vortex-noise frequency spectrum is obtained using the method in Appendix D.B of [13].

A-Weighting Scheme   Human ears have different responses at different frequencies. When it comes to social acceptance, it is more fitting to choose dBA as a metric for perceived sound pressure level, since it amplifies sounds being emitted close to 3kHz. Appendices B.C and D.C in [13] give a procedure on how to apply the weighting for tonal and vortex noise, respectively. The A-weighting response which is superimposed on the SPL frequency spectrum in dB to obtain the dBA metric is illustrated in Figure 9.6a.

Atmospheric Attenuation   On top of the procedure for noise prediction outlined in [13], a model for atmospheric attenuation based on frequency of emitted sound and atmospheric parameters is implemented[1]. Figure 9.6b shows the output of the tool as a function of the queried source frequency and atmospheric parameters such as relative humidity.

(a) A-weighting Response

(b) Sound absorption coefficient per atmosphere for air at 20°C according to relative humidity per atmosphere
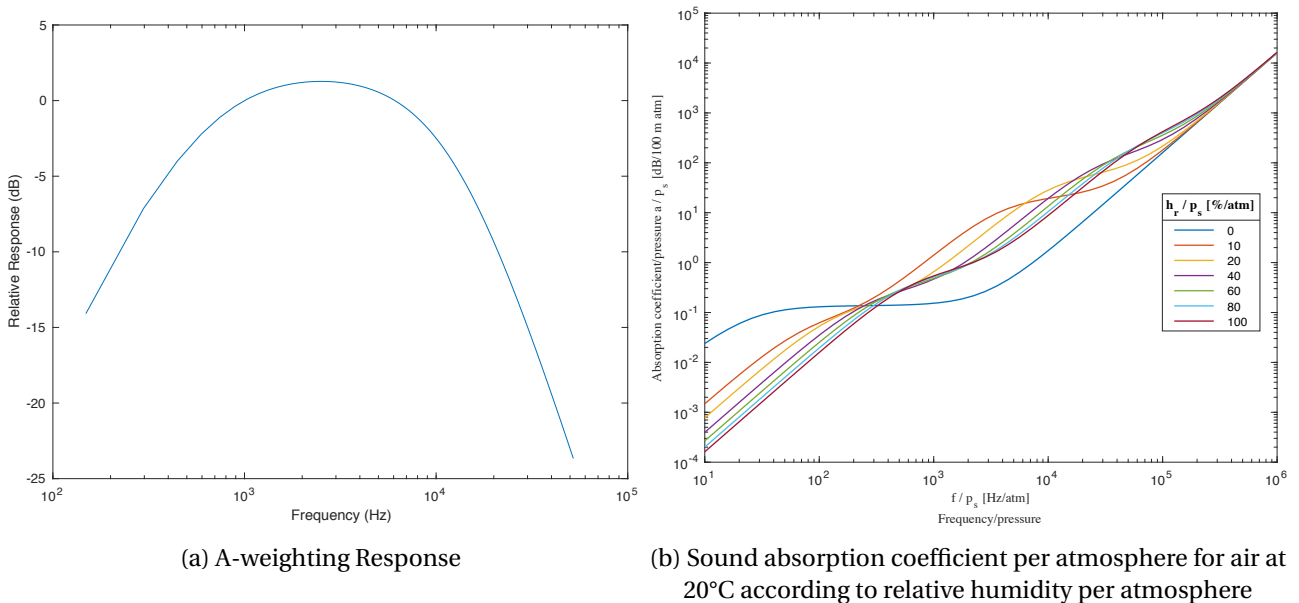
Figure 9.6: A-weighting (a) and atmospheric attenuation weighting (b) applied to the rotor SPL frequency spectrum for both rotational and broadband noise

---

[1]`https://en.wikibooks.org/wiki/Engineering_Acoustics/Outdoor_Sound_Propagation` [accessed 20.05.19]

Limitations

- Blade slap is neglected, under the assumption that the tip Mach number stays below the transonic range (the optimisation discussed later puts a hard penalty on tip mach numbers higher than 0.7).
- The tool does not simulate destructive interference between sound sources. This is a fair assumption only if the sound emitted from these sources is of different frequencies.
- The effect of ground and fuselage interactions/reflectance as well as cabin noise is not modelled.

Verification and Validation   The first mode of verification that is done for the noise tool is a comparison of the order of magnitude of the output with similar vehicles studied in [13]. Even though the blade design is different, the MTOW and rotor area of the tilt-wing concept analysed in [13] (Airbus Vahana) are very similar to that of the Bumblebee concept. The predicted noise signatures are (as expected) within 3 dB of each other.

The second verification method is based on sensitivities. Here it is checked that changes of certain vehicle parameters have the expected impact on the noise signature and its frequency spectrum. For instance, an increase in MTOW should increase the overall noise signature, for the same propulsion system. An increase in solidity should reduce the vortex noise footprint. An increase of tip speed and/or a reduction of blade projected thickness should increase the peak vortex frequency, producing a relatively higher A-weighted noise signature. Some examples of these plots are shown in Chapter 12. Finally, the outputs of the tool for rotational, vortex and total noise for different observer distances and angles (see Figure 9.5b) are compared to the results presented in [13]. A discrepancy is expected since the vehicles being compared are not the same. However, the trend and order of magnitude of the results gives confidence in the correct implementation of the theory presented above. This comparison also shows that vortex noise is predominant and should be mitigated before rotational noise for a vehicle like the Bumblebee.

9.1.3. Propulsion System Optimisation

One of the first trade-offs to make is whether to use fixed pitch propellers or variable pitch propellers (through a collective). The performance benefits of a variable collective versus a fixed collective are shown in Figure 9.7a, where the definition of η_p is given in Equation 9.36. The additional battery mass to be carried on-board (using the battery specifications of the wing propeller circuit) is 20 kg for a fixed collective. However, the additional mass for a variable collective (including the snowball effect discussed in Figure 12.1) would have to be less than 1.6 kg (20/(3 MTOW kg/OEW kg · 4 wing props)) which is unlikely. In addition to this, having additional moving parts, additional actuators and circuits increases failure risks, maintenance costs and in general, the complexity of the propulsion and drivetrain system. Therefore, fixed pitch propellers were finally chosen.

$$\eta_p = \frac{T(V_P + v_i)}{P_{prop}} \tag{9.36}$$

where $T = C_T \rho \pi R^2 (\Omega R)^2$ is the thrust provided by the propeller and $P_{prop} = C_P \rho \pi R^2 (\Omega R)^3$ is the power required by the propeller.
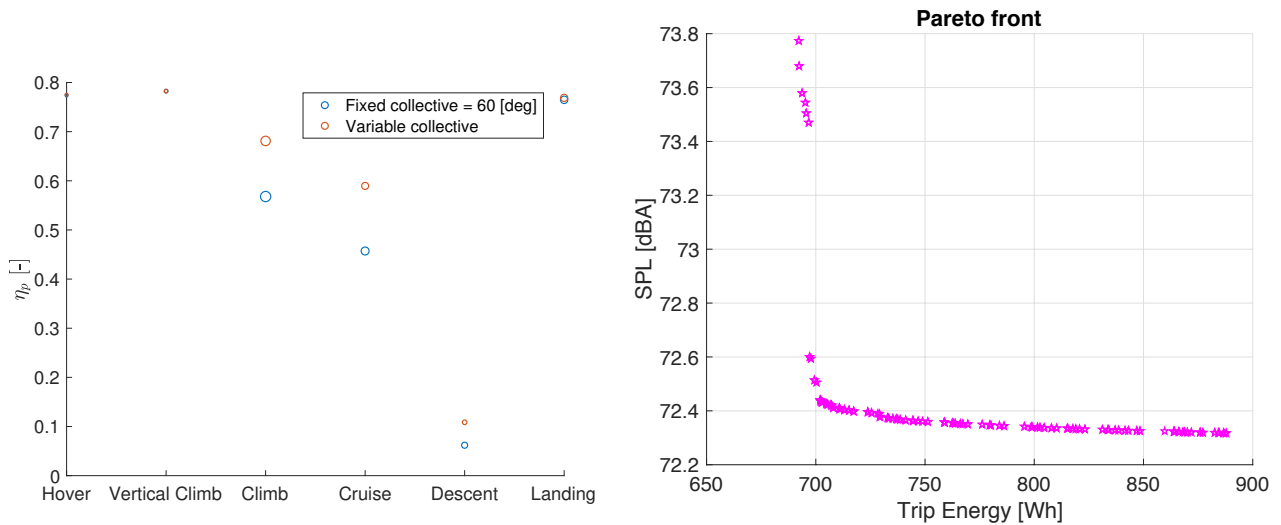
(a) Propulsive efficiency of the wing propellers in all flight phases. Circle size correlates to energy consumption in a particular phase.

(b) Pareto front of the multi-objective optimisation performed by a Genetic Algorithm (GA). The noise objective is plotted on the vertical axis (for an observer distance of 76 m). The energy objective is plotted on the horizontal axis for a typical mission profile.

Figure 9.7: Plots that have guided the propeller design optimisation process

After deciding on a fixed-pitch system for both the canard and wing propellers, an automated multi-objective optimisation framework is developed in MATLAB and integrated with the rest of tools. Thereby, an optimal set of propellers (one for each propulsion unit) could be designed as a function of the mission profile, MTOW and an equivalence factor k_e, which determines which objective to favour. The objectives to be minimised are noise and energy consumption. The design variables to be optimised are rotor solidity, number of blades, root pitch angle (fixed collective setting) and twist (ideal). Since the number of blades is an integer, a Mixed Integer Optimiser[2] is chosen. Upper and lower bounds are put on each of the design variables and a non-linear constraint is added to restrict the minimum allowed chord. The cost function evaluates the noise of the configuration in hover and calculates the power it needs to fly the different phases of the flight profile based on an axial velocity and thrust required, provided for each phase. This power is weighted by the amount of time spent in each phase to end up at an approximate trip energy. Additionally, to prevent the GA from exploiting the limitations of the BEMT tool, a hard penalty is put on configurations which requires a tip mach number higher than 0.7 in any of the flight phases.

The trade-off to be made between noise and energy efficiency of the vehicle for different rotor designs is illustrated in Figure 9.7b for the canard propeller. A higher k_e will favour a low noise design (which would make sense for the canard propeller since it operates for less time than the wing propellers but has a significant impact on the noise footprint in hover) as seen in Figure 9.8.

---

[2]https://nl.mathworks.com/help/gads/mixed-integer-optimization.html [accessed 12.06.19]
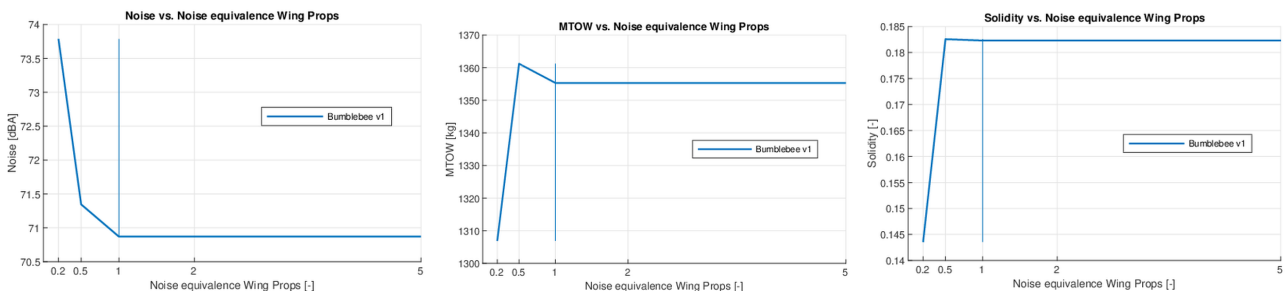
(a) A higher equivalence factor results in a quieter design.

(b) A higher equivalence factor results in a less efficient design (heavier).

(c) A quieter design will usually have a higher solidity, especially if the dominant noise source is broadband

Figure 9.8: Sensitivity plots on the equivalence factor between energy and noise minimisation used to optimise the propeller.

9.1.4. Propulsion System Sizing

Sizing the propulsion system is not only about finding a weight of the propulsion system components, but more importantly, it is used to find the peak power requirements of the vehicle and to calculate the maximum loads on the wing and canard.

The starting point for the sizing is the emergency cases that could occur in case of a failure. The two scenarios with the highest risk are considered: failure of an inboard/outboard propeller on the wing and failure of a canard propeller during hover. A failure in cruise will have to be met with a glide down to a nearby airfield and a belly landing since transition is hard to manage with a failure without over designing the whole vehicle.

The first of the scenarios is dealt with by shutting off the opposite inboard/outboard motor to avoid any net yawing or rolling moments. This implies that the peak thrust of two wing propellers has to be the same as the hover thrust of four. The second scenario implies that a single canard propeller has to be able to carry the load of both.

Technically it might be possible to balance the aircraft if an inboard motor fails with the three remaining wing propellers and the canard propellers although this has been ignored in favour of a more conservative design.

From the maximum thrust required by the propeller, one can find the maximum power $P_{\text{prop,max}}$ that the propeller needs to provide (using BEMT). From this power, the structure of the propeller can be sized based on data. The first empirical method implemented is presented in [14] (Torenbeek adjusted):

$$m_{\text{prop}} = 2.2(RP_{\text{prop,max}}\sqrt{N_{\text{b}}})^{0.52}. \tag{9.37}$$

The weight of the wing propellers based on these statistics is 94 kg combined, which seems like an overestimate by quite a margin considering the weight performance of more modern carbon fibre propellers. A database of carbon fibre fixed-pitch propellers is created based majoritarily on propellers from DUC Helices [3] with power ratings and diameters similar to the wing and canard propellers. A two-dimensional interpolation between power, diameter and mass is performed to obtain the mass of the propellers which is halved for the wing propellers. The choice of carbon fibre blades is thus mainly founded on the lighter design which also results in smaller rotor inertias which are beneficial for differential RPM control.

---

[3] http://www.duc-helices.com/rubrique.php?id_rubrique=76 [accessed 15.06.19]

9.2. Powertrain Subsystem

The powertrain (power and drivetrain) subsystem of the Bumblebee includes all the components necessary to provide power and transfer this power from the source to the propulsion system. The Bumblebee is a fully electric vehicle and is equipped with batteries and electric motors to convert electric energy into mechanical energy. For redundancy and battery design reasons it is chosen to have three main power systems on board. The first one powers the motors on the wings, the second powers the canard propellers and the final is supplies energy to the wing tilt mechanism. Some design decisions that arise are the choice of suitable motors, gearboxes, motor controllers, cables and batteries. The rationale for selecting these components and sizing them is presented in this section.

9.2.1. Drivetrain sizing

The drivetrain is sized directly after the propulsion system and is integrated in the tool such that it does a selection of a combination of off-the-shelf components that both meet the demands of the propulsion system and be as light as possible as well. The inputs that are required by the drivetrain sizing tool from each propulsion unit are:

- Number of motors
- Maximum power required per motor
- Continuous power required per motor

- Maximum torque required per motor
- Continuous torque required per motor

These numbers are used to narrow down the suitable motors and motor controllers from a database of EM-RAX motors and compatible controllers. Motors that cannot provide the peak power or continuous power required are discarded. For the motors that have the sufficient power rating, but not enough torque, a planetary gearbox is sized based on the Willis 1963 method [14] which is a function of the gear ratio, and torque of the motor. The lightest motor controller in the list of compatible motor controllers is selected. Finally, the lightest combination between suitable motor, gearbox (if any) and motor controller is chosen.

Now that the loads of the circuit are known, the cables connecting them to the battery can be sized. The maximum current of the circuit is the minimum between the maximum current of the motor and of the motor controller. This current is used to find the power loss, P_{loss}, with equations Equation 9.39 and Equation 9.38.

$$R_{\text{cable}} = \rho_{\text{copper}} \frac{L_{\text{cable}}}{A_{\text{cable}}} \tag{9.38}$$

$$P_{\text{loss}} = R_{\text{cable}} I^2 \tag{9.39}$$

In these equations R_{cable} is the total resistance in the cable, ρ_{copper} stands for the electrical conductivity of the copper wires, $1.7 \times 10^{-8}\,\Omega\text{m}$, $L_{\text{cable)}}$ is the length of the cabling, a value that varies for each of the three power systems, and A_{cable} is the cross sectional area of the wire. The latter is determined by a fixed cable radius of 0.5 cm. The power losses in the cables is fed into the tool battery sizing as an extra bit of power that must be produced by the battery.

A mass estimation of the cables is found by simply computing the total volume of the cables and multiplying it by the density of copper, 8960 kg/m^3.

9.2.2. Cooling of the motors

The motors can accumulate quite some heat during the operations of the vehicle. It is specified by EMRAX that the motor temperatures must stay within the -40 to 120 degrees Celsius range. The lower bound will not cause any issues, however the upper bound of 120 degrees requires adequate cooling. The motor selected is the air cooled option as this does not require any cooling liquid that has to be taken on board. EMRAX recommends using an airstream of 20 m/s at a maximum of 25 degrees Celsius [15], which matches well with the propeller downwash value of 18 m/s found at hover (based on momentum theory). For cruise, the airspeeds at the motor will likely be higher than the specified 20 m/s by EMRAX, however it is assumed that this will not cause any issues as the motors do not perform at maximum operating powers at this stage of the mission.

9.2.3. Battery sizing

Unlike in the Midterm report, where battery mass estimation is done through an energy and power density linear relationship, the method used in the Detailed Design phase is more elaborate. More constraints are adhered to (such as system voltage and burst power) and an optimal battery architecture and cell selection is performed to ensure an accurate estimation of what is one of the biggest components on the vehicle. The requirements passed to the battery sizing tool (for each main circuit in the vehicle) are the following:

- Maximum energy
- Peak power
- Continuous power

- Motor nominal voltage
- Circuit peak voltage

where maximum energy is calculated for each propulsion unit as explained in subsection 10.4.3, peak power comes from the emergency power required at the propellers, continuous power comes from the power required to hover, motor nominal voltage follows from the selected motor and circuit peak voltage is the minimum between the peak voltage of the motor and motor controller.

The above requirements in addition to a database of existing battery cells, is enough to size the battery pack for each circuit. This is done through a GA, which minimises the number of cells ($n_{\text{series}} \times n_{\text{parallel}}$) in the pack whilst complying with the following constraints:

$$V_{\text{cell}} n_{\text{series}} = V_{\text{circuit}} \tag{9.40}$$

$$n_{\text{series}} n_{\text{parallel}} E_{\text{cell}} V_{\text{cell}} > \frac{E_{\text{max,pack}}}{\eta_{\text{operational}}} \tag{9.41}$$

$$n_{\text{series}} n_{\text{parallel}} E_{\text{cell}} V_{\text{cell}} C_{\text{nom,cell}} > P_{\text{nom,pack}} \tag{9.42}$$

$$n_{\text{series}} n_{\text{parallel}} E_{\text{cell}} V_{\text{cell}} C_{\text{burst,cell}} > P_{\text{max,pack}} \tag{9.43}$$

where V_{cell} is the nominal cell voltage, V_{circuit} is the circuit nominal voltage, E_{cell} is the cell capacity, $E_{\text{max,pack}}$ is the maximum energy required from the pack, $\eta_{\text{operational}}$ is the usable fraction of the battery capacity (67% in our case; since 20% of the capacity never gets charged - for increased life-cycles - and 13% is left for the go-around in case of emergency), $C_{\text{nom,cell}}$ is the nominal C-rate of the cell, $C_{\text{burst,cell}}$ is the burst C-rate of the cell, $P_{\text{nom,pack}}$ is nominal power required from the battery pack, and $P_{\text{max,pack}}$ is the peak power required from the battery. A battery pack is sized using the GA for each of the cells in the database, and the lightest pack is chosen. Some top-level specifications of the three main battery packs in the vehicle, sized with this tool are presented in Section 7.3. The mass breakdown is as shown in Figure 9.9.
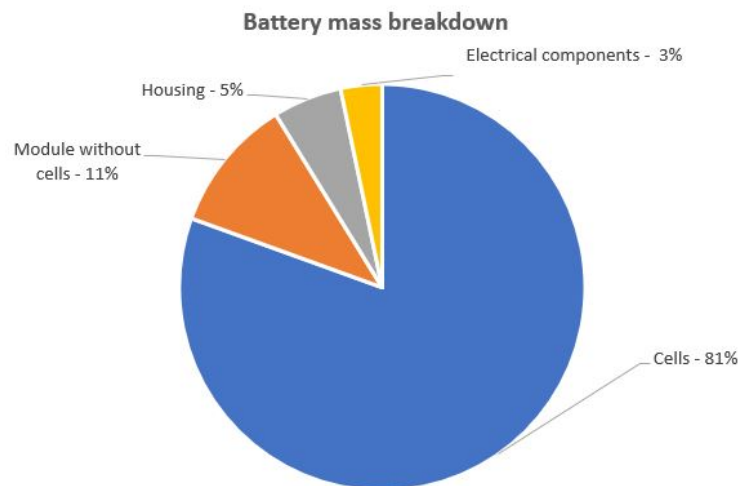
Figure 9.9: Mass breakdown of a reference battery [16]

9.2.4. Failure modes and redundancy

The power subsystem is one of the most vital subsystems that will be on board of the vehicle. Therefore, it is of great importance that the probability of a failure and its consequences, in essence the risks, is minimised as much as possible. Several aspects have been considered to ensure this.

As mentioned before, 3 separate circuits are chosen for the wing rotors, canard rotors and the tilt wing mechanism as these are the most crucial elements in the power system. In case of a failure in between the battery and the motors, for example a cut cable, there must be a method for the system to redirect the power from the malfunctioning cables to the operational part of the circuit. This could be done with the implementation of switches at crucial parts in the circuit.

The device cannot function without one of the propulsion units (especially if a failure occurs during transition). That is why the *battery packs cannot be single points of failure*. Cells have a finite probability of failing which is highly dictated by their operating temperature, the charge level they are stored at, the number of cycles and their DOD%.

For the main battery pack, a single cell failure would result in the loss of 68 operating cells assuming that there is no significant thermal dissipation from the damaged cell (which could onset a thermal runaway of neighbouring cells). The pack would lose 6.3% of its capacity and peak power, which in nominal conditions should not be a problem.

For the canard battery pack the failure of a single cell, if contained, would reduce the capacity and peak power of the battery pack by 14% which without other vehicle subsystem failures is not a problem.

For the tilt-wing mechanism battery, the failure of a single cell would result in a *complete loss of power*, which could be catastrophic in certain flight phases. Therefore, some redundancy needs to be incorporated in the design in the form of switches around each of the cells such that when a cell fails the circuit can be diverted from it.

The above solutions rely on a well-functioning Battery Management System (BMS) which can detect failures and activate switches when necessary. It also relies on sufficient cooling so that the operating temperature of the cells stays within limits. This could be incorporated in the design in the form of air inlets on the side of the fuselage.

9.3. Aerodynamic Characteristics and Thrust and Power Requirements

In this section the calculations of the aerodynamic characteristics are presented. The global goal is to provide thrust requirements to compute power, noise and downwash using the previously introduced BEMT tool (subsection 9.1.1) and the final trip energy using subsection 10.2.1. Versatility is stressed with this tool such that different planforms can be evaluated and the interaction between propeller and wing during cruise and hover are taken into account.

In subsection 9.3.1, an iterative lifting line algorithm for near-straight wings operating behind propellers is discussed after which numerical computations on the fuselage are presented (subsection 9.3.2) and this section concludes with thrust requirements for cruise and hover (subsection 9.3.3 and subsection 9.3.4).

9.3.1. Aerodynamic Analysis of the Wings

As mentioned in the description in Section 5.2, the tools for aerodynamic performance are separate from stability where stability is not included in the main mass iterations and rather analysed in much closer detail on its own (see Section 9.5). While a freely available airfoil and wing tool is used there to estimate coefficients, an integrated lifting line theory is written for use in the mass iterations, offering more flexibility, features and potential for future ideas.

This tool expands the lifting line equations found in [17, p436-469] which are used iteratively, incorporating airfoil characteristics taken from XFOIL via[4] or from JavaFoil[5]. Since swirl and induced velocity estimates are available from Figure 9.1, the equations are modified to include the propeller effect on the wing. Also, a simple method estimating the twisting moment around the tilt axis of the wing is developed.

Limitations   No twist distribution is considered and the effect of the low sweep angle is only considered when integrating the moment arms and not for the actual aerodynamics of the wing.

Wing Definition   The wing and canard are each characterised by their effective span b (excluding the fuselage), their chord distribution following a tapered wing profile with taper ratio λ_w and λ_c, quarter chord sweep $\Lambda_{0.25}$ and surface area S. The wing is discretised along its length using a symmetric grid of k Chebyshev nodes to increase convergence speed near the tip of the wing. Let this grid be called $\underline{\mathbf{y}}^i$. A second grid called $\underline{\mathbf{y}}^{ii}$ using $k+1$ nodes is placed with 2 nodes outside the wing span and the remaining $k-1$ nodes on the geometric mean between every of the original k Chebyshev points. For a visual explanation of this, refer to Figure 9.10.

Initial Circulation Distribution   The method is based on the fundamental Kutta-Joukowski theorem relating local lift to the circulation distribution around an object. The relation can be compactly written as Equation 9.44[17, p.436]:

$$L'(y_n^{ii}) = \rho V_0 \Gamma(y_n^{ii}) \tag{9.44}$$

The iterative lifting line method is based on improving guesses for the circulation distribution Γ on the $\underline{\mathbf{y}}^{ii}$ grid. As an initial estimate, a lift of $L = 0.5\rho V_0^2 S \cdot 2\pi\alpha_{\mathrm{w}}$ is assumed together with an elliptic distribution for lift and circulation distribution: $\Gamma(y_n^{ii}) = \Gamma_0\sqrt{1-(\frac{2y_n^{ii}}{b})}$; matching Γ_0 to satisfy the relationship between L and integral of Equation 9.44.

Effective Angle of Attack   For every element in the grid $\underline{\mathbf{y}}^{ii}$, the effective angle of attack is defined as Equation 9.45:

---

[4] http://airfoiltools.com/, [accessed 12.06.19]
[5] https://www.mh-aerotools.de/airfoils/javafoil.htm, [accessed 25.06.19]
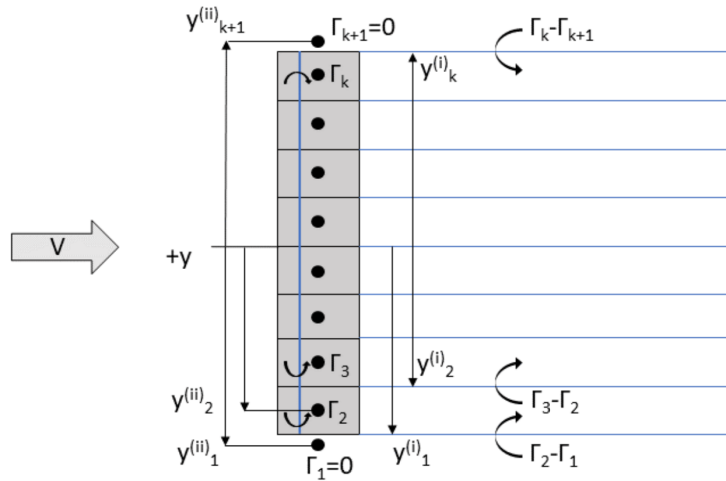
Figure 9.10: Distinction between the two grids $\underline{\mathbf{y}}^i$ and $\underline{\mathbf{y}}^{ii}$. Note that a regular grid is shown, not a Chebyshev grid.

$$\alpha_{\text{eff}}(y_n^{ii}) = \alpha_{\text{w}} + \arctan\left(\frac{w_{\text{i}}(y_n^{ii})}{w_0(y_n^{ii})}\right) \tag{9.45}$$

Where α_{w} is the geometric angle of attack of the wing as measured relative to the root chord line. The vertical induced velocity component $w_{\text{i}}(y)$ (upwards positive) is estimated using the trailing vortexes of the individual horseshoe vortexes evaluated at the $\underline{\mathbf{y}}^i$ grid. This is the first deviation from [17] and important for fast convergence since it categorically eliminates the singularities that would occurs in the denominator of Equation 9.46.

$$w_i(y_n^{ii}) = v_{z_{\text{prop}}}(y_n^{ii}) - \frac{1}{4\pi}\sum_{j=1}^{k}\frac{\Gamma_{j+1} - \Gamma_j}{(y_j^i - y_n^{ii})} \tag{9.46}$$

Note that the circulations at the control points outside the wing (Γ_1 and Γ_{k+1}) are set to zero and merely help making the above formula more compact.

The velocity component aligned with the freestream is simply $w_0(y_n^{ii}) = V_0 + v_{x_{\text{p}}}(y_n^{ii})$. The modelling of the propeller components v_{z_p} and $v_{x_{\text{p}}}$ is discussed later in Equations 9.47 and 9.48.

Propeller-Induced Velocity Components   When applying this method in cruise flight, the effects of the propeller on the wing are quantified by adding components v_{z_p} and $v_{x_{\text{p}}}$ to the local velocities and shown above. Modelling this is done using swirl ω_{s} and induced velocity output v_{i} of the BEMT tool (subsection 9.1.1). The propeller axis is assumed to be on the chordline and close enough to the wing such that wake contraction has negligible effects. Furthermore, the spanwise distance to the vehicle symmetric plane is a design input vector $\underline{\mathbf{y}}_{\mathbf{p}}$ with N_{r} components. Outside of the propeller radius R along the span, quickly decaying exponential functions have been used for the two velocity components to provide continuity.

Equations 9.47 and 9.48 describe the approach for propeller i located at y_{p_i} and a generic spanwise location y at which the interference is evaluated.

$$v_{z_p'}(y) = \sum_{i=1}^{N_r}\begin{cases} -(y - y_{\text{p}_i})\omega_i & |y - y_{\text{p}_i}| \le R_i \\ -R_i\omega_i \cdot sign(y - y_{\text{p}_i}) \cdot \exp(\tau_z \cdot (1 - |y - y_{\text{p}_i}|/R_i)) & (|y - y_{\text{p}_i}| > R_i) \end{cases} \tag{9.47}$$

$$v_{x'_p}(y) = \sum_{i=1}^{N_r} \begin{cases} v_i(|y - y_{p_i}|) & |y - y_{p_i}| \leq R_i \\ v_i(R_i) \cdot \exp(\tau_x \cdot (1 - |y - y_{p_i}|/R_i)) & (|y - y_{p_i}| > R_i) \end{cases} \tag{9.48}$$

Here the function $v_i(r)$ represents radial interpolation from BEMT output.

To arrive at the final values v_{z_p} and v_{x_p} that are aligned with the free stream, a rotation through the angle of attack is performed, but is not shown here for brevity.

Circulation Distribution   The circulation distribution Γ across the $\underline{y}^{ii}$ is updated as Equation 9.49:

$$\Gamma_1 = 0 \quad \Gamma_{k+1} = 0 \quad \Gamma_j = \frac{1}{2} w_0(y_j^{ii}) \cdot c(y_j^{ii}) \cdot C_l(\alpha_{\text{eff}}(y^{ii})_j) \quad j = 2, 3, 4...k \tag{9.49}$$

Here, $c(y_j^{ii})$ is the chord distribution of the wing and $C_l(y_j^{ii})$ is the local lift coefficient interpolated from a table output of JavaFoil.

A numerical damping factor of around $\gamma_{\text{num}} = 0.3$ is introduced when updating the circulation distribution with the just computed value Γ. See equation Equation 9.50.

$$\Gamma_n^s = \Gamma_n^{s-1} \cdot (1 - \gamma_{\text{num}}) + \Gamma_n \cdot \gamma_{\text{num}} \tag{9.50}$$

Lift, Drag and Moment Computations   Once the circulation distribution is converged, lift is computed using the Kutta-Joukowski relation 9.44, numerically integrating over the span. The induced drag is related to the circulation using the product with the induced velocity as described in 9.51 [17, p.442].

$$D_i = \rho V_0 \cdot \sum_{j=2}^{k} (y_j^i - y_{j-1}^i) \cdot \Gamma(y_j^{ii}) \cdot \arctan\left(\frac{w_i(y_j^{ii})}{w_0(y_j^{ii})}\right) \tag{9.51}$$

Profile drag and total drag are estimated using numerical integration as in 9.52, where local profile drag coefficients are read from

$$D_p = \frac{1}{2} \rho \cdot \sum_{j=2}^{k} (y_j^i - y_{j-1}^i) \cdot c(y_j^{ii}) w_0(y_j^{ii})^2 \cdot c_d(\alpha_{\text{eff}})) \tag{9.52}$$

$$D_{\text{total}} = D_p + D_i; \tag{9.53}$$

In a similar way the total moment around the local quarter chords is estimated as:

$$M_{0.25MAC} = \frac{1}{2} \rho \cdot \sum_{j=2}^{k} (y_j^i - y_{j-1}^i) \cdot c(y_j^{ii})^2 w_0(y_j^{ii})^2 \cdot C_{m_{\text{ac}}}(\alpha_{\text{eff}})) \tag{9.54}$$

To arrive at the twisting moment on the tilting mechanism, its position with respect to a fixed point on the wing must be known. For this, the x-offset from the tilt axis to the leading edge of the root chord is chosen Δx_{tilt} and the relation can be formulated as Equation 9.55. This method is similar to the one described in [18, p18] where only the first term of the moment coefficient is considered ($z \approx 0$) and the small angle approximation is assumed to hold such that $\cos \alpha \approx 1$.
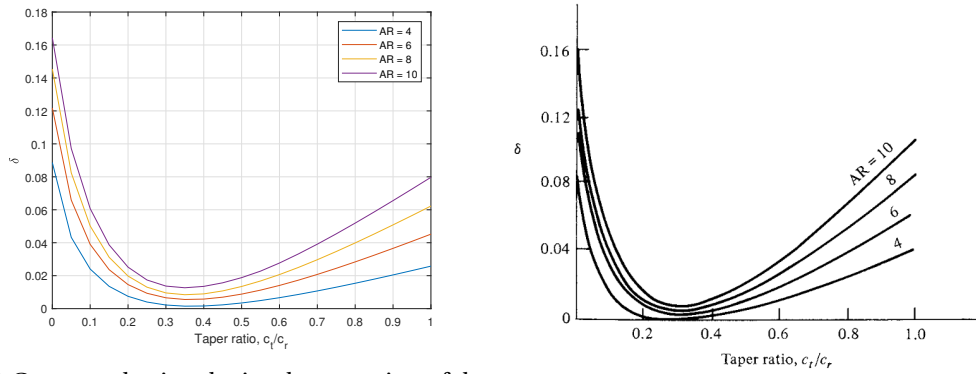
(a) Computed using the implementation of the iterative non-linear lifting line theory

(b) Reference figure from Anderson [17, p452]

Figure 9.11: Custom lifting line implementation largely agrees with textbook results.
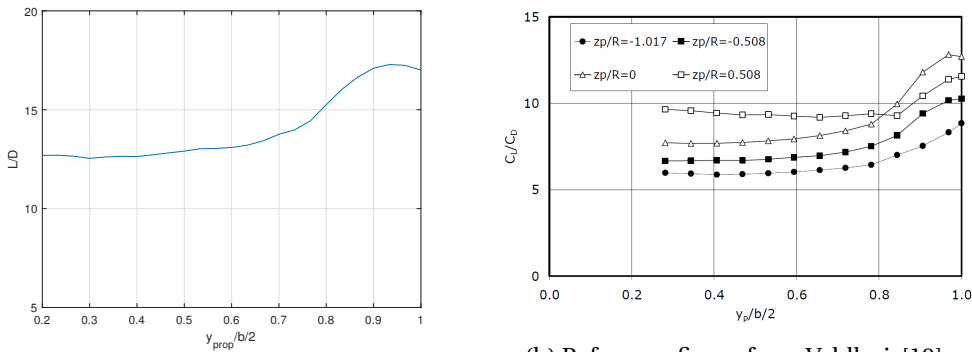
(a) Computed using the implementation of the iterative non-linear lifting line theory

(b) Reference figure from Veldhuis[19].
$z_p/R = 0$ is relevant for comparison

Figure 9.12: Comparison of experimental interaction effects and the adapted lifting line theory shows good agreement in shape. Magnitude was not compared due to lack of data.

$$M_t = M_{0.25\text{MAC}} + \rho V_0 \sum_{j=2}^{k} (y_j^i - y_{j-1}^i) \cdot \Gamma(y_j^{ii}) \cdot |y_j^{ii}| \cdot (-\tan(\Lambda_{0.25}) + \Delta x_{\text{tilt}} - 0.25 \cdot C_r) \tag{9.55}$$

Verification – Basic Lifting Line   The first step in verifying the iterative calculation is by showing that an elliptic planform converges to an Oswald factor $e = C_L^2/(C_D \pi \cdot AR) = 1$ with corresponding lift. After this has been achieved, the function is called using the uniformly tapered wing using different taper ratios λ_w and different aspect ratios AR. The resulting plot 9.11a agrees with 9.11b well for lower taper ratios, but errors persists at high tapers. This could be due to the discretised calculations given larger errors in the high Γ gradient areas near the wingtip. These gradients get more pronounced as the taper ratio increases.

Verification – Propeller Interaction   For certain sets of parameters (low vehicle speed, high propeller pitch, high thrust), the general shape of wind tunnel results from [19]. Not enough characteristic data on propeller operating conditions and geometry is found in the paper so the results are not compared quantitatively. The qualitative comparison is shown in Figure 9.12.

However, when going to higher speeds and lower thrusts, the resulting weighted average swirl from the BEMT computations become negative and the slope of the above plot reverses. Due to negative effective angles of attack near the root of the propeller, the air is computed to swirl the other way near the root, effectively windmilling in this area. This does not comply with the high speed results from [19] and it is clear

that either this method of drag reduction is not beneficial for the operating conditions of the propellers on this vehicle, or the calculation method of the swirl is inaccurate for these conditions. Therefor, the swirl effect is not taking into account in the mass iterations for the vehicle. A recommendation for the future would be a closer analysis of this and other propeller wing effects since it is shown to be very advantageous (around 50% higher L/D) in some cases.

Whether using far outboard mounted propellers results in an overall benefit depends on the structural feasibility as well. Propellers mounted far from the root induce high bending moments during the hover phases which might be limiting for the structure (especially in an inboard-engine-out case) due to the MAC being closer to the root. This dependency needs to be investigated further to reach a trade-off.

9.3.2. Aerodynamic Analysis of the Fuselage

Packaging just 4 passengers in an electrical vertical takeoff and landing ((e)VTOL) vehicle that does not need to be pressurised results in the proposal of a non-circular body with the objective of low drag and interference with the lifting surfaces attached. The body of the vehicle is expected fairly stubby and relatively large compared to the wings which prompted the need for evaluating its aerodynamic behaviour for stability and energy calculations. For long, circular fuselages, estimation schemes for their lift, drag and moment coefficients exist [20], however it did not seem applicable to the present shape. Also, MIT's AVL [6] only supports "slender-body models for fuselages".

It is therefore decided to conduct a standalone CFD analysis of the isolated fuselage to obtain the unknown but important lift, drag and moment forces. Initially, a panel method is preferred for this preliminary computation for ease of setting up and expected speed compared to finite volume methods. The software Caedium[7] is selected as it is acclaimed for its ease of use for beginners and support of the panel method. For a finite wing, results match pressure drag and lift expectation from lifting line theory and airfoil section data quite closely seemingly confirming this approach, but pressure drag for the fuselage returns unrealistically low or negative numbers.

Caedium also supports RANS flow using solvers from openFOAM. However, the obtained numbers must not be taken as final coefficients and contingency measures are taken into account when applying them to energy and stability calculations. Since the CFD knowledge among the members of the group is very low, results are known to depend heavily on chosen turbulence model, parameters and meshing. The pre-set k-omega SST model is chosen and a low turbulent intensity of 0.1% is chosen, since the problem concerns external flow as suggested in[8]. A tet-mesh using a rather modest cell count of $600,000$ elements is chosen to compute more angle of attack cases such that a single simulation ran in approximately 30min on a student laptop.

Also it is decided to not trust the simulation on any details of the vehicle, so only the outside shape of the fuselage is used without wings, propellers and details like landing gear. The resulting number must be understood as fuselage only in subsequent calculations and fuselage interaction with wing and propellers are consciously neglected.

The coefficients that are found in the CFD analysis of the body are shown in Table 9.1. To transform the forces from the CFD to coefficients, they are normalised by $\frac{1}{2}\rho V^2 S$. The moments are normalised by $\frac{1}{2}\rho V^2 S$ $\bar{c}$, with S and $\bar{c}$ both equal to 1. By doing this, the coefficients are only dependent on the dynamic pressure instead of the wing dimensions. The moment coefficient is taken around the centre of gravity of the MTOW configuration. For the calculations for different loading configurations performed in the Stability & Control, the c.g. is moved to their specific x-location by Equation 9.56. The lift and drag relations are later used in the power and energy calculations.

---

[6] http://web.mit.edu/drela/Public/web/avl/
[7] https://www.symscape.com/product/caedium
[8] https://www.cfd-online.com/Wiki/SST_k-omega_model

$$C_{m_{y_b}}(x) = C_{m_{y_b}}(MTOW\,c.g.) - \Delta cg_x \cdot C_{L_b} \tag{9.56}$$

Table 9.1: Fuselage coefficients from coarse RANS flow

C_{L_b}	$0.054 \cdot \alpha - 0.39$
C_{D_b}	$7.52 \cdot 10^{-4} \cdot \alpha^2 - 0.0092 \cdot \alpha + 0.027$
C_{D_b}	$0.25 \cdot C_L^2 + 0.025 \cdot C_L + 0.024$
$C_{m_{y_b}}$ (MTOW c.g.)	$0.11 \cdot \alpha - 0.29$

(a) C_D - α graph of the body

(b) Cm around the MTOW c.g. at varying angles of attack
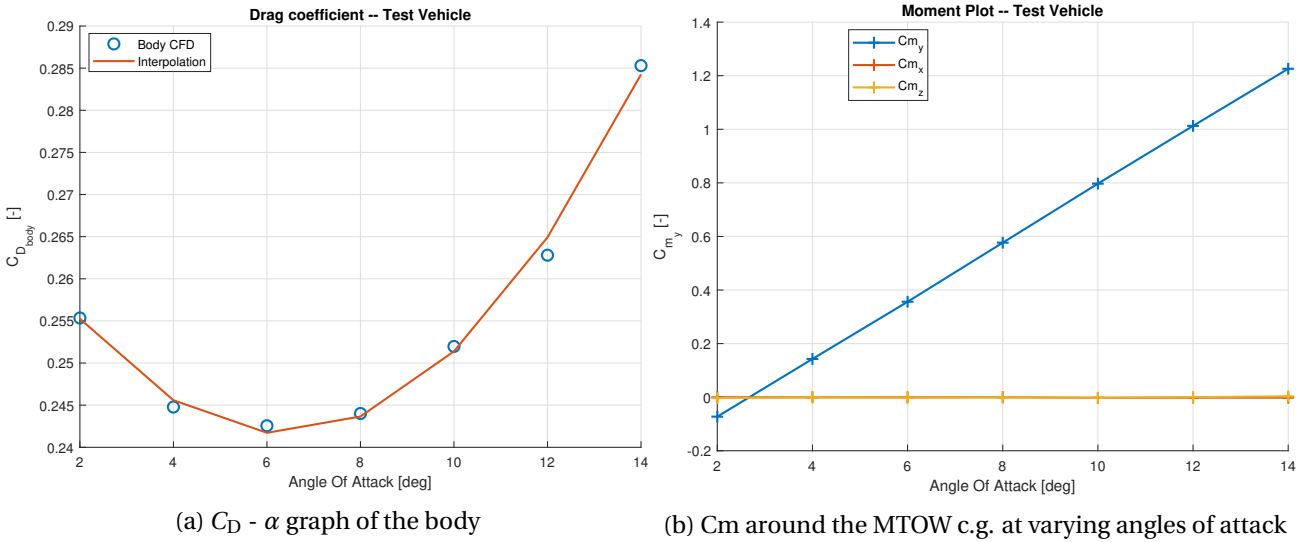
Figure 9.13: Results of the CFD Analysis of the body

As can be seen from Figure 9.13a the drag can be minimised by flying at a certain angle of attack. From the $C_D - \alpha$ relation it is found that this optimal angle of attack is 6.1°. During cruise, the fuselage is kept at this angle of attack as the main wing and canard can be rotated to get the necessary lift and balance. From the moment relation in Figure 9.13b it can be seen that for positive angles of attack, the body creates a pitch up moment. Because the body will always be close to a 6° angle of attack, this moment will have to be countered by the main wing and canard. This is further explained in Section 9.5 about stability and control. The moments around x and y are zero as expected with a symmetric body and only velocity in x-direction.

9.3.3. Thrust and Power during cruise

Having a tiltable main wing allows keeping the fuselage at its minimum drag angle of attack at different cruise speeds, increasing the efficiency but introducing another variable in the equations. In the following it is explained how longitudinal equilibrium is solved iteratively for the vehicle model incorporating variable wing and canard incidence angles. These results are used in power and energy calculations and can help deriving stability coefficients more accurately and adaptively for future design iterations.

In this section the angles of the wing and canard are given relative to the free air velocity, but because the angle of attack stays constant, the following relations can be determined (Equation 9.57 and Figure 9.29):

$$\alpha_w = \alpha_{\text{body}} + i_w \qquad \alpha_c = \alpha_{\text{body}} + i_c \tag{9.57}$$

By keeping only the angles of attack of the main wing and the canard, together with the thrust of the main wing propellers as variables, a system with three equations and three variables is created. Equations are

set up for the sum of forces perpendicular and parallel to the airflow (respectively Equation 9.58 and Equation 9.59 and the sum of moments around the y axis of the c.g. (Equation 9.60).

The total lift contains the lift of the wing, the canard and the upward part of the thrust of the propellers, due to the angle of attack of the main wing. The drag is straightforward and consists of the drag of the main wing, canard and the body. To obtain steady flight and force equilibria, the total lift should equal the total weight, and the drag equals the horizontal part of the propeller thrust.

The moment equilibrium is defined as pitch up positive and contains the aerodynamic moments of the wing and the body. Here the aerodynamic moment of the canard is assumed to be small and is neglected, the moment of the body is found by the CFD analysis described in subsection 9.3.2. The lift of the wing has a negative contribution to the moment as it is located behind the c.g.. This is compensated by the lift of the canard, which results in both the canard and the main wing producing lift. The propellers also add to the negative moment and the thrust is assumed to act in the aerodynamic center of the main wing. Due to the low position of the canard and the high configuration of the main wing, also the drag of the wings is considered in the moment equilibrium. Finally, the drag of the fuselage is expected to have a small influence in the moment and is neglected.

$$\Sigma L = L_\mathrm{w} + L_\mathrm{c} + sin(\alpha_\mathrm{w}) T_\mathrm{wp} = W \tag{9.58}$$

$$\Sigma D = D_\mathrm{w} + D_\mathrm{c} + D_\mathrm{b} = T_\mathrm{wp} cos(\alpha_\mathrm{w}) \tag{9.59}$$

$$\Sigma M_y(c.g.) = M_\mathrm{ac} + M_\mathrm{b} - L_\mathrm{w} l_\mathrm{ac} + L_\mathrm{c} l_\mathrm{c} - T_\mathrm{wp} cos(\alpha_\mathrm{w}) h_\mathrm{ac} - T_\mathrm{wp} sin(\alpha_\mathrm{w}) l_\mathrm{ac} + D_\mathrm{w} h_\mathrm{ac} - D_\mathrm{c} h_c = 0 \tag{9.60}$$

This system of equations uses the geometric parameters and dimensions of the vehicle as inputs for the calculations of the wing using the previously described lifting line theory (subsection 9.3.1) for forces and moments. The body inputs are the polynomial fits from the CFD analysis. The cruise velocity can be changed, and dependent on the amount of passengers transported by the vehicle the weight of the vehicle can also be adjusted. The optimum cruise speed for our application is the one that maximises range (speed over power is maximised). Figure 9.14a shows this relationship for the two limiting payload situations, using the BEMT tool (subsection 9.1.1) for the power computation.

(a) Mass sensitivity of the optimum cruise speed   (b) Optimal C_L relationship of main wing
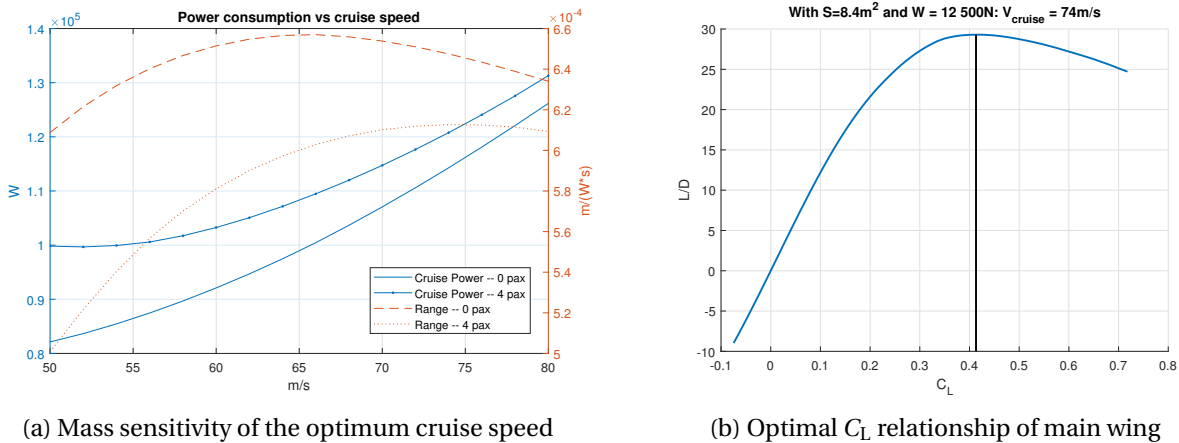
Figure 9.14: Considerations to determine the cruise

It can be seen from Figure 9.14b, that the condition that maximises range can be reached by designing for a cruise C_L of around 0.41. After convergence of the MTOW to a value 25% higher than expected at the midterm and higher than what the stability and control team was using, changes are made to the performance characteristics. At this point in the design process it is already established that stability is sensitive to wing location and it is also found that the sensitivity of the vehicle maximum dimension on vertiport size

requirements and consequently the ticket price is high. In order to not change these aspects of the design, the vehicle speed is increased. Aerodynamic stall speed is 42m/s and is found to be acceptable in transitions since powered lift is available.

The angles of attack of the wing and the canard are outputs, as well as the required thrust of the propellers, which are shown in Table 9.2 for different amounts of passengers. Better estimates would be obtained if the centre of gravity shifts would be taken into account more accurately. Doing this is expected to increase efficiency of the vehicle in empty conditions.

Table 9.2: α_w, α_c, thrust, L/D and total power consumption during cruise different amounts of passengers at the optimum speed for each

Configuration	α_w [deg]	α_c [deg]	Thrust required [N]	L/D [-]	P [kW]
Empty	1.7	4.1	950	8.4	111
1 pax	1.9	4.3	1,020	8.8	116
2 pax	2.0	4.4	1,100	9.0	121
3 pax	2.1	4.6	1,170	9.3	126
4 pax	2.2	4.7	1,250	9.5	131

9.3.4. Thrust and power during hover

Before the vehicle can get into cruise, a vertical take-off and climb is performed. During this hover phase, the balance of the vehicle is obtained by the thrust of the main wing propellers and the thrust of the canard propellers. The wings are tilted up, so the main wing propellers give an upward thrust. Due to the low vertical velocities, the drag during this phase is assumed to be negligible. However, due to the downwash of the main wing propeller, the lift generated by the main wing is considered. The three variables in this phase are the angle of attack of the main wing and the thrust levels of the propellers. The body and canard are assumed to be kept in the same position during this phase. Furthermore, the aerodynamic moments of the wing, canard and body are assumed to be small and negligible.

To go straight up, the sum of forces in x-direction have to be in equilibrium (Equation 9.62). Because the wing generates lift, this force is countered by the x-component of the thrust.

The thrust is dependent on the angle of attack, but because the direction of the airflow is changed due to the propeller, the wing is dependent on the effective angle of attack. The lift is also calculated for this α_{eff}, with the induced velocity behind the propeller (v_i) added to the free stream velocity (V). The equations for this effective angle of attack and new velocity are stated in Equation 9.61. The two velocity vectors are added and the new 'effective' angles and velocities are calculated.

$$V_{\text{eff}} = \sqrt{(V_0 + v_i \cos - \alpha_w)^2 + (v_i \sin - \alpha_w)^2} \qquad \alpha_{\text{eff}} = \alpha_w \cdot \frac{v_i \cos - \alpha_w}{V_0 + v_i \sin - \alpha_w} \tag{9.61}$$

In equation Equation 9.63 the sum of forces in z-direction is shown, which is equal to the weight times an acceleration factor of 1.1 ($T/W = 1.1$). The combined thrust of the main wing propellers and the canard propellers provide the largest part of the thrust, with a small vertical component of the lift pointing downwards for a positive angle of attack.

The third equation considers the moment around the y-axis of the centre of gravity, which has to be equal to zero. Due to the assumptions made at the start of this subsection, the problem is reduced to the wing and canard propeller thrust and the lift of the main wing.

$$\Sigma X = T_{wp} sin(\alpha_w) + L_w cos(\alpha_{eff}) = 0 \tag{9.62}$$

$$\Sigma Z = T_{wp} cos(\alpha_w) + T_{cp} - L_w sin(\alpha_{eff}) = 1.1W \tag{9.63}$$

$$\Sigma M_y(c.g.) = -T_{wp} cos(\alpha_w) l_{ac} + T_{wp} sin(\alpha_w) h_{ac} + T_{cp} l_c + L_w cos(\alpha_{eff}) h_{ac} - L_w sin(\alpha_{eff}) l_{ac} = 0 \tag{9.64}$$

The system of equations is solved to find the thrust of the main and canard propellers. Again, this thrust output is passed to the BEMT tool(subsection 9.1.1) to get the final power values and to the trip energy tool (subsection 10.2.1) to obtain final energy demands for the flightphases.

9.4. Structural Characteristics

This section will focus on the structural design of the vehicle. Firstly, there will be an overview of the load cases that the structure is designed for, after which loading diagrams for the wings will be shown. Based on these two aspects, the sizing of the wing structure and tilt mechanism are elaborated upon. Lastly, there are sections on the fuselage structure and a cost estimation for the vehicle structure as a whole.

9.4.1. Load Factors on Vehicle

Three sets of regulations are researched in order to understand the regulations pertaining to the structural design of the vehicle. The newly proposed eVTOL regulations by EASA [21] do not contain detailed information about the load factor requirements on the vehicle. The CS-23 has detailed information on load factors for small commuter category aeroplanes [22]. The vehicle will likely need to follow these regulations when in cruise flight. The maximum and minimum load factors for the flight profile can be calculated using formulas given in the document. The flight profile includes both the manoeuvring envelope and the gust envelope. The maximum positive load factor is calculated to be 4.3 when a gust of 15 m/s is acting on the vehicle. The vehicle is assumed to be flying at the design cruising speed. The maximum negative load factor is calculated to be -1.5, the vehicle is at the dive speed. The regulations from CS-27 [23] have given the critical conditions during take-off and landing. The vehicle must be able to perform functions near the ground when experiencing wind velocities of 8.6 m/s. These requirements from the regulations are used to determine the structural characteristics of the vehicle.

9.4.2. Free Body and Loading Diagrams

The loads on the wings for the described load cases (factors, tbd) are investigated. They are elaborated upon in this subsections and free body diagrams are created. Next, there is a discussion on the internal moment and loading diagrams.

Free Body Diagrams   The wing can have two configurations (cruise and tilted). Figure 9.15 illustrates the free body diagram of the wing in both of these configurations. The forces and moments are assumed to be acting in the critical loading conditions. The local wing coordinate system is fixed to the centroid of the airfoil. A positive moment is not defined by the right-hand rule. Instead, a positive moment causes tensile stresses in the positive quadrant (indicated by the gray box).

Several aerodynamic and inertial forces can be observed in the free body diagrams. The forces and moments acting on the wing during cruise configuration are lift (L), drag on wing (D), weight of wing (W), torque loading (T), thrust of rotors 1 & 2 ($T1$ & $T2$) and weight of rotors 1 & 2 ($M1$ & $M2$). The lift is assumed to be uniformly distributed in this first order analysis. The uniform lift distribution will overestimate the bending moment caused by the lift at the wing root. In reality, the lift will be less towards the tips as the lift profile will be as elliptical as possible to reduce induced drag. Therefore, the bending moment near the root will be less than currently estimated. Also, the wing weight is assumed to be triangularly distributed.

(a) Wing Configuration During Cruise
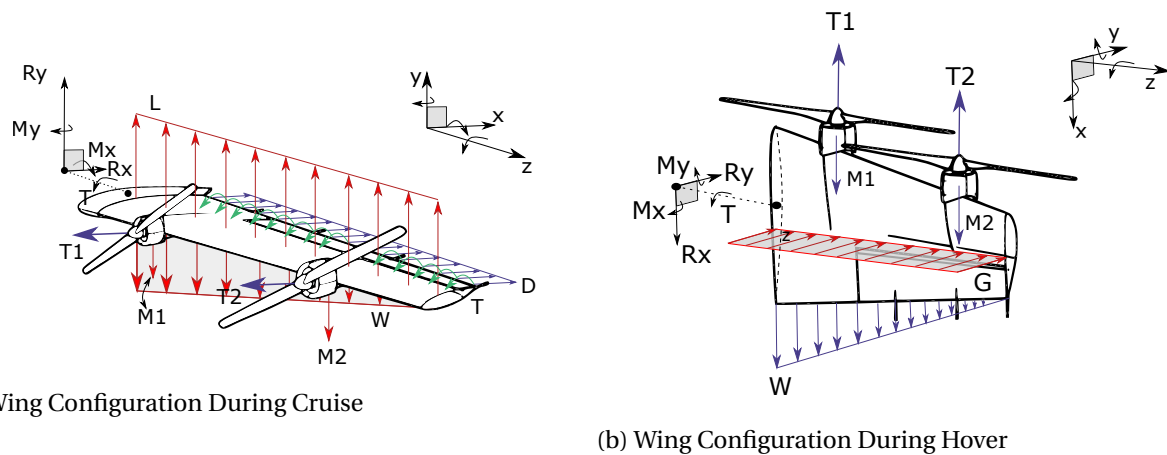
(b) Wing Configuration During Hover

Figure 9.15: Free Body Diagram of Wing

Although the wing does not have significant taper, the wing sections near the root will be significantly heavier than the tip. They have to resist a higher bending moment and extra reinforcements will also need to be added to transfer the loads from the wing to the tilt-wing mechanism. The drag is assumed to be uniformly distributed over the wing. The lift of the wing causes torsion in the wing as it does not act in the shear center of the airfoil. The wing is assumed to have 6 reaction forces and moments to support it. Note that these forces and moments are transferred to the wing-tilt mechanism which transfers it to the fuselage truss structure. The reaction forces and moments are assumed in the positive direction as specified by the coordinate system. The problem is statically determinate. There are six unknown forces & moments, there are 6 equilibrium equations (force and moment equilibrium about all three axes).

A similar force analysis is done in the tilted wing configuration. The coordinate system has rotated with the wing about the z-axis. Rotors 1 and 2 produce lifting forces $T1$ and $T2$. They also have weights $MW1$ and $MW2$. The weight of the wing (W) is assumed to be triangular. A uniform critical gust force is also assumed to be acting on the wing. This force calculated by assuming a drag coefficient of the tilted wing is 1.28, the drag coefficient of a flat plate normal to the flow[9].

Loading Diagrams   The internal forces and moments in the wing are found by traversing along the half-span of the wing and calculating the internal forces and moments necessary to maintain both force and moment equilibrium. These diagrams are shown in Figure 9.16. The first two plots show the internal shear force in the y-direction and the internal moment about the x-axis. Other internal forces and moments also exist on other axes, however the ones shown are considered the most important as they counteract the primary forces of the lift and weight in the wing. Similarly, the lower two plots show the internal shear force along the x-axis and the internal moment about the y-axis. Keep in mind that the coordinate frame rotates with the wing.

Consider the top subplot in Figure 9.16, it illustrates the internal shear force along the y-axis. The lift on the wing is larger than the weight of the wing and the rotors. Therefore, the reaction force at the root are in the negative direction. The internal shear force is positive to maintain equilibrium along the y-axis across the wing. Jumps can be observed at the locations of the rotors. The rotor weights act downwards and thus the internal force must be positive to maintain force equilibrium. The reaction moment is in the negative x-direction. The value of the shear force diagram in the y-direction is equal to the slope of the moment diagram in the x-direction. Both the diagrams have a value of zero at the free-end (tip) of the wing.

Also consider the internal shear force along the x-axis in the tilted configuration (third plot). The reaction force at the root is in the positive x direction (the x axis is pointing downwards). Traversing along the wing, the internal shear force will be negative to maintain force equilibrium in the wing. The jumps can be ob-

---
[9]https://www.grc.nasa.gov/www/k-12/airplane/shaped.html [accessed 24.06.19]

served after at the location of the rotors. The new force of the rotor (rotor thrust minus its weight) also acts in the negative x-direction, this reduces the internal shear force. Furthermore, the slope of the moment in the y direction is equal to the value of the internal force in the x-direction. Both the internal shear force and the internal moment have a value of zero at the tip.
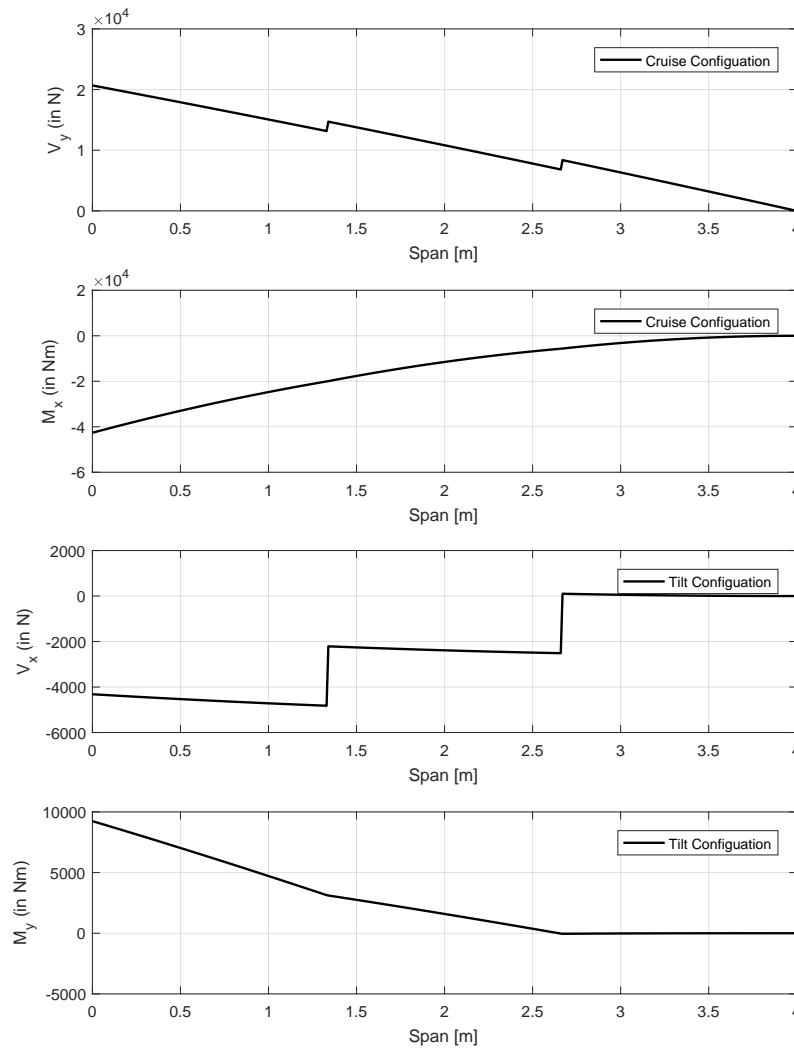
Figure 9.16: Loading Diagram in Tilt Configuration

9.4.3. Wing Mass Estimation

The wing-box structure typically has four components; wing skin, spars, ribs and stringers. The wing skins are primarily loaded in compression (upper skin) and tension (lower skin). They are designed to carry bending and torsional loads.

The initial aim is to create a wing box mass estimator tool. The tool would take inputs such as the internal forces, moments and wing geometry (e.g. span) and calculate the resultant internal stresses. Thereafter, the tool sizes the components to ensure that they do not yield under the limit load. Then, the mass of the

components could be estimated based on their geometry. However, it is realised that creating such a tool would require significant time investment. Instead, the time is used to design other aspects of the vehicle such as the fuselage truss structure or the tilt-wing mechanism.

A wing-box is a very standard component of an aircraft. Therefore, there are already wing box tools which are able to determine the stresses in a wing box and accordingly size the wing box. The structures department decided to use the wing mass tool of the Airbus Vahana project [10]. The Vahana is a urban air mobility project being designed by A^3; the innovation centre of Airbus. There are two reasons why the structures department have decided to use their wing mass tool. First, the tool computes the wing mass using methods and techniques that are also taught at the faculty in the Bachelor's programme. It does not use Finite Element Analysis (FEA) to compute the stresses, instead it discretises the wing into sections and computes the stresses within each section. Secondly, the tool is written in Matlab; this enables it to be integrated with the other tools.

The Vahana software takes several inputs such as MTOW, load factor, percentage of lift carried by lifting surface, geometrical properties of the wing (e.g. span, chord), the location of the motors and the thrust they produce. The program discretises the wing in sections and finds the internal forces and moments in the various wing sections. The program is able to calculate the skin thickness required for both torsion & bending and the shear-web thickness. It assumes that the wing skin and spars are made of composites with the fibres being bi-directional. The ribs are taken to be made of aluminium.

Two adjustments are made to the wing mass program in order to make it more suitable for this design. The wing mass program uses the airfoil shape that would likely be used on the Vahana. This is changed in the Matlab code. It now uses the airfoil chosen for this design. Also, the wing mass program assumes that the lift distribution is elliptical. This is changed and the lift distribution is assumed to be uniform. This is in accordance with the assumption made when drawing the free body and loading diagrams. The drag and torsion distribution is also assumed to be uniform.

The structure of the canard is similar to the wing. It also will be designed as a wing box. Some inputs such as the location of the propellers and span will however change when calculating the mass of the canard.

9.4.4. Tilt Mechanism

The mechanism that is used to tilt the wing in the transition of flight phases is a significant structural component. It is designed as a hollow circular rod. The rod is a carry-through structure from one end of the fuselage to another. This makes the rod lighter but causes the drawback that the wings cannot be tilted independently. This decision is discussed with the Stability and Control department to ensure that the vehicle does not lose its control capabilities. The diameter (d) of the rod is equal to the maximum airfoil thickness at the root. The thickness (t) of the rod depends on the wing bending moments at the root. The cross-section is circular (hence symmetric), also the rod will be made of metal (hence isotropic properties). Therefore, the critical load case is when the wings are in cruise configuration under maximum positive load factor. The load case and cross-sectional properties are shown in Figure 9.17. Designing for this ensures that the rod also is able to withstand the loads under a negative load factor. Also, the loads on the rod in the tilt configuration will be less than in the cruise configuration. This is because the maximum moment at the wing root is higher when the in the critical cruise condition than in the critical tilt condition due to the high positive load factor in the cruise condition.

The thickness t_r of the rod is limited by two constraining factors. The first is to ensure that the stress in the material is less than the yield strength at limit load. However, the beam deflection at the gear should also be limited. Having a large deflection can result in the gear-teeth misaligning with each other. This will lead to the operational failure of the tilt-mechanism. The thickness of the rod is calculated for these constraining cases. The larger thickness is selected as the final thickness.

---

[10], https://github. com/VahanaOpenSource/vahanaTradeStudy [accessed 18.06.19]

(a) Bending of Shaft

(b) Hollow Cross Section
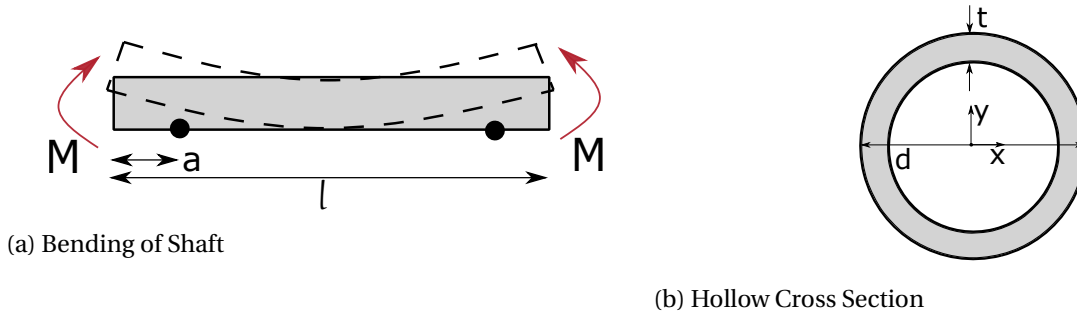
Figure 9.17: Free Body Diagram of Wing

Thickness for Yield Strength Criteria   The flexure formula for bending relates the normal stress due to an internal moment in the structure. It can be rewritten in terms of the thickness of the rod. This is shown in Equation 9.65. Note that the moment of inertia for a hollow rod is equal to $\Rightarrow I_{xx} = (\pi t_{\mathrm{r}} d^3)/8$.

$$\sigma_z = \frac{M_x \rho_t}{I_{xx}} \Rightarrow I_{xx} = \frac{M_x \rho_t}{\sigma_z} \Rightarrow t_{\mathrm{r}} = \frac{8 M_x \rho_t}{\pi d^3 \sigma_z} \Rightarrow t_{\mathrm{r}} = \frac{8 M_x (d/2)}{\pi d^3 \sigma_{\mathrm{yield}}} \tag{9.65}$$

The thickness of the rod can be calculated for the yield strength criteria. Note that this is an iterative process in the MTOW convergence. For instance, a higher maximum take-off weight will result in more lift which will result in a higher bending moment. This will result in a higher rod thickness.

Thickness for Deflection Criteria   Equation 9.66 gives the Euler-Bernoulli equation. This relates the internal moment to the second derivative of the beam deflection along it span. This equation is integrated twice to obtain the expression for the deflection along the span of the rod.

$$\begin{aligned}
M_x = -EI_{xx}\frac{\mathrm{d}^2 v}{\mathrm{d}z^2} &\Rightarrow \frac{\mathrm{d}^2 v}{\mathrm{d}z^2} = \frac{M_x}{-EI_{xx}}\\
&\Rightarrow \frac{\mathrm{d}v}{\mathrm{d}z} = \int \frac{M_x}{-EI_{xx}}dz + C_1\\
&\Rightarrow v(z) = \int \left(\frac{\mathrm{d}v}{\mathrm{d}z} + C_1\right)dz + C_2
\end{aligned} \tag{9.66}$$

The equation has two unknowns, C_1 and C_2, from the integration process. Two boundary conditions must be set to solve for these integration constants. The first boundary conditions assumes that the slope of the beam is zero in the middle; $v'(l/2) = 0$ where l is the length of the rod. The second boundary condition is that the difference in deflection between the bearing and the gear should be less than 1 mm.

Initially, aluminium was the desired choice of material. However, performing the analysis several times has shown that the thickness of the aluminium cross section would need to be larger than the radius of the cross-section. A stronger material needs to be chosen. Therefore, the material of the rod is changed to titanium. The volume of the rod is found by multiplying the cross-sectional area (dependent on the thickness) with the length. Multiplying the volume with the density gives the mass of the rod.

9.4.5. Fuselage structure, Load Paths

The fuselage structure is designed as a 3D truss. The sizing of the truss members is done with the "Direct Stiffness Method". The source [24] is very helpful in explaining the method, it is recommended for further reference. The fuselage truss structure is designed for max positive load factor and a hard landing.

Information on Method Used   The "Direct Stiffness Method" is used to analyse the fuselage truss struc-
ture. This section gives a brief overview of the method. Trusses are assumed to be composed of two-force
members; they either take tensile or compressive forces. Consider Figure 9.18, a truss member can have
forces applied at either end (node 1 and node 2) and consequently, it can also deform at node 1 or node 2.
Furthermore, it can deform from either end.
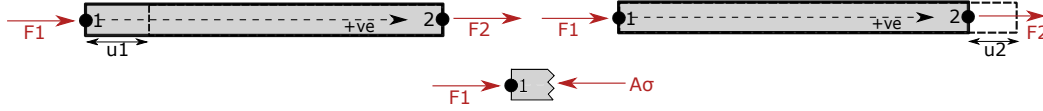
Figure 9.18: The deformation of a truss when forces are applied at the end nodes.

Consider a scenario where the truss member is constrained at node 2 (deformation at node 2 is zero); thus
there is only a deformation δ_1 at node 1. There is a force F_1 acting at node 1 and a force F_2 acting at node 2.
Both these forces act in the local positive coordinate frame. From axial equilibrium $F_1 = -F_2$. The loading
creates an internal normal stress within the truss member. The member is sectioned and axial equilibrium
is applied as in Equation 9.67

$$
\begin{aligned}
F_1 &= EA \cdot \frac{\delta_1}{l} \\
F_2 &= -F_1 = -EA \cdot \frac{\delta_1}{l}
\end{aligned}
\tag{9.67}
$$

Similarly, one can consider the case where the truss member is constrained at node 1; there is only a de-
formation δ_2 at node 2. The same approach is applied of taking the equilibrium of forces. In that case,
$F_1 = -EA \cdot \frac{\delta_2}{l}$ and $F_2 = EA \cdot \frac{\delta_1}{l}$. Lastly, one can consider the case when both ends can deform. The forces
can be found by superimposing the resulting from the above two cases. Therefore, $F_1 = EA \cdot \frac{\delta_1}{l} - EA \cdot \frac{\delta_2}{l}$ and
$F_2 = -EA \cdot \frac{\delta_1}{l} + EA \cdot \frac{\delta_2}{l}$. The results are expressed in a matrix notation:

$$
\begin{bmatrix} F_1 \\ F_2 \end{bmatrix} = \underbrace{\frac{EA}{l} \begin{bmatrix} 1 & -1 \\ -1 & 1 \end{bmatrix}}_{\text{local member stiffness matrix}} \begin{bmatrix} \delta_1 \\ \delta_2 \end{bmatrix} \Rightarrow \underline{F}^{(i)} = \underline{\underline{k}}^{(i)} \, \underline{\delta}^{(i)}
\tag{9.68}
$$

The above expression relates the forces that can act on the member with the deformations that the truss
member experiences. The above expression is analogous to the force-stiffness relationship $F = k\delta$. There-
fore, the first matrix is known as the "member stiffness matrix". Note that in the term $\underline{\delta}^{(i)}$, the i refers to the
fact that the displacements are in the local truss member coordinate frame.

Each member in the truss will have its own force-displacement relation. However, these relations will be
in the local coordinate frame. Both the forces and the displacements must be transformed to the global
coordinate frame of the entire truss. This is done using the "displacement transformation matrix" and the
"force transformation matrix". The "displacement transformation matrix" is denoted by $\underline{T}$. It relates the
global coordinate matrix ($\underline{\delta} = [x \; y \; z]^T$) to the local coordinate frame $\Rightarrow \underline{\delta}^{(i)} = \underline{T} \, \underline{\delta}$. The "force displacement
transformation matrix" transforms the forces from the local coordinate frame ($\underline{F}^{(i)}$) to the global coordinate
frame ($\underline{F}$) $\Rightarrow \underline{F} = \underline{T}^T \, \underline{F}^{(i)}$. The global member load displacement relation can found as follows:

$$
\underline{F} = \underline{T}^T \, \underline{\underline{k}}^{(i)} \, \underline{\delta}^{(i)} = \underline{T}^T \, \underline{\underline{k}}^{(i)} \, \underline{\delta}_i = (\underline{T}^T \, \underline{\underline{k}}^{(i)} \, \underline{T}) \, \underline{\delta}
\tag{9.69}
$$

The term in brackets is known as the "global member stiffness matrix", it essentially gives the stiffness matrix of a particular member in the global coordinate frame. The stiffness matrix for the entire truss (known as the "assembled stiffness matrix") is the sum of the global stiffness matrices for the individual members. The assembled stiffness matrix is denoted by $\underline{\underline{K}}$. The load displacement relationship for the entire truss can be written as $\underline{F}_T = \underline{\underline{K}}\,\underline{\delta}_t$. Some nodes in the truss can be constrained to move (support reactions). These can be incorporated in the load-displacement relationship. The system can be solved to obtain the deformations and the forces within the truss members. An extensive explanation of this method is given in [24].

An assumption of this method is that the truss members are only subjected to axial forces. They are not subjected to moments. This assumption will underestimate the loads acting on the truss members.

Load Cases and Optimisation   The "Direct Stiffness Method" tool is incorporated into Matlab. This is done with the help of resource [11]. The truss structure is loaded in the tool. The initial truss structure was designed in a 3D CAD Software (Rhinoceros), shown in Figure 9.19. The wing-box rests on top of the truss structure as the vehicle is a high-wing configuration. The truss structure is incorporated into Matlab by specifying the coordinates of the points and which points connect with each other.
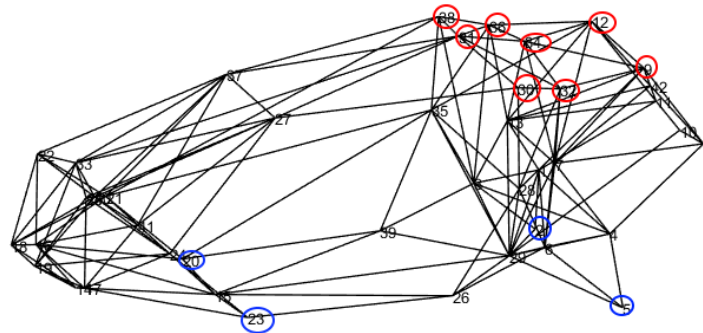
Figure 9.19: Fuselage Truss Structure

Two load cases are investigated for the stress and mass estimation of the truss structure. The first case is when the vehicle is under the maximum positive load factor. This occurs due to gusts acting on the vehicle. A safety factor of 1.5 is also applied. The attachment points with the wing are constrained to move in all 3 directions (x, y and z). This is denoted by the red circle around the points. The loads of the batteries, passengers and cargo are distributed at relevant nodes in the fuselage structure by placing a force in the negative z-direction. Also, weight of the links is distributed evenly at both nodes. Thus the weight of the link going from node 1 to node 2 is evenly distributed between node 1 and node 2.

The second load case is a hard landing. The nodes of the landing gear and their connections are constrained to move. A landing load factor of 1.5 is assumed during landing. This is not the same as the total load factor. The total load factor on the vehicle is 2.5 (1 + landing load factor). This is the typical load factor for conventional aircraft when landing, obtained from [25]. A safety factor of 1.5 is also applied. Because the vehicle is VTOL, the load factor at landing will be less than the load factor for a conventional aircraft. However, in the improbable but critical case when the vehicle performs a conventional landing (due to wing-tilt failure), the landing gear is designed to sustain the initial vertical landing dynamic load.

A stress-margin minimisation algorithm is built into the Matlab tool. All links are given an initial cross-sectional area of 1,000 mm^2. The links are assumed to be made of aluminium (Al 2014) due to its light weight. The stresses in the members are calculated. If the stresses in the members are higher than the ultimate strength, the cross-sectional area is increased. If the stress in the members are lower than the ultimate

---

[11]https://nl.mathworks.com/matlabcentral/fileexchange/68337-finite-element-analysis-fea-of-2d-and-3d-truss-structu
   [accessed 18.06.19]

strength, the cross-sectional area is decreased. This increase or decrease is done in a controlled and damped method using a learning rate of 0.10. The new area for a particular member in the truss is:

$$A_{\text{new}} = (1 - 0.10)\, A_{\text{old}} + 0.10 \cdot \frac{\max(|\sigma_1|, |\sigma_2|)}{\sigma_{\text{ult}}} \cdot A_{\text{old}} \tag{9.70}$$

The term σ_1 represents the stress due to the first load case, σ_2 represents the area due to the second load case. The term σ_{ult} is the ultimate strength, which is equal to 483 MPa [12]. All members in the fuselage structure are manufactured out of aluminium. The mass of the truss structure is found by multiplying the cross-sectional area of each link with its length to obtain the volume; this is then multiplied with the material density.

The method used has two drawbacks. Firstly, only two critical loading cases are considered; max positive load factor under gust and hard landing. More load cases must be considered to properly size the truss structure. There are some links in the structure which have a very small mass because they are zero force members in the structure. However they will carry some loads if a different loading types, this also has to be considered. Also, the trusses are assumed not to be able to transfer moments. This is not true in reality as the truss members will likely be welded together. This will allow them to carry moments as well. The truss structure will therefore become lighter. Notice the offsetting effects of the drawbacks. Analysing more load cases will likely increase the mass of the structure as some zero force members (which have negligible mass) will start taking loads. This will increase their mass. However, in reality the truss members can also carry moments which make the members lighter.

9.4.6. Impact of Material Choices on Sustainability

The choice of material can significantly impact the sustainability of the final design. The main two factors that are considered are the weight of the final structure and the recyclability of the design. Reducing the weight of the material reduces the amount of energy needed for a trip and hence improves environmental sustainability. Having a material that can be recycled at the end of life naturally improves the sustainability of the design as well, as newly manufactured parts can be made from the scrap that is left after a vehicle has ended their service life.

As mentioned before, the fuselage truss structure and spars and ribs of the wing will be made out of aluminium. Next to the fact that this is a light metal and weldable material, it is also recyclable. At the end of the vehicle's life the aluminium will be used to create the next generation vehicles or will be sold on to metal recycling companies. The composites that will be used in the wing skin and fuselage shell are not trivial to recycle at the present time. Therefore their usage is kept to a minimum. The fact that they are used in the vehicle, is thought to be justified by the weight savings that they provide to the entire vehicle.

9.5. Stability, Control & Autonomy Characteristics

This section begins with determining the c.g. ranges for various loading configurations during hover and cruise, subsection 9.5.1. This is followed up by analysis into static and dynamic longitudinal stability in subsection 9.5.2 and subsection 9.5.3 respectively. Next, artificial stability and control methods are elaborated upon in subsection 9.5.5 and the section is closed off with subsection 9.5.6, which contains the method in which autonomy is integrated into the system.

9.5.1. Loading Diagram

Locating the position of the centre of gravity (c.g.) is one of the primary tasks to be executed. In order to do so, the c.g. location and mass of every main vehicle component needs to be estimated, after which they are

---

[12]http://asm.matweb.com/search/SpecificMaterial.asp?bassnum=MA2014T6 [accessed 24.06.19]

inserted into Equation 9.71 to determine the shift of the c.g. due to that particular vehicle component. Once all vehicle components (see Table 7.2) have been added, the c.g. of the entire vehicle at OEW is determined.

$$\bar{x}_{\text{cg}_{\text{new}}} = \frac{m_{\text{comp}} \bar{x}_{\text{cg}_{\text{comp}}} + m_{\text{old}} \bar{x}_{\text{cg}_{\text{old}}}}{m_{\text{comp}} + m_{\text{old}}} \tag{9.71}$$
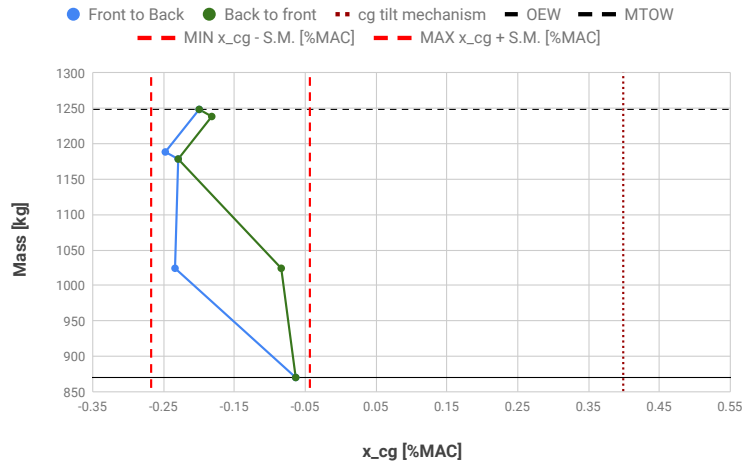
Figure 9.20: Loading diagram in hover configuration

After the c.g. location at OEW is found, the shift in c.g. due to payload loading in the various loading procedures is determined. For this, Equation 9.71 is used again, leading to the c.g. location at MTOW. The shifts due to loading in hover configuration can be seen in Figure 9.20.
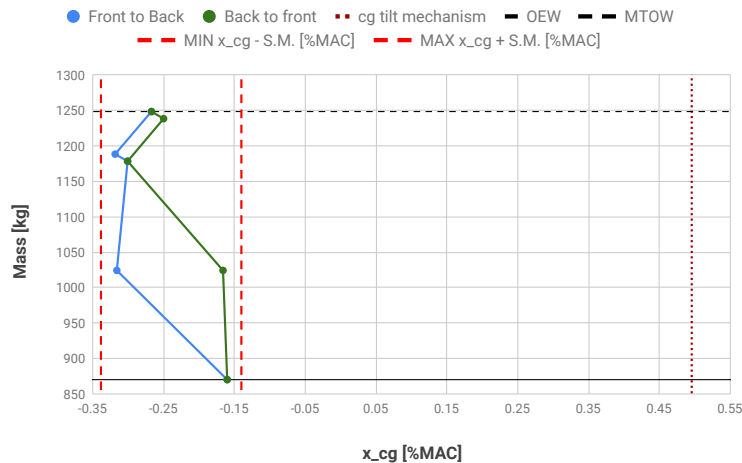
Figure 9.21: Loading diagram in cruise configuration

Furthermore, one should acknowledge the difference between the c.g. location in hover and the c.g. position in cruise due to tilting of the main wing. For this reason, loading with the c.g. position in cruise configuration is analysed as well and can be seen in Figure 9.21. The c.g. location for different passenger configurations must also be analysed as the vehicle is quite small resulting in high c.g. shifts if the vehicle is not loaded until MTOW. Furthermore, this is done in order to establish the critical loading configuration and also identify possible loading configuration(s) which are not feasible. In cruise configuration, the most aft possible c.g. is found to be at -0.10 [MAC] when only cargo in the back is loaded. The most forward c.g. is achieved when two passengers are sitting in the front row and cargo is only loaded in the front and is equal

to -0.34 [MAC]. Furthermore, the x_{cg} at MTOW is at -0.27 [MAC]. Some of these loading configurations are deemed unfeasible and are elaborated upon in subsection 9.5.2

9.5.2. Static Longitudinal Stability

Trim Analysis Before starting analysis into the static stability of the vehicle, ensuring equilibrium of moments in cruise is convenient as consequently, the trim point is determined. For this, Equation 9.72 is used to determine the moment coefficient of an aircraft at varying angles of attack with Equation 9.73 and Equation 9.74 as the moment coefficients induced by the aircraft-less canard and the canard, respectively.

$$C_M = C_{M_{A\text{-}c}} + C_{M_c} \tag{9.72}$$

$$C_{M_{A\text{-}c}} = C_{m_{y_b}} \frac{S_b l_b}{S\bar{c}} + C_{m_w} - C_{L_w}(x_{ac_w} - x_{cg}) + T_c \frac{8d_{wp}^2}{S\bar{c}}(z_{ac_w} - z_{cg})\cos\alpha_{off_w} + T_c \frac{8d_{wp}^2}{S\bar{c}}(x_{ac_w} - x_{cg})\sin\alpha_{off_w} \tag{9.73}$$

$$C_{M_c} = C_{m_c} \frac{S_c \bar{c}_c}{S\bar{c}} + C_{L_c} \frac{S_c(x_{cg} - x_{ac_c})}{S\bar{c}} \tag{9.74}$$

By implementing the various parameters seen in Table 9.3, Table 9.4 and Table 9.5 for the main wing, canard wing and thrust generated by the main wing propellers, and Table 9.1 and Equation 9.56 for the parameters of the body in Equation 9.73 and Equation 9.74, one ends up with the moment curves seen in Figure 9.22 around x_{cg} at MTOW. The trim condition at MTOW is thus found to be at an angle of attack of 1°. Performing this analysis around various c.g. positions results in Figure 9.23. The aerodynamic coefficients of the wing and canard are estimated using JavaFoil and the DATCOM method. Furthermore, this analysis is performed around the maximum aft c.g. and the most forward c.g. in order to determine the range of trimmed angles of attack.

Table 9.3: Parameters of the trim analysis 1

Parameter	Value	Unit
x_{ac_w}	3.2	m
z_{ac_w}	1.1	m
z_{cg}	0.92	m
α_{off_w}	0	°
α_{off_c}	3	°
α_{off_b}	6	°

Table 9.4: Parameters of the trim analysis 2

Parameter	Value	Unit
S	8.4	m^2
S_c	1.1	m^2
d_{wp}	1.4	m
$\bar{c}$	1	m
$\bar{c}_c$	0.4	m

Table 9.5: Main wing, canard wing and thrust coefficients [deg]

C_{m_w}	-0.028 - 0.001 α
C_{m_c}	-0.001 α
C_{L_w}	0.18 + 0.08 α
C_{L_c}	0.082 α
T_c	-0.036

As can be seen in Figure 9.23, the C_{M_α} around the maximum aft c.g. (green line) is positive, which indicates an unstable vehicle. Thus, finding the most aft c.g. around which the C_{M_α} is negative is crucial. This is found to be at x_{cg} = -0.24 [MAC] (blue line). The C_M around the x_{cg} at MTOW is also analysed and can be seen as the yellow line in Figure 9.23. Last but not least, the C_M around the most forward c.g. can be seen as the red line and has a negative C_{M_α}.
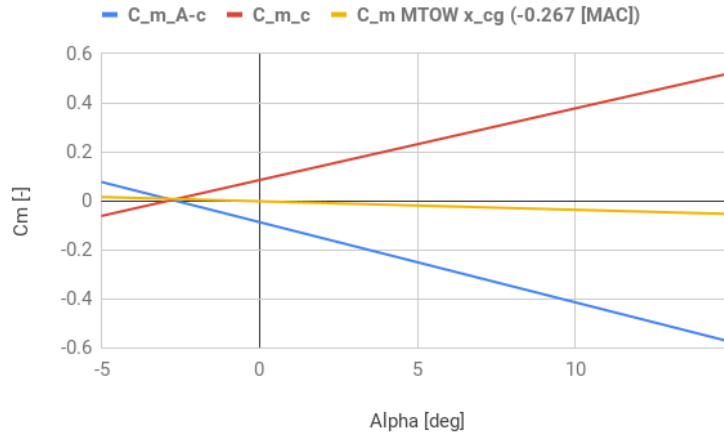
Figure 9.22: Moments generated by aircraft-less canard and canard wing of the aircraft
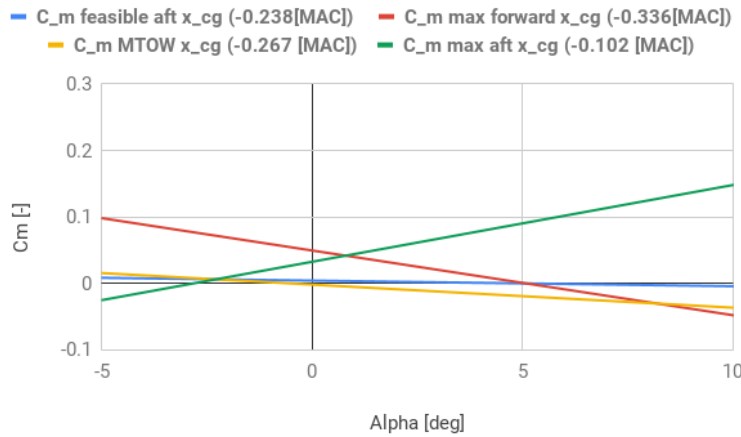
Figure 9.23: Trim analysis around various x_{cg} locations

Stability Analysis Now the trim point is determined, the next step is to analyse the stability of the vehicle. An aircraft is said to be stable if at any point in time the aircraft would return to its equilibrium position after a disturbance has occurred, which happens when the aircraft has a negative C_{M_α}. For this analysis, the critical point is to be used which in this case is any point in the transition phase. However, in the transition phase, the vehicle is in the process of tilting the wing into cruise mode. This stability analysis is done in Equation 9.5.3.

In this stability analysis, a point in cruise is chosen to be analysed, as the vehicle has a very low cruise velocity, meaning no shockwaves occurring throughout the entirety of the velocity range. For this, the neutral point of the vehicle would have to be behind the c.g. of the vehicle, as the change in lift due to an increase in angle of attack acts through the neutral point, causing a negative (pitch down) moment. In order to ensure that this requirement is met, a stability margin (s.m.) of 0.05MAC is taken into account, see Equation 9.75 [26].

$$\bar{x}_{cg} = \bar{x}_{np} - \text{s.m.} = \bar{x}_{ac} + \frac{C_{L_{\alpha_c}}}{C_{L_{\alpha_{A-c}}}} \left(1 - \frac{d\varepsilon}{d\alpha}\right) \frac{S_c l_c}{S\bar{c}} \left(\frac{V_c}{V}\right)^2 - \text{s.m.} \tag{9.75}$$

Rewriting Equation 9.75 to get the ratio of canard wing surface area over main wing surface area leads to Equation 9.76. Using Equation 9.76 by implementing the various aircraft parameters at different horizontal

c.g. positions leads to the blue line seen in Figure 9.24.

$$\frac{S_\text{c}}{S} = \frac{1}{\frac{C_{L_{\alpha_\text{c}}}}{C_{L_{\alpha_\text{A-c}}}} \left(1 - \frac{d\varepsilon}{d\alpha}\right) \frac{l_\text{c}}{\bar{c}} \left(\frac{V_\text{c}}{V}\right)^2} \bar{x}_\text{cg} - \frac{\bar{x}_\text{ac} - \text{s.m.}}{\frac{C_{L_{\alpha_\text{c}}}}{C_{L_{\alpha_\text{A-c}}}} \left(1 - \frac{d\varepsilon}{d\alpha}\right) \frac{l_\text{c}}{\bar{c}} \left(\frac{V_\text{c}}{V}\right)^2} \tag{9.76}$$

Controllability   Apart from the stability analysis, the controllability of the vehicle is analysed as well. For this, Equation 9.77 is rewritten into Equation 9.77, after which it is rewritten again into Equation 9.78 to determine the ratio between canard wing surface area and the main wing surface area needed to maintain moment equilibrium.

$$\bar{x}_\text{cg} = \bar{x}_\text{ac} - \frac{C_{m_\text{ac}}}{C_{L_\text{A-c}}} + \frac{C_{L_\text{c}}}{C_{L_\text{A-c}}} \frac{S_\text{c} l_\text{c}}{S\bar{c}} \left(\frac{V_\text{c}}{V}\right)^2 - \frac{C_{m_\text{b}}}{C_{L_\text{A-c}}} - \frac{T_\text{c}}{C_{L_\text{A-c}}} \tag{9.77}$$

Implementing the range of c.g. positions, aerodynamic parameters and vehicle parameters into Equation 9.78 leads to the red curve seen in Figure 9.24.

$$\frac{S_\text{c}}{S} = \frac{1}{\frac{C_{L_\text{c}}}{C_{L_\text{A-c}}} \frac{l_\text{c}}{\bar{c}} \left(\frac{V_\text{c}}{V}\right)^2} \bar{x}_\text{cg} + \frac{\frac{C_{m_\text{ac}}}{C_{L_\text{A-c}}} - \bar{x}_\text{ac}}{\frac{C_{L_\text{c}}}{C_{L_\text{A-c}}} \frac{l_\text{c}}{\bar{c}} \left(\frac{V_\text{c}}{V}\right)^2} + \frac{\frac{C_{m_\text{bod}}}{C_{L_\text{A-c}}}}{\frac{C_{L_\text{c}}}{C_{L_\text{A-c}}} \frac{l_\text{c}}{\bar{c}} \left(\frac{V_\text{c}}{V}\right)^2} + \frac{\frac{C_{m_\text{Thrust}}}{C_{L_\text{A-h}}}}{\frac{C_{L_\text{c}}}{C_{L_\text{A-c}}} \frac{l_\text{c}}{\bar{c}} \left(\frac{V_\text{c}}{V}\right)^2} \tag{9.78}$$

Scissor Plot   By plotting the ratios of canard surface area over main wing surface area from the stability and controllability analyses, one arrives at the scissor plot as seen in Figure 9.24. Furthermore, Figure 9.24 shows that the c.g. position and canard surface area lie in between the controllability and stability curves, which means that the vehicle is both stable and controllable within the c.g. range at full capacity.
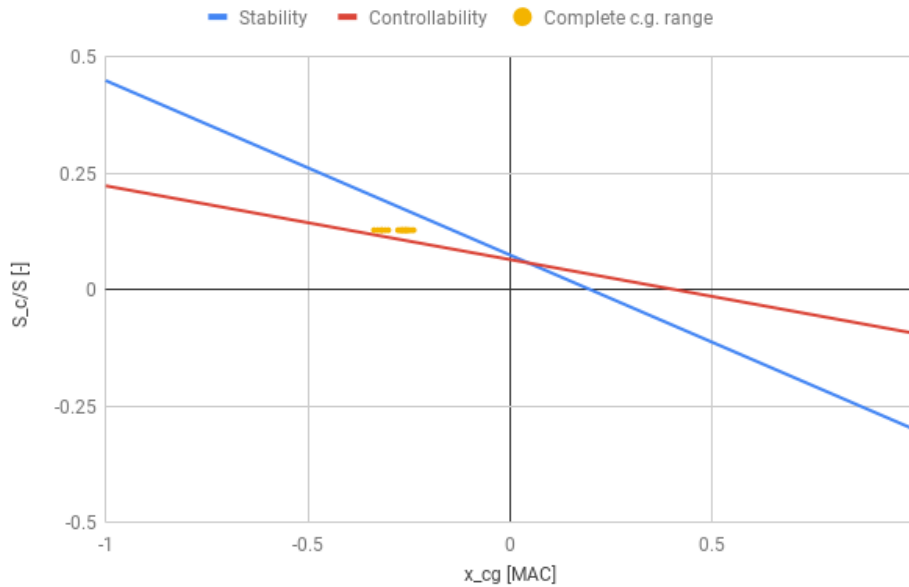
Figure 9.24: Scissor plot including feasible cg range (-0.336[MAC]-0.238[MAC])

Loading Configurations   After the trim analysis has been performed and the scissor plot is created, the feasible loading configurations can easily be determined. This is done by determining the most aft c.g. for which the C_{M_α} is negative and within the stability and controllability curves seen in Figure 9.24. Thus, at full passenger capacity, all possible cargo loading are deemed feasible. Furthermore, for a passenger loading configuration containing three passengers, two passengers are to be seated in the front row and one in the

back row as seen in 29 section view B-B, and when loading only two passengers, both shall be seated in the front row. In the loading configuration containing one passenger, the passenger shall be seated in the front row and only cargo in the front or no cargo at all are feasible loading configurations. To wrap up, an empty vehicle is deemed unfeasible and in order to make this loading configuration statically stable, dummy weights are to be loaded in the front row of the vehicle.

Stall Characteristics From Table 9.2 it can be seen that the angle of attack during trimmed cruise at fully loaded configure is higher for the canard than for the main wing. During the trim analysis it has become apparent that this is given even for the most aft operational c.g. location ($\alpha_c \approx \alpha_w + 2.9°$) and that the canard also features higher C_L values. This higher wing loading is beneficial since the stall angle of attack is similar for both wings ($\alpha_{c, stall} \approx 15°$, $\alpha_{w, stall} \approx 14°$) and therefore the canard is expected to stall earlier in all cases, ensuring stability in this flight regime.

9.5.3. Dynamic Longitudinal Stability

The aircraft must be dynamically stable in hover, transition and forward flight. The aircraft has been designed for static stability in cruise, but a stable transition phase is critical to success. The longitudinal dynamic stability is analysed for the transition from hover to cruise in 3 steps.

Longitudinal Equations of Motion To analyse the dynamic longitudinal stability of the aircraft in transition, a preliminary estimate is made using linearised equations of motion as derived in [20]. The second order derivatives are neglected for simplicity. These equations of motion (Equation 9.79) simplify the notation such that Δu is replaced by u (similarly Δw, Δq and $\Delta\theta$). Furthermore, it is assumed transition will occur at a level pitch condition $\theta_0 = 0$ for passenger comfort.

$$
\begin{aligned}
m\dot{u} &= X_u u + X_w w + X_\theta \theta + X_q q - W\cos(\theta_0)\theta + X_{\delta_c}\delta_c + X_{T_{cp}}T_{cp} + X_{T_{wp}}T_{wp} + X_{i_w}i_w \\
m(\dot{w} - qV) &= Z_u u + Z_w w + Z_\theta \theta + Z_q q - W\sin(\theta_0)\theta + Z_{\delta_c}\delta_c + Z_{T_{cp}}T_{cp} + Z_{T_{wp}}T_{wp} + Z_{i_w}i_w \\
I_{yy}\dot{q} &= M_u u + M_w w + M_\theta \theta + M_q q + M_{\delta_c}\delta_c + M_{T_{cp}}T_{cp} + M_{T_{wp}}T_{wp} + M_{i_w}i_w \\
\dot{\theta} &= q
\end{aligned}
\tag{9.79}
$$

T_{cp}, T_{wp} are the pilot thrust input, δ_c is the canard angle input and i_w is the main wing tilt input.

Equation 9.80 indicates the physical derivatives that compose the X_u term. The same terms also appear in the X_w, X_q and X_θ derivatives which are not given here. Some of these derivatives can be neglected, and their calculated values are given in Table 9.7.

The first term T_{wp}, is the (horizontal) thrust of the main wing propellers. The second term D_{wp}, the (horizontal) drag of the main wing propellers. The third term is the drag of the canard propellers, assuming they are pointing up during transition ($\theta = 0$). Thus, the thrust of the canard propellers always acts in the Z-direction. The final terms in both Equation 9.80 and 9.81 are the lift and drag of the wing, canard and complete aircraft fuselage, where γ indicates the flight path angle ($\gamma = 0$ indicates level flight).

The moment derivative (Equation 9.82) is taken about the centre of gravity and includes the aerodynamic moment of the wing, canard and body. The fuselage moment has been estimated from CFD techniques and includes the moment caused by the lift and drag of the fuselage.

$$
X_u = \frac{dr_{wp}}{du}\cos i_w - \frac{dD_{wp}}{du}\sin i_w - \frac{dD_{cp}}{du} - \frac{dL_w}{du}\sin\gamma - \frac{dL_c}{du}\sin\gamma - \frac{dD_w}{du}\cos\gamma - \frac{dD_c}{du}\cos\gamma - \frac{dD_b}{du}\cos\gamma \tag{9.80}
$$

$$
Z_u = \frac{dr_{wp}}{du}\sin i_w + \frac{dD_{wp}}{du}\cos i_w + \frac{dr_{cp}}{du} - \frac{dD_b}{du}\sin\gamma + \frac{dL_w}{du}\cos\gamma + \frac{dL_c}{du}\cos\gamma \tag{9.81}
$$

$$M_\mathrm{u} = \frac{\mathrm{d}r_\mathrm{wp}}{\mathrm{d}u} \sin i_\mathrm{w}(x_\mathrm{w} - x_\mathrm{cg}) + \frac{\mathrm{d}r_\mathrm{wp}}{\mathrm{d}u} \cos i_\mathrm{w}(z_\mathrm{w} - z_\mathrm{cg}) - \frac{\mathrm{d}r_\mathrm{cp}}{\mathrm{d}u}(x_\mathrm{cg} - x_\mathrm{c}) + \frac{dM_\mathrm{wp}}{\mathrm{d}u} + \frac{dM_\mathrm{cp}}{\mathrm{d}u}$$
$$+ \frac{dM_\mathrm{w}}{\mathrm{d}u} + \frac{dM_\mathrm{c}}{\mathrm{d}u} + \frac{dM_\mathrm{b}}{\mathrm{d}u} - \frac{\mathrm{d}L_\mathrm{c}}{\mathrm{d}u}(x_\mathrm{cg} - x_\mathrm{c}) + \frac{\mathrm{d}L_\mathrm{w}}{\mathrm{d}u} \cos\gamma(x_\mathrm{w} - x_\mathrm{cg}) - \frac{\mathrm{d}L_\mathrm{w}}{\mathrm{d}u} \sin\gamma(z_\mathrm{w} - z_\mathrm{cg}) \qquad (9.82)$$
$$- \frac{\mathrm{d}D_\mathrm{w}}{\mathrm{d}u} \sin\gamma(x_\mathrm{w} - x_\mathrm{cg}) - \frac{\mathrm{d}D_\mathrm{w}}{\mathrm{d}u} \cos\gamma(z_\mathrm{w} - z_\mathrm{cg})$$

Transition Profile   The derivatives must be calculated for each flight condition from hover to transition. Since this a continuous situation, only 3 points in time during this transition are analysed here.

In Figure 9.25, the tilt angle of the wing (i_w) and the horizontal velocity (V_u) are given over time during a level transition from hover to cruise speed. This transition can be done quickly (in about 25 seconds or less), but no altitude is gained. During the acceleration from 0 to 60 m/s, the vehicle covers about 700 m of distance, and does not exceed an acceleration of 3 m/s^2. The passenger will only experience a force of 1.1 g's.

A level transition is very quick, but for many trajectories, some ascending velocity may also be required. Figure 9.26 shows the tilt angle of the wing as the vehicle would complete an ascending transition from hover to cruise. This takes a bit longer than a level transition (about 45 seconds), as power must be used to ascend as well as accelerate. The maximum ascent rate is limited to 5 m/s, although more may be possible. The maximum g-force on the customer is a little under 1.1 while they cover 1,250 meters distance.

Both of these transition modes may be accelerated assuming there is additional power/energy available. It is considered that the g-force on the customer should be less than 1.2 g maximum, for the sake of comfort.
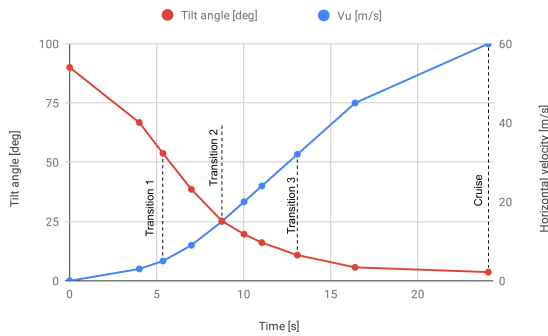
Figure 9.25: Wing tilt angle and horizontal velocity during a level transition from hover to cruise speed. The points used for stability analysis in transition are indicated.
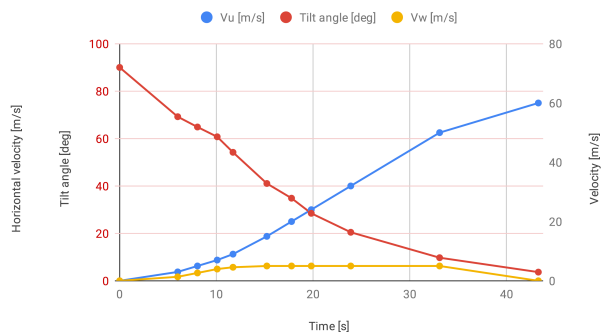
Figure 9.26: Wing tilt angle and horizontal/vertical velocity during an ascending transition from hover to cruise speed (maximum ascent 5 m/s).
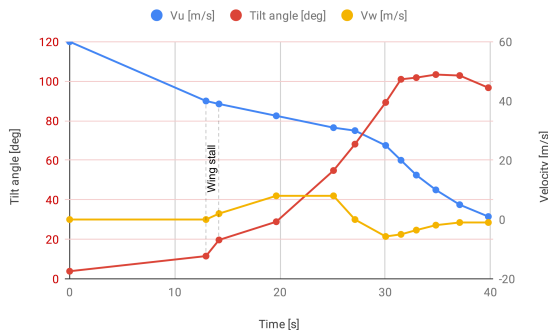
Figure 9.27: Wing tilt angle and horizontal/vertical velocity during transition from cruise speed to hover. The range where the wing stalls is indicated.
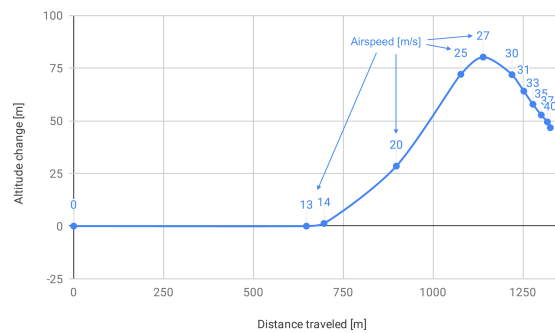
Figure 9.28: Position (relative to start of transition) as the vehicle slows from cruise to hover. The airspeed at certain points is given to indicate the deceleration.

When transitioning from cruise speed back to hover, a more complicated manoeuvre is necessary. It is possible to make a slow transition where the wing never completely stalls while tilting to vertical, however this transition requires nearly 2 minutes of time and covers over 3.5 km of distance. In a fast transition, the aircraft is slowed (using drag) to near stall speed at about 40 m/s. This is depicted in Figure 9.27 during the first 12 seconds. As the wing nearly stalls, the aircraft must pull up and increase the ascent rate. This allows the wing to tilt further back without stalling. The customer experiences the largest g-force during this phase at just under 1.2 g's. Near the end of this ascent, the wing continues to quickly tilt to over 50° while increasing thrust. At this stage, the wing does stall, and the propeller thrust must takeover the majority of the lifting force. There will be a quick vertical deceleration, and the customer will feel partially weightless (about 0.6 g) and the aircraft will decelerate until it is descending at a moderate rate of 4 m/s. During the last phase of transition, the wing is actually tilted backwards slightly to continue to decelerate the aircraft to 0, while also reducing the descent rate to a gentle 1 m/s. This requires the most thrust from the propellers during all flight phases. The entire transition takes about 35 seconds, and covers 1,150 meters distance. The vehicle ascends about 50 meters before descending. The flight path is shown in Figure 9.28

The interaction of the propeller thrust and wing is accounted for using simple momentum theory. It is assumed that the wings sit in a fully developed downwash of the propellers, and the effective velocity is superimposed over the airspeed. The induced velocity of the propellers can be calculated using Equation 9.83 from momentum theory, where v_i is the induced velocity and V is the airspeed ingested by the propeller in the axial direction. While the downwash in a fully developed wake should be twice the induced velocity, empirical measurements show that this generally is only 1.6 times the induced velocity.

$$T = 2\rho A(V + v_i)v_i \tag{9.83}$$

Once the induced downwash is calculated, the adjusted angle of attack over the wing can be determined. The adjustments to the effective angle of attack due to this downwash are shown in Figure 9.29 and given in Equation 9.84. The general effect is that the downwash increases the lift (and drag), while also tilting the angle of the resultant force back with the wing (increasing γ).

$$\alpha'_w = \theta + i_w - \gamma'$$
$$\gamma' = \tan\left(\frac{V_w + v_i \sin i_w}{V_u + v_i \cos i_w}\right) \tag{9.84}$$
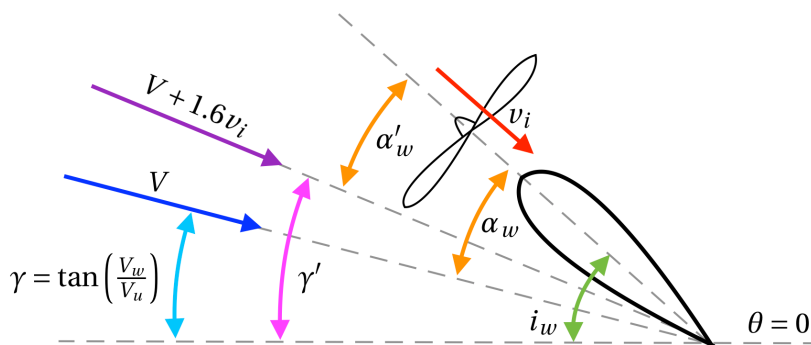
Figure 9.29: Definition of wing tilt, angle of attack and flight path angles due to propeller downwash.

With this, the wing lift and drag can be calculated and the equilibrium states determined. Each of these states are a point in the transition charts, and also the defining characteristics given in Table 9.6. These states are used to determined the derivatives for the dynamic longitudinal stability analysis.

Table 9.6: The four flight conditions that were analysed for longitudinal dynamic stability.

	Transition 1	Transition 2	Transition 3	Cruise
Vel [m/s]	0	15	32	60
γ [deg]	0	0	0	0
i_{w} [deg]	54	25	11	3.7
T_{wp} [N]	9,230	8,380	6,670	800
T_{cp} [N]	2,370	2,280	1,490	0
a_{u} [g]	0.2	0.4	0.4	0

For dynamic stability analysis, only four points during the transition are being considered. These points are labelled in the level transition chart, Figure 9.25 at 0, 15, 32 and 60 m/s velocity. In order to determine the derivatives, first an equilibrium state must be established. By setting a given acceleration, the necessary drag, thrust, lift and moments can be established.

Force Derivatives   Each of the propeller derivatives can be estimated using BEMT tools. A given flight condition during transition is input, and the u, w, θ and q is varied slightly to reveal the gradient. The direction of the results are logical. For example, if the axial flow into a propeller increases, the thrust accordingly decreases. If the lateral flow across a propeller increases, the thrust increases slightly, although it is less significant than the effect of axial flow. The change in drag of the propeller is much less significant than the thrust derivatives.

For the non-propeller derivatives, estimates are made using lifting line and CFD methods. The moment due to change in drag on the canard is neglected. The fuselage characteristics come from Table 9.1 and the aerodynamic coefficients of the wing and canard have been estimated using JavaFoil.

The coefficients can be turned into dimensional derivatives by taking the derivative with respect to each of the state variables, u, w, θ and q as in Equation 9.85.

$$\frac{\mathrm{d}L}{\mathrm{d}u} = \frac{1}{2}\rho V^2 S\frac{\mathrm{d}C_{\mathrm{L}}}{\mathrm{d}u} \qquad \frac{\mathrm{d}D}{\mathrm{d}u} = \frac{1}{2}\rho V^2 S\frac{\mathrm{d}C_{\mathrm{D}}}{\mathrm{d}u} \qquad \frac{\mathrm{d}M}{\mathrm{d}u} = \frac{1}{2}\rho V^2 Sc\frac{\mathrm{d}C_M}{\mathrm{d}u} \qquad (9.85)$$

Table 9.7 shows (as an example) the calculated force derivatives for Transition 3. These values change throughout the transition until cruise. Terms indicated with - are negligible. Table 9.8 shows the complete derivatives that are used in the state space system for the purpose of finding the eigenvalues, and simulating the system response.

Longitudinal Eigenmotions   Once the motion derivatives are calculated, they can be placed in the equations of motion formulated as a state space system. The equations of motion from Equation 9.79 can be formed as Equation 9.86, where the first matrix is the state-matrix, and the second the input-matrix. The mass of the aircraft is taken to 1,250 kg and the inertia I_{yy} is estimated to be 1,340 kg m^2.

The longitudinal eigenmotions of the system are found by determining the eigenvalues of the state-system. The results of this are given in Table 9.8.

$$\begin{bmatrix} \dot{u} \\ \dot{w} \\ \dot{\theta} \\ \dot{q} \end{bmatrix} = \begin{bmatrix} \frac{X_{\mathrm{u}}}{m} & \frac{X_{\mathrm{w}}}{m} & \frac{X_\theta - W\cos\theta_0}{m} & \frac{X_{\mathrm{q}}}{m} \\ \frac{Z_{\mathrm{u}}}{m} & \frac{Z_{\mathrm{w}}}{m} & \frac{Z_\theta - W\sin\theta_0}{m} & \frac{Z_{\mathrm{q}}}{m} + V \\ 0 & 0 & 0 & 1 \\ \frac{M_{\mathrm{u}}}{I_{yy}} & \frac{M_{\mathrm{w}}}{I_{yy}} & \frac{M_\theta}{I_{yy}} & \frac{M_{\mathrm{q}}}{I_{yy}} \end{bmatrix} \cdot \begin{bmatrix} u \\ w \\ \theta \\ q \end{bmatrix} + \begin{bmatrix} \frac{-X_{\delta_{\mathrm{c}}}}{m} & \frac{-X_{\mathrm{T_{cp}}}}{m} & \frac{-X_{\mathrm{T_{wp}}}}{m} & \frac{-X_{i_{\mathrm{w}}}}{m} \\ \frac{-Z_{\delta_{\mathrm{c}}}}{m} & \frac{-Z_{\mathrm{T_{cp}}}}{m} & \frac{-Z_{\mathrm{T_{wp}}}}{m} & \frac{-Z_{i_{\mathrm{w}}}}{m} \\ 0 & 0 & 0 & 0 \\ \frac{-M_{\delta_{\mathrm{c}}}}{I_{yy}} & \frac{-M_{\mathrm{T_{cp}}}}{I_{yy}} & \frac{-M_{\mathrm{T_{wp}}}}{I_{yy}} & \frac{-M_{i_{\mathrm{w}}}}{I_{yy}} \end{bmatrix} \cdot \begin{bmatrix} \delta_{\mathrm{c}} \\ T_{\mathrm{cp}} \\ T_{\mathrm{wp}} \\ i_{\mathrm{w}} \end{bmatrix} \qquad (9.86)$$

If the real parts of the eigenvalues are negative, this means the eigenmotions are stable. Cruise is a dynamically stable flight condition, however the transition phases are not. By simulating disturbances to u, w, θ,

Table 9.7: The estimated force/moment derivatives with respect to changes in state for Transition 3 condition.

Derivatives	d/du	d/dw	d/dθ	d/dq
L_w	45	-1,100	34,000	-580
D_w	-0.02	0.48	-15	-
T_wp	-760	-3.3	-110	-230
D_wp	0.16	-73	-2,300	-26
L_cw	14	-99	-3,200	280
D_cw	0.42	-	-	-
T_cp	22	-44	-1,400	93
D_cp	4.0	0.80	26	-1.7
L_b	-15	-1.7	53	-
D_b	11	0.19	-	-
M_w	0.36	-8.5	270	-
M_b	-31	-0.69	21	-
M_c	-	-	-	-
M_wp	0.20	29	940	10
M_cp	4.1	-4.8	-150	10

and q, the form of these eigenmodes can be examined. The plots of Figure 9.30 and Figure 9.31 show the system response from an initial state disturbance. The disturbances damp very quickly for cruise, but grow exponentially during the transition phases. Some artificial stability will be required to stabilise the vehicle in transition with the use of feedback in the control system.

$$t_{\frac{1}{2}} = \frac{\ln \frac{1}{2}}{\mathbb{R}\mathrm{e}(\lambda)} \tag{9.87}$$

The time to half amplitude, $t_{\frac{1}{2}}$, for each eigenmotion is calculated using Equation 9.87 taken from [20]. For cruise (which is stable), the longest time to half amplitude is 1.4 seconds. Little extra effort will be required from the pilot as disturbances will damp very quickly. For the unstable modes, the shortest time to double amplitude is only 0.5 seconds. While this is quite short, the autonomous pilot in hover is already working to handle disturbances. During Transition 3 (about halfway through transition) this time to double is 3 seconds, making it easier for the system to handle the disturbances. The response time of the control system is quite a bit faster and should be able to dynamically stabilise the system with feedback in the loop.
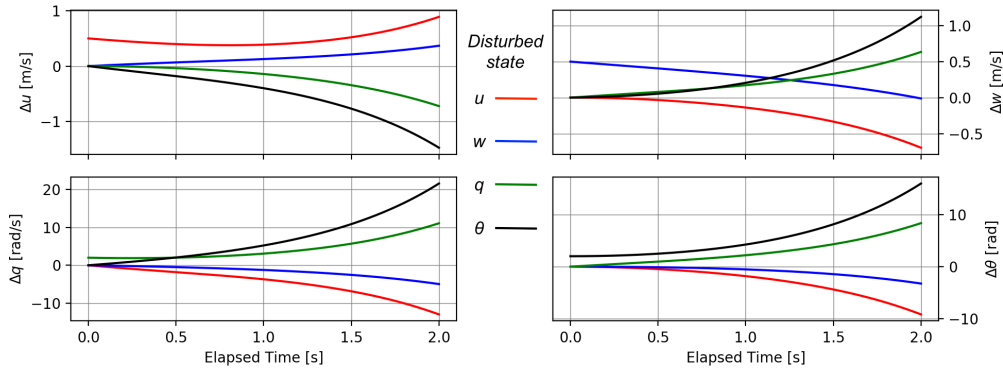
(a) Response of the vehicle to an initial disturbance in state during transition at 5 m/s (Transition 1).

Table 9.8: The complete derivatives calculated for the state space systems.

	Tilt 1	Tilt 2	Tilt 3	Cruise
X_u	-652	-575	-765	-729
X_w	403	203	54.0	5.00
X_q	32.0	-70.0	-199	-211
X_θ	-1,570	-2,480	-1.10	183
Z_u	35.0	-18.0	-62.0	-18.0
Z_w	-465	-908	-1,275	-1,830
Z_q	-118	-274	-272	-379
Z_θ	1,425	10,500	33,100	100,000
M_u	-172	-260	-320	-287
M_w	-31.0	-436	-641	-1,050
M_q	-610	-905	-1,400	-1,980
M_θ	2,410	7,260	14,400	21,100
Eigenvalue 1	1.35	1.16	$-1.05 + 2.15i$	$-0.86 + 5.51i$
Eigenvalue 2	$-1.15 + 0.6i$	$-1.18 + 1.04i$	$-1.05 - 2.15i$	$-0.86 - 5.51i$
Eigenvalue 3	$-1.15 - 0.6i$	$-1.18 - 1.04i$	0.23	-0.51
Eigenvalue 4	-0.4	-0.66	-0.79	-1.3
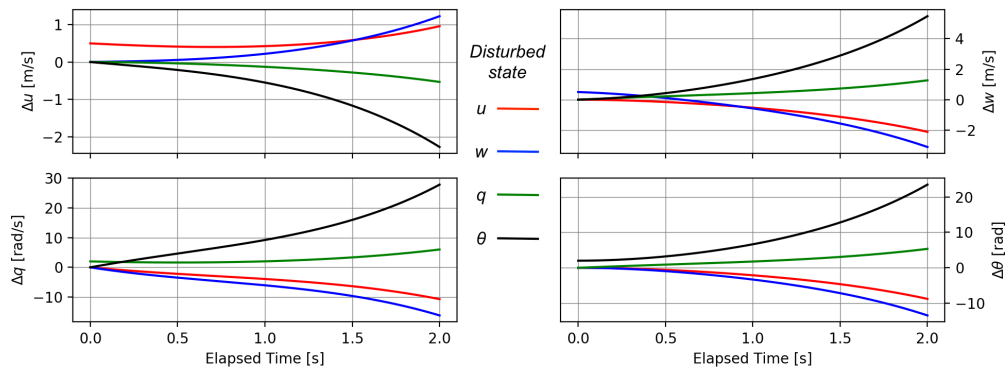
(b) Response of the vehicle to an initial disturbance in state during transition at 15 m/s (Transition 2).
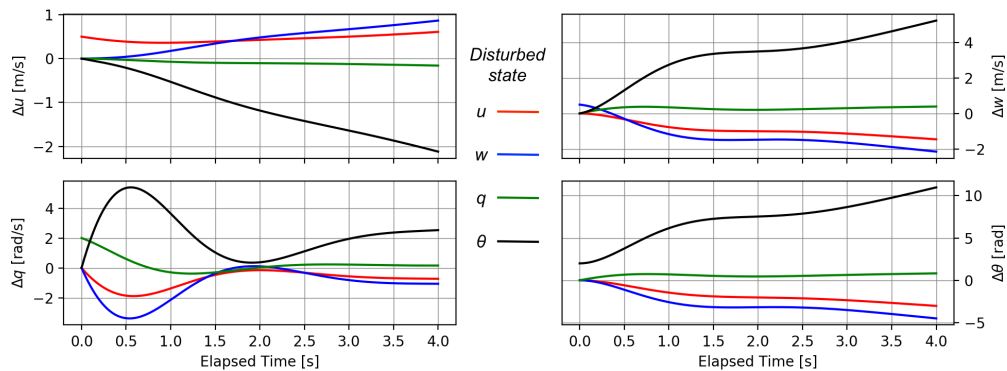
(c) Response of the vehicle to an initial disturbance in state during transition at 32 m/s (Transition 3).

Figure 9.30: Simulation of longitudinal system response.
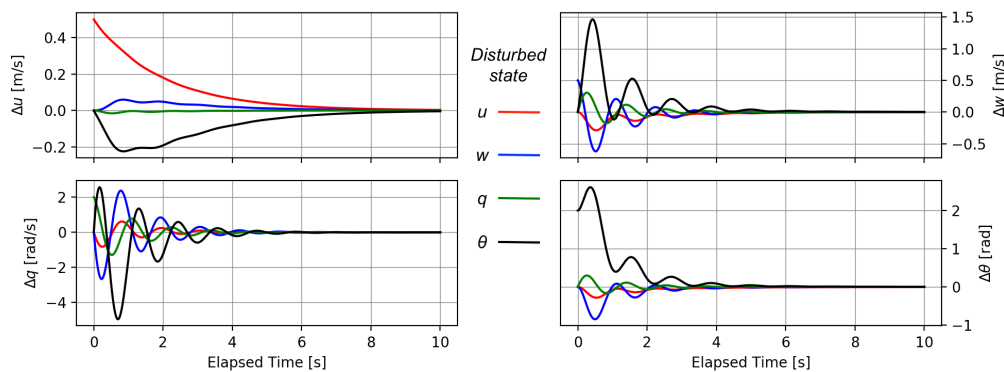
Figure 9.31: Response of the vehicle to an initial disturbance in state during cruise. This mode is longitudinally dynamically stable.

Verification and Validation   This method of analysis is a first level dynamic stability analysis, and may be subject to estimation error. To minimise this error, two versions of BEMT code are used to compare the output forces and moments, and found to be within a reasonable margin of error. In addition, different blade parameters (solidity, RPM, taper, twist) are input to determine if the derivatives are highly sensitive to different input. The resulting eigenvalues show some sensitivity to the change in input, but overall the order of magnitude and the sign of the eigenvalues remain unchanged. Sensitivity to the mass and inertia is tested and found to be insignificant even for large variation in mass and inertia estimates.

Further investigation should be done to increase the accuracy of this analysis. The aerodynamic derivatives could be simulated using higher resolution CFD methods. Furthermore, wind tunnel tests of scale models can also be used to provide some empirical assessment of the stability. As the design progresses, this will be critical to mission success.

9.5.4. Lateral and Directional Stability

As has been done for the longitudinal stability, the lateral and directional stability can also be estimated. The fuselage of the aircraft causes a significant destabilising moment when a sideslip is present. This induces a further yaw moment. However, when the wing rotors are subjected to a yaw rate, they act as a yaw damper (assuming constant RPM governance from the motor controller), which reduces the yaw rate. This effect was estimated through simulation. In the case that the rotors are not functioning, an initial yaw disturbance of 1° will rotate the aircraft to 35° in about 2 seconds. With the rotors spinning (at cruise speed) this is estimated to reduce the effect to only 8° in 2 seconds, which should be sufficient time for the control system to compensate.

The response time of the rotors can be calculated by estimating the time it takes the rotors to increase RPM and the resulting thrust/moment. The moment of inertia of the wing rotors is estimated conservatively to be less than 1.2 kg m^2 (for the canard it is 0.52 kg m^2). In cruise, the torque on the rotors is 77 Nm, with an available maximum torque of 330 Nm from the motor (which does not exceed the maximum power of the motor at 2100 RPM). The rate of acceleration/deceleration is the difference in torque required and torque available divided by the moment of inertia; a range of 200 rad/s^2 to -64 rad/s^2. If the rotors on one side of the fuselage double in thrust, while the others reduce to 0 N, this occurs in about 0.12 seconds (the RPM must only increase/decrease by about 80 RPM). At that point, the main rotors induce 2,400 Nm of torque to oppose the instability. For reference, the instability caused by the fuselage at 5° sideslip angle is about 1,200 Nm. It is likely this is sufficient to maintain stable flight with active control response, however further testing would be required. The exact blade design will also impact the response time.

For lateral stability, there are 3 primary effects to be accounted for: the (lack of) dihedral, the negative sweep and the placement of wing on the fuselage. Typically, positive dihedral and positive sweep provide a

stabilising roll response to sideslip. Thus, with a lack of dihedral and negative sweep, the Bumblebee may be somewhat unstable, however the high wing position provides some stabilising effects, depending on the fuselage interactions. This will need to be further studied to determine how much active control is required to maintain static and dynamic stability.

9.5.5. Artificial Stability & Control

For artificial stability and control, differential thrust, aileron deflection and independent half span deflection of the canard wing are used. The various methods and their respective use cases are elaborated upon in the following paragraphs. Furthermore, the reference frame as seen in Figure 9.32 is used in the following paragraphs.
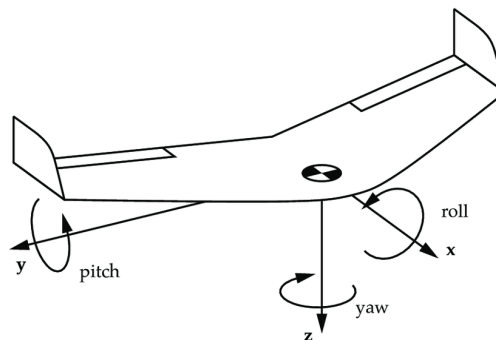
Figure 9.32: Body reference frame [13]

Hover, (H)   While in the hover phase, the propellers positioned on the main wing provide around 80% of the thrust required for take-off, whereas the propellers on the canard wing provide around 20% of the thrust. This leads to the fact that moment and force equilibria during hover are provided and maintained by the ratio of thrust produced by the canard wing propellers over the main wing propellers. Furthermore, the ailerons located on the trailing edge of the main wing may be used as vanes to control the direction of the thrust, also known as thrust vectoring.

H, Roll   Roll manoeuvres during hover are initiated by applying differential thrust between the left and right side of the vehicle. This causes moment imbalance around the x-axis, which in turn triggers a roll rate. During this manoeuvre, force equilibrium in all directions and moment equilibrium around the y-axis are maintained by applying the correct ratio of thrust between the main wing propellers and the canard wing propellers. In order to return back to complete equilibrium or , differential thrust is applied again.

H, Pitch   The pitch angle and rate are controlled by yet again applying differential thrust, but between the canard propellers and main propellers. Thus, the ratio of thrust provided by the canard propellers over the main propellers would have to decrease in order to achieve a negative pitch rate (pitch down), and vice versa. This is done while maintaining force equilibrium in all directions, but causing a moment imbalance around the y-axis.

H, Yaw   In order to introduce a yaw rate, two options are available. The first option is applying differential thrust between the clockwise rotating propellers and the counter clockwise rotating propellers on the main wing. However, this method will be elaborated upon in Section 19.7 as further analysis into the effectiveness and consequence(s) on the cruise efficiency is required before implementation is possible. The second option includes deflection of the ailerons located at the trailing edge of the main wing for thrust vectoring. For a positive yaw rate (clockwise rotation), the aileron located in the right half span of the wing is deflected downward (positive deflection) and the aileron located in the left half span is deflected upwards (negative deflection). This results in a loss in lift, which is counteracted by increasing the rpm of the propellers on

---

[13]`https://www.researchgate.net/figure/Coordinate-system-of-the-body-attached-reference-frame-\`
`The-common-names-for-the_fig2_40754972`[accessed 21.06.19]

the main wing, which means in an increase in thrust and thus lift. This also means an increase in moment created around the z-axis. However, as the thrust generated to counteract the weight for take-off is rather high, the aileron deflection needed to induce a yaw rate is fairly low, which indicates a small loss of lift.

Cruise, (C)   During cruise, the various control methods are applied as well; the difference in application of the methods between hover and cruise lies in their use cases. Apart from thrust vectoring, applying differential thrust and deflecting the ailerons, the half spans of the canard wing may be tilted independent of one another, as well as the propellers located on the canard wing. This introduces another degree of freedom, usable for control and manoeuvring of the vehicle. The various methods belonging to their respective use cases are elaborated upon in the following paragraphs.

C, Roll   During cruise, the ailerons located in the main wing are used to initiate a roll rate. Apart from the ailerons, the half spans of the canard wing are also deflected to support the roll rate. The ailerons of the UAM vehicle deflect very similar to a conventional aircraft, the only difference lies in deflection of the half spans of the canard wing, which only support the ailerons.

C, Pitch   Initiating a pitch rate during cruise is done by deflecting both half spans of the canard wing in the same direction and over the same angle. Another option would be to deflect the ailerons, but as the moment arm of the canard wing is bigger than of the aileron, the effectiveness of the canard deflection is higher. Due to the rather large moment arm, only a small canard tilt angle is required for initiation of a pitch rate, resulting in a fairly small increase or decrease (depending on the pitch direction) in lift.

C, Yaw   In order to introduce a yaw rate, differential thrust between the propellers located on the left half span and the right half span of the main wing is applied. This difference in thrust causes a resultant moment around the z-axis to occur. Thus, if a positive yaw rate is desired, an increase in thrust provided by the propellers on the left half span of the wing and a decrease (the same amount as increase in thrust provided by left half span) in thrust provided by the propellers on the right half span is required. The increase and decrease in thrust eliminate one another out, resulting in conservation of force equilibrium in the x-direction.

Weather Handling   Any reliable service must be able to handle the most common weather conditions, and some more extreme conditions. During catastrophic weather (e.g. tornado, hurricane, hail) the fleet will be grounded for safety. However the vehicle must be able to handle winds, precipitation and fog/smog.

In turbulent winds, the vehicle will use differential thrust (via rapid RPM changes) to maintain equilibrium. While the ailerons are used for roll control in horizontal flight (with the canard), they are sized for adequate yaw manoeuvres in hover as well.

Static wicks have been added to the rear of the aircraft to discharge static buildup that may occur in precipitation. Advancements in material technology may present another solution for this phenomenon.

9.5.6. Autonomy

In this subsection, some crucial background information about autonomy is given. Afterwards, the method in which the vehicle is made fully autonomous is elaborated upon and the subsection is closed off with the challenges one faces when designing a fully autonomous vehicle and the overall system.

Background Information   Autonomy plays a big role in the design phase of a vehicle and more importantly, the overall system. A fully autonomous vehicle is associated with many advantages, with one of the most important being a vast reduction in operating cost (especially when designing 4 passenger UAM vehicle). Apart from the advantages, one should also notice that nowadays around 80% of aircraft accidents are caused by human error, whereas only 20% is caused by machine failure [14]. However, autonomous vehicles come with a set of challenges which will be elaborated upon at the end of subsection 9.5.6. Before the

---

[14]http://www.boeing.com/commercial/aeromagazine/articles/qtr_2_07/article_03_2.html [accessed 19.06.19]

method in which the vehicle is made fully autonomous, one should acknowledge the distinction between the several levels of autonomy[15]:

- Level 0: No automation; vehicle without any assistance

- Level 1: Driver assistance; cruise control

- Level 2: Partial automation; automated steering manoeuvres (parking, lane guidance)

- Level 3: Conditional automation; vehicle controls itself for the most part

- Level 4: High automation; limited to known sections of road

- Level 5: Full automation; autonomous in every environment and all situations

Method   Now the distinction between the various levels of autonomy is clear, it is safe to say that by 2050 the vehicle is designed to be a level 5 autonomous vehicle. However, for now, the aim is to reach level 4 autonomy with a remote pilot in case of an emergency or rough weather conditions. This is achieved by implementing a range of different types of systems and sensors in the vehicle, as well as a vehicle network. The various systems and sensors are stated below and their respective weights and dimensions are stated in Table 9.9.

Systems & Sensors:

- **Traffic Collision Avoidance System III, TCAS III** For the TCAS, the chosen system is the L3 ACSS T^3CAS 4-MCU as it is a highly integrated system containing multiple systems needed for automation purposes of the vehicle [16]. It is an integrated system containing the TCAS, a Terrain Awareness Warning System (TAWS), a Automatic Dependent Surveillance Broadcast system (ADS-B in) and a mode S transponder (ADS-B out). As the name of the system already states, it is used for traffic collision avoidance, but is in essence an integrated surveillance and communication system.

- **Inertial Measurement Unit, IMU** Two Lord 3DM-GX5-45 IMU are used (one for redundancy) as it already contains a Global Navigation System GNSS, which adds some redundancy to the navigation system [17]. This unit contains a Global Navigation Satellite System (GNSS), a triaxial magnetometer, gyroscope and accelerometer, and a pressure altimeter. These sensors allow for measurement of accelerations, angular rates and atmospheric pressure amongst many other parameters. Furthermore, the noise in the data obtained by the various sensors within the unit is filtered out by use of a Kalman filter. For redundancy purposes, the vehicle contains two IMUs.

- **Laser Imaging Detection and Ranging, LiDAR** The Phoenix Ranger-LRT is chosen as it allows for high resolution construction of 3-D maps of the terrain underneath and in front of the UAM vehicle. Apart from 3-D mapping, the system allows for remote data feed, which enables remote piloting of the UAM vehicle [18]. Furthermore, 3-D mapping of the terrain allows for altitude determination, obstacle avoidance and terrain reconnaissance.

- **Cameras** Three micro cameras (VTX20 800TVL HD Micro CMOS FPV [19]) will be implemented in the vehicle. The first will be pointed towards the ground, the second to the front of the vehicle and the third to the back of the vehicle. This allows for a remote pilot to properly and accurately see the environment surrounding the UAM vehicle and avoid potentially dangerous situations if for some reason none of the sensors produced a warning; especially during take-off and landing procedures.

---

[15]https://www.popularmechanics.com/cars/car-technology/a27269684/self-driving-cars/ [accessed 13.06.19]

[16]https://www.l3commercialaviation.com/avionics/products/t3cas/?_ga=2.217215952.771716189. 1560932266-1145034677.1560932266 [accessed 19.06.19]

[17]https://www.microstrain.com/sites/default/files/3dm-rq1_datasheet_8400-0053.pdf [accessed 19.06.19]

[18]https://www.phoenixlidar.com/ranger-series/ [accessed 19.06.19]

[19]https://www.gearbest.com/camera/pp_009235714117.html?wid=1433363 [accessed 19.06.19]

- **Linear Magnetic Encoder** For the tilt angle of the main wing two (1 for redundancy) linear magnetic encoders are installed. Linear magnetic encoders were chosen due to the ease of application and the robustness of the sensor. The magnetic scale is wrapped around the shaft of the main wing and the encoder is located on top of the shaft. For this sensor, the Baumer MIL10 is chosen[20].

Table 9.9: Sensors specifications

System	Weight [kg]	Dimensions; L x W x H [mm]
TCAS	7.5	190 x 120 x 400
IMU	0.21	88 x 76 x 22
LiDAR	5.4	340 x 190 x 130
ADC	1.0	140 x 100 x 84
Micro camera (x4; forward, backward, down & interior)	0.004 (x4)	15 x 15 x 70 (x4)
Linear magnetic encoder (x6)	0.13 (x6)	10 x 15 x 46 (x6)

Furthermore, the vehicle will be fitted with the following sensors:

1. 5-hole air data probe (x2; one for redundancy): measure airspeed, angle of attack and static pressure
2. Thermometer: measure temperature
3. RPM sensor (incorporated in motor control unit):

The systems and sensors mentioned above only allow a level 4 autonomous vehicle as a level 4 autonomous vehicle requires human control in situations which are unknown to the vehicle. In order to design a level 5 autonomous vehicle, artificial intelligence (AI) and a vehicle network need to be implemented as well[21]. The data obtained by all sensors and systems will be processed by the Air Data Computer (ADC) and AI, and afterwards distributed through the vehicle network to all other vehicles within the system. For the ADC, the ADC developed by Meggitt Avionics will be implemented in the vehicle[22]. It is important to analyse critical conditions during the design phase of the vehicle, but for a fully autonomous system, all possible situations and conditions have to be acknowledged which is impossible. This leads to the necessity of implementing artificial intelligence (AI) and a network between all vehicles. Each vehicle gains experience and learns to respond to certain situations correctly through AI and share this experience with the rest of the vehicles within the system via the vehicle network. However, as of today, AI has not reached the technological readiness level needed to be implemented into the system, which leads us to the challenges faced when designing an autonomous vehicle.

Challenges The first challenges to be faced are the legislation and regulations or rather the lack thereof when it comes to autonomy, but as the aim for this project is 2050, it is safe to assume that by that time this will have changed. Apart form this, cyber security is another major challenge, as fully autonomous vehicles do not allow for the passengers to manually control the vehicle from within the vehicle. If a breech in the system would occur and the people hacking the system would turn off all of the vehicles, the consequence would be huge, as the vehicles in hover at that time would in a sense "fall out of the sky", causing an enormous amount of damage to the area in which the vehicles operate. This introduces the next challenge, safety. Safety has been a very important aspect during the entirety of the design phase of the vehicle and still plays a very important role. At no point should a UAM vehicle "fall out of the sky" and cause catastrophic damage, as this has very negative effects on the social acceptance aspect of the system, leading to the final challenge; social acceptance. As of now, the majority of people in Los Angeles would accept and use autonomous vehicles, but this would rapidly change if failure leading to catastrophic damage would occur.

---

[20]https://www.baumer.com/nl/en/product-overview/rotary-encoders-angle-sensors/bearingless-encoders/linear-encoders/mil10/p/28114 [accessed 19.06.19]

[21]https://future-markets-magazine.com/en/innovators-en/challenges-of-autonomous-vehicles/ [accessed 13.06.19]

[22]https://www.meggitt-avionics.co.uk/wp-content/uploads/2017/10/Meggitt-Avionics-Data-Sheet-\ADC-Sept-2017.pdf [accessed 19.06.19]

10

Operations and Infrastructure

Throughout this chapter, the design of the UAM system in which the vehicle will operate will be presented. The goal is to develop a system that is able to most effectively solve the foreseeable congestion problems in the most efficient, sustainable, and socially integrated manner possible. In Section 10.1 the use case is described. Thereafter, in Section 10.2, the mission profile is determined. This is followed by a description of the airspace design in Section 10.3. Then, the system sizing method is explained in Section 10.4.Thereafter, the different stages for the development of a UAM is explained in Section 10.5. The method to size the vertiports is explained in Section 10.6. Afterwards, the vertiport design is discussed in Section 10.7. The air traffic management is explained in Section 10.8. Hereafter, the maintenance plan for the vehicle and vertiport is presented in Section 10.9. Finally, the system function diagrams are shown in Section 10.10.

10.1. Use Case

The use case defines the specific manner in which the mobility system will be used. Therefore, it also defines how the demand of the system will be satisfied. The two major types of use cases for such a transportation system are the on-demand and scheduled models. A research study by NASA highlights the typical characteristics, which are summarised below [27]:

On-Demand   Routes are unscheduled and un-planned, and are in service once a trip is individually ordered. It is expected that the average amount of passengers per vehicle would be close to one. A high density of infrastructure is required for the system to truly be able to accommodate this service. A 3 minute last mile travel is required for such a system, making it adapt to a large range of possible destinations. High infrastructure costs are therefore required, which makes the business model harder to sustain. In addition, the level of visual and noise disruption is high due to high exposure of landing sites near private homes.

Scheduled   For an on-demand use case, routes are predetermined and scheduled well in advance of flight time. Vertiports are capable of handling numerous vehicles at once, and always provide charging facility. The main competition to this form of a UAM system are public transport services such as busses, metros and cars. In LA, public transport has a very low utilisation percentage, making cars the only real form of competition. It is predicted that a scheduled UAM system may have a viable market in 2028. A relatively low infrastructure cost is required, as last minute travel is up to 10 minutes for such system, meaning a lower density of hubs is needed.

As a conclusion, the scheduled use case is more convenient as a business case due to the lower infrastructure costs, higher utilisation rate, and lower total noise and visual disruption. As a target system size for 2050, all the PUMAs that are able to be served within the maximum range of the aircraft shall be served. This implies a vertiport system of 105 hubs, with optimal routing and fleet management to operate the vehicles between them. Moreover, it is estimated that around 4,470 vehicles can be operated with that amount of hubs.

10.2. Mission Profile

The mission profile is defined in order to later size the system, and to compute the routes that serve the largest travel time gain compared to using a car. The mission profile is shown in Figure 10.1.
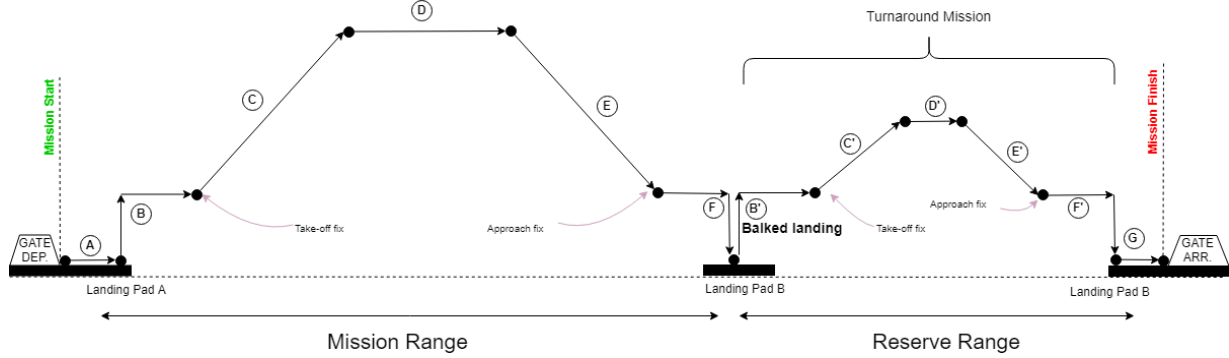
Figure 10.1: Mission profile including balked landing

The different stages are listed and described in Table 10.1.

Table 10.1: Trip features throughout mission profile

Stage	Mission phase		Vertical Velocity (m/s)	Horizontal Velocity (m/s)	Altitude range (m AGL)
A	Taxi from gate to landing pad		0	$0 \leqslant V_u \leqslant 1.1$	0
B + B'	Step up take-off	Vertical take off	$0 \leqslant V_w \leqslant 10$	0	$0 \leqslant h \leqslant 200$
		Cruise/hover to take-off fix	0	$0 \leqslant V_u \leqslant V_{climb}$	200
C + C'	Climb to cruise height		$V_{climb} \cdot sin(\gamma)$	$V_{climb} \cdot cos(\gamma)$	$200 \leqslant h \leqslant h_{cruise}$
	Cruise Phase		0	V_{cruise}	h_{cruise}
E+E'	Descent to approach fix		$-V_{climb} \cdot sin(\gamma)$	$V_{climb} \cdot cos(\gamma)$	$h_{cruise} \geqslant h \geqslant 200$
F+F'	Step down landing	Cruise/hover to approach fix	0	$V_{climb} \leqslant V_u \leqslant 0$	200
		Vertical descent	$-V_{desc} \leqslant V_w \leqslant 0$	0	$200 \geqslant h \geqslant 0$
D'	Turnaround cruise		0	V_{cruise}	$h_{emergency}$
G	Taxi from landing pad to gate		0	$0 \leqslant V_u \leqslant 1.1$	0

From Table 10.1 a few particular characteristics can be observed and are hereafter shortly described, namely the step up/down phases, the climbing/descending trajectories and the turnaround mission.

Flight Phases   A step approach and take off trajectory is established, with the vehicle performing vertical take off to a height of 200 m Above Ground Level (AGL), before horizontally transitioning for 135 m to the take off fix. This allows clearance of infrastructure, minimising noise pollution and traffic exposure to neighbourhoods surrounding the vertiport. Also, according to a study, this trajectory has shown to be effective in minimising delay of arrivals [28]. The climbing and descending phase is expressed in terms of climb angle, γ, and is performed until a modular cruise altitude, h_{cruise} is reached. These values are determined according to the airspace design implemented for the routes, highlighted in Section 10.3. The turnaround mission phase is used to define the minimum extra energy that the vehicle must have available at all times. The turnaround mission involves a balked landing where the vehicle will again be following the original step up trajectory. The turnaround cruise will be performed in the low altitude emergency flight layer, further defined in subsection 10.3.1. The total range of the turnaround mission determines the reserve range for the trip, a value is set at 9 km.

Energy Breakdown for a 60km trip -- Reserve: +28%
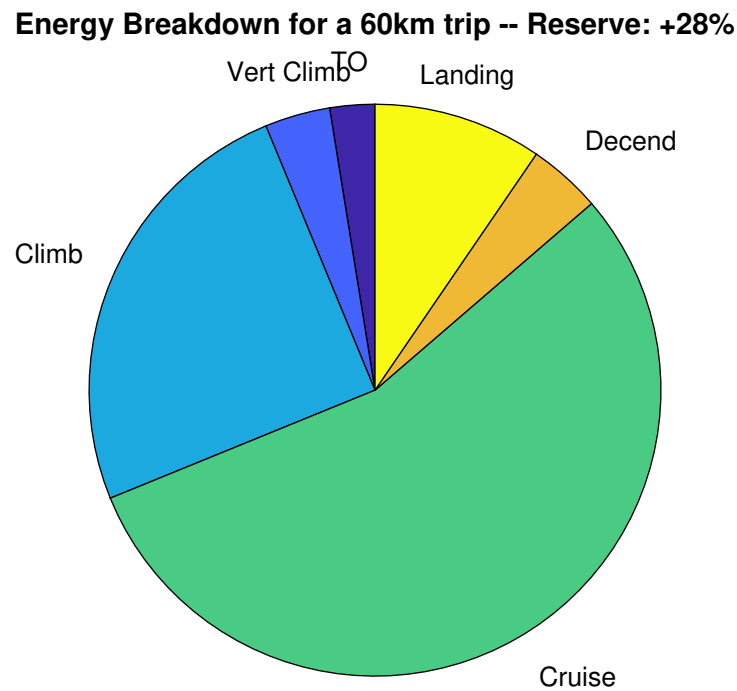
Figure 10.2: The distribution of energy required to perform different phases of flight

10.2.1. Trip Energy

The energy required to fly a trip for the given mission profile is computed using a tool that sums the energy required for each individual phase, N. The distance of the phase trajectory, D_N, a function of the total trip range and cruise height, is divided by the flight velocity at that phase, V_N, to the airtime of N at T_N. Then, the power required to perform flight at each phase P_N is a summation of the power required by each propulsion unit. This is a function of the thrust required to fly at V_N, and of the wing configuration. See subsection 9.3.3 and subsection 9.3.4 for the power computations. The energy required to perform the trip is simply the summation of the product of T_N and P_N for all flight phases, N.

10.3. Airspace Design

It is expected that other operators will be using the urban airspace of LA for UAM too. Furthermore, a foreseeable large UAV last-mile delivery industry will almost certainly be present by 2050 as well. As subsection 10.8.1 will later on also highlight, the vehicles will be operated in a decentralised system, meaning a large amount of free flights will take place in very restricted areas. An airspace design that optimises the capacity of the airspace must be found. Furthermore, information of routes that every vehicle will fly should be shared between the different vehicles occupying the airspace. The design space for the airspace design will firstly be presented, before different concepts are compared

10.3.1. Design Space

Types of constraints include altitude limits, separation constraints, and vertiport constraints. Assumptions that are made are a uniform ground altitude Above Sea Level (ASL) of 80 meters throughout the entire area covered by the system, and that by 2050 the urban skyline compares to that of today in terms of peak alti-

tudes. The peak altitudes of buildings are found in central LA district which are in the range of 200 to 250 meters AGL [29].

The altitude limits of the airpsace are firstly discussed. The allowable airspace to operate en route flights is set at a minimum of 380 m ASL, and a maximum of 1,370 m ASL. The minimum is set in order to maintain low noise pollution and limit traffic exposure to residential urban areas. It is also intended to maintain a 60 meter separation margin with the urban skyline of the city. This therefore sets the minimum en route altitude at 300 m AGL, corresponding to 380 m ASL. The maximum height is set to stay safe from commercial aviation, which is therefore the minimum altitude at which aviation is permitted to cruise at. According to visual flight rule restrictions, this corresponds to flight level 35, which corresponds to an allowable flight altitude of 1,300 m ASL, or 1,370 m AGL [30]. The airspace of 330 to 380 m ASL will always be designated to emergency and balk flight cases.

Furthermore, separation constrains must also be implemented. A vertical separation is dependent on factors such as the position and velocity measurement accuracy and efficacy in conflict avoidance. An acceptable value from literature study is taken to be 50 m [31].

10.3.2. Airspace Design

The Metropolis project at TU Delft in 2016 published a paper which identified different airspace designs adapt to "Extreme Traffic Densities", where simulation of air traffic densities led to certain conclusions. Capacity was modelled as a combination of safety, a function of the number of simulated separation conflicts, and efficiency as a function of the optimally flight trajectories. According to the Metropolis study [31], the design concepts that displayed largest capacity performance are the flight layer and free flight concepts, which are described below.

Flight Layers   The urban airspace is segregated into sets of altitude ranges at which vehicles must fly at depending on the heading angle and trip distance. The vehicles are free to choose their own paths and avoidance trajectories within the flight layer. Each flight layer will encompass trips with a heading angle range of 45 degrees. This reduces the relative velocity between vehicles in each layer, reducing the chance of collision. The height of each flight layer is 100 m, twice the vertical separation requirement. Two sets of flight layers allow trips of long distance and low traffic to be assigned to the high altitude layer set, increasing the fuel efficiency of the system. The route distance divided by number of vehicles on the route per hour for every route is computed, with the top 50th percentile being assigned to the top flight layer set. The optimal way to traverse flight layers is to climb and descent vertically as proven in the Metropolis study. This implies that the vehicle will take a vertical flight path to its cruise altitude, before horizontally cruising at its assigned cruise altitude. An illustration of this concept is shown in Figure 10.3.

Free Flight   For this concept, no segregation of airspace is implemented within design space altitude limits. The operator is given the freedom to choose the most conflict free and efficient flight trajectory. Efficient climb angles are permitted to be taken as there are no layers that limit the heading angle one must fly on. The height at which the vehicles will cruise is modelled as linear with respect to the distance of the trip. This is because it is expected that to find the most optimal, conflict free trajectory, the vehicles travelling long distances will have to fly above low altitude traffic flying short trips. The illustration of this concept is shown in Figure 10.4.
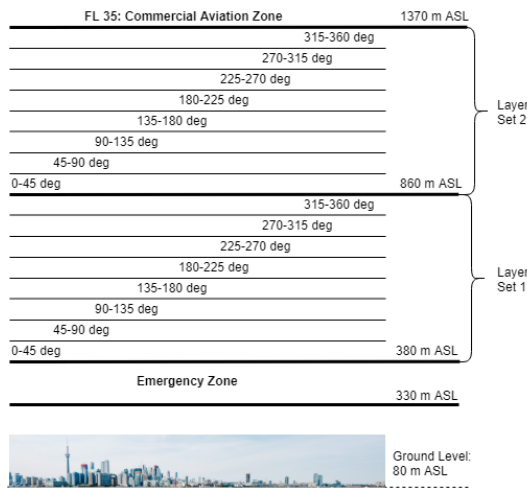
Figure 10.3: Flight layers airspace design and designated heading angle ranges
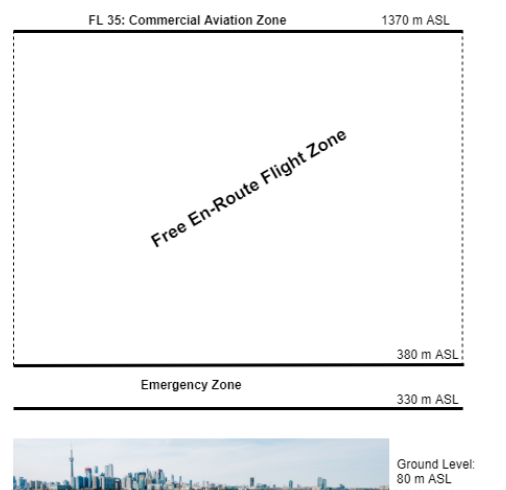
Figure 10.4: Free flight layer airspace design

10.3.3. Airspace Design Evaluation and Energy Usage

The flight layer concept is implemented using the requirement that the vehicle must traverse the flight layers vertically. Therefore, a climb angle of 85 degrees is implemented to also attempt to use some of the vehicle's efficient cruise capabilities during climb. For the free flight concept, freedom to use the most energy efficient climb trajectory is exercised. This corresponds to climb with non-powered lift at lowest possible climb angle. A climb angle of 5.8 degrees is chosen, which allows the aircraft to still reach the en-route cruise flight layer without spending too much time in the emergency layer. Also, this allows for the aircraft to descend at the same angle without entering vortex ring state. The question of how much more energy efficient the free flight layer is compared to the flight layers is investigated by energy required to complete 200 routes.

Results   Taking the average energy of all routes, the flight layer system has shown to require 6.3 times more energy than the free flight system. These results can be explained by the exponential increase in energy required for the vehicle to perform powered climb compared to non-powered flight. This vehicle performance characteristic is visualised in Figure 10.5, showing the energy required to complete different trip distances at an arbitrary cruise altitude of 1,000m, via powered climb for a layers concept with respect to non-powered climb permitted by the free flight concept.
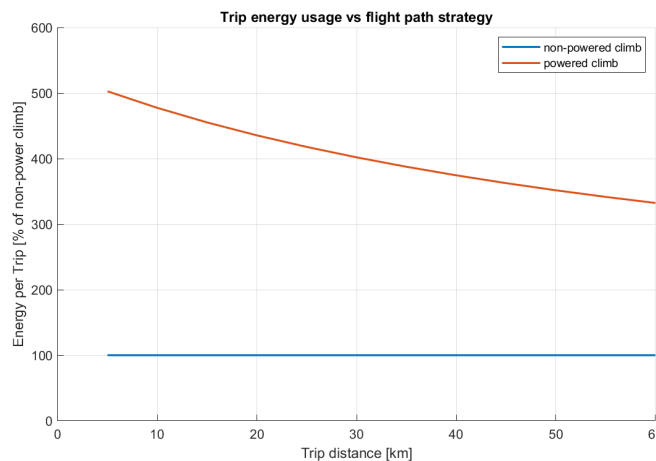
Figure 10.5: Energy required to perform trip using powered climb (for flight layers) vs non-powered climb (for free flight)

Energy Breakdown for a 60km trip -- Reserve: +28%
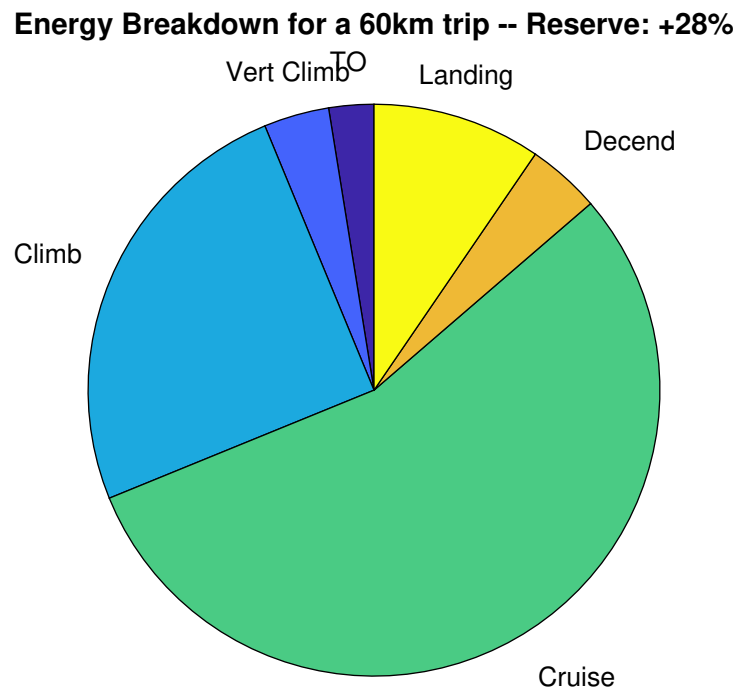
Figure 10.6: The distribution of energy required to perform different phases of flight

Even though air traffic density and conflict probability is much more spread out in the flight layer system, the proven energy inefficiency is deemed in acceptable. The free flight system will therefore be implemented. Figure 10.6 shows the energy usage distribution per flight phase for the selected free flight concept. What can still be observed is the outstanding large portion of energy required for vertical hover, which highlights the energy heftiness of takeoff and landing operations.

10.4. System Sizing Methods

With full knowledge about the mission profile permitted and the airspace design, the optimal routes to serve, fleet size and number of required hubs can be found. This section will highlight the tools implemented to size the system.

10.4.1. Route Selection

With full knowledge about the mission profile permitted and the airspace design, the most optimal routes to serve can be computed. A revenue proxy is constructed to evaluate the demand that certain routes offer over others.

Revenue Proxy   An a priori proxy for revenue is set up based on trip time advantage with respect to cars on the same trip. The total number of passengers per unit distance is also included, to account for the volume of potential customers of the route:

$$G(\text{trip}, t_{\text{day}}) = \left(T_{t_{\text{car}}}(\text{trip}, t_{\text{day}}) - T_{t_{\text{UAM}}}(\text{trip}) \right) \cdot \frac{\#\text{pax}(\text{trip}, t_{\text{day}})}{D} \tag{10.1}$$

Here, #pax is the amount of people commuting the trip in question at the time of day in question and D is the direct distance from origin to destination. The necessary data is known from the CTTP[1]. This is the same data that is used to make a quantitative market analysis as described in subsection 3.2.4. The UAM trip time $T_{t_{\text{UAM}}}$ is estimated based on a simplistic, user specified model involving cruise speed, trip distance information and a constant estimate of boarding and first/last mile transport time.

Alternative (car) Model   From the more detailed market study of LA (subsection 3.2.4) a set of morning commutes is known showing the hourly flow of commuters between 113 districts. Because of the high combinatorics of this problem and available computational resources, the top $N = 2{,}800$ trips are sampled for each hour from 5am to 10am representing 75% of the by-car commuters. These 14,000 data points are queried to Google Maps' "Directions" API asking for the local time traffic-corrected and average traffic-corrected trip time on Monday the 13th of May, 2019. This puts numbers to the metrics $T_{t_{\text{Car,avg}}}$ and $T_{t_{\text{Car}}}(t_{\text{day}})$ and their ratio $C(t_{\text{day}}) = T_{t_{\text{Car}}}(t_{\text{day}}) / T_{t_{\text{Car,avg}}}$ as a congestion index for every of the 2,800 trips.

Trip Selection   All known trips are sorted in descending order by metric 10.1 and stored in a table. The cumulative sum of the gain metric is defined as equation 10.2, with $0 \le n \le N$ where N is the total number of distinct trips available in the dataset. When a value for n is selected, these top trips can be used as the design input for the system.

$$S_n = \zeta \sum_{i=1}^{n} G_i \tag{10.2}$$

The constant factor ζ represents the percentage of the total people commuting these routes that are now transported by the UAM system. It is necessary, since it may depend on the mobility concept, whether all people on a small number of routes n should be targeted, or a smaller percentage on a larger n.

S_n can be set to a value S_{target} which can be reached by setting appropriate values of the routes to serve n and ζ with $S_{\text{target}} / \sum_{i=1}^{N} G_i \le \zeta \le 1$. Figure 10.7 illustrates this concept.
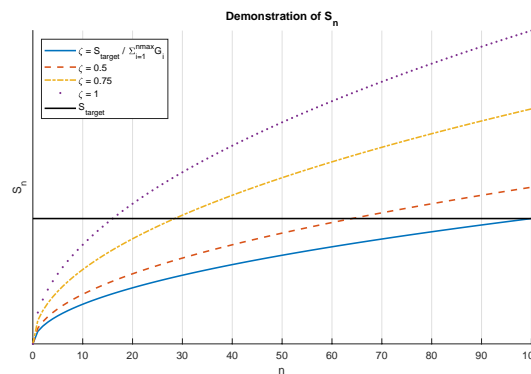
Figure 10.7: The target S value can be reached by different combinations of ζ and n

Verification   To verify the scripting, same information for a few randomly chosen trips is requested manually on `www.google.com/maps` and via the API from MATLAB. After running the full Google Maps query the average time loss due to traffic is evaluated to be 33% of average trip time added which do not not match the TomTom traffic index[2] which reports 62% for the morning peak in 2016 (with an upwards trend in the recent years), at the same time of day as predicted by this algorithm (8am to 9am). To investigate this, the traffic model that Google provides is configured from "best-estimate" to "pessimistic". This overestimates the average trip time added by 80%, which is closer to the TomTom data when carfully extrapolating it for 2019.

---

[1] `https://ctpp.transportation.org/2012-2016-5-year-ctpp/` [accessed 08.05.19]
[2] `https://www.tomtom.com/en_gb/trafficindex/city/los-angeles` [accessed 21.05.19]

10.4.2. Fleet Sizing

In the previous subsection 10.4.1, the routes best served by the vehicle are found. This flows down into determining the system characteristics such as zombie flight trip flux, zombie flight ratio, total system energy, and fleet sizing.

Vehicle Trip Model and Zombie Flights   A vehicle trip model is defined in order to model the vehicle flux serving the chosen routes. The vehicle trip model is defined as follows: the trips taken on each route are modelled for the maximum throughput obtained during commute travel between 5am and 9am. A return trip for every commute morning commute in the afternoon is assumed, and each individual vehicle only travels back and forth on a designated route. It must be taken into consideration that not every trip is served with full passenger payload. For the sake of simplicity, it is assumed that for each trip, the vehicle is either fully loaded with passenger payload ("revenue flight") or is empty ("zombie flight").

This model is applied to first compute the number of trips per unit of time Ψ, to then compute the zombie ratio (percentage of trips travelling empty). Equation 10.3 and Equation 10.5 show the applied expressions. The input ζ factor is explained in Equation 10.4.1, and represents the fraction of commuters using the UAM service. The maximum number of vehicles, on route number i is governed by the maximum of the number of passengers on that route, R_i or its inverse route ($\bar{R}_i$), timed by two. The multiplication factor of 2 counts for the vehicles that are on the return route. This is shown in Equation 10.3. There are m unique routes pairs (a pair is a route and its inverse) to iterate over.

$$\text{maxveh} = \lceil \max(\frac{pax(R_i)}{veh_{\text{pax}}}\zeta, \frac{pax(\bar{R})}{veh_{\text{pax}}}\zeta) \rceil \quad \text{minveh} = \lceil \min(\frac{pax(R_i)}{veh_{\text{pax}}}\zeta, \frac{pax(\bar{R})}{veh_{\text{pax}}}\zeta) \rceil \quad (10.3)$$

$$\Psi(R \cup \bar{R}, t_{\text{day}}) = 2 \cdot \text{maxveh} \quad (10.4)$$

A more precise definition of the zombie ratio is given in Equation 10.5:

$$z(R \cup \bar{R}, t_{\text{day}}) = \frac{\text{total trips - revenue trips}}{\text{total trips}} = \frac{(\Psi(R \cup \bar{R}, t_{\text{day}}) - (\text{maxveh} + \text{minveh}))}{\Psi(R \cup \bar{R}, t_{\text{day}})} \quad (10.5)$$

The mean zombie ratio obtained for the arbitrary system serving 600 routes for 105 vertiports at peak commute time of 8-9 am is 0.45. This gives an indication that some trips have revenue return trips, however the vast majority do not and can be considered an operational setback to the vehicle trip model in place.

Fleet Size Computation   The vehicle trip model and zombie ratio is defined, allowing for the fleet size to be estimated. The time for one flight cycle is required for this computation. The time for one cycle is approximated as the sum of air time AT and the turnaround time $t_{\text{Turnaround}}$. The air time computed using the flight profile and cruise altitudes defined in Section 10.3. The turnaround time is dependant on the boarding time, taxi time, and time to vertically hover to the approach fix. Next to that, it is assumed that the vehicles are charged before every flight. The fleet size calculation is shown in Equation 10.6. Effect of wind on airtime, as well as time vehicles are in operation while travelling to maintenance and storage facilities are neglected. The fleet size is computed for the most critical commute time, being the time of maximum flux. This corresponds again to the 8-9 am time range.

$$\text{fleet size} = \sum_{i=1}^{m} \lceil \left((AT + t_{\text{turnaround}})_{i,\text{zombie}} \cdot z + (AT + t_{\text{turnaround}})_{i,\text{revenue}} \cdot (1 - z) \right) \cdot \Psi((R \cup \bar{R})_i, t_{\text{peak}}) \rceil \quad (10.6)$$

The turnaround time is derived from the vertiport design, which is analysed in Equation 10.15. The fleet size needed to fly the arbitrarily selected 600 routes is equal to 4,470 vehicles.

10.4.3. Passenger Kilometres and Energy Footprint

For each trip at each of the 5 discrete time slots the required vehicle energy, air-time and turnaround time is calculated. The trip energy E depends on whether the flight is a revenue trip or zombie flight, with the latter having significantly lower energy required (Equation 10.7). Passenger kilometres pax_{km} on a certain route during a discrete time slot are simply the sum of the revenue trips multiplied with the route length D as shown in Equation 10.8.

$$E(R \cup \bar{R}, t_{\text{day}}) = \Psi(R \cup \bar{R}, t_{\text{day}}) \cdot (E_{\text{zombie}} \cdot z + E_{\text{revenue}} \cdot (1 - z)) \tag{10.7}$$

$$\text{pax}_{\text{km}}(R \cup \bar{R}, t_{\text{day}}) = (\text{maxveh} + \text{minveh}) \cdot veh_{\text{pax}} \cdot D(R \cup \bar{R}) \tag{10.8}$$

10.4.4. Verification

To verify the flux calculations, a shortened trip definitions file is created and the fluxes are manually computed for the low amount of trips. This is compared and confirmed to match with the scripted calculations and also associativity with the GEOIDS (specifying the location within LA country) is confirmed to be kept. Although not shown here for brevity, these unit testing files are available from the team on request.

Correct operation of the tool integration needs to be confirmed, especially with regards to keeping the associativity of the PUMAs and treating the route inverses correctly. This is achieved by inputting a trip database of only two trips with 100 passengers going one way on a route and 60 passenger going to opposite way on the same route, at each time of the day. The smaller database allowed to do hand calculations with which to compare the tool outputs. ζ is set to 1 initially and then varied.

After correcting a forgotten ceiling function in calculation of the number of gates, the results matched one-to-one when comparing all six quantities above (which caused a few percent of relative error), which increases confidence in the implementation.

10.5. System Sizing in Different Stages

Section 10.4 describes the tools needed to compute the fleet size and number of vertiports in terms of target gain and number of trips one would like to serve. This section applies these tools to size the system at the different stages of development of the UAM system.

An appropriate ratio of vertiports and vehicles is approximated at 1:10, as estimated in Section 11.2. This ratio is used to define the target system size at different stages of development, as shown in Table 10.2. An initial investment phase for a 20 vertiport system and 200 vehicles, an intermediate second phase of 50 vertiports and 500 vehicles and a final phase, when 105 vertiports covering the pumas reachable within the range limits of the vehicle are implemented. To obtain the system size requirement, the correct inputs to the system need to be found, namely the target system velocity gain, S_n and number of routes to serve, n. The sensitivities displayed in Figure 10.8 are used to obtain these values. It can be seen that the value for n is directly proportional to the required number of routes to serve, and the value for S_n determines the required fleet size for the selected number of routes to serve.

The Table 10.2 displays the corresponding total target gain metric (see subsection 10.4.1) and number of routes to serve. Other significant parameters such as number of passengers served, system PREE and average time gain are also displayed.

As can be seen from the table, an increase in fleet size and hubs as defined in Table 10.2 result in an increase in passengers served and market share, defined as percentage of total car commutes served. The efficiency of the system decreases however, as seen by a decrease in PREE from 0.47 to 0.33. This can be explained by
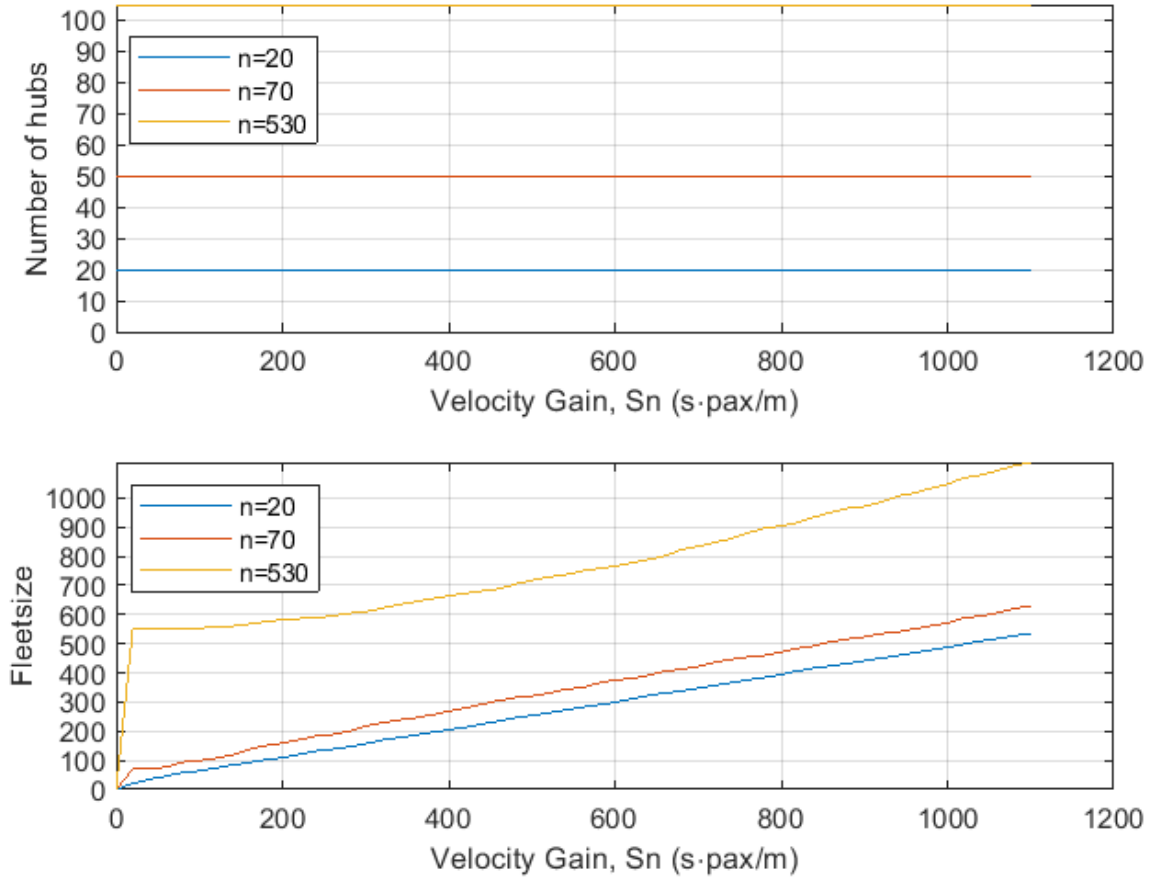
Figure 10.8: Variation in system fleet size and number of vertiports for varying number of hubs and target total velocity gain

Table 10.2: Comparison of system's stages of development using 1:10 target vertiport to fleet size ratio, and corresponding system parameters and efficiency metrics

	Phase 1	Phase 2	Phase 3
Number of Vertiports	20	50	105
Fleetsize	200	500	1,000
System Gain, S_n	20	70	530
Number of routes served, n	388	848	933
Number of Passengers Served	6,300	15,800	23,500
Marketshare (%)	0.055	0.13	0.17
Mean time gain (minutes)	27.4	27.2	25.9
PREE	0.47	0.46	0.33

the fact that if n is increased, trips with a smaller velocity gain that the previously selected routes are offered. This requires more vehicles to operate for a smaller increase in passengers to serve. This gives indication that the hub to fleet size ratio is not optimal as the system is scaled up.

Optimal Target System   Due to the inefficacy of the defined ratio in Table 10.2, a new optimal ratio is defined. A PREE is set which is at least that of phase 1, while keeping the required fleet size at a achievable amount. The the target gain, S_n, is scaled up to a value of 6,000 to serve a fleet size of 4,470 around 105 hubs. The obtained system parameters are shown in Table 10.3. In addition, the PREE for a single trip at maximum payload (not for the system which takes into account the zombie ratio) for the mean trip distance is 1.0.

Table 10.3: Optimal target system size for maximised efficiency, and corresponding system parameters

Number of vertiports	Fleetsize	Number of routes served	Mean route distance (km)	Number of pax served per day	Market-share (%)	Mean time gain (min)	PREE	Zombie ratio
105	4,470	600	18	155,000	1.10	26	0.49	0.45

10.6. Vertiport Sizing

To design the vertiport it the passenger throughput is calculated, the approach used is explained in subsection 10.6.1. The passenger throughput is an input to calculate the size of a hub (subsection 10.6.2). Afterwards, the maximum throughput per gate is calculated in subsection 10.6.3, based on the operations on the ground. Using the requirements on the vertiport design a final design will be shown in this subsection.

10.6.1. Passenger Throughput

A measure of the maximum passenger throughput is firstly computed. This puts a preliminary throughput requirement on the set of selected PUMAs which can be used to subsequently compute an estimate of size and cost of the landing infrastructure necessary.

In order to determine a throughput requirement for the different hubs selected in subsection 10.4.1, a metric called flux can be computed for all PUMAs districts, based on the selected n number of trips. This is the maximum of commuters flowing into a district and the outflow of commuters, as seen in equation 10.9:

$$\Phi(\text{PUMA}, t_{\text{day}}) = \max\left(\sum_{i=1}^{n}\left(\text{pax}(\text{trip}_i, \text{into PUMA}, t_{\text{day}})\right), \sum_{i=1}^{n}\left(\text{pax}(\text{trip}_i, \text{out of PUMA}, t_{\text{day}})\right)\right) \qquad (10.9)$$

10.6.2. Hubs Sizing

Knowing the vehicle flow per hour on every unique route enables sizing of the hubs as well. For simplicity, one "lumped" hub is placed at the centre of each served PUMA. The hub is variable in size and may contain a number of vertiports which are comprised of one touchdown and liftoff (TLOF) pads and a number of gates where vehicle ground operation takes place.

Instead of assuming a fixed gate ratio (as done in the midterm report [7]), with estimates of taxi time and gate time, a feasible but not optimal gate ratio was calculated for every hub k, assuming that all vertiports in that hub share the same number of gates.

$$\text{gates}_k(t_{\text{day}}) = \left\lceil \sum_{j=1}^{\text{routes from k}} t_{\text{turnaround}_j} \cdot \Psi(R \cup \bar{R}_j, t_{\text{day}}) \right\rceil \tag{10.10}$$

$$\text{pads}_k(t_{\text{day}}) = \left\lceil \sum_{j=1}^{\text{routes from k}} t_{\text{taxi}} \cdot \Psi(R \cup \bar{R}_j, t_{\text{day}}) \right\rceil \tag{10.11}$$

$$\text{gate2pad}_k = \left\lceil \max t_{\text{day}} \left(\text{gates}_k(t_{\text{day}}) / \text{pads}_k(t_{\text{day}}) \right) \right\rceil \tag{10.12}$$

$$\#\text{gates}_k = \max t_{\text{day}} \left(\text{gates}_k(t_{\text{day}}) \right) \tag{10.13}$$

$$\#\text{pads}_k = \text{gate2rat} \max t_{\text{day}} \left(\text{pads}_k(t_{\text{day}}) \right) \tag{10.14}$$

Note that turnaround time $t_{\text{Turnaround}}$ and taxi time t_{taxi} are in units of hours, just like Ψ is in 1/hours.

10.6.3. Maximum Throughput per Gate

The maximum throughput of the system is of great importance. It shows how many customers the system can handle and how many gates and TLOF's should be placed. Previous researches have stated that the vertiport design is the most limiting factor for the throughput. Next to that, the throughput is dependent on the operations/scheduling of the vehicles. In this subsection, both aspects will be discussed. Firstly, the operations/scheduling of the vehicles will be explained then the vertiport design will be discussed.

Gate Efficiency at System Level   The gate efficiency contains the number of customers that can be ideally served per hour. The turnaround time is defined as the time for all activities from the moment the vehicle touches down, to the moment it takes off again. The taxi time is just 15 seconds, based on a taxi speed of 15 km/h. The complete turnaround time (in minutes) is given in Equation 10.15 as a function of the number of passengers (n_{pax} fully loaded).

$$\underbrace{1.5}_{\text{land}} + \underbrace{0.25}_{\text{taxi in}} + \underbrace{0.5}_{\text{despin}} + \underbrace{0.5}_{\text{spin}} + \underbrace{0.25}_{\text{taxi out}} + \underbrace{0.5}_{\text{take-off}} = 3.5 = t_{\text{taxi}}$$

$$\underbrace{0.25 \cdot n_{\text{pax}}}_{\text{deboarding}} + \underbrace{2}_{\text{inspection}} + \underbrace{0.5 \cdot n_{\text{pax}}}_{\text{boarding}} + \underbrace{0}_{\text{downtime}} = t_{\text{boarding}} \tag{10.15}$$

$$t_{\text{turnaround}} = \max \left(t_{\text{boarding}}, t_{\text{charging}} \right) + t_{\text{taxi}}$$

Figure 10.9 shows the steps accounted for in the turnaround time.
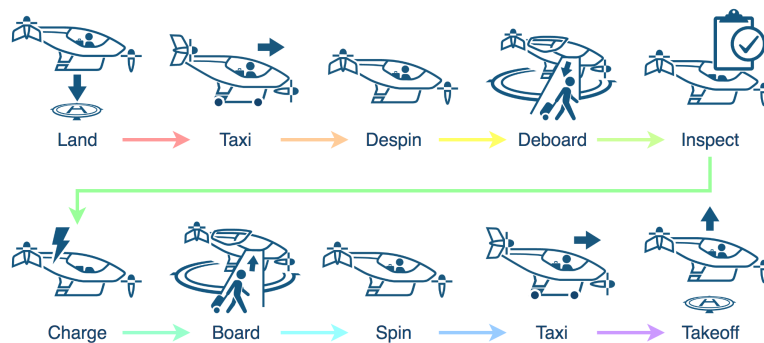
Figure 10.9: The "turnaround" time of a vehicle accounts for all time on the ground. Charging/refuelling can occur concurrently with boarding and inspection.[3]

---

[3]Icons courtesy of Vahana - `https://github.com/VahanaOpenSource/iconography` [accessed 20.05.19] `https://vahana.aero/urban-air-mobility-iconography-5ad4de1fbca0` [accessed 20.05.19]

Type of Network   The network will be based on a port-to-port system, Figure 10.10 shows a cycle for this system. Using this type of network, the vehicle can be charged after every journey. A disadvantage of this network is that the locations of the vertiports are set, which means that that the customer needs to travel to a vertiport. However, this last mile transportation has already been taken into account.
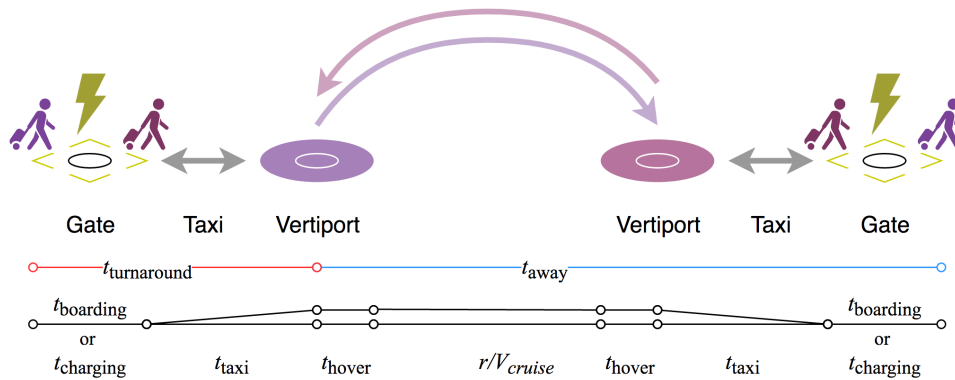
Figure 10.10: When all customers travel vertiport to vertiport, the vehicle can charge after every flight. This diagram shows a complete cycle of two customer journeys.

10.7. Vertiport Design

As known the airfield capacity is the primary bottleneck for commercial aviation and the expectation is that this will also be the constrain for a UAM system. The vertiports have to be capable of supporting the throughput of aircraft and passengers. The number of operations for an UAM system exceed the number for current heliports. Next to that, it is of great importance that the vertiports are integrated with the existing transport modes.

There are requirements on the dimensions of vertiport designs. The Touchdown and Liftoff Area (TLOF) should have a maximum dimension of 3/2 of the maximum dimension of the vehicle with an additional space of 1/3 tip-to-span. The ground taxi way should be 1.5 times the tip-to-tip span to make sure there is enough clearance. In previous studies it has been concluded that ground taxi is recommended for a higher throughput. Moreover it is assumed that, "the gates have a diameter equal to the maximum vehicle dimension plus either 10 ft for ground taxi operations, or the greater of 10 ft or 1/3 rotor span for hover taxi operations"[3]. A taxiroute may not come within 1/3 of the tip-to-span distance between the gates and taxiways. These restrictions will lead to complex design of the vertiport and should be optimised to create the highest throughput. In Figure 10.11 the restricted dimensions are shown.

Using these requirements, the team has designed an example vertiport. The vertiport has been designed for the city centre of LA on top of the Los Angeles Convention Center West Hall. The expectation is that the Convention Center will be used as a vertiport for 2050 as it is located in the city centre of LA and it has a enough space on top of the roof to create a big vertiport. Moreover, it is placed closely to the highway and just 5 minutes walk from the Pico metro station. Underneath the Convention Center there is enough space to park cars, which makes it easily accessible for commuters. The rooftop has a length of 175 meters and a width of 113 meters, this makes the vertiport suitable for 8 TLOF pads and 14 gates. These TLOF pads are 18 by 18 meters and the gates have a size of 10 by 10 meters. The terminal is placed in the middle and the energy for this building will be provided by solar panels on the roof. The terminal is 63 meters long and 25 meters wide. As the vertiport is placed on top of an existing building, the building should be reinforced. However, these adjustments are for now not taken into account. In front of the gates two sliding doors are placed so that the passengers can leave/enter the terminal after/before their trip. The design of the vertiport can be seen in Figure 10.12.
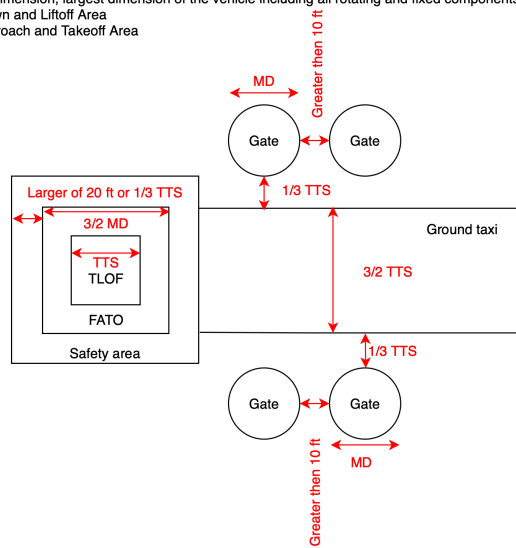
Figure 10.11: Vertiport design

Figure 10.12: Vertiport design on top of the Los Angeles Convention Center

The vehicle will land at the TLOF pad and taxi to the closest available gate. The taxi procedure is done by taxibots. These are robots which make sure that the vehicle is able to taxi. For each vehicle two taxibots are needed, one will go underneath the vehicle at the front and one at the back. The vehicle will be lifted and is able to taxi. The taxibots operate at a speed of 15 km/h, this will lead to a maximum taxitime of 15 seconds. There is one set of taxibots, consisting of two taxibots, for each gate to ensure the optimal operation. Once arriving at the gate the rotors will despin and afterwards the deboarding procedure starts. The customers leave the vehicle and the inspection will take place. During the process the vehicle will be charged. The customers will leave the vehicle and enter the terminal via the two doors placed in front of the gate. Once the vehicle gets a clearance the boarding procedure will start. The customers will enter the vehicle, thereafter the rotors will start spinning and start the taxi procedure to the TLOF. Finally, the vehicle will take-off and a new vehicle can arrive/departure at that TLOF.

10.8. ATM System

An urban airspace shared by numerous operators working on different schedules brings forth demands that ATM systems in today's day and age are not adapt to deal with. This section will give an overview of the design choices to be implemented in order to obtain an ATM system that is able to effectively manage the urban air mobility system at hand.

10.8.1. Decentralisation of ATM

One of the first decisions to make when designing the ATM system is the degree to which it is decentralised. In an ATM system such as the one in place today for commercial aviation, a centralised air traffic controller (ATCo) manages the airport flux, ensures separation in en-route air spaces, and manages the transition between airport and en-route traffic. To reduce ATCo workload for tasks such as collision avoidance, pre-determiflight trajectories along specific airways are assigned resulting in structured but slow air traffic, and air crafts are forced to take indirect and less efficient flight paths [32]. The lack of efficiency has become evident, as in 2017 for an air traffic increase in Europe of 3.8 % , the number of en route delays radically increased by 104 % [33].

A decentralised system is more adapt to a dense and chaotic airspace. ATCo workload is distributed amongst all vehicles in the airspace, and all pilots have a situation overview of surrounding traffic and have the choice to fly at direct and more fuel efficient routes [34]. Freedom of free flight also brings improvement to the level of safety as a more distributed use of the airspace results in smaller chances of collision, compared to locally congested airways required to reduce workload on centralised ATCos [31]. A decentralised system for trajectory determination and conflict resolution is therefore implemented.

Nevertheless, the airspace will always be to a degree semi-segregated even though free flight is permitted within the given constraints, giving the need of a centralised surveillance entity. subsection 9.5.6 also describes that before level 5 technological maturity for automation is achieved, a centralised entity must have authority and control over the vehicles for when unpredictable operating circumstances arise. A centralised Air Navigation Service Provider (ANSP) will therefore be required for traffic management during unpredictable situations, as well as surveillance and other communication services such as weather conditions.

Required On Board Technology   Subsection 9.5.6 describes the on board technology required for autonomous communication. Namely, an Automatic Dependent Surveillance Broadcast system (ADS-B in) and a mode S transponder (ADS-B out) will be equipped on each cockpit allowing for periodic signalling of position, velocity, trajectory and identity between all vehicles in operation [35]. ADS-B information is communicated to the conflict detection and resolution (CD&R) automated system, which uses algorithms to compute the conflict free trajectory.

10.8.2. ATM Communication Flow

The entities involved in the system are the show in Figure 10.13. The Air Navigation Service Provider (ANSP) is the centralised entity that provides surveillance and policing for all operators using the urban air space. The fleet management is the private operator owned entity and coordinates the vehicles with respect to the demand, vertiport capacities, and restrictions placed by the ANSP. The communication flow is displayed in Figure 10.13, and the order of communication throughout different stages of operation is subsequently described in Figure 10.14.
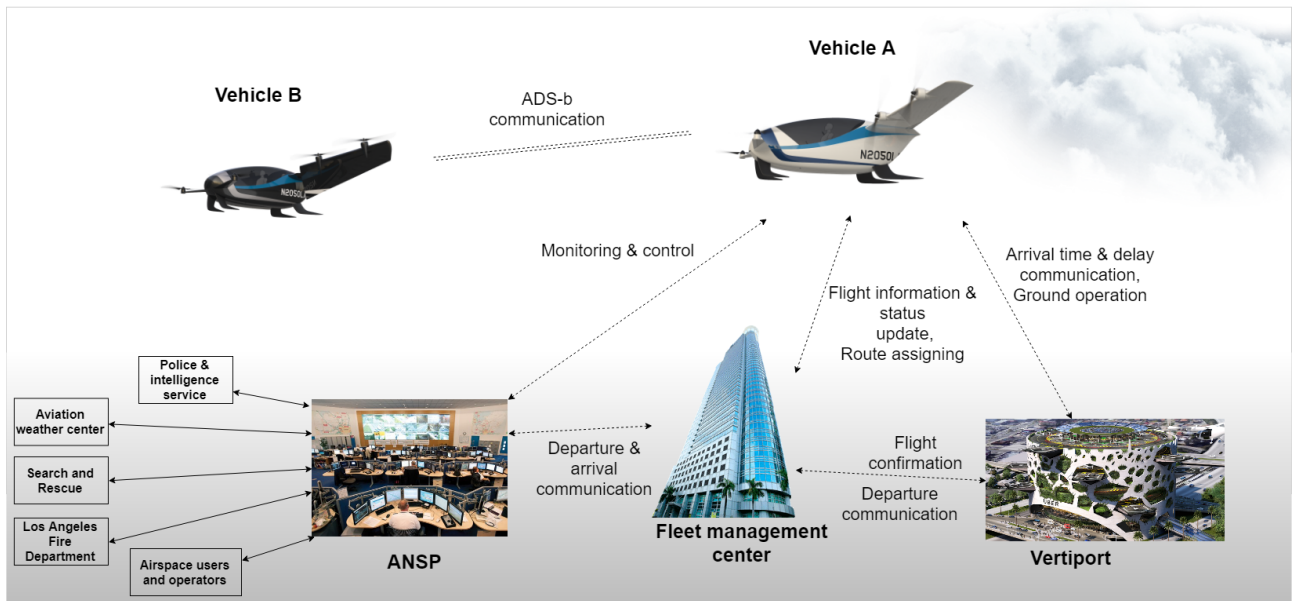
Figure 10.13: Communication links between Entities involved in ATM
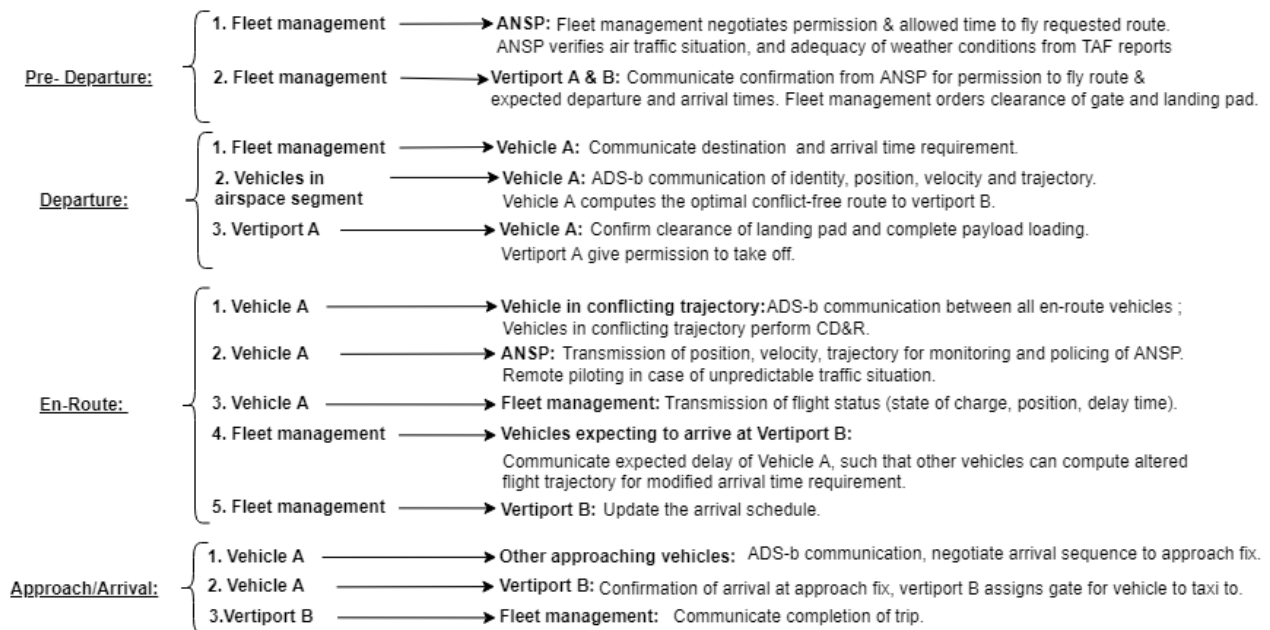
Figure 10.14: Communication flow at different stages of operation

10.8.3. Emergency Procedure

Cases of emergency apply to any case in which passenger safety is put jeopardy. Cases may involve vehicle malfunctions, vehicle collisions, passengers urgently needing medical attention, criminal or terrorist attacks on board or at vertiport site. A few major important steps are always followed regardless of the situation at hand, and are listed below.

1. **Alarming the ANSP & surrounding vehicles** The procedure starts with an emergency notification of the emergency and nature of the problem from the vertiport or vehicle to the ANSP. The ANSP has direct contact with all emergency operators, and other operators using the airspace, and therefore must be contacted first.

2. **Calling emergency services** The ANSP will immediately notify the fire department, ambulance, search and rescue teams and local police.

3. **Executing emergency operation** The first step to all emergency operation execution is notifying all the nearby vehicles such that appropriate route deviation can be performed. Depending on the nature of the emergency, different procedures will follow.

   - Vehicle emergency landing: Necessary if further cruise is not possible, for example due to empty battery or severe rotor malfunction. The ANSP will assign the most nearby stable horizontal ground location for the emergency landing to be executed. Emergency responses are ordered to swiftly arrive at the landing spot and evacuate the area.

   - Non-critical vehicle malfunction: The vehicle will be permitted to cruise at the emergency fight layer to the most nearby vertiport or preferably a maintenance facility, and will be given landing pad priority.

   - Landing accident at vertiport: all approaching vehicles will be deviated to nearby vertiports. Emergency responders are ordered to swiftly arrive at the vertiport.

4. **Notifying operators** The ANSP will directly notify surrounding vehicles as well as the UAM operators, such that appropriate routing schedule modification can take place, and customers can be notified.

10.9. General Maintenance Plan

Before a new aircraft can be brought on the market, it should have an Approved Maintenance Plan (AMP). This AMP is created by the operator and is subsequently approved by the National Aviation Authority (NAA). This AMP contains a list describing all maintenance tasks that are required to be performed after a certain amount of time or after a set amount of flight hours or cycles have been performed by the vehicle. Most of the maintenance will consist of verifying that certain components still comply with their corresponding requirements. In case a component does not meet these requirements, it should either be fixed or replaced depending on the reason of defiance.

The maintenance of the vehicle consist of three parts. First, there is the daily maintenance. This maintenance consist of a visual check which will performed after every flight. It is a brief check of all components, which is mainly focused on verifying no damage has been done to the vehicles. Secondly, there is the software and hardware check that will be performed prior to every flight. This type of maintenance is performed by the autonomy kit itself. During this check it verifies that all the different software and hardware systems are functioning adequately. Software systems that will be checked are for example the communications system as constant connection with ATM is very important. For the hardware system, it is checked for example if the tilt mechanism responds appropriately to certain inputs. Finally, the actual maintenance plan is usually structured in the form of a so called ABC check system[4]. The A and B checks mostly consist of visual type of inspections, while the C and D checks are more thorough checks, and more specific tests of the sub-components are performed. At this stage of the design, it is not yet possible to determine the exact lay-out of the A, B, C and D check. The following rules therefore only define a preliminary setup for the ABC check of the vehicle. The rules are likely to change in accordance with manufacturers' instructions.

The A check is performed after every 300 cycles. One cycle is defined by first taking-off, then cruising, then landing. An A check will need roughly 20 hours of maintenance work. The B check shall be performed every 1,500 cycles. This check shall require approximately 100 man-hours of maintenance. The C check shall be done after 5,000 cycles. This check is much more thorough then the A and B checks. It therefore also requires many more man-hours of maintenance. For larger aircraft, such as the A320, this check may take up to 6,000 man-hours[5]. However, since this vehicle is a lot smaller, this will probably be more in the

---

[4]`https://www.aircraftengineer.info/aircraft-maintenance-checks/` [accessed 22.06.19]
[5]See footnote 4

range of a 1,000 man-hours. During the C check, also the interior of the vehicle could be renewed if this is deemed necessary. Finally, the D check should be performed after 25,000 cycles. This is the most time-demanding check as the whole vehicle is practically taken apart and all components and sub components shall be inspected. Due to the fact that it requires many man-hours of maintenance and that the vehicle is out of service for an extended amount of time, it is also the most expensive check. For standard commercial aircraft the D check is performed about every 6 years. On average, the D check is completed three times before an aircraft is retired[6]. It is expected that this maintenance plan will be the same for the Bumblebee EX.

Furthermore, it is assumed that the manufacturers of all components of the vehicle will provide a very detailed maintenance plan for their individual components. Based on the advised maintenance procedures, they will be incorporated in a suitable manner in the ABC check system. Special attention should be paid to the maintenance of the autonomy kit. For obvious reasons, it is of utter most important that all these components function adequately. In subsection 9.5.6 a description of several components of the autonomy kit is given. The manufactures of these components provide own personnel to perform specific maintenance procedures. Therefore, the expected maintenance moments of the vehicle should be communicated with these manufacturers, such that the right maintenance personnel is present at the time of the different checks.

Below, an example is given of what kind of maintenance procedures could be performed during an A, B and C check of the propulsion system. Thereafter, an exemplary replacement procedure of one of the batteries is described. These two examples show how all the other maintenance checks and replacement procedures will be described in the actual final AMP.

Maintenance Plan Propulsion System   According to the FAA [36] propellers are, in general, designed to be able to endure higher levels of stress for long periods. Even though proper safety factors are taken into account, failures still occur. A maintenance plan is made to decrease the failure rate of certain components and therefore, extend the service life. During the propeller's service life, it is highly subjected to bending, flexing and vibratory loads. The propeller can also be exposed to external sources causing stresses, such as bird strikes or up shooting debris on take-off and landing pads.

In [36], an overview is given of the main components that should be inspected during different maintenance checks. A summary of these points is shown below. A more extensive inspection procedure shall be created at a later phase of the design to either prevent or postpone certain failure modes from occurring.

A type A check might be in the form of a pre-flight / walk-around inspection. This check would include careful inspection of each of the blades for surface damage, crack forming, oil and grease leakage at odd locations and looseness of the blades. Furthermore, the spinner and bulkhead should be checked for similar reasons for defiance. Finally, the general condition of the control system should be inspected as well. Every blade shall have a separate maintenance logbook in which the history performed repairs are logged.

The B check shall include the following for the propeller blades: tip tracking inspection and verification of correct functioning of protective coatings. Again, a check for surface damage should be performed. For the spinner and bulkhead assembly, the propeller-to-engine attachment should be inspected. Additionally, it should be investigated if there are any signs of fatigue that may harm the air worthiness of the vehicle. For all components, it should be verified that the condition of bolts and fasteners is still appropriate.

For the C check, the whole propulsion system should be disassembled. All components shall be inspected for any kind of wear and crack forming. Also, the tachometer, an instrument which measures the rpm of the shaft spinning the propellers, should be carefully tested. As over speed is one of the main causes for failure of propellers.

Replacement Procedure of a Battery   After a certain amount of flight hours, the performance of a battery degrades to an unacceptable level. The performance of the battery can be measured by means of a smart

---

[6]See footnote 4

sensor, capable of measuring the voltage level[7]. An optimal voltage is important to maximise the battery capacity. It will also provide a form of safety, since it can give a warning to the system in case the battery is malfunctioning. Once the type of batteries are known, a threshold can be determined that sets the amount of flight hours that the vehicle should have flown after which the battery performance should be checked by other means than just the smart sensor. In case the battery needs to be replaced, the following steps should be followed (these steps are based on the instructions on how to replace a car battery[8]):

1. Verify that the battery indeed needs to be replaced.
2. In case different types of batteries are used in the vehicle, verify that the correct replacement battery is present.
3. Create a secure working environment. Batteries contain highly corrosive materials, therefore gloves should be worn.
4. Open the space where the batteries are stored.
5. Identify the battery that has to be replaced.
6. Locate the positive and negative terminals of the battery.
7. Disconnect the terminals, the negative terminal should be disconnected prior to disconnecting the positive terminal.
8. Remove the battery.
9. Put the replacement battery in to place.
10. Reconnect the positive terminal prior to reconnecting the negative terminal.
11. Close and lock the storage location of the batteries.
12. Dispose the old battery in the correct location.

Not only for the vehicle a maintenance plan has to be created, but also for the vertiports. The vertiports have similar functions to an airport. Therefore, the following steps are advised to follow to setup a preventive vertiport maintenance plan. The instructions are based on those given in Chapter 5 of [37] to setup a preventive maintenance plan for an airport.

1. Determine what the requirements for the vertiports infrastructure and conditions are.
2. For all of the components of the infrastructure identify what preventive maintenance is needed.
3. Based on safety, operations and economics of the vertiports prioritise the required maintenance.
4. Gather all the necessary resources to perform the maintenance tasks. Also, ensure that the staff of the vertiports is trained to execute the tasks in a satisfactory manner.
5. Construct an extensive check-list which can be used to verify if maintenance has to be done and if it is done correctly.
6. Implement the program and update is regularly.

10.10. System Function Diagrams

In this section the (FFD) and the (FBS) of the system are described and shown. A FFD shows in which order the functions of a system must be performed. This diagram is created by different blocks, each describing the functions of the system by the use of a verb. A FBS shows of what sub-functions a top level function is composed of. A FBS is therefore shown in the form of an AND tree. A FBS goes into more detail than a FFD. In subsection 10.10.1 the FFD of the system is described. This section is followed by subsection 10.10.2, in which the Functional Breakdown Structure is explained.

---

[7]https://www.fierceelectronics.com/components/monitor-your-electric-vehicle-s-battery-a-smart-sensor [accessed 21.06.19]

[8]https://www.wikihow.com/Change-a-Car-Battery [accessed 21.06.19]

10.10.1. Functional Flow Diagram

The FFD of the system shows the order in which the functions of the system are performed. The system interacts with its environment and therefore this interaction is also taken into account in the FFD. The FFD of the system is shown on the foldout page 98 of this report. Each block in the FFD represents a function or a sub-function.

The colour coding of the FFD from top level functions to lower level sub-functions is as follows: Pink (top level function), blue, green, orange (lowest level sub-function). Furthermore, it should be noted that the FFD is a cycle. It starts and ends with the stage when the passenger is waiting to make use of the system.

10.10.2. Functional Breakdown Structure

The FBS of the system is shown on the foldout page 99 . It provides a more clear insight into what sub-function specifically should be performed to completely fulfil a top level function. Where necessary the FBS goes one level deeper than the FFD shows. The same colouring system is used as in the FFD. In addition to this, the lowest level sub-functions are shown in purple.

Functional Flow Diagram

1 Wait for passengers

2 Perform pre-flight inspection

2.1 Test Hardware

2.2 Test Software

2.3 Analyse Test Results

OR

3 Boarding of Passenger(s) (& Cargo)

3.1 Open port from terminal to gate

3.2 Let max 4 passengers through

3.3 Unlock passenger- & cargo-doors

3.4 Let passengers load cargo

3.5 Load passengers

3.6 Decide loading sequence

3.7 Perform safety check

AND

3.4.1 Confirm seat belts are on

3.4.2 Confirm (Cargo)doors are locked

3.4.3 Confirm center of gravity is within allowance

4 Determine Flight Path

4.1 Communicate with ATC

4.2 Adjust Path if neccessary

4.3 Make estimate of residual power at end of journey

4.4 Determine next possible journeys

5 Fly to destination

5.4 Check flight path continously

5.1 Vertical takeoff

5.1.1 Start propulsion system

5.1.2 Initiate vertical climb to desired altitude

5.1.3 Transition to cruise phase

5.2 Cruise

5.2.1 Determine most efficient cruise speed

5.2.2 Increase speed to cruise speed

5.2.3 Engage in-flight entertainment

5.3 Land Vehicle

5.3.1 Communicate with Ground Segment

5.3.2 Transition back to hover

5.3.3 Decent to vertiport

5.3.5 Negotiate landing position and speed

6 Taxi to gate

6.1 Vehicle is picked up by taxibots

6.2 Taxi to gate

6.3 Taxibots carefully put the vehicle down

6.4 Go into Safe-Standby-Mode

7 Unboarding of Passenger(s) (& Cargo)

7.1 Unlock passenger- & cargo-doors

7.2 Verify that all passengers are out fo the vehicle

7.3 Verify that all cargo is taken out of the cargo compartment

7.4 Close and lock passenger- & cargo-doors

7.5 Open port from gate to terminal

7.6 Verify all passengers have gone through the port

8 Analyse Vehicle

8.1 Analyse Battery Power / Fuel Level

OR

8.1.1 Recharge / Refuel Vehicle

8.1.2 Communicate range/endurance for given capacity

8.1.3 Determine next journey

8.2 Analyse Maintenance necessity

OR

8.2.A Continue without doing maintenance

9 Schedule Maintenance

OR

9.1 Perform Maintenance on-site

9.2 Perform Maintenance off-site

9.2.1 Fly vehicle to maintenance site

9.3.1 Determine if Vehicle is at End of Life

OR

9.3.1A Perform required maintenance

9.3.1B Dispose Vehicle

Functional Breakdown Structure - Urban Air Mobility System

1. Wait for passengers
- 1.1 Declare ready for dispatch
- 1.2 Get info from dispatch
- 1.3 Charge/Fuel as needed

2. Perform pre-flight inspection
- 2.1 Test Hardware
  - 2.1.1 Test Propulsion system
  - 2.1.2 Test Power system
  - 2.1.3 Test Control system
- 2.2 Test Software
  - 2.2.1 Test Communication system
  - 2.2.2 Test Passenger Info
  - 2.3.3 Test Telemetry
- 2.3 Analyse Test Results

3. Boarding of Passenger(s) (& Cargo)
- 3.1 Open port from terminal to gate
- 3.2 Let max 4 passengers through
- 3.3 Unlock passenger- & cargo-doors
- 3.4 Let passengers load cargo
  - 3.4.1 Open cargo bay
  - 3.4.2 Balance Cargo
  - 3.4.3 Close cargo bay
- 3.5 Load passengers
  - 3.5.1 Open doors, provide steps
  - 3.5.2 Close doors, retract steps
- 3.6 Decide loading sequence
- 3.7 Perform safety check
  - 3.7.1 Confirm seat belts are on
  - 3.7.2 Confirm (Cargo) doors are locked
  - 3.7.3 Confirm center of gravity is within allowance
    - 3.7.3.1 Determine Passenger Locations
    - 3.7.3.2 Determine Cargo Locations
  - 3.7.4 Check Payload Capacity — 99
  - 3.7.5 Make safety briefing available (1st time mandatory)

4. Determine Flight Path
- 4.1 Communicate with ATC
  - 4.1.1 Deconflict route with service
  - 4.1.2 Request route from ATC
  - 4.1.3 Get confirmation
- 4.2 Adjust Path if neccessary
- 4.3 Make estimate of residual power at end of journey
- 4.4 Determine next possible journeys

5. Fly to destination
- 5.1 Vertical takeoff
  - 5.1.1 Start propulsion system
    - 5.1.1.1 Send commands to start system
    - 5.1.1.2 Set propulsion system into 'Flight Mode'
  - 5.1.2 Initiate vertical climb to desired altitude
    - 5.1.2.1 Analyse environment
    - 5.1.2.2 Increase Throttle
  - 5.1.3 Transition to cruise phase
    - 5.1.3.1 Tilt main wing
    - 5.1.3.2 Turn to face destination
- 5.2 Cruise
  - 5.2.1 Determine most efficient cruise speed
  - 5.2.2 Increase speed to cruise speed
  - 5.2.3 Engage in-flight entertainment
- 5.3 Land Vehicle
  - 5.3.1 Communicate with Ground Segment
  - 5.3.2 Transition back to hover
  - 5.3.3 Decent to vertiport
  - 5.3.4 Negotiate landing position and speed
    - 5.3.1 Identify and track target landing space
    - 5.3.2 Measure location / speed w.r.t target
    - 5.3.3 Verify target space is sufficient
    - 5.3.4 Manually confirm landing site
  - 5.3.5 Verify ground stability
- 5.4 Check flight path continously
  - 5.4.1 Communicate with ATC
  - 5.4.2 Communicate with other vehicles
  - 5.4.3 Maintain adequate stability
  - 5.4.4 Check battery capacity
  - 5.4.5 Track and avoid hazards
    - 5.4.5.1 Locate static objects
    - 5.4.5.2 Track and evade dynamic bogeys

6. Taxi to gate
- 6.1 Vehicle is picked up by taxibots
  - 6.1.1 Taxi bots approach vehicle
  - 6.1.2 Taxi bots put carriage in correct position
  - 6.1.3 Taxi bots lift off vehicle
- 6.2 Taxi to gate
- 6.3 Taxibots carefully put the vehicle down
- 6.4 Go into Safe-Standby-Mode

7. Unboarding of Passenger(s) (& Cargo)
- 7.1 Unlock passenger- & cargo-doors
  - 7.1.1 Open doors
  - 7.1.2 Give clearance to the passengers to leave
- 7.2 Verify that all passengers are out of the vehicle
- 7.3 Verify that all cargo is taken out of the cargo compartment
- 7.4 Close and lock passenger- & cargo-doors
- 7.5 Open port from gate to terminal
- 7.6 Verify all passengers have gone through the port

8. Analyse Vehicle
- 8.1 Analyse Battery Power / Fuel Level
  - 8.1.1 Recharge Vehicle
    - 8.1.1.1 Open safety cap
    - 8.1.1.2 Connect vehicle to charging facilities
  - 8.1.2 Communicate range/endurance for given capacity
- 8.2 Analyse Maintenance necessity
  - Schedule Maintenance — to 9

9. Schedule Maintenance
- 9.1 Perform Maintenance on-site
- 9.2 Perform Maintenance off-site
  - 9.2.1 Fly vehicle to maintenance site
  - 9.2.2 Determine if Vehicle is at End of Life
    - 9.2.2A Perform required maintenance
    - 9.2.2B Dispose Vehicle
      - 9.2.2.1 Recycle all possible parts
      - 9.2.2.2 Compact and Landfill

Cost estimation

It is expected that the market for a UAM will grow quickly. In 2030 the global UAM market will reach 7.9 billion US dollars[1]. However, to achieve this market share it is important that the ticket price is competitive with existing transport modes. The urban mobility system will have a market share of 1.1 %. The ticket price is highly dependent on the cost estimation of the system. For each system two types of costs are estimated, namely production costs and operational costs. Afterwards, these costs are combined and a break even point is determined. This is the point where the total costs are exactly the same as the incoming costs over a few years. If the break even point is known, the ticket price can be determined. In Section 11.1 this procedure is explained. Afterwards, the investment plan is explained in Section 11.2.

11.1. Ticket Price

The production costs of the system are based on the production costs of the vehicles and the production costs of the hubs. The production costs of the vehicle is divided in battery costs, structural costs, autonomy kit, propulsion units and the manufacturing costs. The costs for these subsystems can be find in Table 11.1. The total production cost for one vehicle is 1.2 million US dollars. The production costs for the initial vertiports are based on the cost estimation of Uber Elevate [2]. These costs are based on adjusting existing buildings, such that their roofs can be used as vertiports. Moreover, on each vertiport 12 high voltage chargers will be placed. These building modifications will cost 3.6 million dollars for each vertiport. This investment in buildings will be amortised by 30 years. The total production costs is the sum of these two components. Finally, the system will operate with 105 vertiports within LA.

The operational costs are divided in two parts, the energy costs for the vehicle and the operating costs for the vertiport. The energy costs are dependent on the amount of trips per vehicle. The energy used for these trips is calculated and multiplied with the cost of energy. It is assumed that the cost per one kWh is 0.12 dollars. Moreover, the operating costs of the vertiport is also taken into account. These costs incorporate lease fees, maintenance, personnel, security, etc. This is determined to be 300 dollars per day per vehicle.

It is very difficult to stick a number on the development costs at this stage in the design process. It is, however, possible to create an initial breakdown of these costs in terms an estimate of what the major components would probably require. Based on a study by Porsche Consulting [38], the development costs are determined to be 1-4 million dollars for concept exploration, 10-90 million dollars for concept validation, 200-600 million dollars for the development and 200-300 million dollars for the industrialisation. To calculate the ticket price the maximum amount of development costs is taken into account, namely 994 million US dollars.

The break even point is set on 15 years to calculate the ticket price. The amount of trips made during those 15 years can be easily determined. This will be done by multiplying the trips served per day times the total operating days in a year (250 days) and then multiplied with the number of years required to reach the break even point. Then, the revenue of the system is determined by the ticket price multiplied with the amount of

---

[1] https://globenewswire.com/news-release/2019/03/18/1756495/0/en/Urban-Air-Mobility-Market-To-Reach-USD-7-9-Billion.html [accessed 22.06.19]

[2] https://www.uber.com/elevate.pdf [accessed 24.06.19]

Table 11.1: The cost break down of the urban air mobility system

Production costs		Dollars [USD]
Vehicle	Battery costs	20,000
	Structural costs	6,000
	Autnomy kit	120,000
	Propulsion units	140,000
	Manufacturing costs	910,000
Veriport	Charging facilities fast charger	250,000
	Charging facilities low charger	10,000
	Initial investment for 1 vertiport	3,600,000
Operational costs		
	Price per 1 kWh	0.12
	Vertiport costs/day/vehicle	300

trips. This will be a linear relation as the total number of trips increase linearly to the break-even point. The costs are dependent on the production costs and operational costs. The production costs are determined by how many vehicles are needed. The operational costs will also increase linearly over these years, because the amount of trips is assumed to increase continuously. Of course, because of the made assumptions, this is only a very rough and thus only preliminary estimate. The break-even point is set on a certain amount of trips and the total desired revenue is set equal to the costs. Then, ticket price per trip per vehicle has been determined. Dividing the price per trip by the number of passengers per vehicle yielded the individual ticket price. The final ticket price for the system is 1.71 dollars per km per passenger. The ticket price of the system is competitive with existing transport modes in LA as the taxi price in LA is $4.67 per kilometre and the public transport costs $2.1 per kilometre. The result can be seen in Figure 11.1, the first jump in the graph is based on the production and development costs.
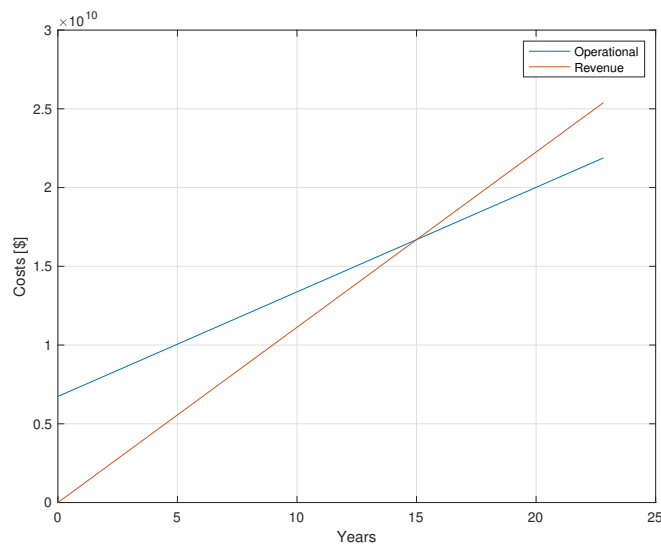

Figure 11.1: Break even analysis

11.2. Investment Plan

Since February 2019, more than 1 billion US dollars is invested in this new transportation system[3]. Partnerships are necessary to invest in all the market segments. The passenger vehicle and the new air traffic managements system need the most investment. However, the ecosystem of this market just started and is expected to undergo a lot of challenges before it is part of an electrified mobility system. For the investors there are also various risks if they step into this market. There are risks in the technical development, certification and above all the social acceptance. As this is an unpredictable market and it is highly dependent on the degree of innovation, the investments can vary[4]. It is important that there is a good collaboration with the regulation agencies, because if the regulation differ per city the production and operational cost might grow.

To create a fully operated system for 2050 it is important to have an investment plan. Investments are needed for the operations, infrastructure and the vehicle itself. Initially, only 20 vertiports will be created within the city of LA. This is of course a big investment, but this is related to modifications that should be made to existing buildings to create vertiports. Next to that, existing helipads will be adjusted to make them suitable for the system. Afterwards, the system will be expanded with more vertiports. The 20 vertiports will be occupied by 200 vehicles. At later stages of implementing the system, the production line for the vehicles will be increased. Once the vehicle production is doubled, the cost will decrease by 15%, this is a typical learning curve for aerospace and automotive products[5]. This means that in the near future vehicles can cost 600,000 US Dollars, this leads to a ticket price of $1.44 per kilometre per passenger. In the long term future, vehicles can cost 200,000 US Dollars, this leads to a ticket price of $1.26 per kilometre per passenger. The effects of these costs can be seen in Figure 11.2 and Figure 11.3
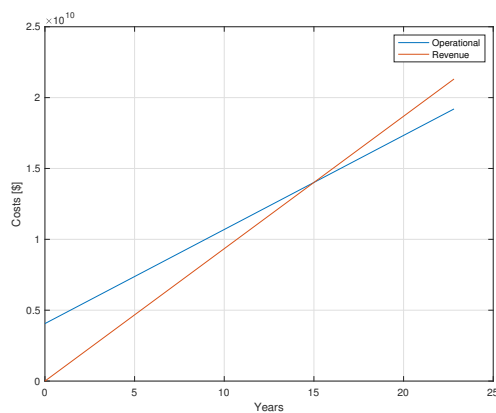
Figure 11.2: Break even analysis for the near future
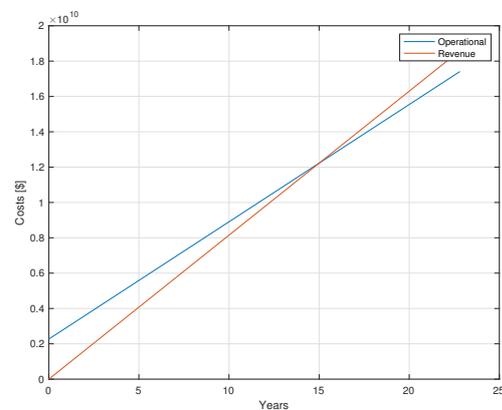
Figure 11.3: Break even analysis for the long term future

---

[3]https://www.globenewswire.com/news-release/2019/03/18/1756495/0/en/Urban-Air-Mobility-Market-To-Reach-USD\
 -7-9-Billion-By-2030-Reports-And-Data.html [accessed 21.06.19]
[4]https://fedotov.co/wp-content/uploads/2018/03/Future-of-Vertical-Mobility.pdf [accessed 20.06.19]
[5]https://www.uber.com/elevate.pdf [accessed 23.06.19]

12

Sensitivity Analysis

The tool-chain developed and presented in the previous chapters for converging and evaluating vehicle and operations designs is useful on its own, but with simple scripting, input parameters can be perturbed separately and responses to any output measured. This was already used in the concept selection phase and to show risky area in the models by revealing the significance of uncertainty in a constant or assumption on the overall system performance (see the midterm report of this group [7]).

12.1. Results

For this final version of the toolchain, more expensive simulations and optimisation's have been performed, such that the available computational power limited the scope of the results. Also, a large number of the results of the sensitivity study are not shown here as to save space but have been considered by the team. Note, that the plots presented concern an intermediate iteration of the design, not the final design. The relative sensitivities however are not expected to differ much, since no big conceptual changes have been performed.

Operational Characteristics   Since operational characteristics and assumptions have not changed much, a short review of these sensitivities is presented first, while the interested reader is referred to the midterm report [7]. Ticket price and efficiency of the system goes down significantly as the system focuses on serving longer trips and the investment cost as well as the operational costs for landing pad operation are a main driver of that ticket price. Connected to that, it is crucial to limit ground time: reducing the sum of pad vacation and taxi time from 6 min to 4 min results in reducing overall system area by 15% which has very significant influence on the ticket cost. A similarly big sensitivity is present with charge and boarding times.

Mass   Most commonly known and very important in aircraft design is the sensitivity of overall weight increase as a response to "dead" weight increase; the snowball effect. If each person is assumed to weight 3 kg more (12 kg more in total), an increase of 40 kg is predicted. This is a high sensitivity that means that focus needs to be put on lightweight design and making sure that the design structural weight is maintained. Also important in the case of this urban vehicle, is the sensitivity to noise as a heavier vehicle requires higher disk loading; Figure 12.1 shows how take off weight and noise correlate.

Battery   The battery is an expensive, hazardous and currently not sustainable component, so understanding the effect of different design parameters on the mass and cost is important. Figure 12.2 clearly shows that the current vehicle is limited by the cell energy density and not by power. This may change however future design iterations when MTOW increases, or when changing the mission to longer trips. Battery costs are also an output of the tools using a database of suitable cells and their prices and otherwise interpolating. However, battery cost is not just driven by their energy and power density and of course pricing is always up to the manufacturer, so something discrete jumps can occur in output of the the tool, most notably in the costs when the optimisation algorithm which is tuned for efficiency and low battery weight "snaps" to a different, more or less expensive cell; see Figure 12.3.

(a) Noise vs individual gross passenger mass   (b) MTOW vs individual gross passenger mass
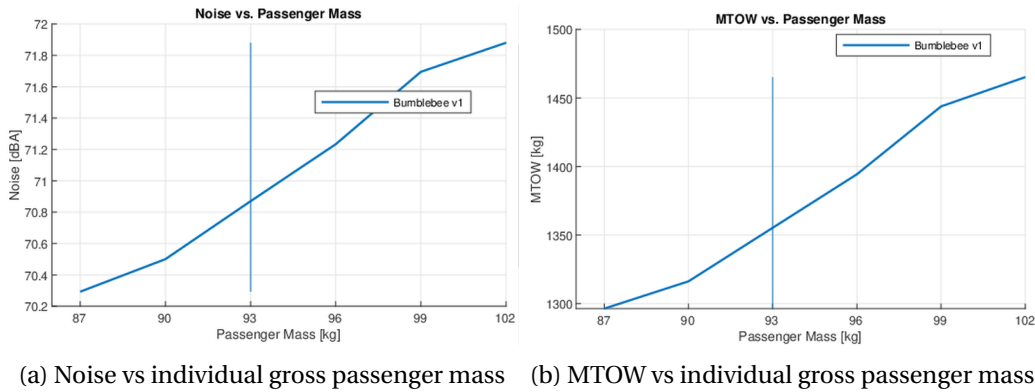
Figure 12.1: MTOW sensitivities can help with trade-offs by predicting snowballing

(a) Battery mass vs battery cell energy density   (b) Battery mass vs battery cell power density
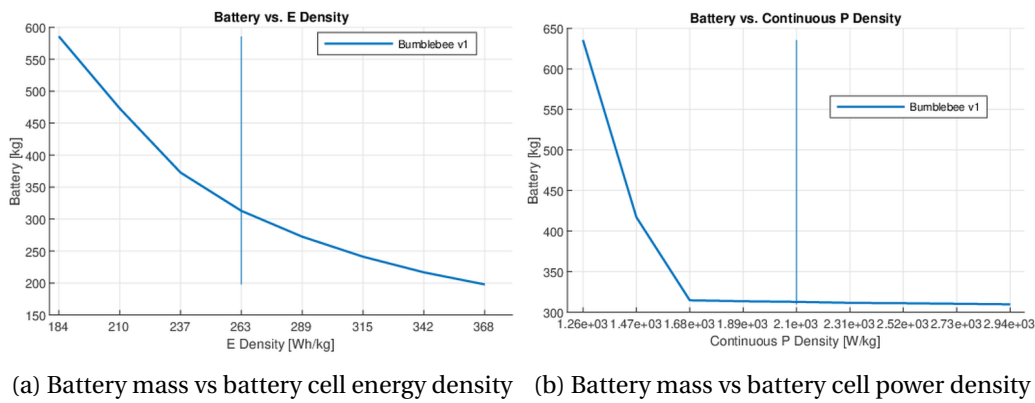
Figure 12.2: Battery mass sensitivities clearly show that the main battery is energy-limit

(a) Battery cost vs passenger mass   (b) MTOW vs individual gross passenger mass
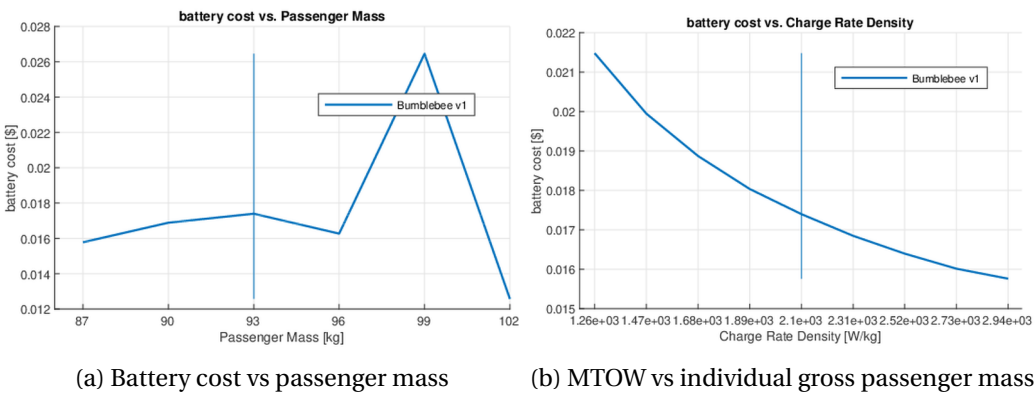
Figure 12.3: Battery Cost sensitivities are less predictable due battery pack optimisation for mass.

<div style="text-align: right; font-size: 3em;">13</div>

<div style="text-align: right; font-size: 2em;">RAMS</div>

The RAMS is an essential part of vehicle and transport system design. In this chapter, the Reliability (Section 13.1), Maintainability (Section 13.2), Availability (Section 13.3) and Safety (Section 13.4) of the designed UAM system are discussed.

13.1. Reliability

This section gives a short overview on the level of reliability of different subsystems to find which parts of the system are vulnerable to failure and need extra attention. Reliability is defined as "the probability that an item will not fail to perform its function(s) when used under stated conditions over a defined time period" or the Mean Time Between Failure (MTBF) [39]. Not only the vehicle is studied in terms of reliability but also the infrastructure and operations are looked at. Subsystems with high failure rates should be more frequently inspected and maintained, this will be further discussed in Section 13.2.

Power   When developing an electric air vehicle, the power system is one of the subsystems that has to be thoroughly looked at. Due to the lack of experience with electric propulsion in aircraft and helicopters, also the failure modes are less known. Degradation of the batteries over their lifetime is something to take into account, to make sure the range of the vehicle is not overestimated. To prevent this, the batteries should often be inspected. Furthermore, the temperature of the batteries should be watched to make sure the battery performance remains optimal over all possible temperature ranges. Finally, charging should be carefully regulated to avoid overcharging and destroying the battery [40]. For a reliable system, the power system and mainly the batteries are delicate systems that need to be used in the correct way to get optimal performance from it.

Airframe   Failures that could occur on the airframe are rivets or screws coming loose due to high forces or vibrations. Because the main airframe is connected by welding, this does not apply for the main structure. However, smaller parts might be connected in this way and it should be prevented that screws or rivets could do damage to the cabin or the passengers. Furthermore, cracks in welds should closely be monitored to avoid larger failures. As the cabin is not pressurised, the fatigue loading due to the pressurisation does not have to be considered. The landing struts have to be able to resist hard landings without failure, to make sure the vehicle does not have to be grounded due to a landing strut failure. Finally, moving components like the hinges on the doors should be tested for durability and have to withstand years of use. Altogether, with regular checks large failures can be avoided without too much effort.

Aerodynamic Structures   Next to the airframe, the wings and the tilt-wing mechanism are points where failure may occur. Because the wing is tilted between the hover and cruise-phase, it is loaded in multiple directions. It should be designed to handle the propulsion loads during take-off, the aerodynamic loads in cruise and the impact forces during the landing. As failure of the wing will probably be fatal, regular inspections should take place and sufficient safety margins are taken into account. The tilt-wing mechanism is also a critical part of the vehicle, therefore a second tilt motor is added for the sake of redundancy. Emergency plans are created in case the wing cannot tilt back from cruise, so in the worst-case scenario an airport landing is possible.

Propulsion   Because the vehicle is equipped with a total of 6 rotors, there are some probabilities of failure. This does however give the advantage of redundancy in case one of the motors fails. The electric motors should be operated within their power limits and operating at peak power should be limited to avoid damage to the motors. The motors that are used are of the shelve and have therefore already proven their reliability. The complexity of the system is reduced, because a fixed pitch propeller is used. This increases the reliability as less moving parts are used. A final failure mode is the possibility that the canard propellers cannot be fixed to their least drag position after they have served their purpose during take-off. This would lead to an increase in drag and chance that the canard has less effect on stability and control. The same could occur during transition back to hover, if the canard propellers cannot be turned on again. Because these failure modes would require an emergency landing, the locking system and the motor itself should regularly be inspected and tested.

Communications   With an autonomous vehicle, the largest risk is losing communication and thus external control over the aircraft. To avoid this, the communication system should have multiple redundancies, such that the odds of losing communication with the vehicle are extremely small. If the communication would fail, the aircraft should be able to land autonomously at the nearest landing pad or landing location. A great amount of tests should be performed to ensure the reliability of this subsystem is as high as possible.

Infrastructure   The vertiport is a fairly robust system with little chances of failure. A thing that could fail are the taxibots, however a human controlled back-up that can taxi a vehicle to a gate could prevent any delays of occurring. Furthermore, the charging system could fail or a power outage could occur. As such a high voltage charging system can be developed and improved in the coming years, reliability should not be a main concern in 2050. However, power outs would result in the total system coming to a halt, just like train or metro networks. In the event of a power out, there might be vehicles in the air. Therefore, an auxiliary power system should be available at every vertiport that has enough power to recover communication with these vehicles, such that a safe landing can be assured. Nonetheless, this is an external factor that is not in our control and, apart from the auxiliary power and a quick restart of the system after a power out, there is not much that can be done.

Conclusion   Overall, the system is mostly dependent on the autonomous systems working properly, so the main priority is to get the reliability of that system as high as possible. Furthermore, the batteries and power system are relatively prone to failure and should regularly be checked to increase the reliability. Finally the tilt-wing mechanism has to be tested extensively to make sure the system is reliable enough that emergency landings do not regularly occur. Due to the relatively low detail during this design phase, no numerical values can be allocated to the reliability of different components and subsystem. This should be done during the next phase of the design and development.

13.2. Maintainability

Maintainability describes the ease at which the aircraft can be inspected, repaired and parts can be replaced. This maintenance should not only be performed with high quality, but also in an efficient and economically sustainable manner. It is also referred to as Mean Time To Repair (MTTR). An extensive maintenance plan is already described in Section 10.9, describing the procedures for maintaining the vehicle and steps needed to take to replace certain components.

Maintenance consists of preventive and corrective maintenance. Preventive measures range from inspections to scheduled replacement of parts of the vehicle. When parts or systems of the vehicle failed, corrective maintenance should take place to repair the part in question. The total time that the vehicle is out of service during any maintenance routine is called the Mean Downtime (MDT). This also includes logistics, paperwork and other actions that need to be taken before the vehicle can fly again [39].

The maintenance should be optimised in such a way that the time the vehicle cannot be used is as short as possible. This can be achieved by efficient scheduling of the preventive maintenance and quick response to

corrective maintenance. The maintenance crew should be highly trained to make sure the vehicle stays on the ground for the shortest time possible. The vehicle should also be designed in a way that parts are easily accessible for inspection or repair. The crew should be able to replace parts like the propellers, motors or batteries with ease to reduce the downtime. In a further design stage, these objectives should be thought of to make the vehicle as maintainable as possible.

13.3. Availability

A combination of reliability and maintainability is the availability of a system. Availability means the readiness level of the system to perform its mission at any time during its lifetime. Three different types of availability are considered: Inherent, achieved and operational availability.

Inherent Availability   When only looking at the reliability and maintainability in terms of unscheduled maintenance, inherent availability is considered. This defines the quality of the design and the manufacturing process, so a vehicle with few unscheduled repairs has a very high inherent availability. Equation 13.1 shows the equation that defines the inherent availability and consists of the metrics earlier discussed in the reliability and maintainability parts: Mean time before failure and mean time to repair. The MTBF should be kept as high as possible and the repair time should be minimised [39].

$$A_i = \frac{MTBF}{MTBF + MTTR} \tag{13.1}$$

Achieved Availability   This form of availability also considers scheduled preventive maintenance besides the corrective maintenance. A new metric is introduced: mean time between maintenance (MTBM), sometimes also referred to as operating time. It can simply be deduced from Equation 13.2 that the MTBM is preferred to be high, with the time to inspect and/or repair the vehicle as short as possible [41].

$$A_a = \frac{MTBM}{MTBM + MTTR} \tag{13.2}$$

Operational Availability   The final availability deals with the complete downtime of the vehicle, so including necessary transport of parts or personnel and administrative delays. Because the vertiports are located relatively close to each other, mechanics can quickly go to the vehicle with a failure to repair it. Spare parts can also be stored in a central point of the network, so that logistic time is minimised. Equation 13.3 shows the equation to calculate A_o [39].

$$A_o = \frac{MTBM}{MTBM + MDT} \tag{13.3}$$

Due to the lack of numerical values for reliability and maintainability, no actual values for the different availability can be calculated yet.

13.4. Safety

To ensure the safety of the passengers and non-users on the ground, safety measures and failure modes should be considered. Especially because the system operates within densely populated areas failures can have catastrophic consequences. In Chapter 14, technical risks that might occur during development or operations of the system are described and a mitigation strategy is discussed. Other ways of how safety is considered during the design process are discussed in the sizing and design of the subsections and are shortly summarised in this section.

Safety is taken into account in all phases of the design, for example with extra safety factors on structures. This means the structure is designed to carry larger loads than the vehicle will ever endure. The vehicle is also designed to still land in the case of motor failure, or for other failure modes described in Section 13.1. As stated in the proposed eVTOL regulations [8], the vehicle has to land on an operating site in case of an engine failure. To meet this requirement, also the non-users on the ground must not be endangered.

The safety of passengers and ground personnel on the landing pad should also be considered. As the charging happens at high voltage, the vehicle should always be grounded while it is charged, so no risk of electrocution exists. This is also the case during maintenance or repair. Furthermore, the passengers should not be able to come close to the canard propellers, as they might hurt themselves or damage the aircraft. Therefore the time users spend outside the gate and not inside the vehicle should be minimised.

Technical Risk Assessment

Technical risk assessment is a very important aspect of designing a new concept. The first step of this process is identifying technical risks that might occur and the possible consequence of these risks. Then, for every risk an estimation is made on the likelihood that it occurs and the severity to the success of the overall mission if it occurs. This last step is done to be able to plot all the risks on Risk Map. On the x-axis the severity of the event happening is plotted and on they y-axis the likelihood. In the top right corner the highest-ranking risks will be mapped, as not only the likelihood of these risks occurring is very high, but they also have a large consequences for the success of the mission as a whole. After the mapping is done, a risk mitigation strategy is thought of for the highest-ranked risks. A good mitigation strategy decreases at least the severity or the likelihood of the risk occurring. Ideally, the risk mitigation strategy decreases both the severity and the likelihood of the event happening, however, this is not always possible. The final step of the risk assessment is to create a "post-mitigation" Risk Map, which visualises the effect of the different mitigation strategies.

The severity of the risks occurring is ranked using the following scale:

- **Catastrophic**: The consequences are calamitous to the success of the system
- **Critical**: Primary functions of the system are lost or heavily degraded
- **Marginal**: Secondary functions of the system are lost or heavily degraded
- **Negligible**: The consequences have a minimal effect on the technical performance of the system

The likelihood of the risks occurring is ranked using the following scale:

- **Almost certain**: In case of new technologies which have never been used before.
- **Likely**: In case technology is used which has only proven to work in a few applications)
- **Possible**: In case technology is used which is based on existing non-flight engineering
- **Unlikely**: In case of the shelve technologies are used
- **Rare**: In case technology is used which has already been proved to work for such a system

In Table 14.1 the risks related to the development phase of the system are outlined. Thereafter, in Table 14.2 the risks related to the infrastructure and the operations of the system are listed.

Table 14.1: Risks related to the development phase of the system.

D1	The certification process is too time consuming.
D2	Operations of the vehicle require more energy than anticipated, due to which the battery end of life is reached much faster than expected.
D3	Expected operational hours are not accepted due to city regulations.
D4	In order to meet the estimated power demand the batteries have to be larger than the vehicle can fit.
D5	Autonomous VTOL are not trusted (yet) by society.
D6	Lateral artificial stability augmentation is too hard to maintain during flight, therefore redesign for static stability is required.
D7	Wing - Propeller-interaction is underestimated.
D8	It is not possible to get a smooth transition from cruise to hover, which increases the energy usage and decreases the user experience.
D9	Noise interference with the canard is underestimated.
D10	Certain components have been missized, due to which the stability of the aircraft is overestimated.

Table 14.2: Risks related to the infrastructure and operations of the system.

I1	Distance between take-off and landing pads has to be bigger due to new requirements.
I2	The required reinforcement of high-rise buildings is too expensive.
I3	Vertiports are not accessible enough (too far from connection points to other modes of transport or parking spaces at departure locations).
I4	A grid failure occurs, due to which there is a loss of connection of the in-air vehicles with the ground system.
O1	The motor that provides energy to tilt the wing fails.
O2	Some of the cables within the vehicle are incorrectly sized, due to which they burn-out during peak power demand during flight.
O3	The cooling equipment on board is not good enough, causing the batteries to degrade faster than expected.
O4	One of the batteries catches fire due to overheating or excessive usage.
O5	The system overall noise is too high.
O6	The grid is not capable of meeting the peak-demands.
O7	In-air traffic jams occur at a vertiport due to a difference in incoming and outgoing flow of vehicles.
O8	There is no interference allowed with airports (restricted fly areas).
O9	Two vehicles collide in the air.
O10	Due to an emergency procedure of another vehicle there are no landing pads available at the aimed vertiport.
O11	The propulsion system is often overheated causing higher maintenance and reduced lifetime.
O12	Due to a misalignment of the propellers they are underbalanced, causing them to be not only less efficient, but they also cause higher vibrations on the wings.
O13	The system is attacked by remote hackers.
O14	One of the passengers travelling in a vehicle starts to feel unwell during transport.

For each of the risks mentioned in Table 14.1 and Table 14.2 a risk mitigation strategy is proposed. The mitigation strategy for the operations and infrastructure are shown in Table 14.3 and those for the development related risks are shown in Table 14.4. All the mentioned risks are continuously taken into account while designing the vehicle. Therefore, some of the risks have in reality already been mitigated or will be

mitigated once the actual production starts. For example, risk I4 will be mitigated by ensuring that auxiliary power is present at every vertiport. Also, risk O1 is already mitigated by installing two motors which are able to drive the tilt mechanism. Furthermore, the likelihood of risks such as batteries overheating or catching fire are also minimised by adding cooling equipment to the design. In addition to this, the severity is decreased by making fire resistant walls between different compartments. Furthermore, systems that will prevent vehicles from colliding in air will, of course, also be installed.

Table 14.3: Risks mitigation strategies for the operations and infrastructure.

I1	Build vertiports on buildings with a larger roof, such that the new requirements can be met.
I2	Aim to build vertiports at buildings with a lower height which need less reinforcements, such as the LA convention centre.
I3	Collaborate with LA Metro to expand public transport further and also increase their usage.
I4	Every vertiport has an auxiliary power source that will be able to provide communication with the in-air vehicles. No vehicles will be allowed to take-off until the grid is up again.
O1	Redundancy is important everywhere, so two motors could be responsible for tilting the wing.
O2	Smart rerouting of the power should be possible.
O3	More money should be invested in better quality air cooling equipment. Also, more research should be conducted to get a better estimate of how heat can best be dissipated.
O4	A voltage and temperature monitor should be installed near every battery. In addition to this, all major subsystems shall be powered by different battery packs, such that one battery failure does not cause the system to be uncontrollable.
O5	All the vehicles should fly at higher altitude. However, this requires more energy and time, so the energy budget should be reevaluated as well.
O6	More money should be invested in charging facilities that provide not only voltage frequency and power frequency control, but also "peak-shaving".
O7	ATM planning should be improved. The system knows which vehicles are going where and when they will arrive, so empty vehicles should be sent somewhere else where they can be used or are not in the way of vehicles that have to land. In any case, every vehicle should be able to hover above a vertiport for a certain while.
O8	Introduce no-fly zones. Routes that initially flew over these zones will be rerouted. However, this increases the energy requirements for certain trips, so the energy budget should be reevaluated.
O9	Introduce procedural separation: prior to flying, the planned route of every vehicle is verified, in case of interference with the route of another vehicle, one of the vehicles will be rerouted.
O10	Either the vehicle has to be able to hover for a while, or it will reroute to the nearest vertiport (enough battery capacity should be available for this).
O11	Aluminium could be added to the frame to absorb more heat.
O12	Checking the alignment of the propellors will be part of the regular maintenance, such that it can be caught in an early stage.
O13	Cybersecurity can be improved by installing software such as Intrusion Detection Systems (IDS) and Intrusion Prevention Systems (IPS).
O14	An emergency button shall be present in every vehicle to immediately get connected with customer services. If deemed necessary, the vehicle will be rerouted to nearest vertiport to help the passenger.

Table 14.4: Risks mitigation strategies for the development phase.

D1	Allow safety management systems (SMS) and stimulate selected industry self-regulation.
D2	Invest in batteries with a longer life cycle.
D3	Adjust the size of the network and the fleet to meet the changed demand.
D4	Decrease the trip lengths, such that the power demand decreases to an allowable size.
D5	In the beginning of the project "Bunker Pilots" can be used to gain trust of the society. (Bunker pilots monitor multiple vehicles from the ground and can intervene if this is necessary)
D6	A vertical-tail should be added to the design of the vehicle.
D7	More wind-tunnel tests should be performed to overcome this problem.
D8	The battery design should be improved, such that it can store more kW. In addition to this, the seats should provide full neck and spinal support.
D9	Perform more wind-tunnel tests to gain more knowledge on the effect of a canard on noise.
D10	A small demo-model of the aircraft should be built prior to the start of manufacturing.

As explained earlier, all the risks are ranked on severity and likelihood of occurring. The ranking is visualised in a risk map. On the left of Figure 14.1 the risk map before the risk mitigation strategies have been applied is shown and on the right the post-mitigation risk map can be seen. Most of the mitigation strategies decreased the likelihood of occurrence. However, for some also the severity is possible to reduce. For example, by ensuring redundancy for certain components, the severity of a default of one of the components is decreased. It can be clearly seen, that all of the risks have been removed from the most catastrophic areas. However, certain risks are hard to mitigate properly. For example, the chances of a cyber attack on the system will always exist. For future development, the focus should be on how the likelihood of success of such attacks can be minimised by installing proper software which is extremely hard to crack. If it is possible to develop this software, this would further reduce the likelihood of occurrence of this risk.
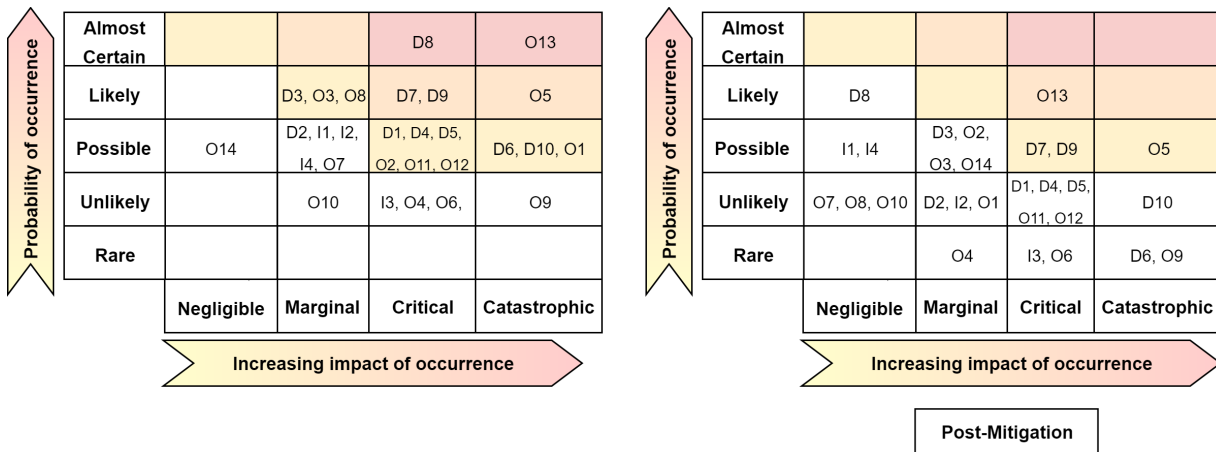

Figure 14.1: Risk map before and after risk mitigation strategies have been applied.

Production Plan

This chapter outlines the production processes that will be used to produce the vehicle. The production techniques to manufacture the fuselage structure are given in Section 15.1. The production techniques to manufacture the main wing and canard is given in Section 15.2. Information regarding the batteries and power and propulsion systems are given in Section 15.3. Other vehicle parts which will be bought from third parties is given in Section 15.4. The assembly of the various components is discussed in Section 15.5, while Section 15.6 gives an overview of the of the production process. It also presents a flow diagram which shows the main steps in the production of the vehicle.

15.1. Fuselage Structure

The fuselage truss structure consists of aluminium members which are welded together. These members will be hollow tubes that will be bought on the market. These tubes will likely be produced by the process of extrusion from the supplier. This is a common metal forming technique that is often used for the creation of hollow tubes [42]. It is possible that not all desired diameters for the optimal design are available. In this case, the diameter which is closest yet larger than the required diameter will be chosen. The tubes will likely need to cut to the correct length. This will be done within the production facility. They will be cut by performing a shearing operation on the rods. The punch will be made of steel. It will be necessary to ensure proper clearance between the tube and the punch. Lubrication will also be applied when performing the shearing operation. This will reduce the tool wear and increase the longevity of the tools. It will also improve the quality of the sheared edge.

The aluminium members will need to be welded to create the space frame. Initially, the manufacturer of the vehicle must invest in a welding jig to ensure proper welding occurs [1]. This jig will have a high stiffness because it also acts as a measuring tool. The welding process that will be performed is "gas tungsten arc welding" (GTAW). This is a relatively clean process; it "prevents aluminum from being contaminated by the atmosphere" [2]. The filler material will be "Al 4043" to ensure a proper weld [43]. The in-plane welds will be I-welds [42]. The out-of-plane welds will be K-welds [42]. Welding will induce some residual stresses in the space-frame. Therefore, some parts of the space-frame will be reheated to remove the residual stresses [42].

For the the carbon fibre body that is to cover the majority of this truss structure use will be made of Automated Tape Laying (ATL). In this process a part is built up with unidirectional tapes that are laid on a mould using a loaded roller system. It is similar to the manual layering of uni-directional tape, but faster and more precise method to construct composite parts [44]. The moulds that will be used in the manufacturing process of our vehicle will be reused as much as possible to ensure economic and environmental sustainability.

---

[1] https://www.weldingschool.com/blog/welding/what-is-a-welding-jig/ [accessed 2.07.19]
[2] https://www.metalsupermarkets.com/what-type-of-welding-is-used-for-aluminum/ [accessed 2.07.19]

15.2. Main Wing and Canard

The main wing of the vehicle and the canard are designed as a traditional wing-box structure. It consists of 2 C-channel spars, ribs, top-skin and bottom skin. The aluminium ribs will be made by rubber forming, a process where the shape desired of the rib or spar is pressed out of a thin sheet of metal. Rubber forming is a universal technique used in aircraft manufacturing. An initial investment must be made in the press machine. The rubber die used in the process has a relatively low cost. The soft surface of the die ensures that the ribs will not get damaged during the process. The sheet metal will be in a soft condition. After, the forming, they will be put in the refrigerator.

The fibre placement on the wing skins will be done using Automatic Fibre Placement (AFP). This will significantly reduce the manufacturing time. A trained technician "can place just about over 1kg per hour" of pre-pregs [45]. The AFP can lay approximately 6.5 to 11 kg/hour of pre-pregs [45]. An initial investment will be required in the AFP machine; however this can be easily compensated for by the increase in the fibre placement rate. The stringers on the skins will be integrated in the skin. The skins will be cured after the placement of the pre-pregs. The composite spars will also be made using AFP. The AFP machine will lay pre-pregs on a rectangular rotating mandrel [3]. Each side of the rotating mandrel will have one of the spars. The spars will be cured after the lay-up is performed.

The tube for the tilt wing mechanism will be made out of titanium. These tubes for the vehicles are readily available on the market and will thus be bought from a supplier. It is likely that the tubes will have been made by titanium extrusion, a commonly used manufacturing process for a metal in this shape.

15.3. Batteries, Power and Propulsion Systems

The battery cells will be bought from a supplier as well, but the battery pack will be assembled within the factory. Things that must be added to cells to form a pack are some non load-carrying structure to keep the cells together, a fire retarding material around the pack and a load carrying structure such that the weight of the battery can be properly withstood. The material that is to hold the cells in the correct place can simply be a plastic of some sort, it is not required that this part of the pack has any load carrying capabilities. Furthermore, there will be thin aluminium cooling plates that run between the battery cells and are connected to a cooling plate to dispose of excess heat that may be generated during the operations. The load-bearing structure around the battery pack will also incorporate the use of fire-retardant materials to prevent the need for an extra layer of material around the battery pack. For the resin in the carbon fibre composite structure an epoxy will be used that is fire retardant. Furthermore, a layer of foam is added between the two layers of composites to form a sandwich structure. The product that will be used is ROHACELL S, a foam with good fire retarding properties and that is used in aerospace[4].

The motors will be bought from a supplier, 'EMRAX', that specialises in light weight, high power motors, while the propeller/hub combination will come from 'Duc-Helices'. The propeller blades will be made out of carbon fibre composites with inserts to an aluminium hub[5]. The motor controllers will be bought from various suppliers, that are each selected based on the recommended motor controller by EMRAX. Suppliers that will be used are Drivetrain Innovation (DTI), Emisio and Unitek.

15.4. Other Parts for the Production

Now that the main subsystems have been discussed, some of the other parts of the vehicle will be looked at as well. The glass that will be used for the windows will be laminated glass. When it breaks, the glass it

---

[3]`https://www.youtube.com/watch?v=_ouF_YmZpNc` [accessed 2.07.19]

[4]`https://www.rohacell.com/product/rohacell/en/products-services/` [accessed 02.07.19]

[5]`http://www.duc-helices.com/rubrique.php?id_rubrique=76` [accessed 28.06.19]

is kept in place by layers of Polyvinyl Butyral (PVB) that are nested in between layers of glass, thus reducing the risk of injuries in the case of a birdstrike [46]. This glass will be bought from an external supplier; "Aviation Glass". The interior of the cabin will consist of, among others, seats, baggage compartments and infotainment screens. The components will be bought from "Collins Aerospace". The interior and exterior lighting on the vehicle will also be bought from "Collins Aerospace". TaxiBots will help the vehicle taxi from the gate to the TOLF pad. The TaxiBots will be directly bought from "Amazon Robotics". Consultation with them will be required to ensure that the design of the TaxiBots is able to meet the requirements set on it. The electrical system includes, among others, wires. This will be bought from the "Safran Group". The Avionics part includes sensor, navigation and communication equipment. This also includes the 5-hole Pitot tube and the angle of attack vane. This will be developed with "Honeywell Aerospace".

15.5. Assembly

A proper assembly line layout is necessary to have a cost-effective production process. The production of the fuselage, main wing and the canard are sub-assemblies in the production process. Assembling the battery pack is also such a sub-assembly. Ideally, the production of these sub-assemblies will take place in the same factory. This will reduce transportation costs of the production; it will also reduce waste when considering lean manufacturing. Independent teams will work on the various work packages associated with the sub-assemblies. They will not switch between sub-assemblies. This is due to the learning effect. Working on the same work packages will help the production staff work faster and likely also make less mistakes.

The exact scale of the production plant still has to be determined. This will be done when a more detailed business plan is made. That business plan will outline the production rates required to carry out the first phase of the business plan. This essentially translates into a delivery interval for the production facility. An initial estimate will be made of the number of workers and the tooling at each sub-assembly. This will give an initial production time for each sub-assembly. The initial delivery interval can be determined from this. Additional workers can be added to the various sub-assemblies if the initial delivery interval is less than the planned delivery interval. It also might be the case that there are additional sub-assemblies producing the same product. For instance, it is possible that manufacturing the wing will likely take longer than the fuselage structure. In this case, extra sub-assemblies can be created who also manufacture the wing. The phasing of the sub-assemblies must be decided beforehand. Expensive parts such as the motors will be installed as late as possible to avoid high interest costs associated with buying them before-hand. The buy order for these parts must also be phase with the production process. This will also require knowledge on the delivery interval of these components.

15.6. Summary of Production Plan

The following pages summarise the production plan. Table 15.1 gives an overview of the materials and manufacturing processes that will be used in the production of the vehicle. Table 15.2 gives an overview of the parts which will be bought from third parties. A flow diagram of the production process is also presented. This gives the order of the steps that will be used to produce the vehicle.

Table 15.1: Overview of materials and manufacturing techniques used

Part	Material	Manufacturing Technique
Wing and Canard		
Ribs	Al 2014	Rubber Forming
Spar	CFRP	Automatic Fiber Placement
Skin (with integrated stringer)	CFRP	Automatic Fiber Placement
Fuselage		
Frame Members	Al 2014 (filler Al 2043)	Extrusion and Welding
Shell	CFRP	Automatic Tape Laying

Table 15.2: Components from third parties

Part	Supplier
Motors	Emrax[2]
Motor Controller	Drivetrain Innovation (DTI), Emsiso & Unitek [3]
Propeller	Duc-Helices[4]
Avionics	Honeywell Aerospace[5]
Battery Cells	Kokam[6]
Interior Design	Collins Aerospace[7]
Lighting (interior and exterior)	Collins Aerospace
TaxiBots	Amazon Robotics[8]
Window Glass	Aviation Glass[9]
Electrical System	Safran-Group[10]
Titanium Tube	Plymouth Tube Co.[11]
Bearings	SKF[12]

[2] https://emrax.com/, [accessed 1.07.19]

[3] https://www.drivetraininnovation.com/products, https://www.emsiso.com/products, https://www.unitek-industrie-elektronik.de/ [accessed 2.07.19]

[4] http://www.duc-helices.com/, [accessed 1.07.19]

[5] https://aerospace.honeywell.com/en, [accessed 1.07.19]

[6] http://kokam.com/data/Kokam_Cell_Brochure_V.1.pdf?PHPSESSID=127ce197928d82d81619847c0b83f2f5, [accessed 02.05.19]

[7] https://www.rockwellcollins.com/, [accessed 1.07.19]

[8] https://www.amazonrobotics.com/#/, [accessed 1.07.19]

[9] https://aviationglass.aero\/e, [accessed 1.07.19]

[11] https://www.plymouth.com/products/net-and-near-net-shapes/, [accessed 1.07.19]

[12] https://www.skf.com/group/splash/index.html, [accessed 2.07.19]

Production Plan of the Bumblebee

Step	Sub-steps
Produce fuselage truss structure — 1	Produce jig for the truss — 1.1 Cut the truss elements to the right size — 1.2 Weld the truss members together — 1.3 Remove jig — 1.4
Produce the wings — 2	Produce the spars — 2.1 Produce the ribs — 2.2 Produce stiffeners — 2.3 Produce carbon fibre wing skin — 2.4 Assmble the wing components — 2.5 Integrate tilt wing mechanism — 2.5
Integrate structural elements — 3	Verify dimensions of wing and fuselage — 3.1 Arange bolts to connect parts — 3.2 Connect wing and fuselage — 3.3 Install landing skids — 3.4 Add carbon fibre fuselage body — 3.5 Integrate the windows — 3.6
Install the interior of the vehicle — 4	Install the passenger seats — 4.1 Install the displays — 4.2
Install the motors and propellers — 5	Check if the motors match the specifications from supplier — 5.1 Connect the motors to the propulsion shaft — 5.2 Connect propulsion shaft to propeller — 5.3 Fix the motor/prop combination to the front spar — 5.4 Integrate the cowling around the motor — 5.5 Connect tilt the motor to the tilt shaft — 5.6
Install the batteries and cables — 6	Check if the batteries match the specifications from supplier — 6.1 Install the batteries — 6.2 Check the cable lengths — 6.3 Connect the batteries to the wing/canard/tilt motors — 6.4 Install the motorcontrolers corresponding to each motor — 6.5

Final Vehicle

Compliance Matrix

To check of the requirements stated in Chapter 6 are met, compliance matrices are set up. Table 16.1 shows the compliance of the requirements of the transport system and the top level requirements of the operations and infrastructure. The top-level requirements of the vehicle and the compliance of the design are shown in Table 16.2, followed by the subsystem requirements in Table 16.3.

The following requirements are not met by the design or still to be determined. These requirements can be checked during the next design phase. This can be done via wind tunnel tests, flight tests or detailed computations:

- **TL - VEHI - 28:** The noise requirement based on the Uber White Paper [1] has not been met

- **TL - CERT - 14:** No vibration analysis on the vehicle has been performed

- **TL - VEHI - 33:** Noise inside the cabin has not been computed

- **TL - VEHI - 34:** Noise inside the cabin has not been computed

- **TL - CERT - 09:** Wind handling has not been studied

- **TL - CERT - 15:** (De)icing measures have not been investigated

Table 16.1: Compliance matrix for the system requirements and top-level Operations & Infrastructure requirements

Transport system requirements											
SYS-01	✓	SYS-02	✓	SYS-03	✓	SYS-04	✓	SYS-05	✓	SYS-06	✓
Top Level Operations & Infrastructure requirements											
TL-VERT-01	✓	TL-VERT-02	✓	TL-VERT-03	✓	TL-VERT-04	✓	TL-VERT-05	✓	TL-VERT-06	✓
TL-VERT-07	✓	TL-VERT-08	✓	TL-VERT-09	✓	TL-VERT-10	✓	TL-VERT-11	✓	TL-VERT-12	✓
TL-VERT-13	✓										
TL-INFR-01	✓	TL-INFR-02	✓	TL-INFR-03	✓	TL-INFR-04	✓	TL-INFR-05	✓	TL-INFR-06	✓
TL-OPER-01	✓	TL-OPER-02	✓	TL-OPER-03	✓	TL-OPER-04	✓	TL-OPER-05	✓		
TL-OPER-07	✓	TL-OPER-08	✓	TL-OPER-09	✓	TL-OPER-10	✓	TL-OPER-11	✓	TL-OPER-12	✓
TL-OPER-13	✓	TL-OPER-14	✓	TL-OPER-15	✓	TL-OPER-16	✓	TL-OPER-17	✓	TL-OPER-18	✓
TL-OPER-19	✓										

Table 16.2: Compliance matrix for the top-level Vehicle requirements

TL Vehicle Requirements											
TL-VEHI-01	✓	TL-VEHI-02	✓	TL-VEHI-03	✓	TL-VEHI-04	✓	TL-VEHI-05	✓	TL-VEHI-06	X
TL-VEHI-07	✓	TL-VEHI-08	✓	TL-VEHI-09	✓	TL-VEHI-10	✓	TL-VEHI-11	✓	TL-VEHI-12	✓
TL-VEHI-13	✓	TL-VEHI-14	✓	TL-VEHI-15	✓	TL-VEHI-16	✓	TL-VEHI-17	✓	TL-VEHI-18	✓
TL-VEHI-19	✓	TL-VEHI-20	✓	TL-VEHI-21	✓	TL-VEHI-22	✓	TL-VEHI-23	✓	TL-VEHI-24	✓
TL-VEHI-25	✓	TL-VEHI-28	✓	TL-VEHI-29	✓	TL-VEHI-30	✓	TL-VEHI-31	✓	TL-VEHI-32	✓
TL-VEHI-33	X	TL-VEHI-34	X	TL-VEHI-36	✓	TL-VEHI-37	✓				
TL-CERT-01	✓	TL-CERT-02	✓	TL-CERT-03	✓	TL-CERT-04	✓	TL-CERT-05	✓	TL-CERT-06	✓
TL-CERT-07	✓	TL-CERT-20	✓	TL-CERT-23	✓	TL-CERT-37	✓	TL-CERT-38	✓	TL-CERT-43	✓
TL-CERT-44	✓										

Table 16.3: Compliance matrix for all subsystem requirements

Manufacturing Requirements									
MANU-01	✓	MANU-02	✓	MANU-03	✓	MANU-04	✓	MANU-05	✓
Propulsion Subsystem Requirements									
VEH-PROP-01	✓	VEH-PROP-02	✓	VEH-PROP-03	✓	VEH-PROP-04	✓	VEH-PROP-05	✓
TL-CERT-16	✓	TL-CERT-19	✓	TL-CERT-27	✓	TL-CERT-28	✓	TL-CERT-29	✓
TL-CERT-30	✓	TL-CERT-36	✓						
Power Subsystem Requirements									
VEH-POW-01	✓	VEH-POW-02	✓	VEH-POW-03	✓	VEH-POW-04	✓	VEH-POW-05	✓
VEH-POW-06	✓	VEH-POW-07	✓	VEH-POW-08	✓	VEH-POW-09	✓		
TL-CERT-26	✓	TL-CERT-31	✓	TL-CERT-32	✓	TL-CERT-33	✓		
Structures Subsystem Requirements									
VEH-STRUC-01	✓	VEH-STRUC-02	✓	VEH-STRUC-03	✓	VEH-STRUC-04	✓	VEH-STRUC-05	✓
VEH-STRUC-06	✓	VEH-STRUC-07	✓	VEH-STRUC-08	✓	VEH-STRUC-09	✓	VEH-STRUC-10	✓
VEH-STRUC-11	✓	TL-CERT-14	X	TL-CERT-17	✓	TL-CERT-22	✓	TL-CERT-24	✓
TL-CERT-25	✓	TL-CERT-26	✓						
Stability & Control Subsystem Requirements									
VEH-STAB-01	✓	VEH-STAB-02	✓	VEH-STAB-03	✓	VEH-STAB-04	✓	VEH-STAB-05	✓
VEH-STAB-06	✓	VEH-STAB-07	✓	VEH-STAB-08	✓	VEH-STAB-09	✓	VEH-STAB-10	✓
VEH-STAB-11	✓	TL-CERT-08	✓	TL-CERT-09	X	TL-CERT-11	✓	TL-CERT-12	✓
TL-CERT-13	✓	TL-CERT-21	✓						
Aerodynamic Subsystem Requirements									
VEH-AERO-01	✓	VEH-AERO-02	✓	TL-CERT-16	✓				
Electrical Subsystem Requirements									
VEH-ELEC-01	✓	VEH-ELEC-02	✓	VEH-ELEC-03	✓	VEH-ELEC-04	✓	VEH-ELEC-05	✓
VEH-ELEC-06	✓	VEH-ELEC-07	✓	VEH-ELEC-08	✓	VEH-ELEC-09	✓	VEH-ELEC-10	✓
VEH-ELEC-11	✓	VEH-ELEC-12	✓	VEH-ELEC-13	✓	VEH-ELEC-14	✓		
TL-CERT-40	✓	TL-CERT-41	✓	TL-CERT-42	✓				
Interior Subsystem Requirements									
VEH-INTER-01	✓	VEH-INTER-02	✓	VEH-INTER-03	✓	VEH-INTER-04	✓	VEH-INTER-05	✓
VEH-INTER-06	✓	VEH-INTER-07	✓	VEH-INTER-08	✓	VEH-INTER-09	✓		
TL-CERT-15	X	TL-CERT-34	✓						

17

Post DSE

For the next phase (post DSE), the activities are divided into six time spans. The diagram containing the various time spans and their respective tasks can be seen in Figure 17.1. In the first time span, an investment plan is created, as money is required to perform further analysis, and in a later stage start production. It includes the set-up and execution of various presentations, market strategies and meetings in order to attract investors.

The next time span focuses on the creation, analysis and confirmation of a more detailed vehicle design and with it the system. Once the detailed design is created, a 3D model of the vehicle is created and the network is optimised, after which both are analysed and improved. After sufficient design iteration, the design is confirmed and the next time span in which a prototype is produced may begin. Once the prototype is produced, the vehicle can be analysed on experimental level by performing wind-tunnel and flight tests. This is done in order to gain more detailed data on the various aerodynamic, control and stability specifications of the vehicle. The results of these tests are analysed and the design is further improved. The last step of this time span is yet again confirmation of the design. In the next phase, the subsystems for the vehicle will be produced and tested. A structural test and performance test will be executed. These tests will give insights into the design and can lead to further improvements for the design of the subsystems. Like the other phases, the improvements will be implemented and new tests will be performed until the design may be confirmed.

After the subsystems are fully designed, the vehicle will be produced. Again, a flight test will be performed and an autonomous flight testing must also be executed. The insights of these tests will be used to further improve the design. Finally, the certification process will start and adjustments can be made. Afterwards, the final design of the vehicle is confirmed and prepared for production. The final phase includes setting-up of the production line for the vehicles. To create this, a detailed production plan should be made. Afterwards, the production line will be set-up and the production will start. Once a vehicle has been made, a market launch will take place, and the vehicle and the system are ready to start operation and transport people.
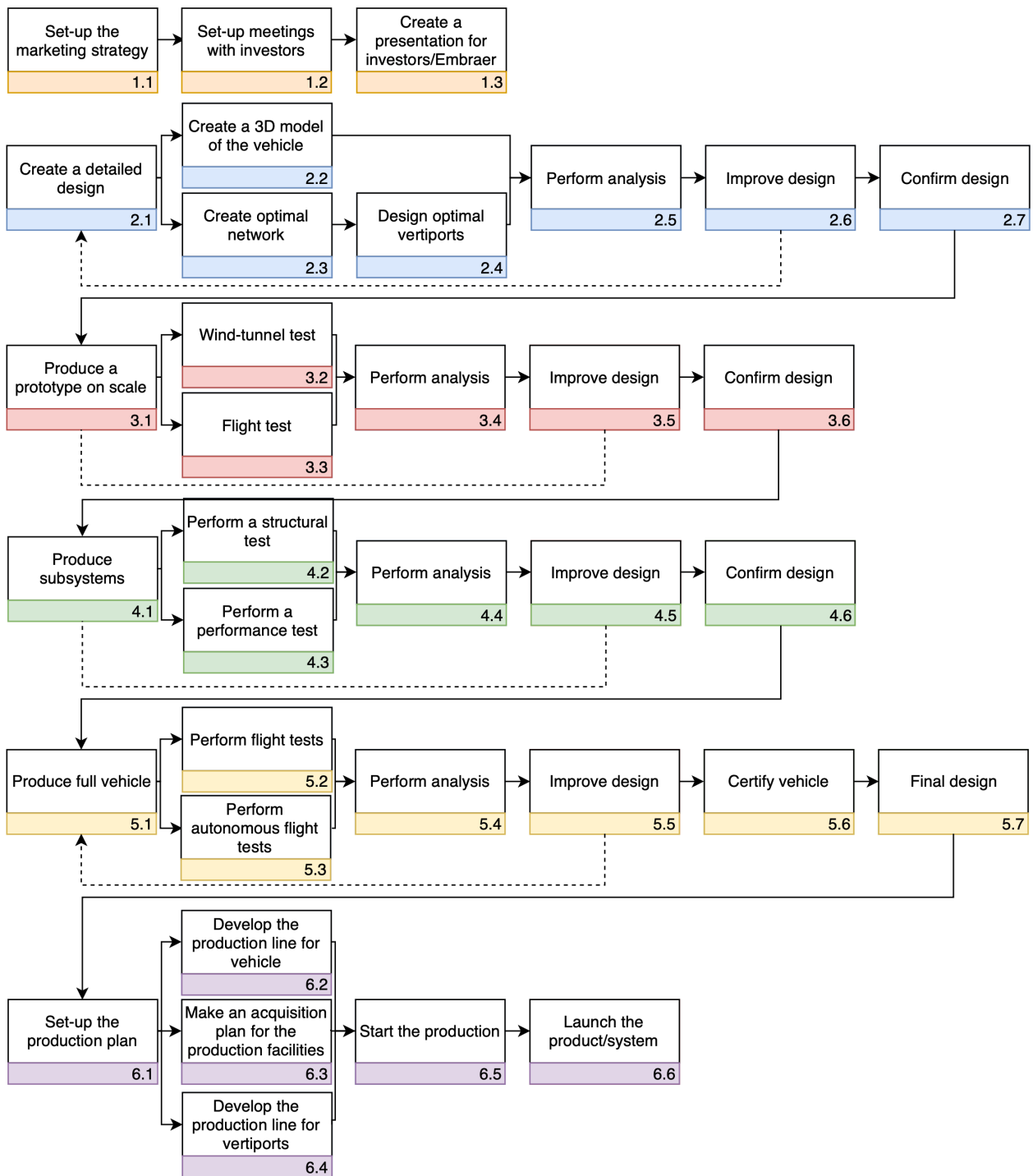
Figure 17.1: Recommended work flow diagram for activities following the Design Synthesis Exercise

Gantt Chart Post DSE

ID	Task Name	Start	Finish
1	**1.0 Create a presentation for investors/Embraer**	**1 Jan '20**	**1 Jan '21**
2	**1.1 Set up the marketing strategy**	**1 Jan '20**	**1 Jan '23**
3	**1.2 Set up the meetings with investors**	**1 Jan '23**	**1 Jan '25**
4	**2.1 Create a detailed design**	**1 Jan '25**	**1 Jan '30**
5	2.2 Create a 3D model of the vehicle	1 Jan '25	1 Jan '28
6	2.3 Create optimal network	1 Jan '25	1 Jan '28
7	2.4 Perform analysis	1 Jan '27	1 Jan '28
8	2.5 Improve design	1 Jan '28	1 Jan '30
9	2.6 Confirm design	1 Jan '28	1 Jan '30
10	**3.1 Produce a prototype on scale**	**1 Jan '30**	**1 Jan '32**
11	3.2 Wind tunnel tests	1 Jan '30	1 Jan '31
12	3.3 Perform flight tests	1 Jan '30	1 Jan '31
13	3.4 Perform analysis	1 Jan '30	1 Jan '31
14	3.5 Improve design	1 Jan '31	1 Jan '32
15	3.6 Confirm design	1 Jan '31	1 Jan '32
16	**4.1 Produce subsystems**	**1 Jan '32**	**1 Jan '35**
17	4.2 Perform a structrual test	1 Jan '32	1 Jan '34
18	4.3 Perform a performance test	1 Jan '32	1 Jan '34
19	4.4 Perform analysis	1 Jan '32	1 Jan '34
20	4.5 Improve design	1 Jan '34	1 Jan '35
21	4.6 Confirm design	1 Jan '34	1 Jan '35
22	**5.1 Produce full vehicle**	**1 Jan '35**	**1 Jan '45**
23	5.2 Perform flight tests	1 Jan '35	1 Jan '39
24	5.3 Perform autonomous flight tests	1 Jan '35	1 Jan '39
25	5.4 Perform analysis	1 Jan '39	1 Jan '40
26	5.5 Improve design	1 Jan '39	1 Jan '40
27	5.6 Certify vehicle	1 Jan '40	1 Jan '45
28	5.7 Final design	1 Jan '44	1 Jan '45
29	**6.1 Set up the production plan**	**1 Jan '45**	**1 Sep '49**
30	6.2 Make an acquisition plan for the production facilities	1 Jan '45	1 Jan '47
31	6.3 Develop the production line	**1 Jan '47**	**1 Sep '49**
32	**6.4 Start the production**	**1 Sep '49**	**1 Jan '50**
33	**6.5 Launch product and system**	**1 Jan '50**	**1 Jan '51**

18
Conclusion

Congestion issues are a growing inconvenience for the population of cities all over the globe. The projected population growth and rapid urbanisation will only increase the mobility issues that are faced in cities today. The time that citizens lose in heavy traffic and the unnecessary air pollution of the urban environment are drivers for a new approach to urban mobility. In this report the design of an Urban Air Mobility (UAM) system, including both the vehicle and the operations around it, has been described. The city of Los Angeles is taken as a pilot city for the implementation of this UAM system in 2050.

The vehicle has been named 'Bumblebee EX' and seats a maximum of four people at any one time. It is a fully autonomous, all electric vertical take-off and landing ((e)VTOL) air vehicle that makes use of a tilt-wing mechanism to tilt the wings into the desired configuration (hover or cruise). It has a fuselage length of 4.82 m, a wingspan of 10 m and a maximum height of 2.15 meters in hover configuration. The bumblebee has a maximum take-off weight of 1,250 kg, a maximum range of 60 km and will operate in urban areas to alleviate congestion. To obtain this performance it has 4 propellers on the wing and 2 on the canard that require a combined maximum continuous power of 410 kW. The wing has an aspect ratio of 8. The vehicle has a longitudinal statically stable and controllable x_{cg} range of -0.34 [%MAC] to -0.24 [%MAC], with the MTOW x_{cg} at -0.27 [%MAC]. Artificial stability and control in the cruise and hover flight cases is provided by combinations of differential thrust, tilting of the canard wing and even thrust vectoring with the ailerons (in the case of hover, when the wing is vertical). For the wing, a NACA2410 airfoil is used, with which the bumblebee can achieve an estimated lift-over-drag ratio of 9.5. The vehicle body will have an angle of attack of 6°during cruise to obtain minimum fuselage drag.

The optimal fleet will consist of 4,470 vehicles travelling 600 different routes. These routes are selected by specifying a metric called the 'travel time gain', defined as the time gain versus a car on the same route. The average trip time gain over cars during peak traffic hours is 26 minutes for a mean mission of just below 18 km. The cruise speed lies at 65 m/s. The vehicles will operate within the system with a PREE of 0.49, however for a single mean mission at maximum payload the vehicle is able to perform at a PREE of 1.0. Looking on a system level, the vehicle is less energy efficient than other modes of transport with cars, busses and rail that have a PREE of 0.76, 3.3 and 27 respectively. The vehicles will fly at altitudes of between 300 and 1,400 meters Above Ground Level (AGL) in a decentralised Air Traffic Management (ATM) system. After vertical take-off, the climb to the desired cruising altitude will happen at a vertical climb rate of 10 m/s, while also accelerating in the horizontal direction as well. There will be 105 vertiports in use, and a preliminary vertiport design has implemented on top of the Los Angeles Convention Centre. Other vertiports will be integrated with current public transport as much as possible.

The total development costs are estimated to be 410-990 million USD. Also, it is estimated that the production of a Bumblebee EX will cost around 1.2 million USD per vehicle. Furthermore, the investment for one vertiport will lie around 3.6 million. The operating costs for the vertiport is 200 USD per day per vehicle, this consists of fees, maintenance, personnel, security, etc. The price to charge the vehicle is 0.12 USD per kWh and dependent on the energy used per trip. The transportation of 180,000 passengers per day and break-even point after 15 years leads to an average ticket price of 1.70 USD per kilometre travelled. With that, the Bumblebee is a fast, economically competitive and sustainable solution to mobility in urban areas and will be a valuable addition to the future transport systems of many cities around the world.

19

Recommendations

During this design process some assumptions have been made, which led to a "simplified" design to some extend. For further improvement of the design, there are several recommendations. These recommendations will lead to a more optimal design. In Section 19.1 the recommendations for the route network and scheduling will be described. Afterwards, further improvements for the charging facilities will be discussed in Section 19.2. Afterwards, the vehicle recommendations will be presented. The recommendations for stability and control can be found in Section 19.7. Finally, the improvements for the noise of the vehicle are discussed in Section 19.8.

19.1. Route Network & Scheduling

This section will outline the steps that need to be taken to determine an optimised route network. Specifici software is recommended in theis section, but alternate methods may be available. First, it will be explained how an accurate estimate of the demand can be made. Then, a preliminary setup of the route network should be created. With this network, two optimisation steps can be performed to minimise the fleet size and the total travelled distance by all the vehicles. This two-step optimisation process is based on the Master's thesis by M. Balac [47]. Unfortunately, due to the time constraint of the project the steps described in this section are not actually executed.

A UAM system provides an extra mode of transportation for (daily) commuters. Commuters have the choice to use either this system or other modes of transport, such as a car or public transit. To analyse the choices and the consequences of the choices commuters make, an agent based modelling program should be used. For large-scale agent-based transport simulations MATSim [48] can be used. In MATSim commuters will be represented as agents. Agents have a plan, for example: travelling from A to B. The agent has multiple options of executing this plan. These options are then scored based on different criteria, such as the cost, the time and effort of executing the agent's plan. In general, agents prefer to execute the plan with the highest score. For example, travelling by car might get a high score for the amount of effort required to use it, however, it might score low for the time required to execute the plan. On the contrary, using UAM to execute the plan, might require more effort, since you have to travel to a vertiport first, but it would score high on the required time to execute the plan, as the UAM System is much faster. MATSim is capable of maximising the total score of all the agents. Based on the outcomes, the demand for the UAM system can be determined.

Once the demand is known, an update of the first estimate of locations for the vertiports can be done. Initially, a vertiports has been created in the centre of every PUMA, however, from the results it might already become clear that from certain PUMA's no commuters use the system. The found demand and the given network can then be used to solve the minimum-cost flow problem (MCFP). Solving the MCFP yields the cheapest way to send a certain amount of flow through a network. A problem that arises is that the MCFP assumes a certain size of the flow that travels over a link at once. However, the operating vehicle has a capacity of 4 commuters, which does not necessarily have to filled. To be able to get a preliminary result, an average occupancy of, for example, 2.5 passengers per vehicle should therefore be assumed. Firstly, a direct graph will be made where each starting point and end point are connected. Due to the maximum range of

the vehicle, some connections are removed. The problem can then be solved using a Gurobi optimiser. This will lead to a (preliminary) minimum fleet size.

Now the second optimisation may be performed. This is done by applying an adjusted version of Graph Theory[1]. Graph Theory can be used to minimise the travelled distance by the fleet size as a whole. However, since shorter routes are not necessarily more energy efficient than longer routes, instead of minimising the distance travelled, the total energy used by the system shall be minimised.

Since the energy efficiency of the system now also is optimised, an iteration on the demand or fleet size can be performed. The more energy efficient usage of all the vehicles might lead to a bigger demand capacity, but it might also mean, not as many vehicles are required to transport all the currently estimated demand. This iterative process continues until a desired optimisation of fleet size and demand has been achieved.

19.2. Charging Facilities

Fast charging capabilities of batteries are one of the limiting factors for the turn around time of the vehicles. However, the batteries are not the only limiting factor, also the capacity of the grid forms a limitation. First it has been assumed that the grid would be able to deliver the required power to charge all the vehicles with fast chargers. However, after consulting *PRE Power Developers*[2], a company which is an expert in the field of EV Charging facilities, this assumption should be rejected. By using the energy tool that is created (subsection 10.2.1), it has been determined that the average trip requires around 30 kWh. At the moment, the charge capacity of most batteries is 1 C. This means that if you want to charge 30 kWh in only 5 minutes, a power supply of 360 kW should be available for just one vehicle. Ones the system is fully operational, it is expected that every 15 minutes, about 20 vehicles arrive on and leave a vertiport. If all of these vehicles would have to be charged at approximately the same time, this would require already more than 3 MW for just one vertiport. It is expected that at one point there will be at least a hundred vertiports in use. This would mean that the whole system requires at least 300 MW of power. Even if the charge rate of batteries would improve majorly by 2050, meaning that the required power to charge a vehicle would decrease, it would still be an excessive amount of power.

Energy is transported via transmissionlines and cables at very high voltages, as this minimises energy losses during transport[3]. However, standard consumers only require low voltage to meet their every day electricity needs. Therefore, transformers are installed which transform the high voltage energy to low voltage energy. In North America, the normal voltage is 110 V [4]. However, fast charging requires much higher voltages. For example, the super charger from Tesla requires 480 V [5]. New transmission lines would have to be installed to connect the fast charging facilities of all the vertiports with the grid. The cost of such lines are approximately 1 million USD per km [6]. To connect all the vertiports, many kilometres of lines would be required which would form a major cost burden for the system. Instead of providing fast charging facilities at every vertiport, it would be much more cost and time efficient to create charging-ports. These charging-ports should be build close to power plants, such that the high voltage power that is generated can directly be used to charge the vehicles. The higher the voltage, the faster the batteries can be charged[7]. It should be noted, that depending on the chemistry of the battery there is a limit to what voltage can be used to fast charge this batteries.

A charging-port does not necessarily have to have only the function of a charging location. In some cases

---

[1] https://en.wikipedia.org/wiki/Graph_theory [accessed 10.07.19]

[2] http://www.pr-electronics.nl/

[3] http://www.betaengineering.com/high-voltage-industry-blog/transmitting-electricity-at-high-voltages [accessed 22.06.19]

[4] https://en.wikipedia.org/wiki/Continental_U.S._power_transmission_grid [accessed 22.06.19]

[5] https://en.wikipedia.org/wiki/Tesla_Supercharger [accessed 22.06.19]

[6] https://www.elp.com/articles/powergrid_international/print/volume-18/issue-2/features/underground-vs-overhead-power-line-installation-cost-comparison-.html [accessed 22.06.19]

[7] http://www.microhydropower.net/mhp_group/portegijs/firefly_bm/ffbm_4_9_5.html [accessed 22.06.19]

it might be possible to integrate a vertiport with a charging-port. This could be determined by analysing if the demand is high enough near a power plant to create a vertiport there. In any case, the tool should be updated to this particular system. The number of zombie-flights and the overall energy use of the system would increase, as a vehicle would have to fly back and forth to these charging-ports without any passengers (assuming it is not yet integrated with a vertiport). However, the turn-around time at a vertiport is no longer limited by the charging time, which means that the throughput of every vertiport may be increased. This obviously leads to more revenue. This, in combination with not having to install many kilometres of transmission lines, would lead to a much more feasible system.

19.3. Contingency Management

In Section 7.1 it has been explained what the expected weights are of the major components of the vehicle. The maximum weight that is found should not be exceeded, of course, a decrease in weight would be acceptable. The mass calculations that are done to determine the mass of the components is fairly simple. Many different elements that will account for a part of the total weight of the vehicle are not yet taken into account. Systems such as air-conditioning, actuators of the main wing and the canard and the general interior of the vehicle are to be sized in later stages of the design. While the tool was created, no contingencies are taken into account. However, for the current weight calculations, it is also not taken into account that there will be improvements to the density of certain components. For example, the power density of batteries will probably increase and materials that are stronger, but weight less might be developed. Since the design approach cannot easily be restructured, it will be of utter most importance that while further designing all the components the aim should be to decrease their total weights. To be able to accomplish this, several things can be done such as investigating how the structural efficiency can be improved and examining how the power train can be more efficient. Also proper cabling could provide a weight reduction by reducing the overall weight of the cables, while also minimising energy losses. Finally, in case it is really impossible to meet the designed MTOW, certain design changes could still be made. By using a more reflective paint for the vehicle, it might not be necessary to have air-conditioning in the vehicle. Not only for the vehicle itself improvements can and have to be made, also in the operations part of the system there is still room for a lot of improvement. For example, it should be further investigated what the most energy efficient flight path is. This would decrease unnecessary energy losses due to an inefficient take-off and landing. Which in turn would lead to less required battery capacity, leading to a lighter battery. However, everything considered, the challenge to meet the designed MTOW should definitely not be underestimated.

19.4. Powertrain

It should be investigated if it is possible to interpolate values from the database of battery cells or motors instead of choosing discrete items. This is something that has not been done extensively so far, but might lead to faster convergence of the tools and it could be assumed that in 30 years time these in-between cells and motors could be available or developed. Another recommendation that could be used in a new iteration could be the implementation of a variable cable radius to form the connection between the batteries and the motors. In the design so far, a fixed radius is specified and a power has been computed. In a new iteration this process could perhaps be switched around by first finding an low resistance cable and then sizing it such that the mass is minimal.

Finally, the group would like to mention that the power system has been designed based on the technology that is currently available and that no extrapolation has been made into the future. For some technologies in the subsystem, like for example the motors and batteries, it is deemed reasonable to assume some rate of improvement in power density. If this is something that is assumed in further designs or researches, it would likely be possible to optimise the design even further. Due to the snowball effect, other subsystems would decrease in mass as well.

19.5. Aerodynamics

Because very basic methods are used to find the aerodynamic performance of the vehicle, future design and performance could be improved. The fuselage drag that is computed is found to be twice as large as the drag of the wing and canard. The aerodynamic characteristics of the body are computed with a very simple CFD analysis, but as there is very little expertise in the group on this field, not much value can be given to the results. With a proper CFD analysis, the body could be optimised for low drag during cruise and transition. Furthermore, the interaction between the wings and propellers and the fuselage are completely neglected for the sake of simplicity, but might introduce considerable effects on the aerodynamic performance. To find the consequences of this interaction, wind tunnel testing or advanced CFD should be performed. The same is valid for the interaction of the rotors on the wing, which is only taken into account by parametric equations on induced velocity and angle of attack behind the rotors. As rotors almost cover the whole span, this effect on the lift and drag of the wing might differ in a real environment. To validate that methods used during this project give the correct results, further analyses and testing should be performed.

The aerodynamics and stability characteristics during transient phases have been studied separately during this project, but these methods have not been integrated with the other components of the aerodynamics tools and potential exist for faster iterations using stability derivatives and estimates of the static controllability directly from the lifting line tools. The stability and aerodynamic behaviour of the body during the extreme angles of attack or in strong winds during take-off and ascend should be analysed. Also, while descending the vehicle has to lose a large amount of energy; it should be investigated if flying with the body at large angles of attack is stable and controllable and may slow the vehicle down enough. If that is not the case, air brakes or propeller windmilling might be necessary. A trade-off between these options should be made in a more detailed analysis of this flight phase.

A better trade-off should have been performed on the aerodynamics-structure interface of the wings. A thicker airfoil for the main wing, like NACA2421 would have only penalized the Lift over profile drag ratio by around 10% [8] while providing similar stall and moment characteristics. Transsonic flight is not expected and the main drag contribution is the fuselage, so the team estimated that the bending stresses in the wing skin due to lift can almost be halved due to the higher moment of inertia of a NACA2421. This interface has been overlooked and all subsequent sizing should take a thicker airfoil into account significantly lowering structural weight and improving packaging of actuators, motors and possibly motor controllers. Also, more iterations on the wing geometry should be performed with the interfacing partners being aerodynamics, stability and operations. Larger wing and canard could have lowered stall speed and induced drag which could have improved robustness during transition and cruise efficiency, but repackaging for adequate centre of gravity location must be performed and a possibly larger landing pad would be necessary.

19.6. Structural Analysis and Manufacturing

In the report the structural analysis of the wing and fuselage sections has been elaborated upon. The first recommendation the group would like to make is with regards to the analysis of the fuselage. The method used only computes the axial loading in the truss members, no bending is currently taken into account. This bending of the elements would likely be interesting and relevant inclusion as in reality they would bend under the loads that the vehicle encounters.

Another recommendation that the group would like to make is for future design iterations, is to take into account the dynamic and vibrational analysis of the wing structure. This has been omitted for the first iteration of this vehicle. Checking and designing for such dynamic phenomena, like for example flutter, is a vital step that must be performed before any flight tests are performed.

As the Bumblebee is a vehicle that is to enter service in 2050, it expected that techniques such as additive manufacturing will have become more accessible and affordable. At the present time such techniques are

---

[8] http://airfoiltools.com/airfoil/details?airfoil=naca2421-il

ideal for parts with a relatively small production number and part volume, but it is imaginable that such '3D printing' will be a logical design decision for a lot more components. If indeed the costs can be reduced or the structure can be optimised even further by the use of such methods, the group recommends investigating these options.

19.7. Artificial Stability & Control

As mentioned in subsection 9.5.5, another option for initiating a yaw rate during hover is available. This alternative method uses differential thrust, but differs significantly from the way it is applied in subsection 9.5.5 as it is based on conservation of angular momentum. As one can see in Figure 19.1, the propellers on the main wing rotate in different directions such that the angular momentum caused by them are cancelled out by one another.
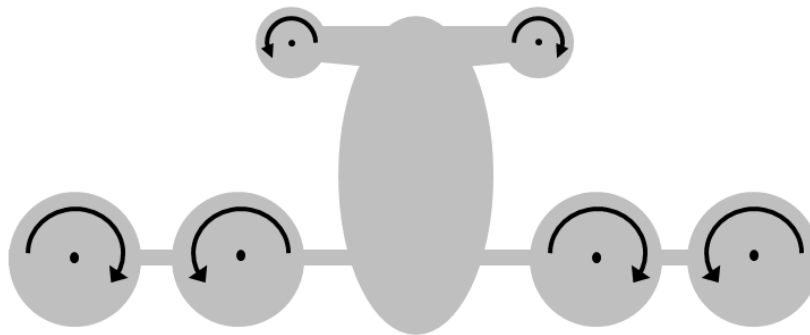

Figure 19.1: Rotational direction of the propellers

For a positive yaw rate (using Figure 9.32 as reference frame), one would have to increase the amount of thrust produced by the clockwise rotating propellers and decrease the thrust produced by the counterclockwise rotating propellers on the main wing by the same amount. Furthermore, the ratio of increase in thrust produced by the outer propeller on the left half span of the main wing over the increase in thrust provided by the inner propeller on the right half span of the main wing should be equal to the ratio of the arm of the inner clockwise rotating propeller over the arm of the outer clockwise rotating propeller in order to maintain moment equilibrium around the x-axis (using Figure 9.32 as reference frame). The same applies to the ratio of decrease in thrust of the counterclockwise rotating propellers. The total amount of thrust produced by the propellers (main wing & canard) should still be equal to the weight of the vehicle. However, this method still requires quite some analysis into its effectiveness.

Apart from initiating a yaw rate during cruise, this method may also be used for roll during cruise by applying the same principle as stated above. This method allows for a reduction in weight as the ailerons are not needed any longer. Furthermore, this means a reduction in technical risk as there is one less moving part. Further analysis into the stability characteristics during application of this method is required just as analysis into the effectiveness and consequence on cruise efficiency before it can be implemented and applied.

Further analysis of the lateral stability of the aircraft is required. The large outboard propellers provide some yaw stability in forward flight, but, as in the longitudinal case, the aircraft may not maintain stability through every flight phase. It is possible to add a vertical stabiliser to the back of the aircraft, however, since the centre of gravity is so far aft, it may provide little additional support to yaw stability, or may be required to be very large. Further analysis is required to determine the extent of any instability, and whether a control system is sufficient to artificially correct.

The canard has a slight dihedral, which may support some roll stability, however due to the tilting mecha-

nism, the main wing has no dihedral. The effect of this on roll stability should be further investigated.

19.8. Vehicle Noise

Despite not meeting the ambitious Uber noise requirement of 67 dBA at 250ft (comparable to a Prius at 25 ft from the listener, driving by at 35mph) it must be stated that the noise footprint of the Bumblebee of 72 dB is significantly lower than a helicopter like the Robinson R44, which has a certified noise metric of 81 dB at 250 ft (almost three times louder) [1].

This report shows some of the directions that propeller design has to go in order to achieve a quiet propulsion system. These are illustrated in the sensitivities of Chapter 12 and can be summarised as follows: high rotor solidity is desired, as is a low disk loading and low tip speed, which can be achieved through high collective angles (high thrust coefficients and in turn high power coefficients). A large angle of attack and large chord yields a high projected blade thickness which can reduce the vortex peak frequency which in turn can reduce the A-weighted signature. In addition to these first-principle design rules, more novel design solutions such as porous blades, serrated trailing edges, tip sweep, etc can be investigated.

Several limitations of the noise model stated in subsection 9.1.2 need to be removed in further iterations of the design. For instance, tools like PowerFLOW can be used to model the interaction between the propellers and the wing which might introduce additional sources of unsteady noise.

The noise metric discussed in this paper are limited to dB and dBA which is only a small fraction of the metrics used for current aircraft certification. On top of that, an eVTOL network would potentially deploy a fleet of hundreds of aircraft which could be continuously passing overhead. New certification metrics are being investigated by NASA [49] to quantify the annoyance that repetitive sound events can have on citizens.

19.9. RAMS

Because of the preliminary state of the design, no numerical values for the RAMS could be found yet, but during a more detailed design stage, values for the reliability of all components and subsystems should be estimated. When using off-the-shelf parts, these values can be requested from the manufacturer. If parts or software are produced in-house, simulations and tests should be performed. The components with low reliability should be improved or replaced, to get the reliability of the complete system as high as possible. The same is valid for the maintainability and the availability. Detailed studies into preventive and corrective maintenance could give an inside in the average downtime, which can be combined with the operating time without failures or maintenance to find the availability.

Bibliography

[1] Holden, J. and Goel, N., *Fast-Forwarding to a Future of On-Demand Urban Air Transportation (white paper)*, UBER, 2016.

[2] SUBRAMANI, T., "Study of air pollution due to vehicle emission in tourism centre," *International Journal of Engineering Research and Applications*, Vol. 2, No. 3, 2012, pp. 1753 – 1763, WESC 2006 Advances in Energy Studies.

[3] National Centre of Sustainable Transport, "Evaluating Environmental Impact of Traffic Congestion in Real Time Based on Sparse Mobile Crowdsourced Data," 2 2018.

[4] SCAG, "Mobility Go Zone & Pricing Feasibility Study," 3 2019.

[5] Giuliano, G., Chakrabarti, S., and Rhoads, M., "Using Regional Archived Multimodal Transportation System Data for Policy Analysis: A Case Study of the LA Metro Expo Line," 9 2015.

[6] Konstantinos, P., *The Analytic Hierarchy Process*, International Hellenic University.

[7] DSE Group 18, "Sustainable Urban Air Mobility: Midterm Report," Tech. rep., TU Delft, May 2019.

[8] EASA, "Proposed Special Condition for small-category VTOL aircraft," 2018.

[9] Leishman, J. G. and Ananthan, S., "An Optimum Coaxial Rotor System for Axial Flight," *Journal of the American Helicopter Society*, Vol. 53, No. 4, 2008, pp. 366–381.

[10] Drela, M., "Xfoil: An interactive program for the design and analysis of subsonic isolated airfoils," December 2013, Accessed 10.06.19.

[11] Pavel, M., "Helicopter Performance, Stability and Control course slides: Helicopter descent velocities," June 2019, Personal correspondence.

[12] Harrington, D., "Full-Scale Tunnel Investigation of the Static Thrust Performance of a Coaxial Helicopter Rotor," Tech. rep., NACA Technical Note 2318, 1951.

[13] Brown, A. and Harris, W., *A Vehicle Design and Optimization Model for On-Demand Aviation*, AIAA SciTech Forum, American Institute of Aeronautics and Astronautics, Jan 2018.

[14] Teeuwen, Y., *Propeller Design for Conceptual Turboprop Aircraft*, Ph.D. thesis, Delft University of Technology, 2017.

[15] EMRAX, "Technical Data and Manual for EMRAX Motors / Generators," `https://emrax.com/standard-emrax-motors/`.

[16] Miller, P., "Automotive Lithium-Ion Batteries," 2015, pp. 11.

[17] Anderson, J., *Fundamentals of Aerodynamics*, McGraw-Hill, 6th ed., 2017.

[18] Sivells, J. C. and Neely, R. H., "NACA TN No. 1269 – METHOD FOR CALCULATING WING CHARACTERISTICS BY LIFTING-LINE THEORY USING NONLINEAR SECTION LIFT DATA," Tech. rep., Langley Memorial Aeronautical Laboratory Langley Field, Va., April 1947.

[19] Veldhuis, L., "REVIEW OF PROPELLER-WING AERODYNAMIC INTERFERENCE," *24TH INTERNATIONAL CONGRESS OF THE AERONAUTICAL SCIENCES*, 2014, p. 21.

[20] Mulder, J., van Staveren, W., van der Vaart, J., de Weerdt, E., de Visser, C., in ´t Veld, A., and Mooij, E., "Lecture Notes AE3202 Flight Dynamics," Delft University of Technology, 2013.

[21] European Aviation Safety Agency (EASA), "Proposed Special Condition for small-category VTOL aircraft," oct 2018.

[22] European Aviation Safety Agency, *Certification Specifications for Normal, Utility, Aerobatic, and Commuter Category Aeroplanes*, a, a ed., jul 2012, Amendment 3.

[23] European Aviation Safety Agency, *Certification Specifications and Acceptable Means of Compliance for Small Rotorcraft CS-27 Amendment 6 17 December*, dec 2018.

[24] CE, I. K., "Analysis of Statically Indeterminate Structures by the Direct Stiffness Method," Lecture Notes, Lesson 24: The Direct Stiffness Method: Truss Analysis.

[25] Currey, N. S., *Landing Gear*, chap. Initial Layout, Lockheed-Georgia Company, 5th ed., jan 1982, pp.

1–12.

[26] Oliviero, F., "Systems Engineering and Aerospace Design – Lecture Series," 2019.

[27] NASA, McKinsey & Company, "URBAN AIR MOBILITY (UAM) MARKET STUDY," Tech. rep., NASA, November 2018.

[28] Kleinbekman, I., *eVTOL Arrival Sequencing and Scheduling in On-Demand Urban Air Mobility*, Ph.D. thesis, TU Delft, 2019.

[29] Chandler, J. and Chiland, E., "Mapping the rise of LA's tallest towers," 2019.

[30] International Virtual Aviation Organization, "VFR Cruise ALtitude or Flight Level," 2016.

[31] Sunil, E., Ellerbroek, J. H. J., Bussink, F., Nieuwenhuisen, D., Vidosavljevic, A., and Kern, S., "Metropolis: Relating Airspace Structure and Capacity for Extreme Traffic Densities," Eleventh USA/Europe Air Traffic Management Research and Development Seminar, 2016.

[32] Sunil, E., *Analyzing and Modeling Capacity for Decentralized Air Traffic Control*, Ph.D. thesis, Delft University of Technology, 2019.

[33] Air Navigation Services (ANS), "Executive Summary - draft Performance Review Report 2018," 2018, PRR 2018 presents an assessment of the performance of Air Navigation Services in the EUROCONTROL area for the calendar year 2018.

[34] Tuna, A., "Free FLigth; A Modern Approach to Air Traffic Management," *Leonardo Times*, Vol. 1, 04 2019.

[35] Udluft, H., "Decentralization in Air Transportations," Delft University of Technology, 2017.

[36] Federal Aviation Administration, "ADVISORY CIRCULAR - AIRCRAFT PROPELLER MAINTENANCE," *Flight Standards Service Washington, D.C.*, 09 2005, pp. 39.

[37] National Academies of Sciences, Engineering, and Medicine, *Preventive Maintenance at General Aviation Airports Volume 2: Guidebook*, The National Academies Press, 2015.

[38] Porsche Consulting GmbH, "The Future of Vertical Mobility, Sizing the market for passenger, inspection, and goods services until 2035," 2018.

[39] Reliability Analysis Center (RAC), *Operational Availability Handbook*, Reliability Analysis Center, -.

[40] Lebkowski, A., "Temperature, Overcharge and Short-Circuit Studies of Batteries used in Electric Vehicles," *Przeglad Elektrotechniczny*, Vol. 5, 05 2017, pp. 8.

[41] Stapelberg, R. F., *Handbook of Reliability, Availability, Maintainability and Safety in Engineering Design*, Springer Science & Business Media, 2009.

[42] Sinke, J., "AE3211-II Production of Aerospace Systems Reader," TU Delft, 2018/2019.

[43] AlcoTec, "Aluminum Filler Alloy Selection Chart," Brochure.

[44] A. Crosky, C. Grant, D. K. X. L. G., *Advances in Composites Manufacturing and Process Design*, Woodhead Publishing, 2015.

[45] de Boer, R. K., "Development of a cost effective composite wingbox for small aircraft," Tech. rep., NLR, aug 2010, Chapter 3, Manufacturing.

[46] Schimmelpenningh, J., "Acoustic Interlayers for Laminated Glass – What makes them different and how to estimate performance," *Glass performance days*, 2012.

[47] BALAC, M., *EMERGING MOBILITY SOLUTIONS AND THEIR IMPACTS IN ZURICH, SWITZERLAND*, Master's thesis, ETH ZURICH, Switzerland, 2019.

[48] Axhausen, K., Nagel, K., and Horni, A., *The Multi-Agent Transport Simulation MATSim*, Ubiquity Press, 2016.

[49] Ilario, C., "NASA UAM Noise metrics and regulations," June 2019, Personal correspondence.